The catalytic applications of titanium complexes in epoxide/anhydride ring opening copolymerization and umpolung cross-coupling reactions

A thesis submitted to Cardiff University in accordance with the requirements for the degree of Doctor of Philosophy School of Chemistry

Sahar Al Fayez
2021

Acknowledgment

First and foremost, all the praises and gratitude goes to God, the Almighty, for granting me countless blessing during my study and in completing this thesis. For giving me a supporting and encouraging family and country, and for every challenging I had to overcome to grow and learn.

My deep and sincere gratitude and thanks to my supervisor, Dr. Ben Ward, for his help, patience, supervision, understanding and endless support. He granted me the honour of joining his group as his PhD student. His immense knowledge and understanding of the subject guided me throughout my years. I will always appreciate all your help and everything you have done for me. Your spiritual and moral support has directed me from the first day I stepped in your lab to the closing of this thesis.

I am especially indebted to my second supervisor, Dr. Emma Richards for her valuable comments and treasured support. She helped me complete my work efficiently and with her plentiful experience she helped me avoid errors. You certainly helped me throughout this journey.

I am also grateful to my colleagues in the lab, their cooperation and support were important to me and working with them was a real pleasure. And I would specially thank Noha Alghamdi, for providing consistent interest and attention, reliable cooperation and support, and rich observation and insights. Moreover, I would like to extend my sincere gratitude to Matthew Shaw for the time and effort he spent with some of my GPC measurements.

I also owe a lot to my family, especially my parents, who always encouraged me and overwhelmed me with prayers and love. They have always given me moral support and assistance throughout my studies and life. To my husband, you are the one who has always supported me, encouraged me, and believed in my abilities. I also want to tell my kids, my motivators, and my supporters that I believe this work would not have been possible without you and your ongoing consideration every step of the way. I would also like to take this opportunity to express my gratitude to my sisters and brothers, for their constant support, encouragement, love, and care.

Last but not least, I would like to thank Imam Abdulrahman Bin Faisal University for giving me this opportunity.

Without all of you, this thesis would not have been possible. Thank you!

Abstract

A number of Salen-type complexes based on titanium(III) and titanium(IV) were synthesized and used as catalysts in the ring opening copolymerization of various epoxides and cyclic anhydrides, and in the reductive cross coupling reactions of enones with nitriles.

The first chapter of this thesis provides an overview of Salen-type ligands, their complexes, and uses with a particular focus on titanium complexes. It also provides some background about the ring opening copolymerization of epoxides with anhydrides, and about umpolung reactions.

The second chapter provides details of the synthesis and characterization of Salen-type ligands and their titanium complexes. Two types of ligand have been prepared: Salpn ligands and Salpy. Salen-type ligands can coordinate to a metal via the imine nitrogens and the phenol oxygens and thus offer a (usually) planner N_2O_2 core. The Salpy ligand contains an additional central pyridyl donor, and it therefore contains five donor groups (N_3O_2). The Salpn congeners have been prepared as pyridyl-free comparisons. All of these ligands have been fully characterized. Ti(IV) and Ti(III) complexes bearing these ligands have been synthesized and fully characterized in both solution and in the solid state.

The third chapter deals with the ROCOP of epoxides with cyclic anhydrides. Titanium Salen-type complexes, in combination with organic bases, were found to be efficient ROCOP catalysts. Also, these complexes proved to catalyse the copolymerization alone (without cocatalyst) providing good alternating polyesters with low dispersity. When a cocatalyst was used, PPNCl was more efficient than DMAP. The ROCOP reaction was studied in both solvent and solvent-free conditions; the selectivity of the prepared polymers were evaluated by ^{1}H NMR spectroscopy and the molecular weights / distributions were measured by gel permeation chromatography (GPC).

The fourth chapter of this thesis is focussed on the reductive umpolung reactions using titanium Salen-type complexes as catalysts in the presence of Zn dust. These complexes were found to be effective catalysts in the preparation of 1,6-difunctionalized ketonitriles *via* the cross coupling of enones with ketones.

The fifth chapter contains the experimental data and full characterization for all the ligands and complexes synthesised within the thesis. In addition to the characterizing data of the cross coupling products.

List of abbreviations

Å	Angstrom
Ac	Acetyl
Ar	Aryl
ASAP	Atmospheric Solids Analysis Probe
Bn	Benzyl
br	broad
°C	Degree Celsius
CDCl$_3$	Deuterated chloroform
CHO	Cyclohexene oxide
d	Doublet
dd	doublet of doublets
DCM	Dichloromethane
DFT	Density functional theory
DMAP	4-(Dimethylamino)pyridine
DP	Degree of polymerization
ECH	Epichlorohydrin
EI	Electron ionization spectrometry
EPR	Electron paramagnetic resonance
Et$_3$N·HCl	Triethylamine hydrochloride
EtOAc	Ethyl acetate
EtOH	Ethanol
eq.	equivalent
FT-IR	Fourier transform infrared spectroscopy
g	gram
GPC	Gel permeation chromatography
h	Hour(s)
HOMO	Highest occupied molecular orbital
HRMS	High resolution mass spectroscopy
^{i}Pr	Iso-propyl
J	Coupling constant
LO	Limonene oxide
LUMO	Lowest unoccupied molecular orbital
m	Multiplet

MA	Maleic anhydride
MALDI-MS	Matrix assisted laser desorption/ionization time of flight mass spectrometry (MALDI-TOF MS)
Me	Methyl
MeOH	Methanol
MHz	Megahertz
Min	Minute(s)
mmol	millimole
M_n	Number-average molecular weight
mol	mole
MS	Mass Spectrometry
M_w	Weight-average molecular weight
NBO	Natural Bonding Orbital
Nm	nanometre
NMR	Nuclear Magnetic Resonance
OMe	Methoxy
PDI	polydispersity index
Ph	Phenyl
PhA	Phthalic Anhydride
PO	Propylene oxide
ppda	2-methyl-2-(pyridine-2-yl)propane-1,3-diamine
ppm	parts per million
PPNCl	bis(triphenylphosphine)iminium chloride
Py	Pyridyl
q	quartet
R	Alkyl group
ROCOP	Ring Opening Copolymerization
s	singlet
SA	Succinic anhydride
Salen	Bis(salicylaldimine)
SEC	Size exclusion chromatography
SET	single electron transfer
SO	Styrene oxide
t	triplet
TBPhA	Tetrabromophthalic anhydride
tBu	Tertiary butyl

TCPhA	tetrachlorophthalic anhydride
THF	Tetrahydrofuran
TLC	Thin layer chromatography
TMS	trimethylsilyl
TMSCl	trimethylsilyl chloride
Tol	*p*-tolyl
VCHO	4-vinyl-1-hexene-1,2-epoxide
Vs	Versus
δ	chemical shift in ppm
λ	Wavelength
μl	Microliter
μm	Micrometre

The names and structures of the prepared complexes

1-Ti(III) complexes

[Ti(Salpy)Cl] **(1)**	[Ti(Salpy-Me)Cl] **(2)**	[Ti(tBu,tBu-Salpy)Cl] **(3)**
[Ti(Cl,Cl-Salpy)Cl] **(4)**	[Ti(Naphpy)Cl] **(5)**	[Ti(Salpn)Cl] **(6)**

[Ti(tBu,tBu-Salpn)Cl] **(7)**

2-Ti(IV) complexes

[Ti(Salpy)Cl$_2$] **(8)**

[Ti(Salpy-Me)Cl$_2$] **(9)**

[Ti(^{t}Bu,^{t}Bu-Salpy)Cl$_2$] **(10)**

[Ti(^{t}Bu,OMe-Salpy)Cl$_2$] **(11)**

[Ti(Me-Salpy)Cl$_2$] **(12)**

[Ti(Cl,Cl-Salpy)Cl$_2$] **(13)**

[Ti(Ad,Me-Salpy)Cl$_2$] **(14)**

[Ti(Naphpy)Cl$_2$] **(15)**

[Ti(Salpn)Cl$_2$] **(16)**

[Ti(^{t}Bu,^{t}Bu-Salpy)Cl$_2$] **(17)**

[Ti(Me-Salpy)Cl$_2$] **(18)**

Table of Contents

Chapter 1- An Introduction

Chapter 2- Synthesis and and Characterization of Salen-type Ligands, and their Complexes with Titanium (III) and Titanium (IV)

Chapter 3- Ring opening copolymerization of epoxides with cyclic anhydrides

Chapter 4- Umpolung reactions

Chapter 5- Experimental and characterization data

Chapter 1

An

Introduction

1.1 Salen ligands:

Since the late nineteenth century,[1] Schiff base ligands have received widespread interest due to their ease of synthesis (one step condensation), ability to coordinate to different metal ions, multi coordinating ability (from mono dentate to hexadentate), stability, and the various applications of their metal complexes. These compounds were reported for the first time in 1864 by Hugo Schiff.[2] Since that time a massive variety of stable compounds have been synthesized containing both transition and non-transition metals. The condensation of primary amines with aldehydes or ketones leads to the formation of Schiff bases, which contain an imine functional group ($N=CR_2$). These compounds have much importance in field of medicine due to the presence of imine functional group which can be structurally modified to achieve the desired molecule, targeting a specific disease. A lot of azomethines were reported to exhibit a broad range of biological activities such as anticancer,[3,4] antifungal,[5,6] antibacterial,[7,8] antiinflammatory,[9] antioxidant,[10] and antiviral activities.[11] In addition, Uddin et al. found that bis(2-hydroxy-1-naphthaledehyde)hexanediamine could be a good candidate for inhibition of *COVID*-19, the virus that affected millions of people in the world during the last year (2020).[12]

One of the most common Schiff base ligands is salen, in which a diamine is condensed with a salicylaldehyde (or its derivative) in a 1:2 stoichiometry, leading to the formation of a bivalent tetradentate (ONNO) ligand (Equation 1.1).[13]
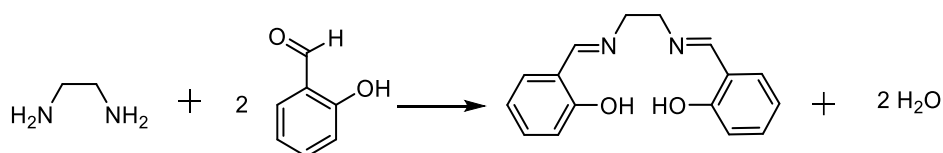
Equation 1.1: Synthesis of salen ligand

The salen ligands coordinate to a metal *via* the imine nitrogens and the phenoxide donors, these latter are invariably deprotonated. Salen ligands offer a rigid and planer N_2O_2 core, leaving two axial sites available for co-ligands.[14] They are suitable for supporting a wide range of transition metals, finding particular applications in catalysis.[14,15] Although the expression salen was used to represent the tetradentate Schiff bases obtained from ethylenediamine, the general expression Salen-type is used in the literature to represent [O,N,N,O] tetradentate bis-Schiff base ligands.[2] Figure 1.1 contains different Salen-type ligands.
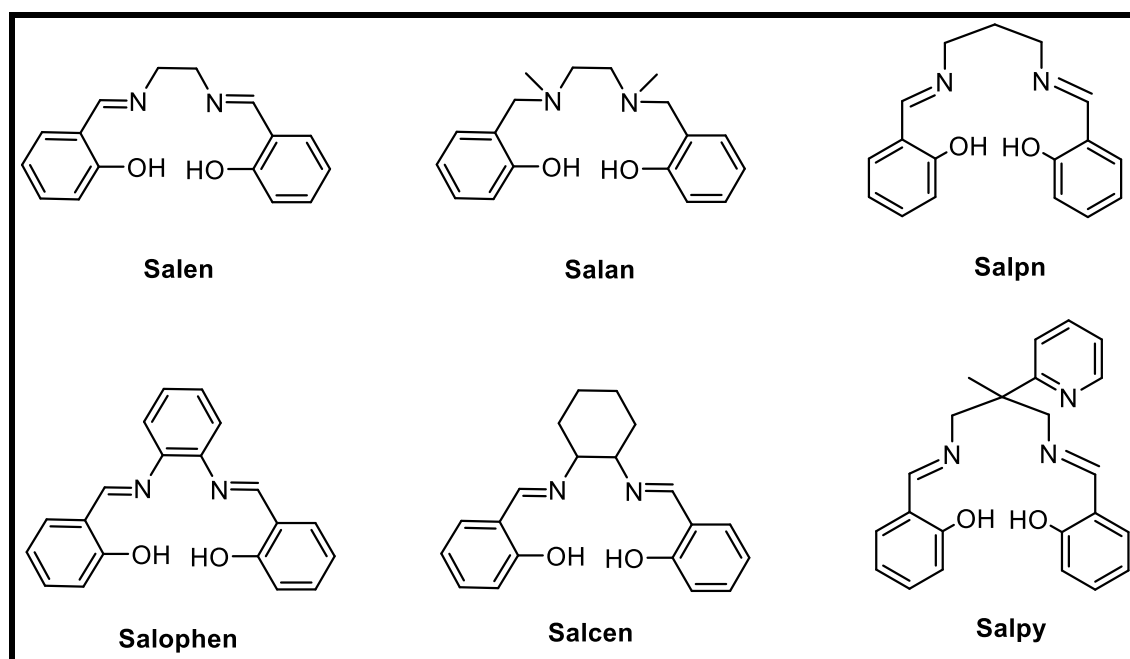
Figure 1.1: Salen-type ligands

The versatility of the starting material (amine and the salicylaldehyde compounds and their derivatives) allows for the preparation of a large diversity of Salen-type ligands with various steric and electronic properties. Their versatility is exemplified by the fact that salen ligands, due to their π conjugate system, have been used as optical sensors for cations including Al(III), Zn(II), Cu(II) and Pt(II).[16–18]

Salen-type ligands can coordinate to most of the metals found in the periodic table. There are many applications of the complexes of these ligands with transition metals, such as electro analysis, as potentiometric sensors,[19] and biochemistry, as some complexes revealed interesting antioxidant[20] and antitumor[21,22] properties. Moreover, they can also be used in stabilizing metal ions in several oxidation states.[23] This is because of the stabilizing efficacy of the *pseudo*-macrocyclic N_2O_2 type coordination motif. Furthermore, metal salen complexes have been used in heterogeneous catalysis, immobilized in different supports such as silicas,[24] zeolites,[25] and organic polymers.[26]

The most important application of these complexes is in homogeneous catalysis. The development of more efficient catalysts has received significant effort. Due to the availability, high asymmetry ability and structural variety, metal salen complexes have been considered one of the most useful class of catalysts.[27] These complexes are able to act as catalysts in a

large selection of reactions, depending on the metal ion, such as olefin epoxidation,[2,28] cyclopropanation,[29] oxygenation,[30] ring-opening of epoxides,[31] hydroxylation,[32] and Diels-Alder reactions.[33] The effect of modifying the salen ligand structure on the redox chemistry of complexes has been investigated during the last few years.[34]

1.2 Titanium chemistry:

Titanium was discovered in 1791 by William Gregor and it is the 9th most abundant of all elements on the earth's crust (second of the transition elements, after iron).[35,36] It occurs in nature as rutile (TiO_2) and ilmenite ($FeTiO_3$).[37] Titanium has many attractive properties: it is corrosion resistance, it is as strong as steel but half as dense, most of its compounds are non-toxic, and it is one of the cheapest transition metals.[38] It has the electronic configuration of [Ar] $4s^2 3d^2$ and upon removal of all the valence electrons resultant in a diamagnetic and tetravalent Ti(IV). Oxidation state (+4) is the highest and most stable oxidation state for titanium. Organometallic complexes containing Ti(II) and Ti(III) can also be prepared, but they tend to be more sensitive to oxygen and require more rigorous glove box and Schlenk line techniques. Due to their coordination number and electronic configuration, organometallic titanium complexes in low oxidation states (III and II) exhibit very high reactivity in molecular activation, almost close to the carbenes and free radicals (it has high tendency to attain d^0 configuration).[23,39] The interests in the chemistry of titanium were focussed mainly on the titanates and alkoxides due to the ease of their preparation from $TiCl_4$ and alcohols, in addition to the use of these derivatives in heat- resistant paints and in the treatment of wood, textiles and paper.[40]

In the 1950s titanium ($TiCl_4$) was used as Ziegler-Natta catalyst in the polymerization of ethylene which required high temperature and pressure to occur. However, with $TiCl_4$ and $AlEt_3$ in a hydrocarbon solvent this process proceeded at room temperature and atmospheric pressure.[41]

The most important geometries for Ti(IV) complexes are octahedral (e.g. $[TiCl_4(THF)_2]$) and tetrahedral (e.g. $Ti(O^iPr)_4$), although, higher coordination numbers such as seven and eight have been reported.[42,43] Titanium (IV) complexes have been identified as good alternatives of cisplatin in anticancer therapy.[44,45] The high toxicity and restricted activity range of cisplatin encouraged researchers to find new alternative inorganic complexes.[46,47] Titanium (IV) complexes, in particular, budotitane ($[(bzac)_2Ti(OEt)_2]$) and titanocene dichloride (Cp_2TiCl_2) were the first to enter clinical experiments after platinum compounds.[48,49] These complexes and their derivatives (Figure 1.2) have shown high and wide anticancer reactivity

with relatively low toxicity *in vitro* and *vivo*, eventually the non-toxic TiO_2 is produced in aqueous solutions.[50–53] However, their rapid hydrolysis in biological systems was the main disadvantage of these complexes, as the labile ligands (Cl, OR) hydrolysed very quickly (seconds to minutes) whereas the more inert ligands (diketonato and Cp) required more time (hours) to dissociate which hampered the mechanistic studies and applicability, due to the formation of undefined aggregates with low solubility.[54–56] On the other hand, titanium (IV) complexes based on diamino bis(phenolato) Salen-type ligands exhibited high cytotoxic activity in addition to the unique hydrolytic stability and *in vivo* activity.[21,57–59]
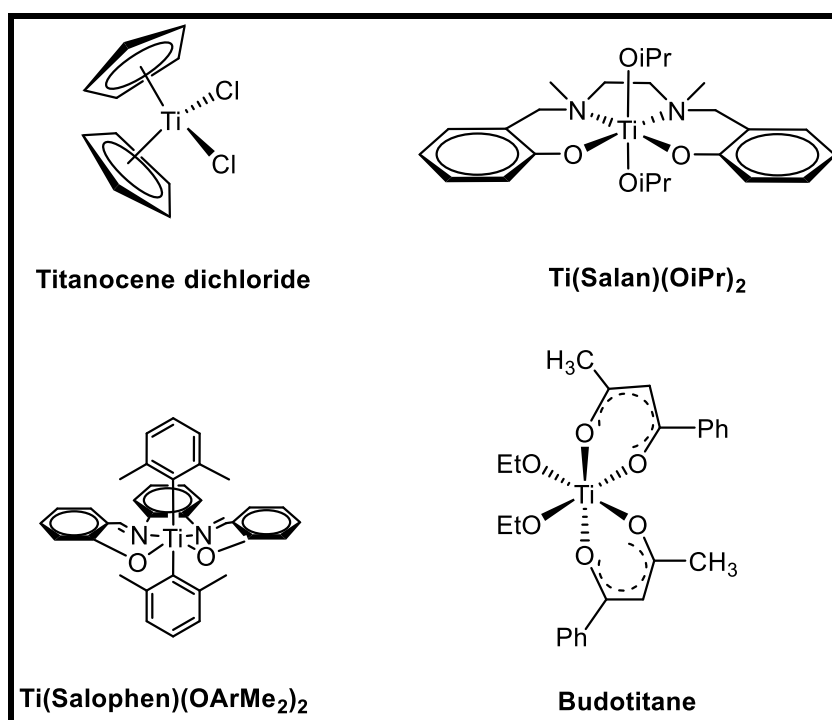
Figure 1.2: Selected titanium complexes used as anticancer therapy

Titanium complexes based on polydentate ligands, especially based upon amido ligands, are well-known complexes and have found widespread implementation in, for instance, catalysts for organic reactions,[60–62] as precursors for ceramic materials,[63] in the synthesis of oligomeric complexes,[64] ethylene polymerization,[65] α-olefin polymerization,[66–68] copolymerization of epoxides with CO_2,[69–71] styrene polymerization,[72,73] ring opening polymerization of cyclic esters,[74–77] trimethylsilylcyanation of aldehydes,[78–81] epoxidation of olefines,[82] and in pinacol coupling.[83] Subsequently, studying these compounds may be considered as an active scientific subject.[62] However, the vast majority of titanium organometallic chemistry is based upon Ti(IV). The high Lewis acidity of titanium in its maximum oxidation states renders it particularly useful for the activation of organic substrates,

and its d^0 electronic configuration makes its complexes diamagnetic, making its chemistry easy to study using NMR spectroscopy. In contrast, the related chemistry of Ti(III) is much less studied, possibly due to its extremely high sensitivity to O_2, as well as its complexes being paramagnetic, thereby making characterization difficult.

The reaction between Salen-type ligands and titanium (IV) precursors do not always lead to the formation of the chelate complex such as [Ti(salen)Cl$_2$], instead, one of three types of complexes may occur; the structures are shown in Figure 1.3.[1] The Schiff base can act as a bidentate donor through nitrogen atoms and form the adduct complex (**I**), it can act as tetradentate donor to form the chelate (**II**) complex and eliminate HX, or tetradentate donor with the coordination of solvent molecule to form the solvate complex (**III**).

Adduct complex
(I)

Chelate complex
(II)

Solvate complex
(III)
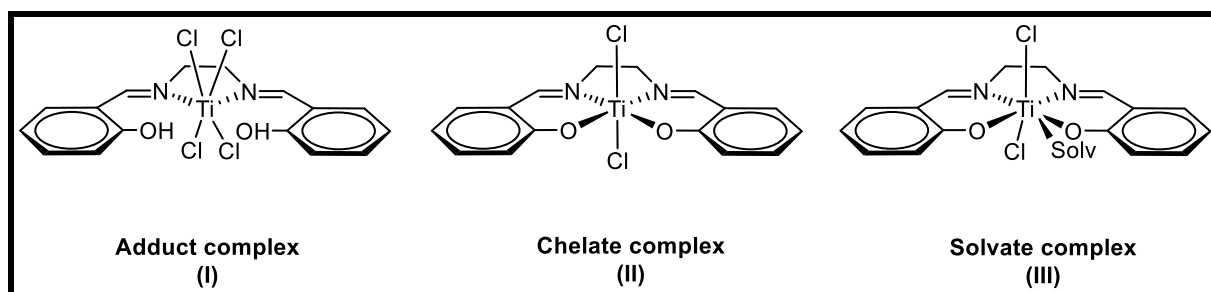
Figure 1.3: Types of different complexes

Reaction conditions play an important role in determining the resulting product, such as the temperature, the choice of solvent the nature of both the Schiff base and metal salt.[1] For example, the reaction between H$_2$salen and TiCl$_4$ in refluxing THF gave type **II** complex, nevertheless, repeating the same reaction with the same solvent at room temperature afforded the solvate complex **III**.

1.3 Ring Opening Copolymerization of Epoxides with Cyclic Anhydrides (ROCOP):

Synthetic polymeric materials have provided many benefits in our daily life and become a significant group of materials since 1941 when the first industrial-scale polyethylene terephthalate (PET) polyester was synthesized.[84,85] The most common polymers are obtained from hydrocarbons derived from crude oil and these polymers are commonly non-biodegradable. With more than 350 million tons per year of plastic production worldwide,[86]

there are growing concerns about their effect on the environment and the resources. These concerns have encouraged scientists to search for biocompatible, biodegradable, and renewable alternatives. Polyesters formed from the ring opening copolymerization of epoxides and anhydrides have been found to be a promising alternative to petroleum-based plastics (Scheme 1.1).[87] The large numbers of available monomers, several of which are from renewable sources[88–90], biodegradability, biocompatibility, and the ability to modify these polyesters through post-polymerization alteration allow a large number of new polymers to be prepared with exceptional properties that could not be obtained using traditional polymers.[91–93]
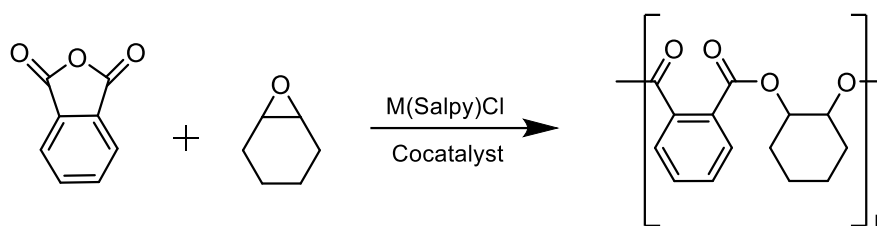
Scheme 1.1: Ring opening copolymerization of cyclohexene oxide with phthalic anhydride

Polyesters can be synthesized by various synthetic routes (Scheme 1.2). Depending on the reaction mechanism, polyesters can be classified into two classes: step-growth polymerization and chain-growth polymerization.[94] The step-growth polymerization involves the condensation of diesters or diacids with dialcohols and is the most common method. However, this process requires a high temperature to eliminate water or alcohol which is produced as byproduct.[92] Also, achieving high molecular weight polymers needs the polymerization to proceed to high monomer conversion (i.e. long reaction time), and the polydispersity is generally about 2 because of uncontrolled growth of the polymer chains and isomerization processes.[95,96] Another route to polyesters is chain-growth polymerization, which in contrast to step-growth polymerization, does not generate byproducts and produces polymers with high molecular weight and with superior control over the polydispersity. Chain-growth polymerization can proceed through several routes, however, the most two common routes are: ring opening polymerization (ROP) of cyclic esters or carbonates and alternating ring opening copolymerization (ROCOP) of epoxides with cyclic anhydrides or carbon dioxide.[91]
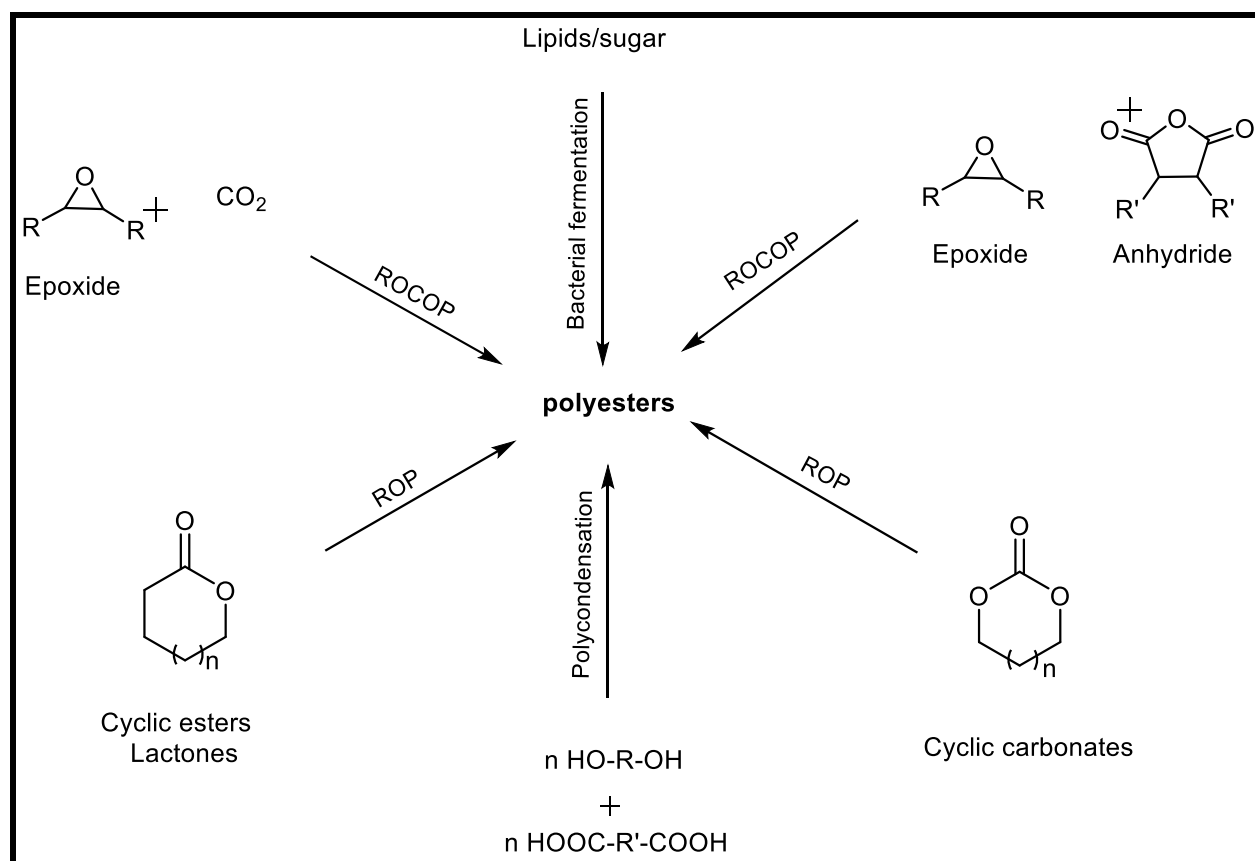
Scheme 1.2: different routes to polyesters

In ROP, especially at the high conversion of lactones, side reactions (like transesterification) can occur, and this gives poor control over the molecular weight. Also, the limited variety of monomers and the deficiency of post-polymerization modification results in polyesters with limited properties.[91,97] However, alternating ring opening copolymerization of anhydrides and epoxides produced polyesters with more variable structures because of the availability of huge numbers of anhydride and epoxide monomers.[98] Moreover, many epoxides and anhydrides reported for the ROCOP can be obtained from renewable resources, like cyclohexene oxide (CHO), epichlorohydrin (ECH), phthalic anhydride (PhA), maleic anhydride (MA), as well as cyclohexanedicarboxylic anhydride (CHA) and succinic anhydride (SA).[99] A list of some popular epoxides and anhydrides used in ROCOP studies are illustrated in Figures 1.4 and 1.5, respectively. Thus, the properties of these polyesters can be tuned by changing the monomer combinations or by post-polymerization functionalization.[100,101] For instance, when using monomers with monocyclic anhydrides and epoxides or monomers with long side chains, low T_g values can be achieved.[96,102] In contrast, high T_g values can be obtained when using rigid backbones monomers like bi- or tricyclic derivatives.[103] Subsequently, these polyesters have been used in diverse applications ranging from films designed for agricultural

properties, drug delivery systems, resorbable medical sutures, wound dressings and other biomedical devices to bulk packaging.[85,97,104,105]
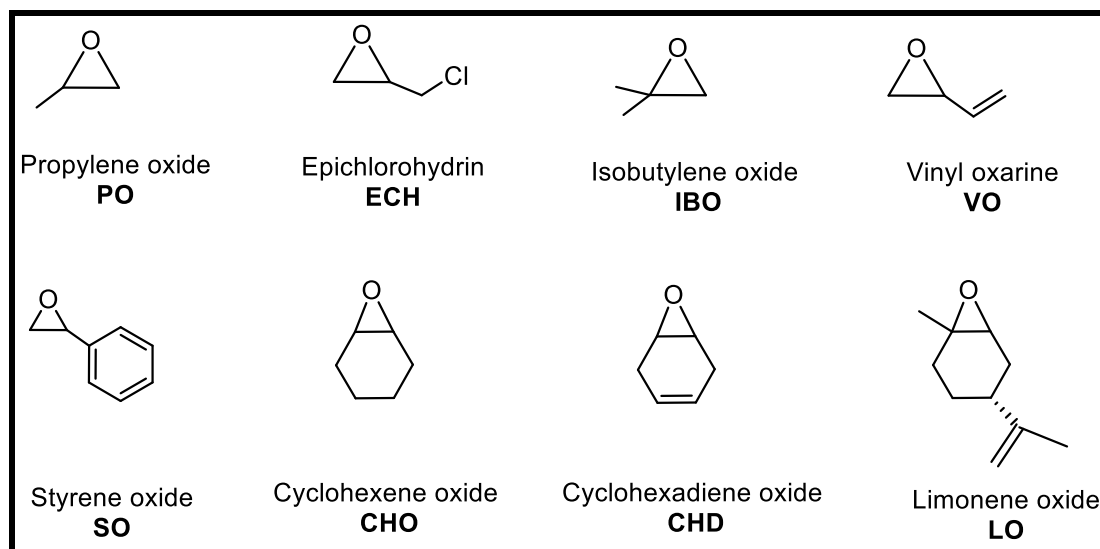
Figure 1.4: Structures and abbreviations of common epoxides used in ROCOP
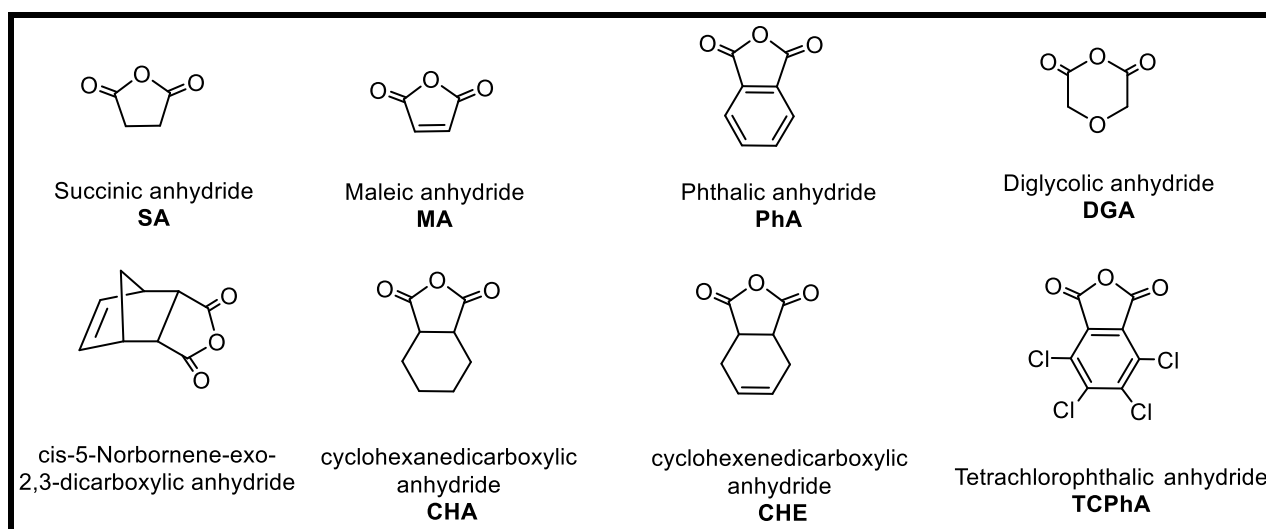
Figure 1.5: Structures and abbreviations of common Anhydrides used in ROCOP

Several studies on the complexes of Lewis acidic metal centres such as aluminium, iron, chromium, manganese, cobalt, magnesium and zinc, with polydentate ligands bearing N and/or O atoms, for example Salen-type[93,96,106,107,107–115], porphyrinate-type[96,109,116] and *β*-

diketiminates[103,117,118] have been examined as catalysts in ROCOP. A wide range of both anhydrides and epoxides have been reported for this copolymerization reaction.

In 1960, Fischer reported the first alternating ring opening copolymerization of anhydride with epoxide using tetrabutyl titanate and tertiary amines as catalysts.[119] Following that several organometallic catalysts (R_3Al, $B(C_2H_5)_3$, $ZnEt_2$ etc.) were described for the copolymerization of epoxides with anhydrides, nevertheless, no significant movement was reached until the recent improvement of new catalysts.[101,120,121] The difficulties in achieving polyesters with high molecular weight and overcoming epoxides homopolymerization (a significant side reaction that generates polyether instead of polyester) have hampered researchers' interest in ROCOP for many years.[98] In 1985, Inoue and Aida reported the first well controlled ROCOP polymerization with aluminium porphyrin complexes ([(TPP)AlX]), **1.1** and **1.2** to catalyse the copolymerization of 1,2-epoxypropane with phthalic anhydride (Figure 1.6).[122] They also found that addition of quaternary ammonium or phosphonium salts (Lewis bases) to the reaction increased the activity of catalyst. Analogous chromium complex **1.3** in combination with 4-dimethylaminopyrdine (DMAP) as cocatalyst were used for the copolymerization of cyclohexene oxide (CHO) and styrene oxide (SO) with phthalic anhydride (PhA), cyclopropane-1,2-dicarboxylic acid anhydride (CPrA), cyclopentane-1,2-dicarboxylic acid anhydride (CPA) or succinic anhydride (SA) and resulted in a completely alternating polyester.[107,110] The substitution of Cr in complex **1.3** by Mn or Co (Complexes **1.4** and **1.5**) decreases the activity of metal porphyrin complex.

	M	X		M	X
1.1	Al	Cl	**1.4**	Mn	Cl
1.2	Al	OCOC(CH$_3$)$_3$	**1.5**	Co	Cl
1.3	Cr	Cl			
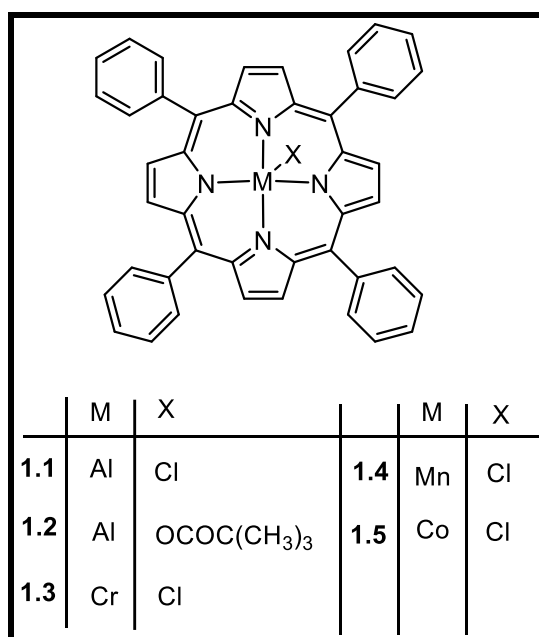
Figure 1.6: Metal-porphyrin complexes as catalysts in ROCOP

In 2007, Coates and co-workers described the first highly active catalyst in the ROCOP of epoxides with cyclic aliphatic anhydrides. They prepared perfectly alternating polyesters with high molecular weight (up to 55000 g/mol) and low dispersity using β-diiminate (BDI) zinc complexes **1.6**-**1.10** (Figure 1.7).[103]

	R_1	R_2	R_3
1.6	Et	Et	H
1.7	Et	Et	CN
1.8	Et	Et	Me
1.9	^{i}Pr	Et	CN
1.10	^{i}Pr	^{i}Pr	CN
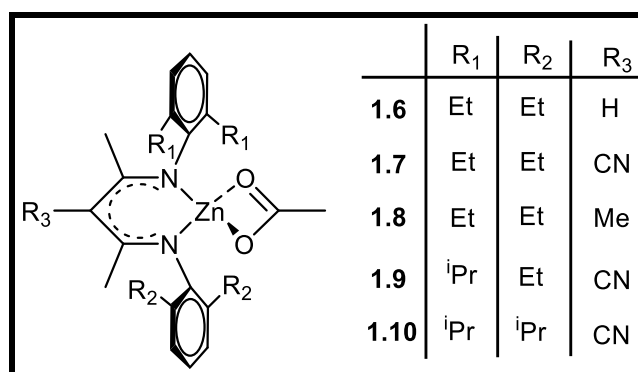
Figure 1.7: Coates's ROCOP catalyst

Coates' report has motivated scientists to explore the effect of other metal complexes on the ROCOP of epoxides with anhydrides. These polymerization reactions required the use of a catalyst, or more precisely, an initiator. The initiator is usually a single site metal complex with the formula LMX, where X is the initiating group at which the propagation proceeds (commonly an alkoxide or halide group), M is the metal site at which the catalysis occurs, and L is an ancillary ligand.

Salen-type complexes also proved to be effective catalysts in ROCOP of epoxides with anhydrides. In 2011, Duchateau and coworkers reported the use of [(Salophen)CrCl] complex (**1.11**) (Figure 1.8) for the ROCOP of CHO with a variety of anhydrides (CPrA, SA, CPA, and PhA).[110] The combination of **1.11** with DMAP produced an alternating CHO-anhydride polyester with M_n values between 1000-16060 g/mol. Complex **1.12** was effectively used for the copolymerization of maleic anhydride (MA) with different epoxides (1-butene oxide (BO), propylene oxide (PO), phenyl glycidyl ether, epichlorohydrin (ECH) etc.) producing completely alternating polymers with high molecular weight (M_n= 21-33 Kg/mol) under mild conditions and without cocatalyst.[123] In 2012, Darensbourg et al. used the same catalyst **1.12** in the ring opening copolymerization of CHO, SO and PO with the anhydrides, SA, MA, PhA, cyclohexane (CHA) and cyclohexene (CHE) and it resulted in completely alternating

copolymers.[108] Unlike the previous study, Darensbourg and coworkers found that **1.12** without cocatalyst was ineffective for the ROCOP of CHO with PhA.
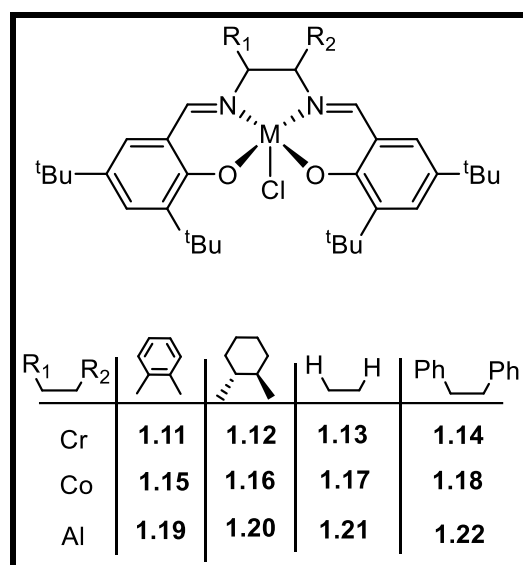
Figure 1.8: Salen-type complexes used in ROCOP of epoxides with anhydrides

Duchateau and coworkers prepared a series of Cr, Co and Al Salen-type chloride complexes **1.11**-**1.22** (Figure 1.8).[106] Employing these catalysts in combination with cocatalyst (DMAP) for the ROCOP of CHO with variety of anhydrides containing different ring strain (SA, CPrA and PhA) provided alternating polyesters with M_n values 800-15000 g/mol. The chromium catalyst proved to be the most reactive while the aluminum catalysts were the least active. Regarding the ligand backbone, the salophen complexes performed best. It is worth mentioning that while some of the bulk copolymerizations produced poly(ester-co-ether)s, all the solution copolymerization afforded perfect alternating polyesters. The same research group studied the ROCOP of limonene oxide (LO) with PhA using (^{t}Bu-salophen)chloride complexes **1.11**, **1.19** in addition to [Mn(^{t}Bu-salophen)Cl] (**1.23**).[116] Again, the chromium complex **1.11** proved to be the most active.

Bimetallic complexes also have been used in ROCOP reactions. The bimetallic Cr(III) salen complex **1.24** (Figure 1.9) was shown to have significant reactivity compared to its monometallic analogues in the ROCOP.[114] The copolymerization of ECH with MA using **1.24** without cocatalyst produced a completely alternating polyester with high molecular weight, M_n= 32.5 Kg/mol.[114] Saini et al. reported two new dinuclear catalysts for the ROCOP of PhA and CHO, **1.25** and **1.26** (Figure 1.9).[124] The di-magnesium complex **1.25**, was found to be

four times faster compared to the zinc counterpart **1.26**, however, their reactivities are closely related to the known chromium salen/ porphyrin catalyst.
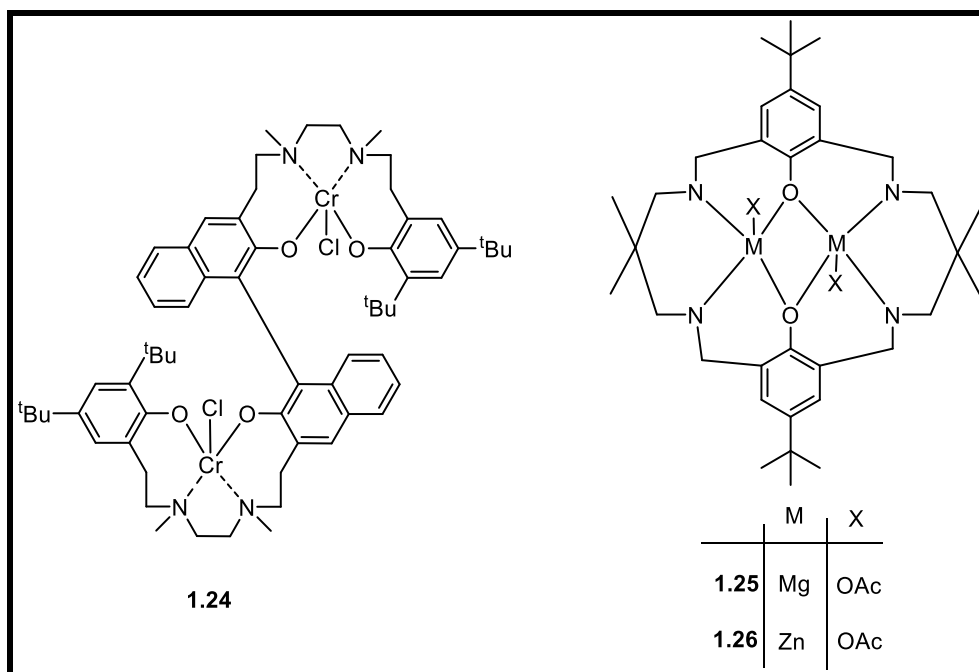
Figure 1.9: Bimetallic complexes used as catalyst in ROCOP

Manganese and iron corrole complexes **1.27-1.31** (Figure 1.10) have been reported by Nozaki and co-workers as effective catalysts in ROCOP of PO, CHO, SO, and ECH with SA, MA and glutaric anhydride GA.[125] These complexes in combination with a cocatalyst [PPN]OBzF$_5$ (OBzF$_5$= pentafluorobenzoate) copolymerized the aforementioned comonomers with molecular masses ranging from 2.9 to 8 Kg/mol.
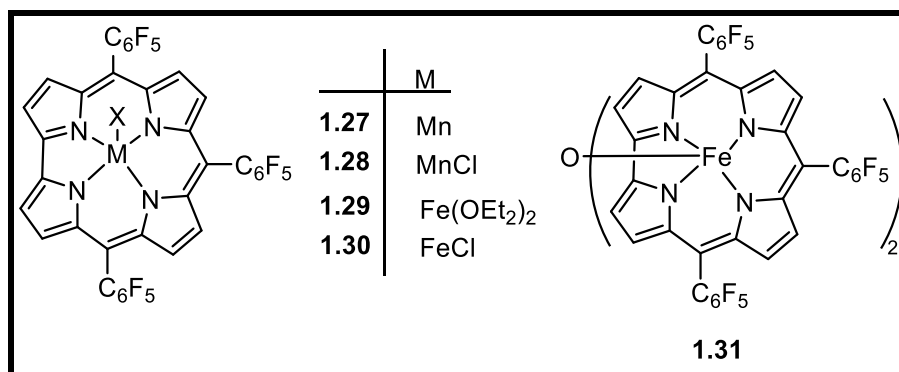
Figure 1.10: Metal corrole used in ROCOP

The ROCOP of epoxides with anhydrides in the presence of catalyst LMX proceeds through several steps (Scheme 1.3):

1- The initiation step at which the metal alkoxide/ carboxylate intermediates are generated by the reaction of the monomers and MX.

2- The propagation reactions. This step involves successive alternating formation of metal alkoxide and carboxylate intermediates. Nevertheless, if sequential epoxide enchainment is involved, the percentage of poly ether will be increased.

3- Chain transfer reactions: the growing polymer chain in this step is equilibrated with added protic compounds (e.g., alcohols).

4- Termination step which could be achieved by manipulating the conditions (monomer removal, reducing temperature) or by addition of acids or water/alcohol.

Initiation

Propagation

Formation of ether linkage

Chain trnsfer

X= halide, alkoxide, carboxylate
OR= alkoxide
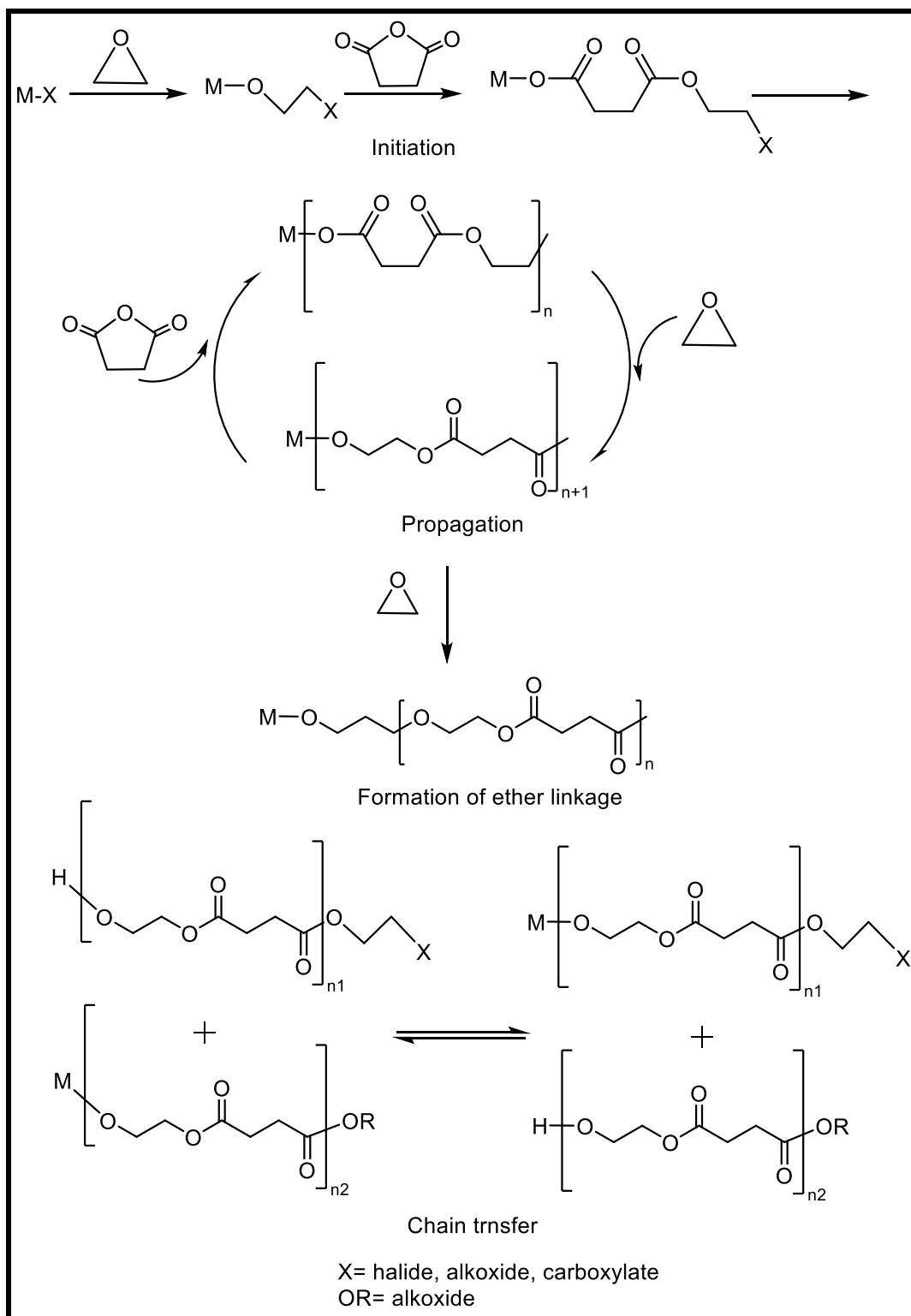
Scheme 1.3: ROCOP steps[91]

Most of the catalysts in ROCOP show higher selectivity and activity when they are combined with nucleophilic cocatalyst (Figure 1.11). The common cocatalysts used are inorganic salts, like ammonium or phosphonium halide, or Lewis bases such as 4-

(dimethylamino)pyridine (DMAP) and methyl imidazole, among them (DMAP) and bis(triphenylphosphine)iminium halides [(PPN)X] are reported as the most effective cocatalysts.[92] Salen-type complexes are generally found to be more active in ROCOP compared to β-diketiminato-type and porphyrin complexes under the same conditions.[96] Deleterious side reactions like, transesterification, epoxides homopolymerization and epimerization tend to occur only when the anhydride monomer is entirely consumed and the polymerization is completed.[93]
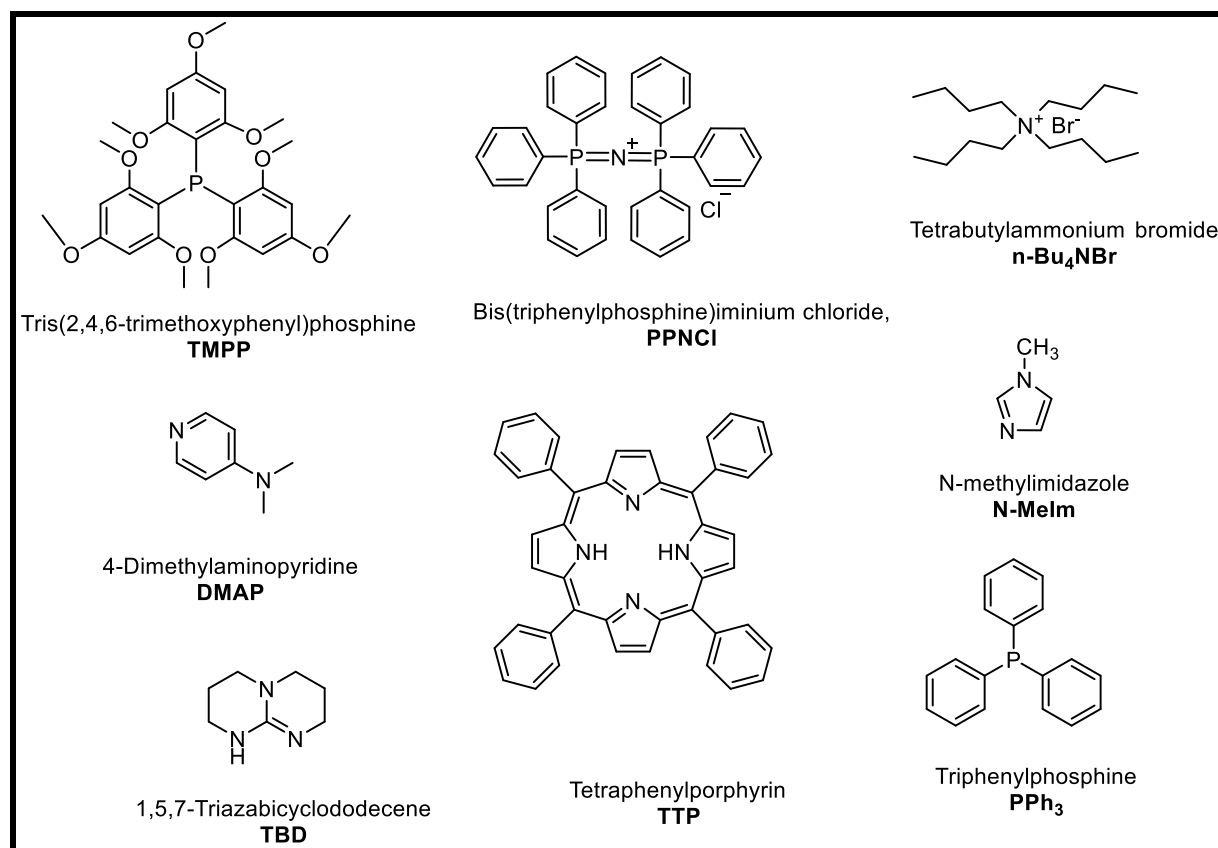
Figure 1.11: Common cocatalysts used in ROCOP

1.3.1 Polymer molecular weight determination:

The synthetic pathways which are used for the synthesis of polymers result in the formation of a mixture of chains that vary in length. The physical properties of a polymer depend on its molecular weight. As a representative example, Table 1.1 shows the effect of the size (molecular weight) on the physical properties of polyethylene.[94]

Table 1.1: Properties of low density polyethylene[94]

DP	Molecular weight	Softening temperature(°C)	Physical state 25°C
1	28	-169 (mp)	Gas
6	170	-12 (mp)	Liquid
35	1000	37	Grease
140	4000	93	Wax
250	7000	98	Hard wax
430	12000	104	Plastic
750	21000	110	Plastic
1350	38000	112	Plastic

Polymer molecular weight can be determined by the number average molecular weight M_n and is described as:

$$M_n = \frac{\Sigma N_i M_i}{\Sigma N_i}$$

Where M_i is the molecular weight of the chain and N_i is the number of chains with that molecular weight.

Also, it can be defined by the weight average molecular weight M_w. Each molecule participates according to the ratio of its particular weight:

$$M_w = \frac{\Sigma N_i M_i^2}{\Sigma N_i M_i}$$

The ratio of M_w to M_n is important and it influences the polymer properties. This ratio is called the polydispersity of the polymer or molecular weight distribution:

$$PDI = \frac{M_w}{M_n}$$

When PDI=1 the polymer is said to be mono-disperse (ie every polymer chain has an identical length), however, a PDI>1 indicates different polymer chain lengths.

There are many methods by which the molecular weight of polymers can be determined. They include membrane osmometry, vapour phase osmometry, light scattering, end group analysis and the size exclusion method.[126] All of these techniques are carried out using polymer solutions.

Size exclusion chromatography method known as Gel-Permeation chromatography (GPC) is used widely for determining molecular weight averages M_n and M_w and the molecular weight distribution PDI of polymers in one operation. This technique is based on exclusion of the molecules above a specific size from entering the pores that are found in a swollen packed column, and that's why it often called size exclusion chromatography. Depending on the molecular size, they are able to permeate different pore volumes and the biggest molecules might not be able to enter any pores and so leave the column first. However, the smallest molecules can permeate every pore and therefore leave the column last.

Another method that can be used to determine the molecular weight is Matrix-Assisted Laser Desorption/Ionization -Time of Flight (MALDI-TOF) mass spectrometry. This method gives the repeat unit of the polymers and to clarify the nature of chain end groups.

1.4 Umpolung reactions:

The development of mild, stereo-, regio-, and chemoselective ways for the construction of C-C bonds has attracted considerable attention over the past years.[61,127] In 1951, the term umpolung was introduced for the first time by Witting to describe the inversion of charge,[127,128] however, it was not accepted by chemists until 1974 when Seebach reintroduced the concept to define inversion of reactivity of 1,3-dithianes (**1.32**) which is now known as an important method for the production of complex natural and unnatural products (Scheme 1.4).[128–132]
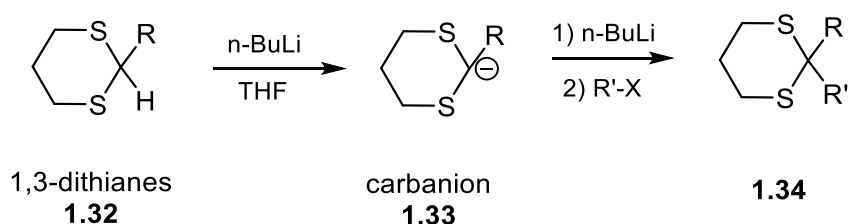
Scheme 1.4: Umpolung reaction of 1,3-dithianes

In general, the concept umpolung describes a modification of a molecule that leads to an inversion of its innate polarization and reactivity which results in formation of new C-C bonds that would be otherwise difficult to form. The removal or addition of electrons in nucleophilic or electrophilic systems (redox reactions), respectively, is considered one of the simplest ways of inducing umpolung reactivity. Consequently, the species' reactivities will reverse, for example, the reduction of aldehydes or ketones to pinacols and esters to

acyloins[133] can be achieved with metals[134] or by photochemical or electrochemical[135] methods (Equation 1.2).

1.35   **1.35**   **1.36**
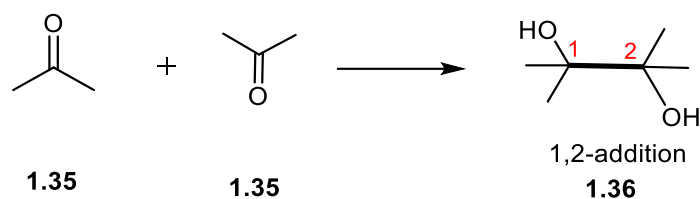
Equation 1.2: Ketones cross-coupling to pinacol

The cross-coupling products are 1,2-, 1,4- or 1,6-bifunctional and are produced by the coupling of two carbon atoms with the same polarity. In these reactions, we can assume that half of the reactants have umpolung reactivity, which couple with the other half that have normal reactivity (in reality, it is radical cations or anions coupling).[132] One of the important industrial applications that use the electrochemical redox coupling protocol is the Baizer-Monsanto process which involves the dimerization of acrylonitrile (**1.37**) to adiponitrile (**1.38**) (an intermediate in the manufacture of Nylon 66, Equation 1.3).[136–138]

1.37   **1.37**   **1.38**
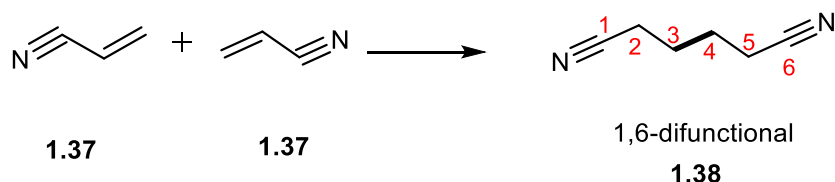
Equation 1.3: Baizer-Monsanto process

Many organocatalysts are able to invert the polarity of molecules such as phosphines.[139,140] N-hetero cyclic carbenes (NHCs) also, were used widely as an organocatalysts in such reactivity umpolung.[141–143] Breslow has proposed a mechanism for this reaction which is illustrated in Scheme 1.5.[128]
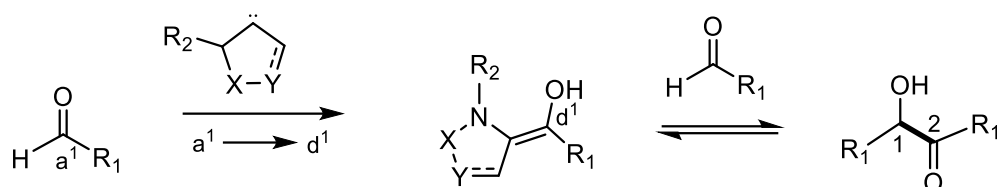
Breslow intermediate

Scheme 1.5: NHC catalysed umpolung reactivity of aldehyde (benzoin condensation)

Several transition metals are known to catalyze these umpolung reactions, such as titanium, copper, nickel, cobalt, palladium and vanadium.[144–146] In particular, low-valent titanium catalysts found widespread applications in cyclization reactions,[147] epoxide opening,[148] conjugate reductions,[149,150] and pinacol coupling.[151,152]

In 1988, Zhang and Liu reported a pinacol coupling reaction using titanocene dichloride (Cp_2TiCl_2) **1.39** as catalyst and Grignard reagent as terminal reductant.[153] Different diaryl ketones were coupled to form diols in good yields, and catalyst inhibition by the product (1,2-diol) was not observed (Scheme 1.6).

reactant	Ar	Product
1.40 a	Ph	**1.40 b**
1.41 a	$4\text{-}ClC_6H_4$	**1.41 b**
1.42 a	$4\text{-}BrC_6H_4$	**1.42 b**
1.43 a	$4\text{-}MeC_6H_4$	**1.43 b**
1.44 a	$4\text{-}MeOC_6H_4$	**1.44 b**
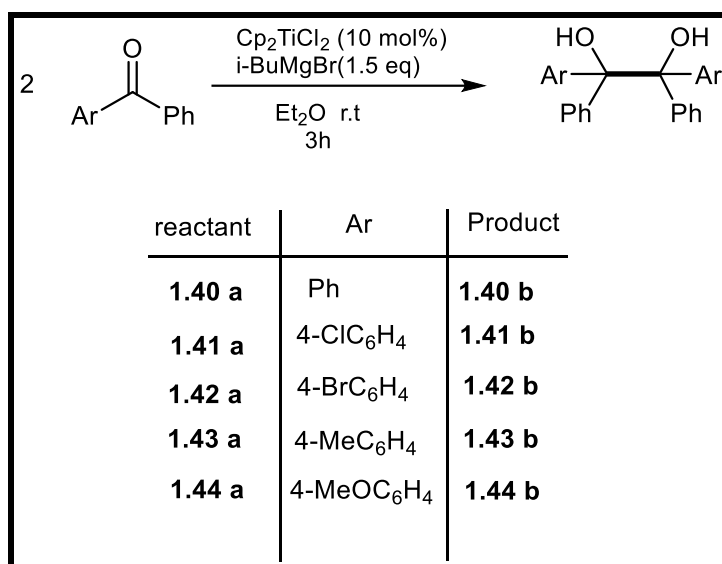
Scheme 1.6: Pinacol coupling reaction with Cp_2TiCl_2

The pinacol coupling of benzaldehyde (**1.45**) was achieved in high yield (90%) when using Ti(III) generated in situ from **1.39** and Zn (Scheme 1.7).[154]
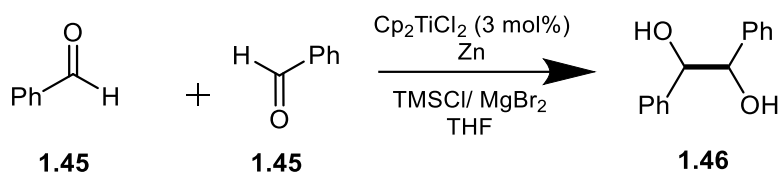
Scheme 1.7: Benzaldehyde pinacol coupling using Cp_2TiCl_2/ Zn

When a zirconium catalyst (Cp_2ZrCl_2) **1.47** in combination with Mg was used in place of the titanium / zinc system, the selectivity and reactivity were slightly lower.[155] In 1996, Endo and coworkers used samarium(II) iodide (SmI_2) (**1.48**) as catalyst and magnesium as terminal reductant which proved to be useful for the coupling of aromatic ketones, aliphatic and aromatic aldehydes (Scheme 1.8).[156]

reactant	R_1	R_2	product
1.45	Ph	H	**1.46**
1.47 a	Ph	Me	**1.47 b**
1.48 a	CH_2CH_2Ph	H	**1.48 b**
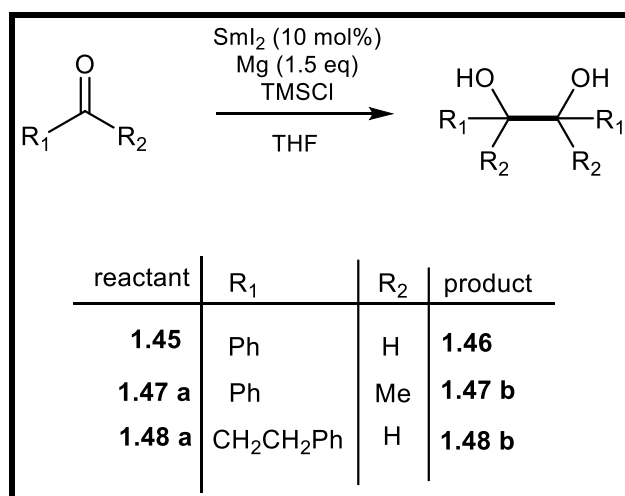
Scheme 1.8: Pinacol coupling using SmI_2

Boland and Svatoš used $CrCl_3$ (**1.49**) / Mn as catalyst for the pinacol coupling of aldehydes and ketones, and the results were excellent.[157] However, when TMSCl was substituted with a bulkier chlorotrialkylsilanes (tert-Butyl(chloro)diphenylsilane,TBDPSCl) this led to lower yield due to the reduction of the carbonyl compound to the corresponding alcohol as a major product.

Uchiyama and coworkers developed a new catalytic electron transfer system consisting of Mn(II), Co(II), and Fe(II) ate complexes, with magnesium as a reductant.[158] Among them, K[(^{t}BuO)$_3$Fe] (**1.50**) was found to be a very efficient catalyst for the aromatic aldehyde / ketone pinacol coupling reaction. Nickel(0)/Zn also showed high activity towards the coupling of aromatic ketones and aldehydes.[159]

The pinacol coupling reactions are highly affected by the reaction conditions. For example, the coupling of cyclohexanecarbaldehyde (**1.51**) in the presence of CpTiCl$_2$/ Zn in 1,2-dimethoxyethane (DME) led to the formation of the trimeric product **1.52**,[160] whereas, with Mn and in THF solvent the corresponding diol **1.53** was observed (Scheme 1.9).[152]

1.52   **1.51**   **1.53**
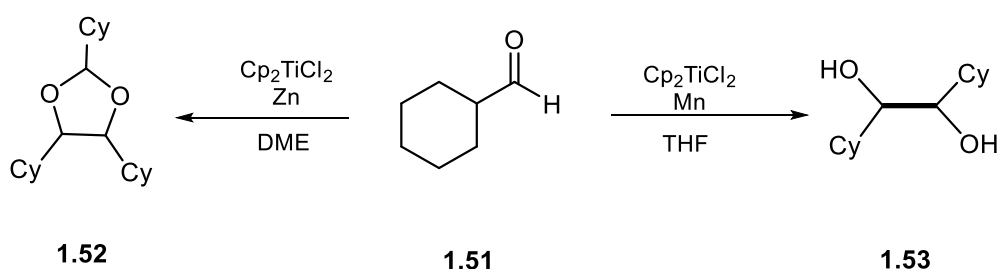
Scheme 1.9: different coupling products with different conditions

McMurry and Fleming used low valent titanium(III) chloride (**1.54**) as a catalyst for the McMurry coupling reaction (the coupling of two ketones or aldehydes to form an alkene) in combination with LiAlH$_4$ as terminal reductant (Scheme 1.10).[161] Later, Fürstner and Hupperts replaced the reductant LiAlH$_4$ with the inexpensive and easy to handle zinc powder, along with the addition of TMSCl, resulting in results comparable to those obtained earlier.[162,163]
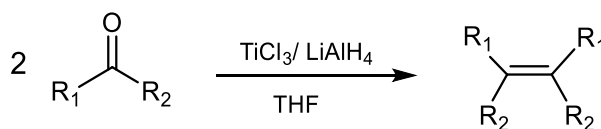
R$_1$,R$_2$= H, alkyl, or aryl

Scheme 1.10: Titanium(III) catalyzed McMurry coupling reaction

The reductive cross coupling of aldehydes, ketones or amines are considerably more difficult than pinacol homocoupling. They usually require either syringe pump addition techniques, or a large excess of one coupling partner to favour the reductive cross coupling

product. In 1989, Freudenberger et al. used [$V_2Cl_3(THF)_6$]$_2$[Zn_2Cl_6] (**1.55**), which was formed in situ from VCl_3 and Zn, and they achieved aldehyde intermolecular cross coupling reactions in good yields and high diastereoselectivities (Scheme 1.11).[164]
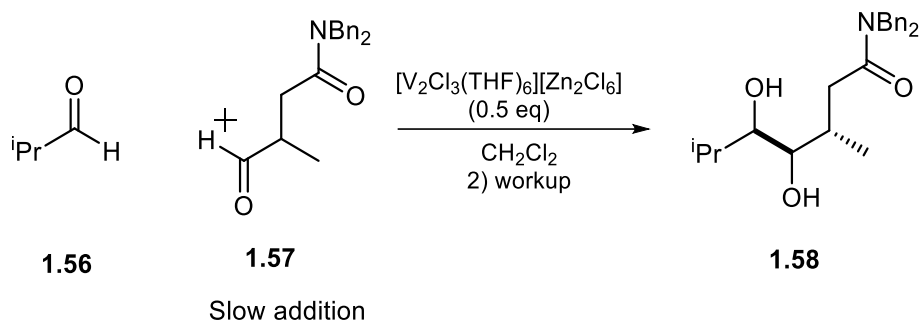
Scheme 1.11: Intermolecular cross coupling

The cross coupling of carbonyl derivatives with Michael acceptors has drawn more attention.[163] Depending on the reaction conditions and the catalyst, the reaction could proceed through reductive coupling (to form normal products) or reductive umpolung reactions (Scheme 1.12). However, even in the reductive umpolung reactions, the products also vary depending on the conditions and transition metal catalyst. For example, the cross coupling between aldehydes and *α,β*-unsaturated carbonyl compounds could lead to either *γ*-hydroxy carbonyl or the vicinal diol compound instead.
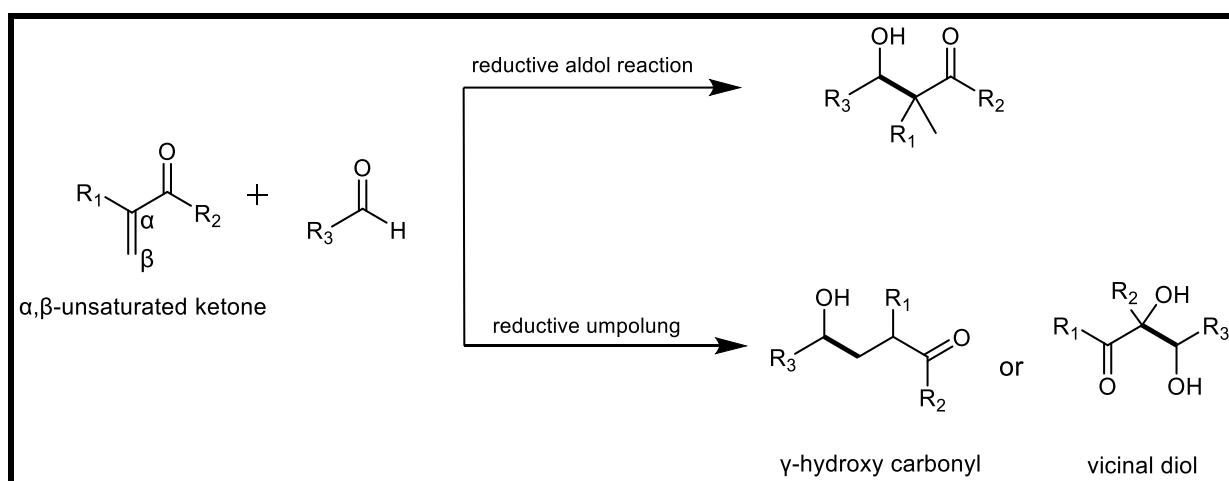
Scheme 1.12: Reductive coupling and reductive umpolung reactions of aldehydes with Michael acceptors

Takai and coworkers reported the use of overstoichiometric amounts of CrCl$_2$ (**1.59**) in the presence of triethylsilylchloride to cross couple nonanal (**1.60**) with a Michael acceptor which leads to the vicinal diol product in excellent yield (99%, Scheme 1.13).[165] Later, the γ-N-hydroxy product was achieved in good yield (76%) by Py, Vallée, and coworkers from the cross coupling of nitrones with α,β-unsaturated esters in the presence of two equivalents of SmI$_2$ (Scheme 1.14).[163]
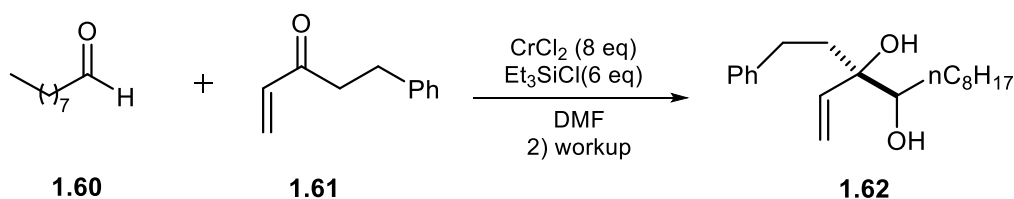
Scheme 1.13: Umpolung reductive to vicinal diol product
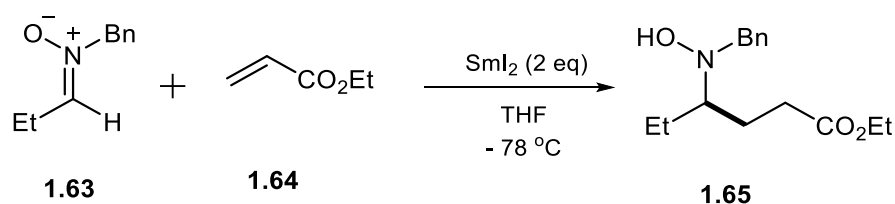
Scheme 1.14: Umpolung reductive to γ-N-hydroxy product

In 2011, Streuff reported the titanium-catalyzed cross coupling of enamides or enones with acrylamides and acrylonitrile, to synthesize unsymmetrical 1,6-bifuncotionalized alkyl compounds (Scheme 1.15).[137] The first attempt to react 2-cyclohexen-1-one (**1.66**) with an excess of an acrylonitrile (**1.37**) (fivefold) in the presence of titanocene dichloride (**1.39**) (10%) as catalyst and Zn dust as stoichiometric reductant in THF led to the formation of the cross coupled product in low yield (35%). However, repeating the reaction in the presence of trimethylsilyl chloride (TMSCl) gave complete conversion and increased the yield to 87% (within 4 hours) by forming the corresponding TMS-enol ether (**1.67**), which hydrolyzed easily to the desired product during workup. Under these conditions several enones with varied substitution were coupled in good yield. Though, increasing the steric bulk on the β-position led to 1,2-addition to the carbonyl function as a major reaction pathway and thus forming 1,4-difunctionalized products.
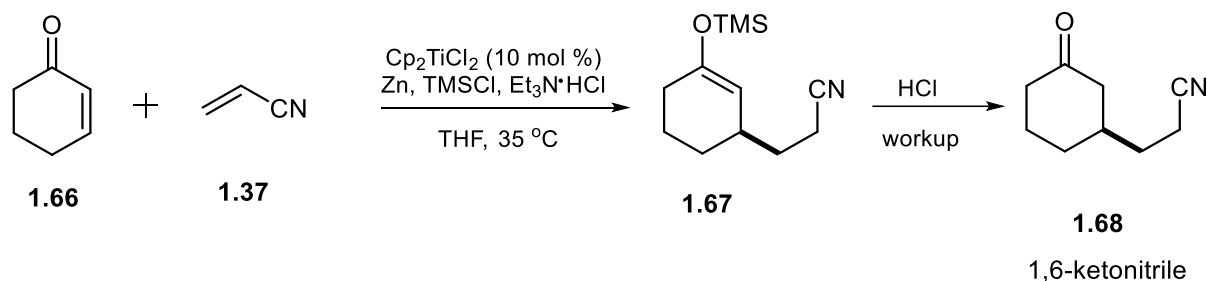
Scheme 1.15: Titanium catalyzed reductive umpolung of cyclohexen-1-one with acrylonitrile

The use of an excess of inexpensive acrylonitrile was found to be necessary to suppress the reduction and homo coupling products. Though, the substitution of TMSCl with another hydrochloride such as collidine hydrochloride and Zn with Mn was less successful.

Titanium complexes also found to be effective to catalyze the reductive cyclization of 1,5 and 1,6-ketonitrile. This reaction is of particular interest because the resulting product is an α-hydroxyketone (acyloin) which is found in more than 1500 known natural products. Streuff et. al. investigated this intramolecular reductive coupling using different titanium complexes (Figure 1.12).[166] They found that catalysts **1.69**-**1.71** are able to catalyze the cyclization of **1.75** to the desired α-hydroxyketone **1.76** in the presence of zinc powder as a reductant (Scheme 1.16), whereas no product was observed with Salen- and TADDOL- based complexes (**1.72**-**1.73**) under the same conditions. The best reactivity was observed with complex **1.69** with 88% yield and high enantioselectivity (91%). Several aromatic and aliphatic substituents were studied and six or five-membered hydroxyketones were formed in good yields and enantioselectivities.
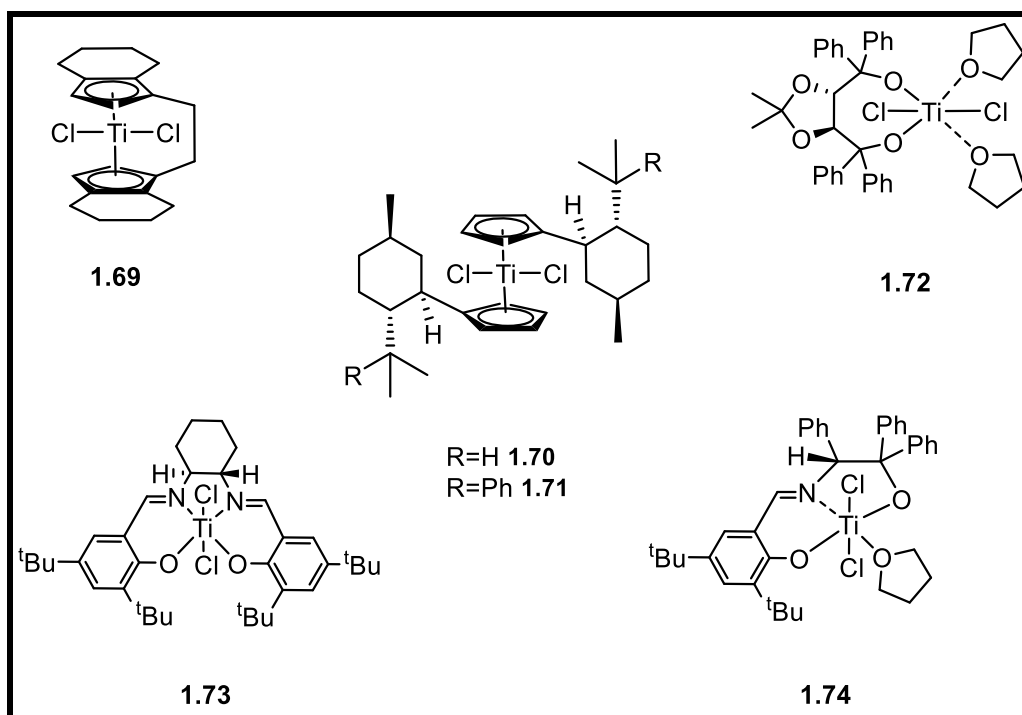
Figure 1.12: Ti complexes used by Streuff et. al. as catalyst for reductive cyclization of ketonitriles
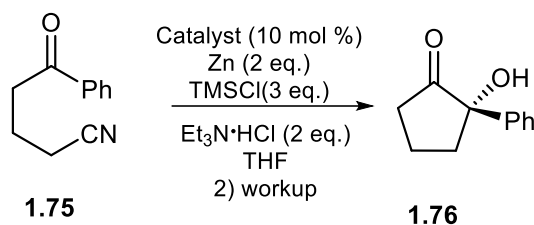
Scheme 1.16: Reductive cyclization of ketonitrile to α-hydroxyketone

1.5 Aims and Objectives:

In this work the main effort was focused on the development of Ti(III) and Ti(IV) Salen-type complexes. A variety of metal complexes have been reported to catalyse the copolymerization of various epoxides with different anhydrides. Among those salen, Salen-type and porphyrin of Cr, Co, Al, Fe and Zn have been widely explored. However, the examples of titanium catalysts that display catalytic performance toward ROCOP of

anhydrides and epoxides are very low. The motivation of this work is to explore the potential of Ti(III) and Ti(IV) Salen-type complexes in ROCOP of epoxides with a variety of anhydrides, which can provide biodegradable and biocompatible polyesters. The titanium Salen-type complexes are environmentally friendly catalysts and they produced polyesters that are non-toxic to the environment as there are concerns about the possible toxic metal residues in the polyester.[70] In addition, the same complexes were explored as catalysts for single-electron transfer cross-coupling reactions in order to explore new ligand environments for this useful transformation in organic synthesis.

This work deals with:

1- Synthesis of Salen-type ligands bearing a hemi labile pyridyl donor (Salpy ligands).
2- Synthesis and characterization of new titanium (IV) and titanium (III) complexes using Schiff base ligands.
3- Investigation of catalytic behaviour of the titanium complexes in the ring opening copolymerization of epoxides with cyclic anhydrides.
4- Use of Ti(III) complexes in single electron transfer (SET) reactions.

1.6 References:

1   S. J. Coles, M. B. Hursthouse, D. G. Kelly, A. J. Toner and N. M. Walker, *J. Chem. Soc., Dalton Trans.*, 1998, 3489–3494.

2   P. G. Cozzi, *Chem. Soc. Rev.*, 2004, **33**, 410–421.

3   L. H. Abdel-Rahman, A. M. Abu-Dief, M. O. Aboelez and A. A. Hassan Abdel-Mawgoud, *J. Photochem. Photobiol. A*, 2017, **170**, 271–285.

4   M. Wang, L.-F. Wang, Y.-Z. Li, Q.-X. Li, Z.-D. Xu and D.-M. Qu, *Transit. Met. Chem.*, 2001, **26**, 307–310.

5   L. H. Abdel-Rahman, M. S. S. Adam, A. M. Abu-Dief, H. Moustafa, M. T. Basha, A. S. Aboraia, B. S. Al-Farhan and H. E.-S. Ahmed, *Appl. Organomet. Chem.*, 2018, **32**, e4527.

6   N. N. Gülerman, S. Rollas, H. Erdeniz and M. Kiraz, *Fabad J. Pharm. Sci.*, 2001, **26**, 1–5.

7   D. P. Singh, K. Kumar and C. Sharma, *Eur. J. Med. Chem.*, 2010, **45**, 1230–1236.

8   L. Abdel-Rahman, A. Abu-Dief, S. Hamdan and A. Seleem, *Int. J. Nano. Chem.*, 2015, **1**, 65–77.

9   R. Nirmal, C. Prakash, K. Meenakshi and P. Shanmugapandiyan, *J. Young Pharm.*, 2010, **2**, 162–168.

10 T. S. Kamatchi, N. Chitrapriya, H. Lee, C. F. Fronczek, F. R. Fronczek and K. Natarajan, *Dalton Trans.*, 2012, **41**, 2066–2077.

11 A. M. Abu-Dief and I. M. A. Mohamed, *beni-Seuf univ. j. Basic appl. sci.*, 2015, **4**, 119–133.

12 M. N. Uddin, M. S. Amin, M. S. Rahman, S. Khandaker, W. Shumi, M. A. Rahman and S. M. Rahman, *Appl. Organomet. Chem.*, 2021, **35**, e6067.

13 Y. Gürsoy Tuncer, K. Gürpınar, N. Acar, H. Nazır, I. Svoboda, O. Atakol and E. K. İnal, *J. Mol. Struct.*, 2020, **1221**, 128789.

14 D. A. Atwood and M. J. Harvey, *Chem. Rev.*, 2001, **101**, 37–52.

15 H. Chen, P. S. White and M. R. Gagné, *Organomet.*, 1998, **17**, 5358–5366.

16 L. Zhou, P. Cai, Y. Feng, J. Cheng, H. Xiang, J. Liu, D. Wu and X. Zhou, *Anal. Chim. Acta*, 2012, **735**, 96–106.

17 L. Zhou, Y. Feng, J. Cheng, N. Sun, X. Zhou and H. Xiang, *RSC Adv.*, 2012, **2**, 10529–10536.

18 S. Samanta, B. Nath and J. B. Baruah, *Inorg. Chem. Commun.*, 2012, **22**, 98–100.

19 O. Fatibello-Filho, E. R. Dockal, L. H. Marcolino-Junior and M. F. S. Teixeira, *Analytical Letters*, 2007, **40**, 1825–1852.

20 M. Mohammadi and R. Yazdanparast, *Food Chem. Toxicol.*, 2009, **47**, 716–721.

21 D. Peri, S. Meker, C. M. Manna and E. Y. Tshuva, *Inorg. Chem.*, 2011, **50**, 1030–1038.

22 K. I. Ansari, J. D. Grant, S. Kasiri, G. Woldemariam, B. Shrestha and S. S. Mandal, *Journal of Inorganic Biochemistry*, 2009, **103**, 818–826.

23 G. Dell'Amico, F. Marchetti and C. Floriani, *J. Chem. Soc., Dalton Trans.*, 1982, 2197–2202.

24 Y.-S. Kim, X.-F. Guo and G.-J. Kim, *Chem. Commun.*, 2009, 4296–4298.

25 S. Ernst, E. Fuchs and X. Yang, *Micropor. Mesopor. Mater.*, 2000, **35–36**, 137–142.

26 C. S. Gill, K. Venkatasubbaiah and C. W. Jones, *Adv. Synth. Catal.*, 2009, **351**, 1344–1354.

27 C. Lv, M. Wu, S. Wang, C. Xia and W. Sun, *Tetrahedron: Asymmetry*, 2010, **21**, 1869–1873.

28 T. Katsuki, *Coord. Chem. Rev.*, 1995, **140**, 189–214.

29 T. Fukuda and T. Katsuki, *Tetrahedron*, 1997, **53**, 7201–7208.

30 N. S. Venkataramanan, G. Kuppuraj and S. Rajagopal, *Coord. Chem. Rev.*, 2005, **249**, 1249–1268.

31 E. N. Jacobsen, F. Kakiuchi, R. G. Konsler, J. F. Larrow and M. Tokunaga, *Tetrahedron Lett.*, 1997, **38**, 773–776.

32 K. Hamachi, R. Irie and T. Katsuki, *Tetrahedron Lett.*, 1996, **37**, 4979–4982.

33 S. E. Schaus, J. Brånalt and E. N. Jacobsen, *J. Org. Chem.*, 1998, **63**, 403–405.

34 J. Fonseca, J. Martinez, L. Cunha-Silva, A. L. Magalhães, M. T. Duarte and C. Freire, *Inorg. Chim. Acta*, 2010, **363**, 4096–4107.

35   S. C. Gad, in *Encyclopedia of Toxicology (Third Edition)*, ed. P. Wexler, Academic Press, Oxford, 2014, pp. 584–585.

36   M. Weller, T. Overton, J. Rourke and F. Armstrong, *Inorganic Chemistry*, Oxford University Press, 6th edn., 2014.

37   T. Jin and M. Berlin, in *Handbook on the Toxicology of Metals (Fourth Edition)*, eds. G. F. Nordberg, B. A. Fowler and M. Nordberg, Academic Press, San Diego, 2015, pp. 1287–1296.

38   B. Rossi, S. Prosperini, N. Pastori, A. Clerici and C. Punta, *Molecules*, 2012, **17**, 14700–14732.

39   M. Pasquali, F. Marchetti, A. Landi and C. Floriani, *J. Chem. Soc., Dalton Trans.*, 1978, 545–549.

40   R. S. P. Coutts and P. C. Wailes, in *Advances in Organometallic Chemistry*, Elsevier, 1971, vol. 9, pp. 135–193.

41   N. N. Greenwood and A. Earnshaw, Eds., in *Chemistry of the Elements (Second Edition)*, Butterworth-Heinemann, Oxford, 1997, pp. 954–975.

42   M. Guo, H. Sun, S. Bihari, J. A. Parkinson, R. O. Gould, S. Parsons and P. J. Sadler, *Inorg. Chem.*, 2000, **39**, 206–215.

43   S. M. Harben, P. D. Smith, R. L. Beddoes, D. Collison and C. D. Garner, *Angew. Chem. Int. Ed. Engl.*, 1997, **36**, 1897–1898.

44   M. Cini, T. D. Bradshaw and S. Woodward, *Chem. Soc. Rev.*, 2017, **46**, 1040–1051.

45   A. Tzubery, N. Melamed-Book and E. Y. Tshuva, *Dalton Trans.*, 2018, **47**, 3669–3673.

46   P. C. Bruijnincx and P. J. Sadler, *Curr. Opin. Chem. Biol.*, 2008, **12**, 197–206.

47   S. H. van Rijt and P. J. Sadler, *Drug Discov. Today*, 2009, **14**, 1089–1097.

48   E. Hadjoudis, M. Vittorakis and I. Moustakali-Mavridis, *Tetrahedron*, 1987, **43**, 1345–1360.

49   Y. Tshuva and M. Miller, in *Metallo-Drugs: Development and Action of Anticancer Agents: Development and Action of Anticancer and Antitumor Agents*, Walter de Gruyter GmbH, Berlin/Boston, GERMANY, 2018, pp. 219–250.

50   G. Kelter, N. J. Sweeney, K. Strohfeldt, H.-H. Fiebig and M. Tacke, *Anti-Cancer Drugs*, 2005, **16**, 1091–1098.

51   E. Meléndez, *Crit. Rev. Oncol.*, 2002, **42**, 309–315.

52   K. Strohfeldt and M. Tacke, *Chem. Soc. Rev.*, 2008, **37**, 1174–1187.

53   F. Caruso, L. Massa, A. Gindulyte, C. Pettinari, F. Marchetti, R. Pettinari, M. Ricciutelli, J. Costamagna, J. C. Canales, J. Tanski and M. Rossi, *Eur. J. Inorg. Chem.*, 2003, **2003**, 3221–3232.

54   P. Manohari Abeysinghe and M. M. Harding, *Dalton Trans.*, 2007, **0**, 3474–3482.

55   A. Tzubery and E. Y. Tshuva, *Inorg. Chem.*, 2012, **51**, 1796–1804.

56   D. Peri, S. Meker, M. Shavit and E. Y. Tshuva, *Chem. Eur. J.*, 2009, **15**, 2403–2415.

57 M. Shavit, D. Peri, C. M. Manna, J. S. Alexander and E. Y. Tshuva, *J. Am. Chem. Soc.*, 2007, **129**, 12098–12099.

58 E. Y. Tshuva and D. Peri, *Coord. Chem. Rev.*, 2009, **253**, 2098–2115.

59 A. Tzubery and E. Y. Tshuva, *Inorg. Chem.*, 2011, **50**, 7946–7948.

60 K. V. Zaitsev, M. V. Bermeshev, A. A. Samsonov, J. F. Oprunenko, A. V. Churakov, J. A. L. Howard, S. S. Karlov and G. S. Zaitseva, *New J. Chem.*, 2008, **32**, 1415–1431.

61 J. Streuff, M. Feurer, G. Frey, A. Steffani, S. Kacprzak, J. Weweler, L. H. Leijendekker, D. Kratzert and D. A. Plattner, *J. Am. Chem. Soc.*, 2015, **137**, 14396–14405.

62 E. A. Kuchuk, B. N. Mankaev, K. V. Zaitsev, Y. F. Oprunenko, A. V. Churakov, G. S. Zaitseva and S. S. Karlov, *Inorg. Chem. Commun.*, 2016, **67**, 1–5.

63 M. Niederberger and G. Garnweitner, *Chem. Eur. J.*, 2006, **12**, 7282–7302.

64 T. A. Immel, M. Grützke, A.-K. Späte, U. Groth, P. Öhlschläger and T. Huhn, *Chem. Commun.*, 2012, **48**, 5790–5792.

65 L. Yangang and J. Guoxin, *Chin.Sci.Bull.*, 2004, **49**, 1236–1240.

66 H. Hamaki, N. Takeda, M. Nabika and N. Tokitoh, *Macromolecules*, 2012, **45**, 1758–1769.

67 S. Segal, I. Goldberg and M. Kol, *Organomet.*, 2005, **24**, 200–202.

68 S. Gendler, A. L. Zelikoff, J. Kopilov, I. Goldberg and M. Kol, *J. Am. Chem. Soc.*, 2008, **130**, 2144–2145.

69 C. C. Quadri and E. L. Roux, *Dalton Trans.*, 2014, **43**, 4242–4246.

70 Y. Wang, Y. Qin, X. Wang and F. Wang, *ACS Catal.*, 2015, **5**, 393–396.

71 Y. Wang, Y. Qin, X. Wang and F. Wang, *Catal. Sci. Technol.*, 2014, **4**, 3964–3972.

72 I. E. Nifant'ev, L. Yu. Ustynyuk and D. V. Besedin, *Organomet.*, 2003, **22**, 2619–2629.

73 I. Kim, Y. S. Ha, D. F. Zhang, C.-S. Ha and U. Lee, *Macromol. Rapid Commun.*, 2004, **25**, 1319–1323.

74 S. Gendler, S. Segal, I. Goldberg, Z. Goldschmidt and M. Kol, *Inorg. Chem.*, 2006, **45**, 4783–4790.

75 A. J. Chmura, M. G. Davidson, M. D. Jones, M. D. Lunn, M. F. Mahon, A. F. Johnson, P. Khunkamchoo, S. L. Roberts and S. S. F. Wong, *Macromolecules*, 2006, **39**, 7250–7257.

76 X. Li, B. Yang, H. Zheng, P. Wu and G. Zeng, *PLOS ONE*, 2018, **13**, e0201054.

77 M. Hu, W. Zhang, W. Ma, F. Han and W. Song, *Polymer*, 2018, **153**, 445–452.

78 M. North, C. Orizu, V. I. Tararov, N. S. Ikonnikov, Y. N. Belokon, D. E. Hibbs, M. B. Hursthouse and K. M. A. Malik, *Chem. Commun.*, 1998, 387–388.

79 Y. Belokon, N. Ikonnikov, M. Moscalenko, M. North, S. Orlova, V. Tararov and L. Yashkina, *Tetrahedron: Asymmetry*, 1996, **7**, 851–855.

80 Y. Belokon', M. Flego, N. Ikonnikov, M. Moscalenko, M. North, C. Orizu, V. Tararov and M. Tasinazzo, *J. Chem. Soc., Perkin Trans.*, 1997, **1**, 1293–1296.

81 V. I. Tararov, C. Orizu, N. S. Ikonnikov, V. S. Larichev, M. A. Moscalenko, L. V. Yashkina, M. North and Yu. N. Belokon, *Russ. Chem. Bull.*, 1999, **48**, 1128–1130.

82 G.-J. Kim and J.-H. Shin, *Catal. Lett.*, 1999, **63**, 83–90.

83 A. Chatterjee, T. H. Bennur and N. N. Joshi, *J. Org. Chem.*, 2003, **68**, 5668–5671.

84 Z. Hošťálek, O. Trhlíková, Z. Walterová, T. Martinez, F. Peruch, H. Cramail and J. Merna, *Eur. Polym. J.*, 2017, **88**, 433–447.

85 W. Amass, A. Amass and B. Tighe, *Polymer International*, 1998, **47**, 89–144.

86 R. Geyer, J. R. Jambeck and K. L. Law, *Sci. Adv.*, 2017, **3**, e1700782.

87 C. K. Williams, *Chem. Soc. Rev.*, 2007, **36**, 1573–1580.

88 M. A. Hillmyer and W. B. Tolman, *Acc. Chem. Res.*, 2014, **47**, 2390–2396.

89 A. J. Ragauskas, C. K. Williams, B. H. Davison, G. Britovsek, J. Cairney, C. A. Eckert, W. J. Frederick, J. P. Hallett, D. J. Leak, C. L. Liotta, J. R. Mielenz, R. Murphy, R. Templer and T. Tschaplinski, *Science*, 2006, **311**, 484–489.

90 R. A. Gross and B. Kalra, *Science*, 2002, **297**, 803–807.

91 S. Paul, Y. Zhu, C. Romain, R. Brooks, P. K. Saini and C. K. Williams, *Chem. Commun.*, 2015, **51**, 6459–6479.

92 J. M. Longo, M. J. Sanford and G. W. Coates, *Chem. Rev.*, 2016, **116**, 15167–15197.

93 M. E. Fieser, M. J. Sanford, L. A. Mitchell, C. R. Dunbar, M. Mandal, N. J. Van Zee, D. M. Urness, C. J. Cramer, G. W. Coates and W. B. Tolman, *J. Am. Chem. Soc.*, 2017, **139**, 15222–15231.

94 A. Ravve, *Principles of Polymer Chemistry*, Springer New York, New York, NY, third., 2012.

95 J. Lustoň and F. Vašš, in *Anionic Polymerization*, Springer, Berlin, Heidelberg, 1984, pp. 91–133.

96 A. M. DiCiccio and G. W. Coates, *J. Am. Chem. Soc.*, 2011, **133**, 10724–10727.

97 P. Lecomte and C. Jerome, in *Synthetic Biodegradable Polymers*, eds. B. Rieger, A. Künkel, G. W. Coates, R. Reichardt, E. Dinjus and T. A. Zevaco, Springer-Verlag, Berlin Heidelberg, 2012, pp. 173–217.

98 K. Bester, A. Bukowska, B. Myśliwiec, K. Hus, D. Tomczyk, P. Urbaniak and W. Bukowski, *Polym. Chem.*, 2018, **9**, 2147–2156.

99 H.-Y. Ji, B. Wang, L. Pan and Y.-S. Li, *Green Chem.*, 2018, **20**, 641–648.

100 X. Yu, J. Jia, S. Xu, K. U. Lao, M. J. Sanford, R. K. Ramakrishnan, S. I. Nazarenko, T. R. Hoye, G. W. Coates and R. A. DiStasio, *Nat. Commun.*, 2018, **9**, 1–9.

101 W. Kuran and A. Niestochowski, *Polymer Bulletin*, 1980, **2**, 411–416.

102 M. Proverbio, N. Galotto Galotto, S. Losio, I. Tritto and L. Boggioni, *Polymers*, 2019, **11**, 1222.

103 R. C. Jeske, A. M. DiCiccio and G. W. Coates, *J. Am. Chem. Soc.*, 2007, **129**, 11330–11331.

104 A. P. Gupta and V. Kumar, *Eur. Polym. J.*, 2007, **43**, 4053–4074.

105 Y. Ikada and H. Tsuji, *Macromol. Rapid Commun.*, 2000, **21**, 117–132.

106 E. Hosseini Nejad, C. G. W. van Melis, T. J. Vermeer, C. E. Koning and R. Duchateau, *Macromolecules*, 2012, **45**, 1770–1776.

107 E. H. Nejad, A. Paoniasari, C. E. Koning and R. Duchateau, *Polym. Chem.*, 2012, **3**, 1308–1313.

108 D. J. Darensbourg, R. R. Poland and C. Escobedo, *Macromolecules*, 2012, **45**, 2242–2248.

109 N. J. Van Zee and G. W. Coates, *Angew. Chem. Int. Ed.*, 2015, **54**, 2665–2668.

110 S. Huijser, E. HosseiniNejad, R. Sablong, C. de Jong, C. E. Koning and R. Duchateau, *Macromolecules*, 2011, **44**, 1132–1139.

111 J. M. Longo, A. M. DiCiccio and G. W. Coates, *J. Am. Chem. Soc.*, 2014, **136**, 15897–15900.

112 R. Mundil, Z. Hošťálek, I. Šeděnková and J. Merna, *Macromol. Res.*, 2015, **23**, 161–166.

113 G. Si, L. Zhang, B. Han, Z. Duan, B. Li, J. Dong, X. Li and B. Liu, *Polym. Chem.*, 2015, **6**, 6372–6377.

114 J. Liu, Y.-Y. Bao, Y. Liu, W.-M. Ren and X.-B. Lu, *Polym. Chem.*, 2013, **4**, 1439–1444.

115 A. M. DiCiccio, J. M. Longo, G. G. Rodríguez-Calero and G. W. Coates, *J. Am. Chem. Soc.*, 2016, **138**, 7107–7113.

116 E. H. Nejad, A. Paoniasari, C. G. W. van Melis, C. E. Koning and R. Duchateau, *Macromolecules*, 2013, **46**, 631–637.

117 R. C. Jeske, J. M. Rowley and G. W. Coates, *Angew. Chem. Int. Ed.*, 2008, **47**, 6041–6044.

118 A. M. DiCiccio and G. W. Coates, *J. Am. Chem. Soc.*, 2011, **133**, 10724–10727.

119 R. F. Fischer, *Ind. Eng. Chem.*, 1960, **52**, 321–323.

120 S. Inoue, K. Kitamura and T. Tsuruta, *Macromol. Chem. Phys.*, 1969, **126**, 250–265.

121 H. L. Hsieh, *J. Macromol. Sci. A*, 1973, **7**, 1525–1535.

122 T. Aida and S. Inoue, *J. Am. Chem. Soc.*, 1985, **107**, 1358–1364.

123 A. M. DiCiccio and G. W. Coates, *J. Am. Chem. Soc.*, 2011, **133**, 10724–10727.

124 P. K. Saini, C. Romain, Y. Zhu and C. K. Williams, *Polym. Chem.*, 2014, **5**, 6068–6075.

125 C. Robert, T. Ohkawara and K. Nozaki, *Chem. Eur. J.*, 2014, **20**, 4789–4795.

126 J. W. Nicholson, *The Chemistry of Polymers*, Royal Society of Chemistry, 2nd edn., 1997.

127 A. B. Smith and C. M. Adams, *Acc. Chem. Res.*, 2004, **37**, 365–377.

128 X. Bugaut and F. Glorius, *Chem. Soc. Rev.*, 2012, **41**, 3511–3522.

129 E. J. Corey and D. Seebach, *Angew. Chem. Int. Ed.*, 1965, **4**, 1077–1078.

130 E. J. Corey and D. Seebach, *Angew. Chem. Int. Ed.*, 1965, **4**, 1075–1077.

131 D. Seebach and K. M, *Chem. Ind.*, 1974, **7**, 687–692.

132 D. Seebach, *Angew. Chem. Int. Ed. Engl.*, 1979, **18**, 239–258.

133 J. J. Bloomfield, D. C. Owsley and J. M. Nelke, *Org. React.*, 1976, 259–404.

134 V. Kalyanaraman and M. V. George, *Journal of Organometallic Chemistry*, 1973, **47**, 225–280.

135 A. J. Fry, *Synthetic Organic Electrochemistry*, John Wiley & Sons, 2nd edn., 1989.

136 M. M. Baizer, *Tetrahedron*, 1984, **40**, 935–969.

137 J. Streuff, *Chem. Eur. J.*, 2011, **17**, 5507–5510.

138 A. J. Bard, G. Inzelt and F. Scholz, Eds., *Electrochemical Dictionary*, Springer Berlin Heidelberg, Berlin, Heidelberg, 2nd edn., 2012.

139 J. L. Methot and W. R. Roush, *Advanced Synthesis & Catalysis*, 2004, **346**, 1035–1050.

140 A. Marinetti and A. Voituriez, *Synlett*, 2010, **2010**, 174–194.

141 J. Douglas, G. Churchill and A. D. Smith, *Synthesis*, 2012, **44**, 2295–2309.

142 A. Grossmann and D. Enders, *Angew. Chem. Int. Ed.*, 2012, **51**, 314–325.

143 A. T. Biju, M. Padmanaban, N. E. Wurz and F. Glorius, *Angewandte Chemie International Edition*, 2011, **50**, 8412–8415.

144 T. Jerphagnon, M. G. Pizzuti, A. J. Minnaard and B. L. Feringa, *Chem. Soc. Rev.*, 2009, **38**, 1039–1075.

145 A. Rudolph and M. Lautens, *Angew. Chem. Int. Ed.*, 2009, **48**, 2656–2670.

146 W. Li, N. Chen and J. Montgomery, *Angew. Chem. Int. Ed.*, 2010, **49**, 8712–8716.

147 A. Gansäuer, D. Worgull, K. Knebel, I. Huth and G. Schnakenburg, *Angew. Chem. Int. Ed.*, 2009, **48**, 8882–8885.

148 A. Gansäuer, C.-A. Fan, F. Keller and P. Karbaum, *Chem. Eur. J.*, 2007, **13**, 8084–8090.

149 A. D. Kosal and B. L. Ashfeld, *Org. Lett.*, 2010, **12**, 44–47.

150 R. E. Estévez, J. L. Oller-López, R. Robles, C. R. Melgarejo, A. Gansäuer, J. M. Cuerva and J. E. Oltra, *Org. Lett.*, 2006, **8**, 5433–5436.

151 A. Gansäuer, *Chem. Commun.*, 1997, 457–458.

152 M. S. Dunlap and K. M. Nicholas, *Synth. Commun.*, 1999, **29**, 1097–1106.

153 Y. Zhang and T. Liu, *Synth. Commun.*, 1988, **18**, 2173–2178.

154 A. Gansäuer, M. Moschioni and D. Bauer, *Eur. J. Org. Chem.*, 1998, **1998**, 1923–1927.

155 M. Lakshmi Kantam, K. Aziz and P. R. Likhar, *Synthetic Communications*, 2006, **36**, 1437–1445.

156 R. Nomura, T. Matsuno and T. Endo, *J. Am. Chem. Soc.*, 1996, **118**, 11666–11667.

157 A. Svatoš and W. Boland, *Synlett*, 1998, **1998**, 549–551.

158 M. Uchiyama, Y. Matsumoto, S. Nakamura, T. Ohwada, N. Kobayashi, N. Yamashita, A. Matsumiya and T. Sakamoto, *J. Am. Chem. Soc.*, 2004, **126**, 8755–8759.

159 S. Ogoshi, H. Kamada and H. Kurosawa, *Tetrahedron*, 2006, **62**, 7583–7588.

160 T. Hirao, B. Hatano, M. Asahara, Y. Muguruma and A. Ogawa, *Tetrahedron Lett.*, 1998, **39**, 5247–5248.

161 J. E. McMurry and M. P. Fleming, *J. Am. Chem. Soc.*, 1974, **96**, 4708–4709.

162 A. Fuerstner and A. Hupperts, *J. Am. Chem. Soc.*, 1995, **117**, 4468–4475.

163 J. Streuff, *Synthesis*, 2013, **45**, 281–307.

164 J. H. Freudenberger, A. W. Konradi and S. F. Pedersen, *J. Am. Chem. Soc.*, 1989, **111**, 8014–8016.

165 K. Takai, R. Morita and C. Toratsu, *Angew. Chem. Int. Ed.*, 2001, **113**, 1150–1153.

166 J. Streuff, M. Feurer, P. Bichovski, G. Frey and U. Gellrich, *Angew. Chem. Int. Ed.*, 2012, **51**, 8661–8664.

Chapter 2

Synthesis and Characterization of Salen-type Ligands, and their Complexes with Titanium (III) and Titanium (IV)

2.1 Ligand synthesis:

The coupling of primary diamines with two equivalents of salicylaldehyde derivative leads to the formation of Schiff base ligands, which contain two imine functional groups (C=N). Salen ligands are one of the most studied chelating Schiff base ligands (Scheme 2.1). The word 'salen' stands for salicylaldehyde (sal) and ethylenediamine (en). Although the expression salen was used only to represent the tetradentate Schiff bases obtained from ethylenediamine, the more general expression Salen-type is used in the literature to represent [O,N,N,O] tetradentate bis(iminophenol) Schiff base ligands.[1] These ligands can coordinate to a metal via the imine nitrogens and the phenol oxygens, which are invariably deprotonated, and thus offer a (usually) planar N_2O_2 core, leaving two axial sites available for co-ligands. The N_2O_2 donor sites offers metal ions to adopt different geometries such as tetrahedral, square planar, square pyramidal or octahedral.
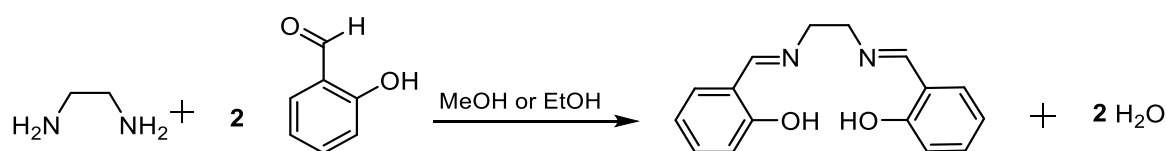
Scheme 2.17: Synthesis of salen ligand

In this thesis, two Salen-type ligands (Salpy and Salpn) have been used in the synthesis of titanium(III) and (IV) complexes. N,N′-bis(salicylidene)propylendiimine ligand (Salpn) has been known since 1946 and can be prepared by the condensation of 1 equivalent of 1,3-diaminopropane with 2 equivalents of salicylaldehyde or its derivatives (Scheme 2.2).[2]
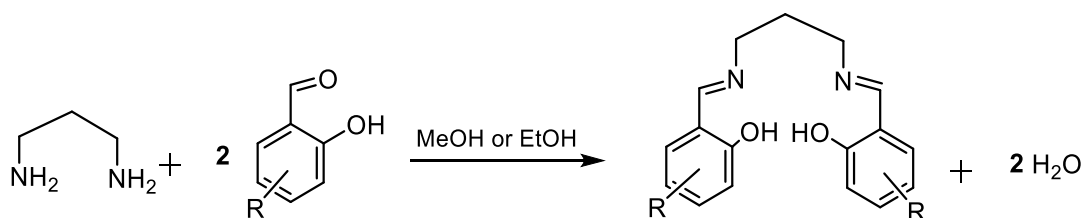
Scheme 2.18: synthesis of salpn ligands

36

Three ligands of this type have been prepared (Figure 2.1): H_2Salpn, $^tBu,^tBu-H_2Salpn$ and $Me-H_2Salpn$ by the condensation of 1,3-diaminopropane with salicylaldehyde, 3,5-di-tert-butylsalicylaldehyde and 3-methylsalicylaldehyde, respectively.
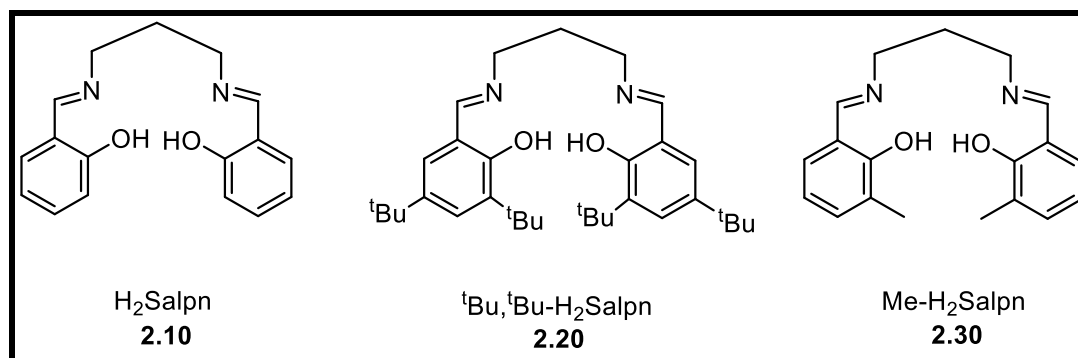
Figure 2.13: Salpn ligands used in this study

All the ligands were prepared in a similar manner following a standard method. Typically, a solution of diamine in methanol was added dropwise to a stirred methanolic solution of the appropriate aldehyde (2 equivalents). The mixture then heated at 50°C for 3-4 hours. Precipitate was formed instantly in most cases, however, in some cases the precipitate was formed after cooling. The precipitate was filtered, washed with cold methanol, and dried under reduced pressure. This reaction is straightforward and led to the formation of the ligands in good yields. The structures and the properties of the Salen-type ligands can be manipulated by changing the substituents on the aromatic rings or the diamine backbone.

The Salpy ligand contains an additional central pyridyl donor, and it therefore contains five donor groups (N_3O_2). The ligand has been previously prepared in the Ward research group, and was first reported by Houser *et al.*[3] The Salpy and its derivatives (denoted R,R'-H_2Salpy, or $H_2Naphpy$ for the naphthyl derivative) were easily prepared by the Schiff base condensation of 2-methyl-2-(pyridine-2-yl)propane-1,3-diamine (**2.40**) (ppda) with salicylaldehyde derivatives or 2-hydroxynaphthaldehyde respectively (Scheme 2.3).
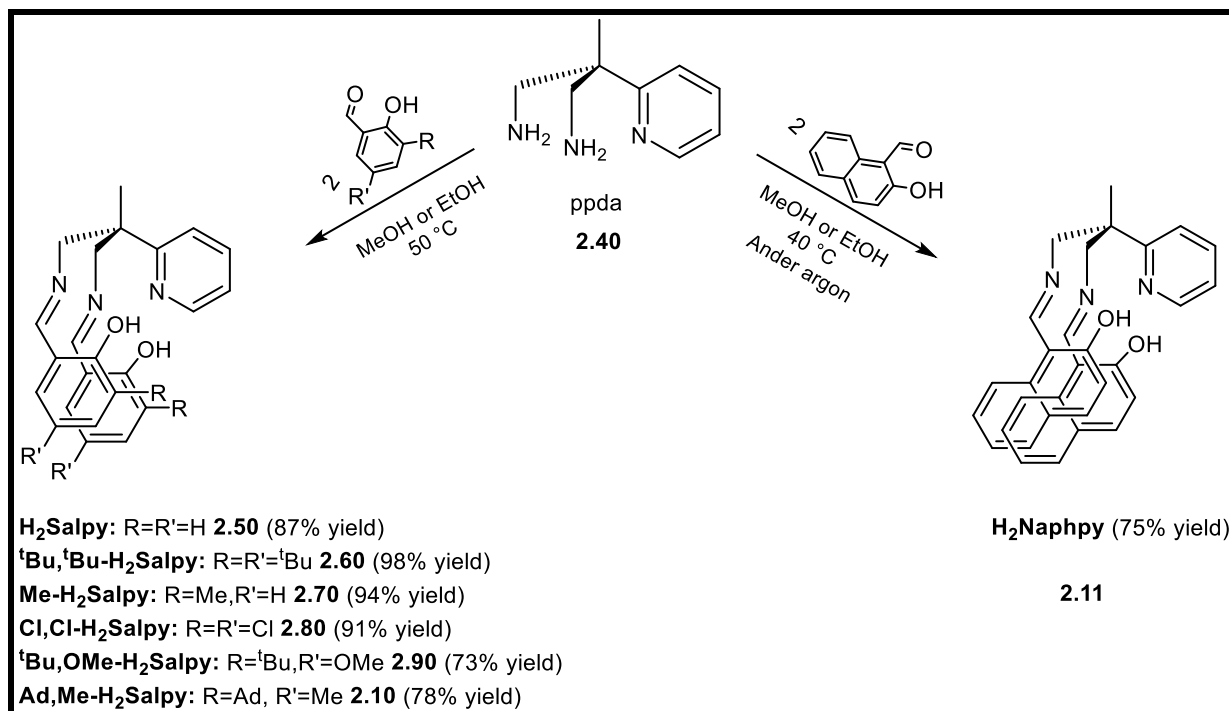
Scheme 2.19: Synthesis of R,R'-H₂Salpy and H₂Naphpy ligands

The precursor 2-Methyl-2-(pyridine-2-yl)propane-1,3-diamine (**2.40**) was synthesized using a modified procedure used by Gade et al.[4] The four steps used in the preparation of ppda (**2.40**) are illustrated in scheme 2.4. Firstly, 2-ethylpyridine was reacted with aqueous formaldehyde (37%) in an autoclave at 150 °C and 5-10 bar for about 40 h to yield a brown mixture of mono- **2.12** and bis-alcohol **2.13** products. Water was removed by atmospheric pressure distillation and then vacuum distillation was used to separate bis-alcohol **2.13** from mono-alcohol **2.12**. The orange viscous oily bis-alcohol **2.13** was obtained in low yield (~20%), but this was increased by 2.5 times by substituting the ethylpyridine reactant for the mono-alcohol **2.12** in subsequent reactions with formaldehyde. Secondly, the bis-alcohol **2.13** was tosylated by adding *p*-toluenesulfonyl chloride gradually at 0 °C in pyridine. The third step involved transformation of the tosyl groups into azide by reaction with sodium azide in DMSO, and finally, the colorless viscous oil (ppda) **2.40** was attained after the treatment of the bis(azide) **2.15** with triphenylphosphine followed by aqueous ammonia.
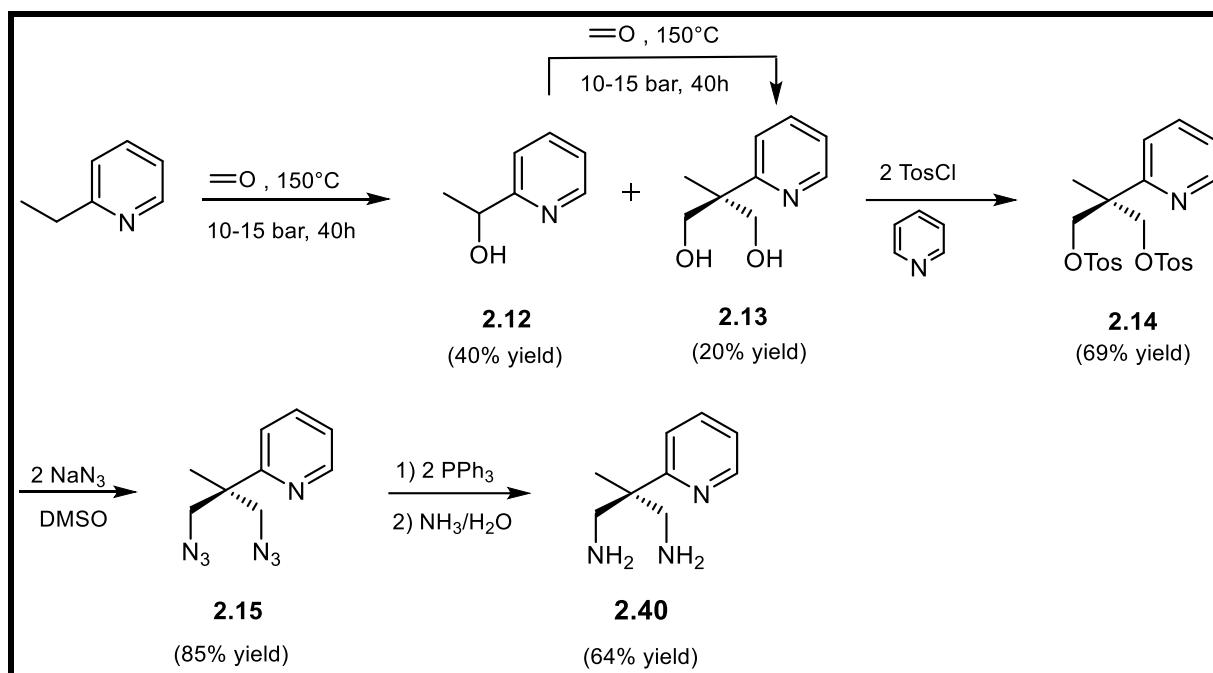
Scheme 2.20: Synthesis of 2-methyl-2-pyridin-2-yl-propane-1,3-diamine (ppda)

H_2Salpy, ^{t}Bu,^{t}Bu-H_2Salpy, Me-H_2Salpy, Cl,Cl-H_2Salpy and H_2Naphpy are all prepared from commercially available precursors whereas the precursors of Ad,Me-H_2Salpy and ^{t}Bu,OMe-H_2Salpy have been prepared by a literature methods. Salicylaldehyde bearing variable substituents are acquired by the introduction of a formyl group into the phenol derivatives in a simple and well-known reaction. The precursor Ad,Me- salicylaldehyde (**2.16**) was prepared following the Sattler et al method.[5] A colorless solution of *p*-cresol and 1-adamantanol in DCM was treated with concentrated H_2SO_4 at room temperature. Followed by the formylation of the resulting 2-adamantyl-4-methylphenol (**2.17**) using hexamethylenetetramine in glacial acetic acid at 110 °C, as shown in Scheme 2.5.
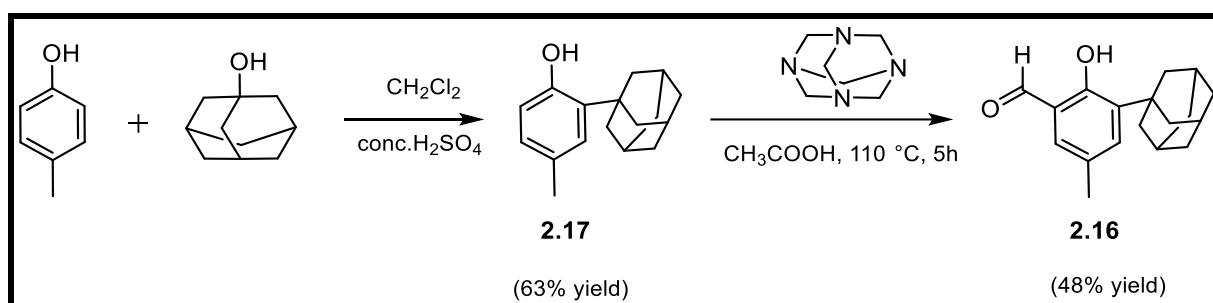
Scheme 2.21: Synthesis of Ad,Me-salicylaldehyde

According to a known procedure, the Duff reaction (hexamine aromatic formylation) was used to synthesise the precursor of (^{t}Bu,OMe-H$_2$Salpy).[6] In this reaction 3-tert-butyl-4-hydroxyanisole and an excess of hexamethylenetetramine were heated in glacial acetic acid at 110 °C for 2 hours, then treated with aqueous H$_2$SO$_4$ (33%) (Scheme 2.6).

2.18

(51% yield)
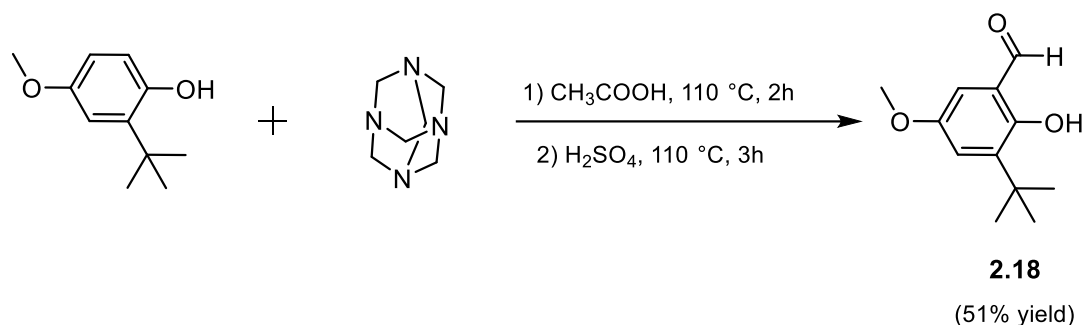
Scheme 2.22: ^{t}Bu,OMe-salicyaldehyde synthesis

All of the Salpy and Salpn ligands were synthesised in an open round bottomed flask, however, the preparation of H$_2$Naphpy (Scheme 2.3) required specific conditions as found by Bahili.[7] He found that to obtain the ligand in a clean condition, the commercially available aldehyde precursor (2-hydroxy-1-naphthaldehyde) needs to be recrystallized prior to use. Then, the condensation between the recrystallized aldehyde and ppda was carried out at 40°C under argon for 5 hours. Relaxing either of these two processes leads to the ligand being formed in an impure state that is difficult to purify.

All the ligands discussed above contain a rigid N=C double bond. In order to study the effect of this bond on the coordination chemistry and subsequent reactivity with this class of ligands, a ligand containing the more flexible single bond C-N was prepared. C=N bonds can be easily reduced to afford a secondary amine, which can be subsequently functionalized. Sodium borohydride was found to be efficient for this reduction and the reaction proceeded in methanol at room temperature. H$_2$Salpy-Me (**2.20**) was thereby prepared from the H$_2$Salpy (**2.5**) ligand in two steps (Scheme 2.7):
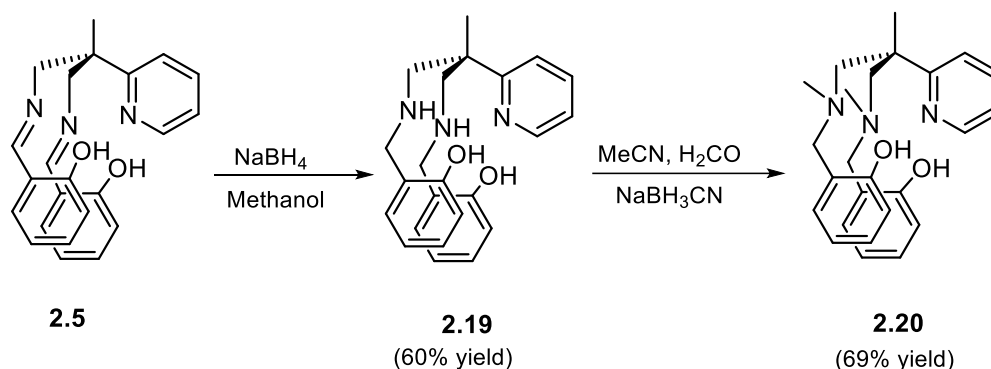
Scheme 2.23: H_2Salpy-Me synthesis

The first step was the reduction of H_2Salpy (**2.5**) according to a modified literature procedure using sodium borohydride.[3] H_2Salpy-H (**2.19**) was obtained as a pale pink sticky product after workup. H_2Salpy-H (**2.19**) was subsequently methylated using the procedure reported by Hultzsch et al.[8] in which **2.19** was reacted with formaldehyde and sodium cyanoborohydride. After workup, H_2Salpy-Me (**2.20**) was obtained as a white powder.

The successful preparation of H_2Salpy-Me (**2.20**) was verified by ^{1}H NMR spectroscopy. A comparison of the spectra of **2.20** and the Salpy ligand (**2.5**) precursor (Figure 2.2) shows the disappearance of the N=CH singlet at 8.31 ppm and the appearance of new N-CH$_2$ signals at 3.65 and 3.56 ppm, as well as the new two Me groups at 1.95 ppm in addition to the upfield shift of the OH chemical shift, which will be discussed later.
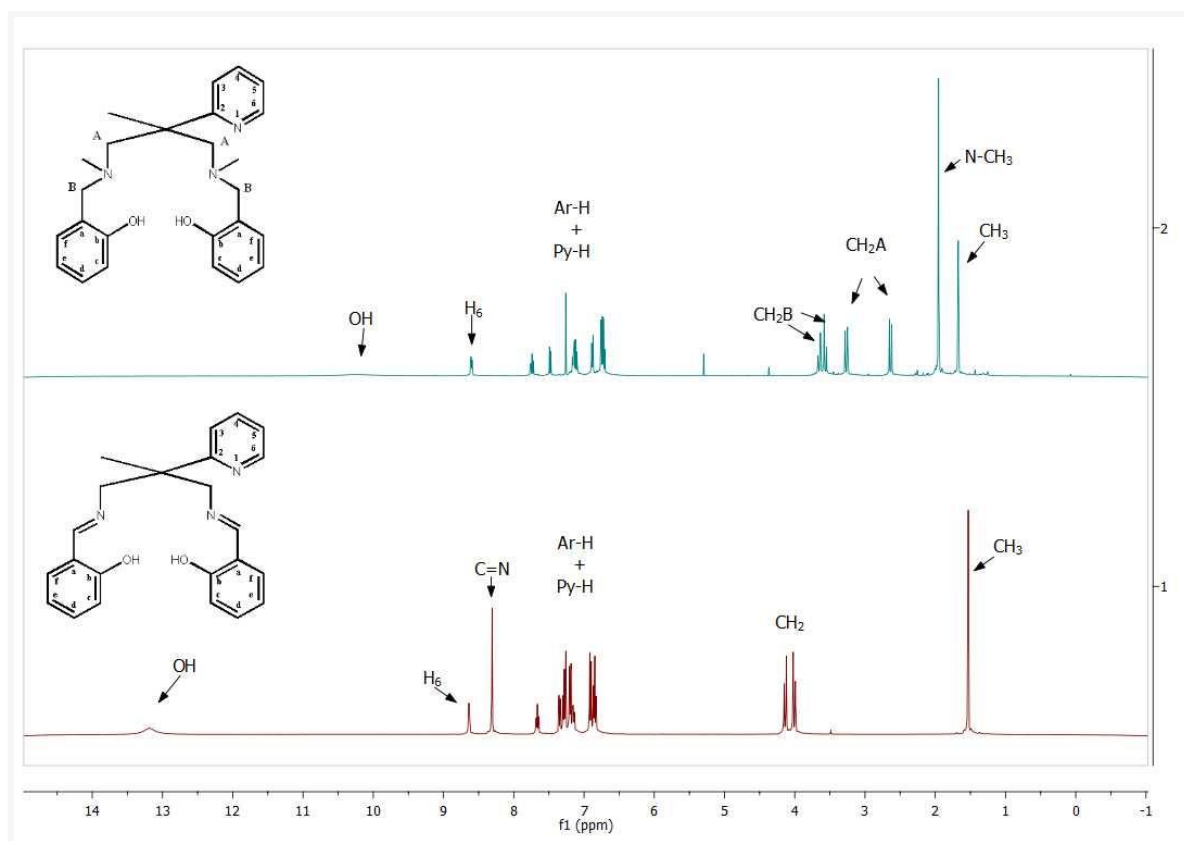
Figure 2.14: ^{1}H NMR spectra (400 MHz, CDCl$_3$, 293 K) of H$_2$Salpy and H$_2$Salpy-Me

This ligand shares a common backbone with H$_2$Salpy ligand; they all present an N$_3$O$_2$ donor set, and both contain two ionizable phenol protons which make them bivalent anionic ligands when deprotonated.

In summary, three different types of ligands have been prepared:

1- Salpy ligands, which contain a pyridyl ring in the backbone making the ligand N$_3$O$_2$ coordinating. The pyridyl in such ligands has been shown to be hemi labile in complexes which could play an important role in catalysis.

2- Me-Salpy ligand, where the rigid imine N=C groups have been reduced to the more flexible amine moiety.

3- Salpn ligands which replace the pyridyl and methyl groups in Salpy ligands with hydrogens, to provide ligands with similar bite angles and steric imposition to Salpy, but without the pyridyl donor so that the effect of the pyridyl can be probed in the structure and reactivity of their complexes.

All of these ligands have been characterized using ^{1}H NMR, ^{13}C{^{1}H} NMR, IR and UV spectroscopies and by high resolution mass spectrometry.

42

2.2 Synthesis of titanium complexes:

2.2.1 Introduction to Ti(IV) Salen-type complexes :

Metal Schiff base complexes can be prepared by different routes using various metal precursors. Essentially, five metal precursors are commonly used in such reactions; metal alkoxide $M(OR)_n$, metal amide $M(NR_2)_n$, metal alkyl MR_n, metal acetate $M(OAc)_n$ or metal halide MX_n.[1,9] However, using metal halide precursors were found to be more effective in obtaining metal salen complexes for the early transition metals. Usually, the synthesis of these complexes with metal halide was performed in THF and consists of two steps: deprotonation of the acidic phenolic hydrogens, followed by the reaction with the appropriate metal halide. KH or NaH are mostly utilized in the deprotonation process as stronger bases such as lithium organometallics can attack the imine group in a nucleophilic attack. The use of tetrahydrofuran adducts like $TiCl_4(THF)_2$ can be preferable to homoleptic metal halides.[1]

The interaction between tetradentate Schiff base (Salen-type) ligands with transition metal compounds can lead to different types of complex (Figure 2.3):[10,11]

1- Commonly, the ligand acts as a tetradentate ligand to form the typical inner chelate complex (**II**) and the coordination occurs through the imine nitrogen atoms and the deprotonated phenol oxygens (HX is eliminated).[12]

2- Sometimes, especially with transition metal halides, the ligand acts as a bidentate ligand and the coordination takes place through nitrogen atoms only and all four halide atoms remain bound to the metal to form the adduct (**I**).[11]

3- Solvent molecules can participate in the coordination with titanium and thus leads to the formation of seven coordinate solvated derivatives (**III**).[10]

4- Less commonly, the reaction involves reduction of the N=CH bonds and the metal in its higher oxidation state coordinates to the secondary amine (**IV**).[11,13]

43
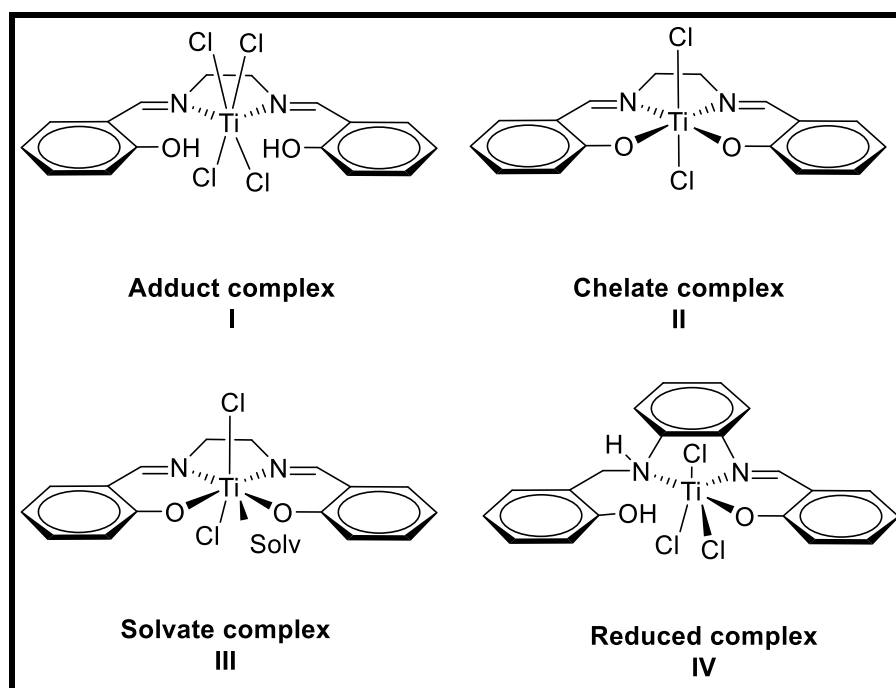
Figure 2.15: Different types of transition metal compounds bearing salen ligands

The adduct complex (**I**) contains acidic hydrogens which might affect its reactivity in catalytic studies. In this thesis, the aim was to obtain the chelate complex (**II**). There are several published reports describing the synthesis of [Ti(salen)Cl$_2$] (**2.21**) and its uses as a precursor for organometallic derivatives. It has been found that when the titanium chloride was reacted with H$_2$salen (**2.22**) in THF at room temperature the solvate complex [Ti(salen)Cl$_2$(THF)] (**2.23**) was formed as an orange precipitate, however, repeating the reaction in refluxing THF leads to the formation of the chelate complex [Ti(salen)Cl$_2$] (**2.21**) as dark red precipitate (Scheme 2.8).[10,14,15] The differentiation between the two complexes can be made by analysis of the ^{1}H NMR spectra, since the solvate complex shows two peaks at δ 3.80 and 1.85 ppm in CDCl$_3$ which are attributed to coordinated THF. The signals were slightly broad and were slightly shifted compared to pure THF, which is evidence that THF is coordinated to the metal.
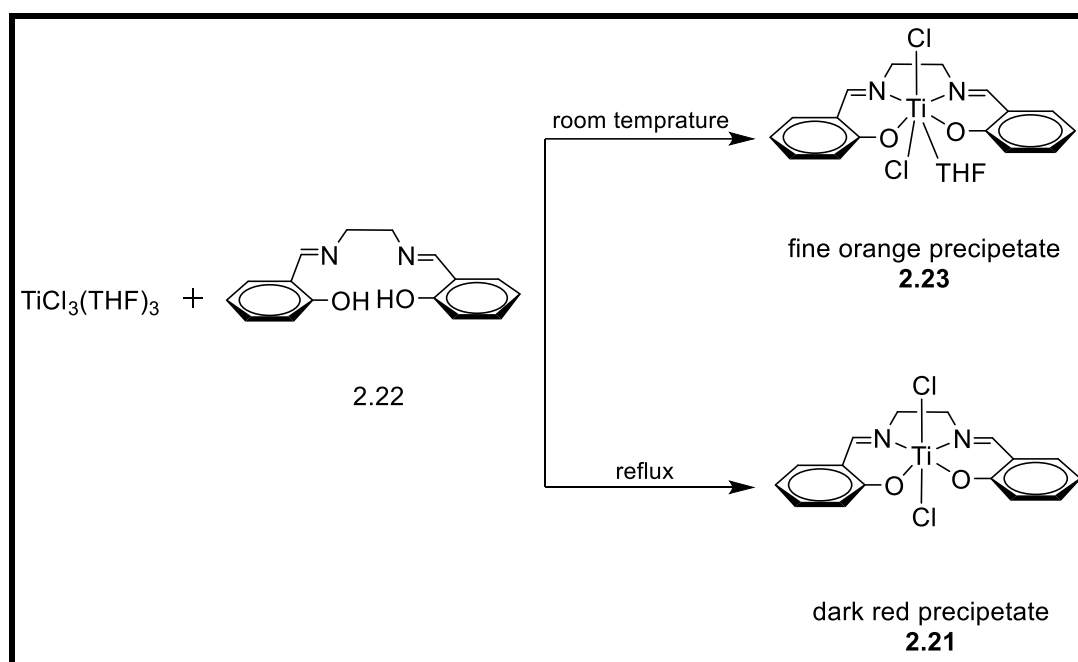
Scheme 2.24: Synthesis of Ti(IV) salen complexes, showing the effect of temperature on reaction product.

The reaction of titanium chloride with H_2dmsalen (**2.24**) in toluene at room temperature afforded the adduct [Ti(H_2dmsalen)Cl$_4$] (**2.25**) as seen in Scheme 2.9 and its structure confirmed by the retention of an imino and hydroxy signals in the IR spectrum.[10]
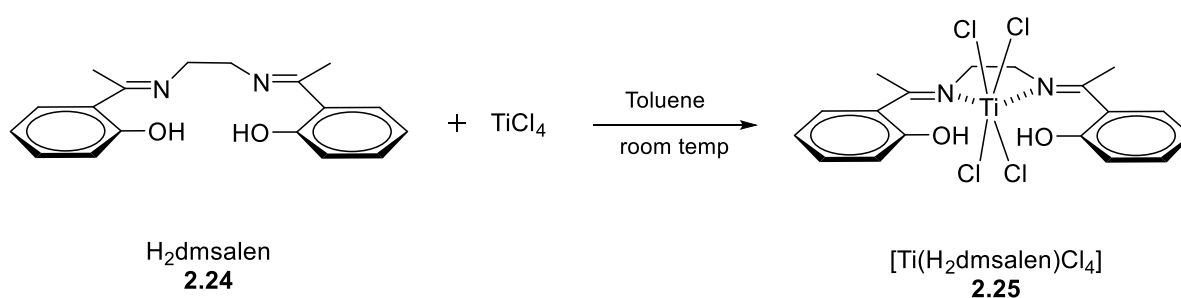
Scheme 2.25: Synthesis of [Ti(H_2dmsalen)Cl$_4$] (**2.25**)

Hence, the direct reaction between the ligand and metal precursor do not always afford the chelate complex and the reaction products can be highly influenced by the choice of solvent, ligand structure and the reaction temperature.

2.2.2 Synthesis of Ti(IV) Salen-type complexes

In the present study $TiCl_4$ and $TiCl_4(THF)_2$ have been tested as precursors for the synthesis of titanium(IV) complexes, however, due to the vigorous and exothermic reactivity of $TiCl_4$, $TiCl_4(THF)_2$ was used as the precursor, which was found to be more suitable.

$TiCl_4$ readily forms an adduct complex with THF to give octahedral $TiCl_4(THF)_2$ (**2.26**), and was synthesized according to a modified known procedure by dissolving titanium tetrachloride in dichloromethane and adding THF (Scheme 2.10).[16] The resulting bright yellow solid $TiCl_4(THF)_2$ (**2.26**) was obtained in high yield.

2.26

(91% yield)
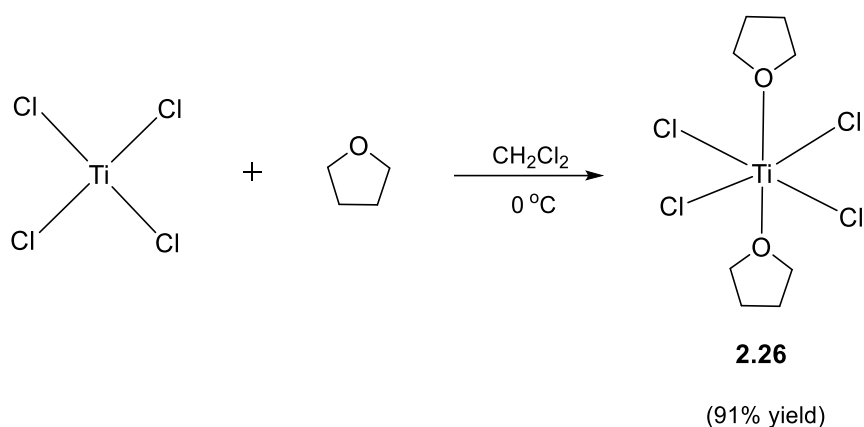
Scheme 2.26: Synthesis of $TiCl_4(THF)_2$

The synthesis and manipulation of all complexes were performed under an atmosphere of dry, oxygen-free nitrogen or argon using glovebox and standard Schlenk techniques with rigorous exclusion of air and moisture. Titanium complexes were prepared via a direct exchange reaction between stoichiometric amounts of $TiCl_4(THF)_2$ (**2.26**) and respective ligands or its potassium salt, liberating 2 equivalents of hydrochloric acid or potassium chloride (which were removed from the reaction medium by high vacuum or filtration).[17] In general, the most successful route involved adding a THF solution of the titanium halide adduct to a stirred solution of the corresponding ligand in THF in 1:1 ratio. The reaction mixture was then heated to reflux for 1-2 hours. Removal of the solvent by filtration and then high vacuum at 80 °C was used to dry the product. Schemes 2.11, 2.12 and 2.13 illustrate the synthesis of $[Ti(L)Cl_2]$ using different ligands.

It should be noted that when the base (Et$_3$N) was used in the synthesis to aid the deprotonation of the ionizable groups,[3,10,18] it leads to an undefined mixture of products, which will be discussed later.

[Ti(Salpy)Cl$_2$] (8): R=R'=H) (91% yield)
[Ti(^{t}Bu,^{t}Bu-Salpy)Cl$_2$] (10): R=R'=^{t}Bu (92% yield)
[Ti(^{t}Bu,OMe-Salpy)Cl$_2$] (11): R=^{t}Bu,R'=OMe (82% yield)
[Ti(Me-Salpy)Cl$_2$] (12): R=Me,R'=H (73% yield)
[Ti(Cl,Cl-Salpy)Cl$_2$] (13): R=R'=Cl (86% yield)
[Ti(Ad,Me-Salpy)Cl$_2$] (14): R=Ad, R'=Me (91% yield)
[Ti(Naphpy)Cl$_2$] (15): Ph=Naphalene (92% yield)
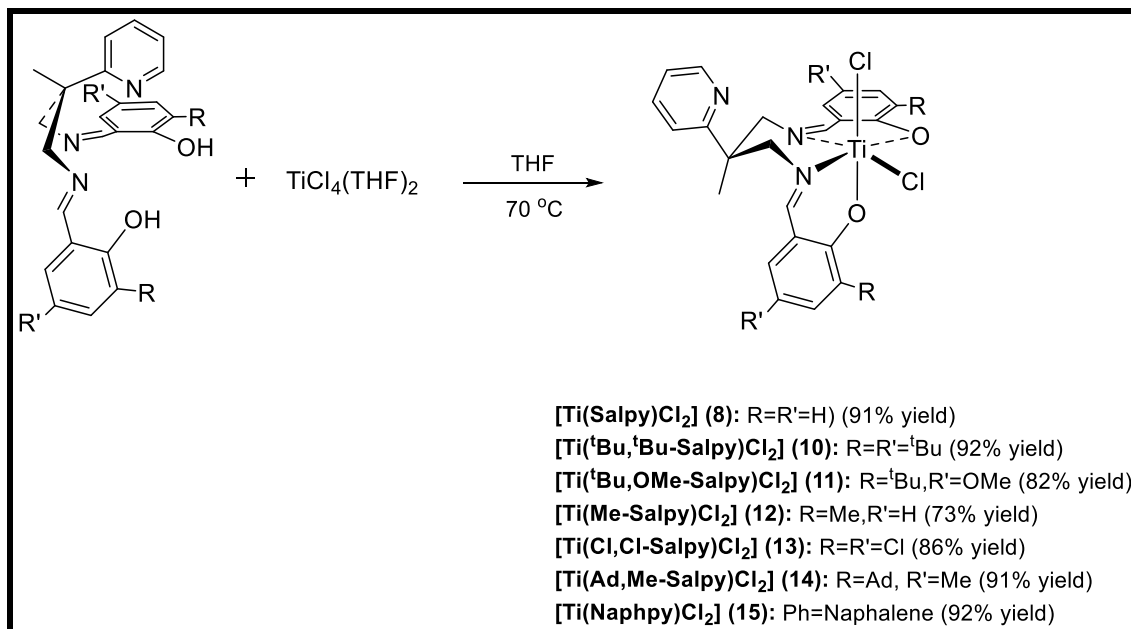
Scheme 2.27: Synthesis of [Ti(R,R`-Salpy)Cl$_2$] complexes

[Ti(Salpy-Me)Cl$_2$] (9)

(84% yield)
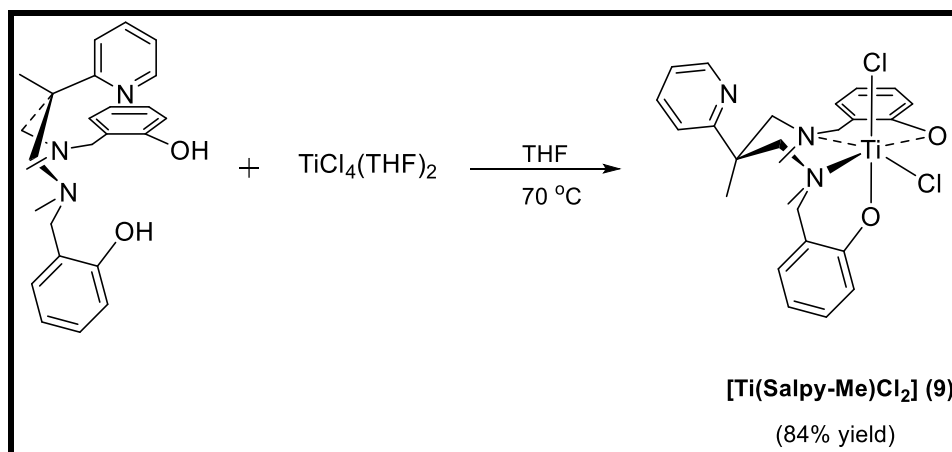
Scheme 2.28: synthesis of [Ti(Salpy-Me)Cl$_2$] **(9)**
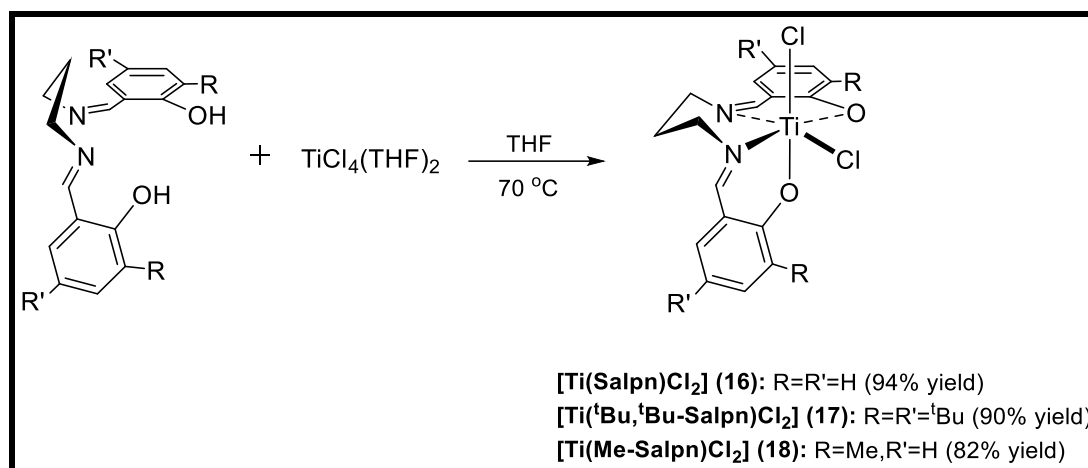
Scheme 2.29: Synthesis of [Ti(R,R'-Salpn)Cl$_2$]

To the best of our knowledge these are the first examples of titanium chloride complexes with Salpy ligands. [Ti(Salpy)Cl$_2$] (**8**), [Ti(Salpy-Me)Cl$_2$] (**9**), [Ti(Cl,Cl-Salpy)Cl$_2$] (**13**), [Ti(Ad,Me-Salpy)Cl$_2$] (**14**), [Ti(Naphpy)Cl$_2$] (**15**) and [Ti(Salpn)Cl$_2$] (**16**) were sparingly soluble in organic solvents which hindered their characterization using NMR and UV analysis. However, their high-resolution mass spectra and FT-IR spectra have proven their existence. A higher number of ^{1}H NMR scans were performed to determine the chemical shift positions.

Introducing groups such as [t]Bu, Me, or OMe to the ligand backbone made the complexes more soluble in organic solvents and allowing for full characterization using ^{1}H and ^{13}C NMR spectroscopy.

2.2.3 Introduction to Ti(III) Salen-type complexes :

Titanium complexes are dominated by the +4 oxidation state; complexes containing titanium in lower oxidation states [e.g. Ti(III) and Ti(II)] exhibit extremely high reactivity in molecular activation, because of their coordination numbers and electronic configuration, they show reactivities comparable to those of carbenes and free radicals.[19]

Most studies of TI(III) salen complexes are focused on the in-situ preparation by reducing the analogous Ti(IV) complexes with zinc, before using them as catalysts in subsequent reactions.[20–24]

The first attempt to prepare Ti(III) complexes with salen and Salen-type ligands was reported by Bowden and Ferguson in 1974.[11] They tried to prepare [Ti(salen)Cl] (**2.27**) by the direct reaction between TiCl$_3$(THF)$_3$ (**2.28**) and H$_2$salen (**2.22**) in THF at room temperature

and with rigorous exclusion of air. However, they obtained a green precipitate of the adduct [Ti(salen)Cl$_3$(THF)] (**2.29**) which oxidized to the red complex [Ti(salen)Cl$_2$] (**2.21**) when the reaction was left for 3 more hours without isolation (Scheme 3). Also, they found that the reaction of TiCl$_3$(THF)$_3$ (**2.28**) with H$_2$salophen (**2.30**) gives two types of complexes in the same reaction medium: dark brown [Ti(salophen)Cl$_2$] (**2.31**) and a complex with partial reduction of the Schiff base, trichloro[(N,N′-(o-hydroxybenzylamino-o-phenylene)salicyalideneiminato]titanium(IV) (**2.32**) (Scheme 2.14).
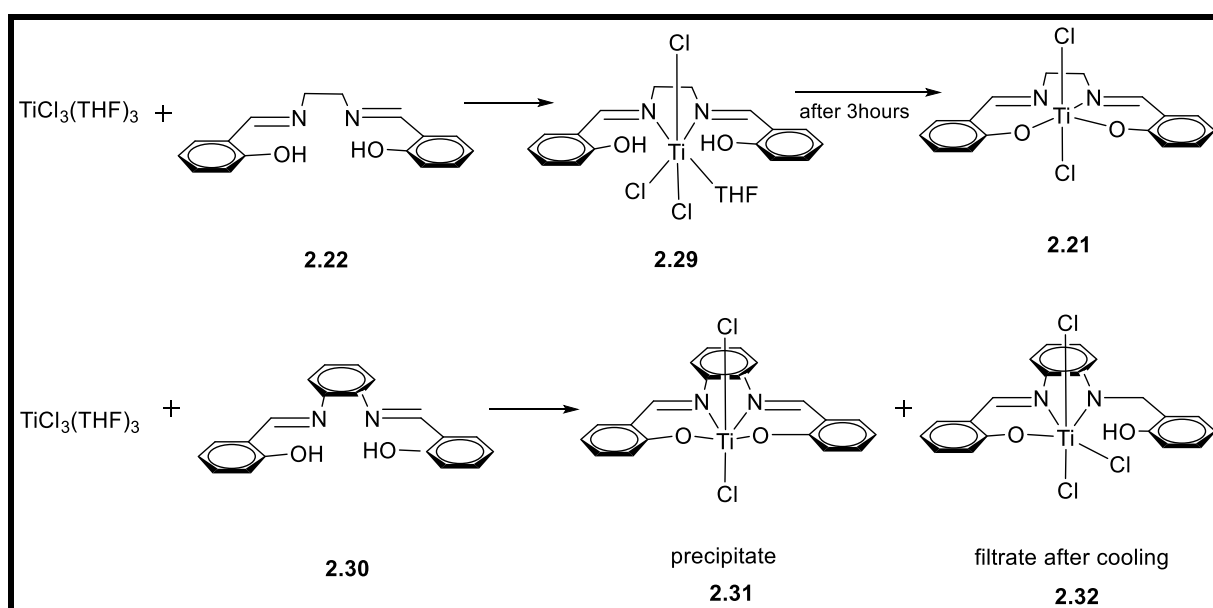
Scheme 2.30: Reaction of TiCl$_3$(THF)$_3$ with salen and salophen ligands[11]

Pasquali and his team found that introducing a pyridine ligand to the reduced complex [Ti(salen)Cl] (**2.27**) led to increases in the stability of the Ti(III) complexes towards oxidation (Scheme 2.15).[19]
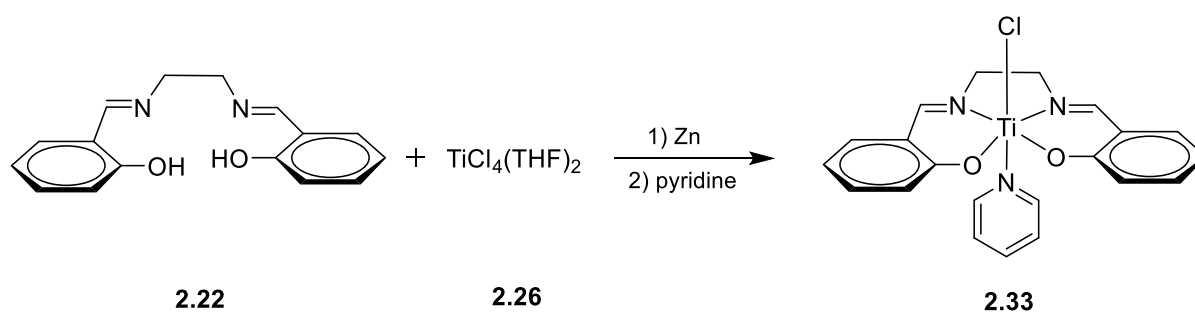
Scheme 2.31: Synthesis of [Ti(salen)Cl(Py)]

It was found that Ti(III) salen complexes can be obtained by the reduction of [Ti(salen)Cl$_2$] (**2.21**) complexes.[19] The choice of reducing agent is crucial, since with Li[BH$_4$] the salen ligand is reduced rather than the titanium,[25] whereas the reduction with zinc dust in tetrahydrofuran gives the desired Ti(III) complexes (Equation 2.1). The reduction process proceeds in THF because of the high solubility of ZnCl$_2$ in THF prevents it from contaminating the complexes.[19]

$$2\ [Ti(salen)Cl_2] \quad + \quad Zn \quad \xrightarrow{\text{THF}} \quad 2\ [Ti(salen)Cl] \quad + \quad ZnCl_2$$

$$\textbf{2.21} \qquad\qquad\qquad\qquad\qquad\qquad \textbf{2.27}$$
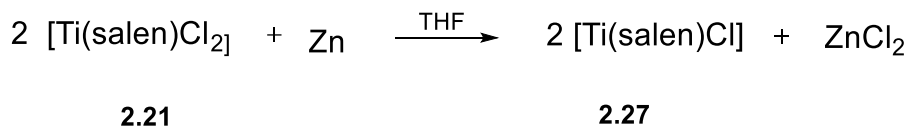
Equation 2.4: Reduction of [Ti(salen)Cl$_2$] to the corresponding Ti(III) complex

However, in 2015, Wang and coworkers successfully prepared [Ti(^{t}Bu,^{t}Bu-salophen)Cl] (**2.34**) by the direct reaction of TiCl$_3$(THF)$_3$ with the ligand salt in THF at -35°C (Scheme 2.16).[26]
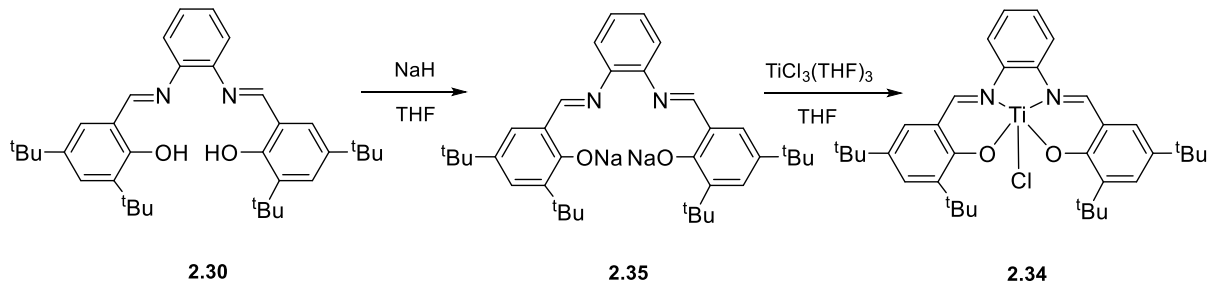
Scheme 2.32: Synthesis of [Ti(^{t}Bu,^{t}Bu-salophen)Cl]

2.2.4 Synthesis of Ti(III) Salen-type complexes :

Since anhydrous TiCl$_3$, which can be used as starting material for Ti(III) chemistry, is very expensive for exploratory synthesis,[27] many attempts have been done to synthesize it in laboratories including: reduction of TiCl$_4$ with H$_2$ at high temperature (650 °C) with removal of the produced HCl to avoid reoxidation,[28] reduction with Na metal in DME,[29,30] or synthesis of [TiCl$_4$(THF)$_2$] (**2.26**) followed by in situ reduction with metal trialkyls.[27] However, these methods required careful precautions to control the byproducts. For that reason, attention has turned to [TiCl$_3$(THF)$_3$] (**2.28**) which is also quite expensive for the laboratory applications, but it can

be prepared in high yield from commercially available $(TiCl_3)_3 \cdot AlCl_3$. $(TiCl_3)_3 \cdot AlCl_3$ is about 13 times cheaper than $[TiCl_3(THF)_3]$ (**2.28**) (Fisher scientific website) and it is easily manipulated. Al(III) and Ti(III) have similar physiochemical properties which hampered the use of this compound in coordination chemistry. Nonetheless, with simple extraction procedure we can acquire $[TiCl_3(THF)_3]$ in excellent yield without generating any corrosive or volatile byproducts (Scheme 2.17).

$$(TiCl_3)_3AlCl_3 \quad + \quad THF \quad \xrightarrow[\text{- AlCl}_3(THF)_n]{\text{Toluene}} \quad 3\ TiCl_3(THF)_3$$

2.28

(97% yield)
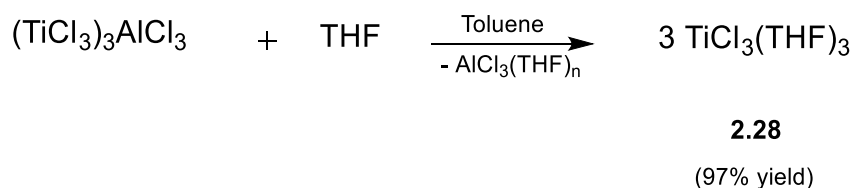
Scheme 2.33: Synthesis of $[TiCl_3(THF)_3]$

In this method $(TiCl_3)_3 \cdot AlCl_3$ was dissolved in toluene in an ampoule under a N_2 atmosphere.[27] The ampoule was then cooled to -50 °C using dry ice / acetone bath and an excess of THF was added to the stirred solution. This reaction is exothermic and the aim of adding toluene is to act as a heat sink during the THF addition. The mixture was heated to reflux overnight to yield the pale blue precipitate of $[TiCl_3(THF)_3]$ (**2.28**) in 97% isolated yield. The isolated titanium trichloride contains no aluminium as the aluminium trichloride dissolves in THF and is removed during the filtration.

In this study both methods have been used in the synthesis of Ti(III) with Salen-type complexes (reaction of the pro-ligand with $TiCl_3(THF)_3$ (**2.28**) and the reduction of a Ti(IV) complex).

At the beginning of this study the complexes were prepared via direct reaction between stoichiometric quantities of $TiCl_3(THF)_3$ (**2.28**) and the corresponding proligand, following a method reported by Wang et al.[26] The reaction was conducted by adding a solution of **2.28** in THF to a stirred solution of the ligand at -35°C, also in THF (Scheme 2.18). The resulting dark green solution was stirred for 2 h at room temperature. Removal of the solvent and washing with dry Et_2O or hexane afforded the complexes as green precipitates in good yields (73-89%).

[Ti(Salpy)Cl] (1): R=H
[Ti(ᵗBu,ᵗBu-Salpy)Cl] (3): R=3,5-di-tert-butyl
[Ti(Cl,Cl-Salpy)Cl] (4): R=3,5-dichloride
[Ti(Naphpy)Cl] (5): Ph=Naphalene
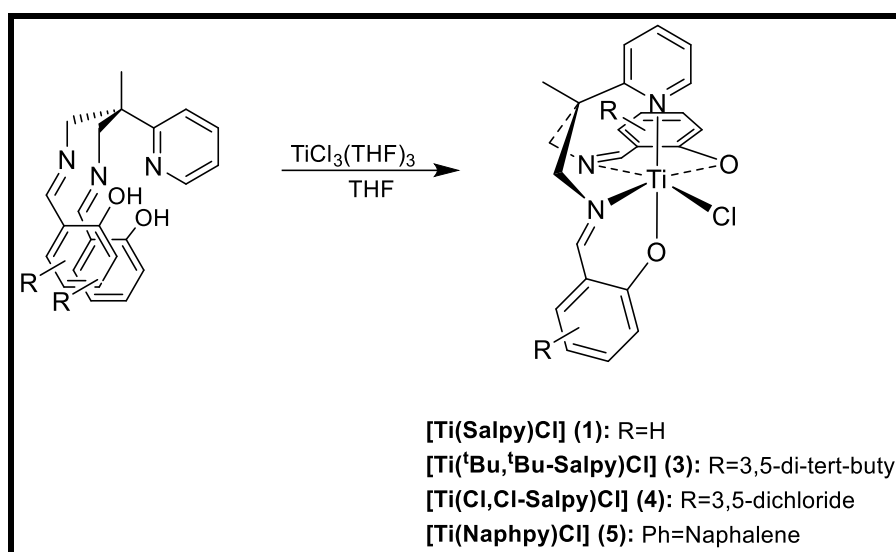
Scheme 2.34: Synthesis of [Ti(Salpy)Cl] complexes

An alternative method was subsequently investigated, such that the Ti(III) complexes were prepared by reduction of the analogous Ti(IV) species with zinc metal. This process was conducted by dissolving Ti(IV) complexes in THF and adding zinc dust. The mixture was stirred overnight then filtered to removed zinc chloride (Scheme 2.19). In case of [Ti(ᵗBu,ᵗBu-Salpy)Cl₂] (**10**) and [Ti(ᵗBu,ᵗBu-Salpn)Cl₂] (**17**), as these complexes are completely soluble in THF, the solvent was removed under vacuum before extracting the product with DCM. Using either of these methods a range of Salpy / Naphpy complexes were prepared as shown in Schemes 2.18. In addition, Ti(III) complexes with the reduced Salpy ligand [Ti(Salpy-Me)Cl] (**2**) and two complexes with Salpn ligand: [Ti(Salpn)Cl] (**6**) and [Ti(ᵗBu,ᵗBu-Salpn)Cl] (**7**) were also prepared.
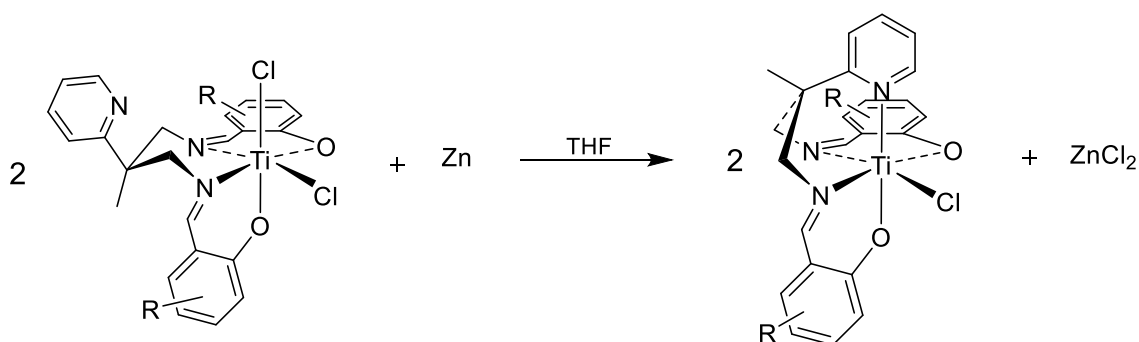
Scheme 2.35: Reduction of Ti(IV) complexes to the corresponding Ti(III) complexes

All of the complexes were characterized by electron paramagnetic resonance spectroscopy (EPR, otherwise known as electron spin resonance, ESR), high resolution mass spectrometry and FT-IR spectroscopy. ^{1}H NMR spectra of paramagnetic complexes show varying degrees of line broadening and chemical shifts that are outside of the normal range. These changes can be a minor effect such that spectra can be used easily (e.g. in many rare earth complexes) or they can be more extreme and can render the method uninformative. The complexes in this thesis were of the latter category; the spectra of the Ti(III) complexes were not informative, showing no meaningful signals. In every case the spectra showed no evidence for any diamagnetic species which evidences the complete conversion of Ti(IV) to Ti(III).

2.3 Characterization of complexes and ligands:

All prepared ligands and complexes were characterized by FTIR spectroscopy, ^{1}H and ^{13}C{^{1}H} NMR spectroscopy (except for Ti(III) complexes), mass spectrometry, and UV-visible spectroscopy. All the ligands are insoluble in EtOH and MeOH but soluble in $CHCl_3$ and THF.

2.3.1 X-ray crystallographic studies:

2.3.1.1 Introduction:

X-ray data for all the structures in this thesis were measured by the EPSRC National Crystallography Service at the university of Southampton (for [Ti(Salpy)Cl] (**1**), [Ti(Salpy)Cl$_2$] (**8**), and [Ti(^{t}Bu,^{t}Bu-Salpy)Cl$_2$] (**10**)) or by Dr. Benson Kariuki at Cardiff University ([Ti(Me-Salpy)Cl$_2$] (**12**), [Ti(^{t}Bu,^{t}Bu-Salpn)Cl$_2$] (**17**), and [Ti(Me-Salpn)Cl$_2$] (**18**)). The structures solved and refined by Dr. Benjamin Ward.

It is known that Ti(IV) complexes with symmetrical Salen-type ligands that have an amine N-C bond often exhibit C_2 symmetrical geometries, with the phenolate oxygens occupying trans donor sites and the two coligands in a cis configuration.[31–37] However, in the presence of the rigid tetradentate Salen-type ligands with an imine moiety, the structures usually have the two labile ligands in trans configuration and the salen ligand occupies the equatorial binding mode.[17,38–43] In these complexes, the basic nitrogen atoms of the azomethine moiety form a coordinative bond and the oxygen of the phenolate groups forms strong covalent bonds to the oxophilic Ti(IV) atom. In 1999, Moore and coworkers successfully synthesized and characterized the first cis [TiLCl$_2$] complexes bearing a Salen-type ligand.[44] They refer their success to the increase of steric effect present in Salen-type ligands (Figure 2.4) which induced the formation of the cis configuration around the titanium centre.
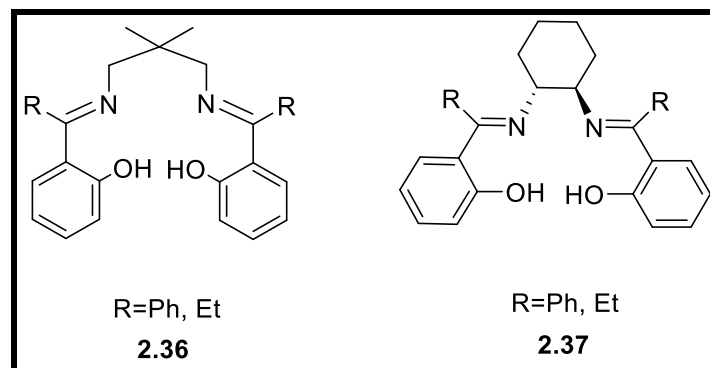
Figure 2.16: Schiff base ligands used by Moore et al.[44]

There are three possible configurations for an octahedral metal complex with a tetradentate ligand and two ancillary ligands. These are (with respect to the mono dentate ligands) *α*-cis with two equatorial ligands, *β*-cis with one equatorial and one apical ligand, or trans with two apical ligands (Figure 2.5).[9,45] It can be seen from Figure 2.5 that the configurations *α*-cis and trans are symmetrical whereas *β*-cis is not (for a symmetrical Salen-type ligands). For that reason, in the ^{1}H NMR spectrum we expect to see one signal set corresponding to the iminophenoxide moieties, whereas in the *β*-cis configuration two sets of signals will be observed.
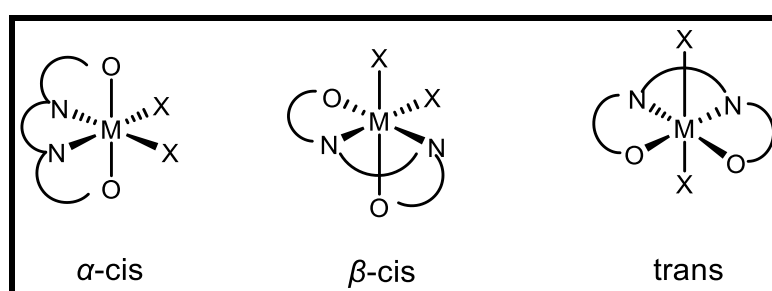
Figure 2.17: Possible octahedral coordination configuration with ONNO tetradentate Schiff base ligands

2.3.1.2 Crystal Structure Determination of [Ti(tBu,tBu-Salpn)Cl2] (17):

X -ray quality crystals of [Ti(tBu,tBu-Salpn)Cl2] (**17**) were obtained from a $CDCl_3$ solution by slow evaporation of the solvent. The molecular structure of (**17**) is depicted in Figure 2.6; selected bond lengths and angles are given in table 2.1. This structure has no pyridyl group on its ligand backbone which makes an interesting comparison with Salpy complexes. The structure consists of discrete $[Ti(C_{33}H_{48}N_2O_2)Cl_2]$ molecules. The equatorial positions are occupied by the substituted Salpn ligand, whereas the chloride ligands occupy the axial positions. The titanium ion lies in a distorted octahedral environment, as found from the angles around the Ti which range from 84.58(8)° (N(2)-Ti(1)-O(2)) to 101.32 (8)° (O(1)-Ti(1)-O(2)). The Ti-Cl bonds are (2.3429 (8) and 2.3455 (8) Å) and the Cl-Ti-Cl angle (164.20(3)°) are very close to those found in [Ti(5-tBu-salen)Cl2] (**2.38**) (Table 2.2).[46] The Ti-O bond lengths are 1.8310(18) and 1.8290(17) Å which are within the normal range found in titanium salen complexes (Table 2.2). The Ti-N bond lengths are 2.209(2) and 2.184(2) Å and are within the range of those reported in the Cambridge structure database (1.849-2.477, mean=2.179 Å for 740 examples).[47]
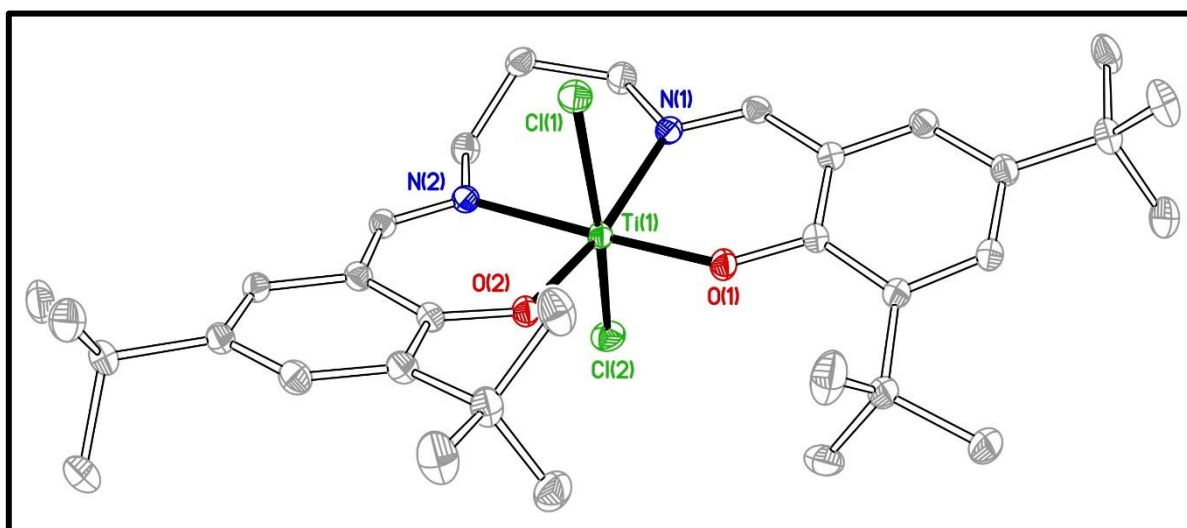
Figure 2.6: Molecular structure of [Ti(tBu,tBu-Salpn)Cl2] (**17**) with thermal ellipsoids drawn at 30% probability and hydrogen atoms omitted for clarity.

Table 2.1: Selected bond lengths (Å) and bond angle (°) for [Ti(^{t}Bu,^{t}Bu-Salpn)Cl$_2$] (**17**)

Bond	Bond length(Å)	Bond	Bond length(Å)
Ti(1)-O(2)	1.8290(17)	Ti(1)-N(1)	2.209(2)
Ti(1)-O(1)	1.8310(18)	Ti(1)-Cl(1)	2.3429(8)
Ti(1)-N(2)	2.184(2)	Ti(1)-Cl(2)	2.3455(8)
Bond	Bond Angle(°)	Bond	Bond Angle(°)
O(2)-Ti(1)-O(1)	101.32(8)	N(2)-Ti(1)-Cl(1)	85.94(6)
O(2)-Ti(1)-N(2)	84.58(8)	N(1)-Ti(1)-Cl(1)	81.69(6)
O(1)-Ti(1)-N(2)	173.36(9)	O(2)-Ti(1)-Cl(2)	99.24(6)
O(2)-Ti(1)-N(1)	170.34(8)	O(1)-Ti(1)-Cl(2)	93.56(7)
O(1)-Ti(1)-N(1)	84.98(8)	N(2)-Ti(1)-Cl(2)	82.41(6)
N(2)-Ti(1)-N(1)	89.57(8)	N(1)-Ti(1)-Cl(2)	87.56(6)
O(2)-Ti(1)-Cl(1)	90.21(6)	Cl(1)-Ti(1)-Cl(2)	164.20(3)
O(1)-Ti(1)-Cl(1)	96.98(7)		

Table 2.2: A comparison of selected bonds(Å) and angles (°) in titanium salen complexes including those in the literature and in this thesis

	[Ti(5-tBu-Salen)Cl2][46] **2.38**	[Ti(tBu,Me-Salen)Cl2][42] **2.39**	[Ti(3-tBu-Salen)Cl2][40] **2.40**	[Ti(tBu,tBu-Salen)Cl2][40] **2.41**	[Ti(3-tBu-Salcen)Cl2][48] **2.42**	[Ti(Me,Me-Salcen)Cl2][48] **2.43**	[Ti(tBu,tBu-Salpn)Cl2] **(17)**	[Ti(Me-Salpn)Cl2] **(18)**	[Ti(Salpy)Cl2] **(8)**	[Ti(Me-Salpy)Cl2] **(12)**
Ti-Cl	2.340(2)	2.345(3)	2.370(5)	2.359(3)	2.3563(10)	2.3436(7)	2.3429(8)	2.3653(4)	2.3501(6)	2.3618(7)
	2.342(2)	2.345(3)	2.326(5)	2.343(3)	2.3551(10)	2.3436(7)	2.3455(8)	2.3396(4)	2.3625(6)	2.3146(7)
Ti-O	1.807(3)	1.816(4)	1.818(8)	1.845(4)	1.830(3)	1.856(2)	1.8290(17)	1.8419(10)	1.825(2)	1.8402(18)
	1.814(4)	1.820(5)	1.843(8)	1.830(4)	1.827(3)	1.856(2)	1.8310(18)	1.8298(10)	1.827(2)	1.8235(18)
Ti-N	2.174(5)	2.110(6)	2.134	2.125	2.140(3)	2.156(2)	2.184(2)	2.1920(11)	2.205(3)	2.206(2)
	2.198(4)	2.136(5)	2.145	2.123	2.139(3)	2.156(2)	2.209(2)	2.1843(11)	2.208(3)	2.198(2)
N-Ti-N	89.0(2)	76.7(2)	75.79	75.29	76.45(17)	76.22(12)	89.57(8)	88.71(4)	88.55(7)	87.33(8)
O-Ti-O	100.9(2)	112.0(2)	112.93	112.72	111.38(17)	112.79(13)	101.32(8)	101.64(4)	99.55(7)	102.41(8)
Cl-Ti-Cl	165.23(8)	169.18(10)	170.9(2)	171.4(1)	170.14(6)	169.04(5)	164.20(3)	165.938(16)	167.72(3)	164.52(3)

2.3.1.3 Crystal Structure Determination of [Ti(Me-Salpn)Cl$_2$] (18):

Suitable crystals for the structural determination of [Ti(Me-Salpn)Cl$_2$] (**18**) were obtained by the slow evaporation of a deuterated chloroform solution. Complex **(18)** crystallizes in the monoclinic space group *P2$_1$/n.* The structure of (**18**) is depicted in figure 2.7 and the selected bond lengths and angles are listed in Table 2.3. The structure consists of discrete monomeric [Ti(Me-Salpn)Cl$_2$]. The equatorial plane of the octahedron is provided by the N$_2$O$_2$ core of the Me-Salpn ligand with trans binding of the chloride ligands, which are skewed from the equatorial plane defined by the Cl(1)-Ti(1)-Cl(2) angle of 165.938(16)° towards the nitrogen atoms. The two nitrogen atoms are situated in cis position, with N(1)-Ti(1)-N(2) angle being 88.71(4)°. The two oxygen atoms subtend an angle with the titanium of O(1)-Ti(1)-O(2) = 101.64(4)°. The bond angles between the two chloride and the two oxygen atoms are smaller than the analogous in Ti-salen complexes whereas the angle N-Ti-N is larger (Table 2.2). The Ti-O bond lengths of 1.8419(10) and 1.8298(11) Å are analogous to the Ti-O bond lengths reported for titanium chloride complexes with N$_2$O$_2$ ligands donor set. Likewise, the Ti-N bond lengths of 2.1920(11) and 2.1843(11) Å are in close agreement with the Ti-N bond lengths for Ti-salen complexes. The Ti-Cl bond lengths are 2.3653(4) and 2.3396(4) Å and are comparable to the Ti-Cl bond lengths.
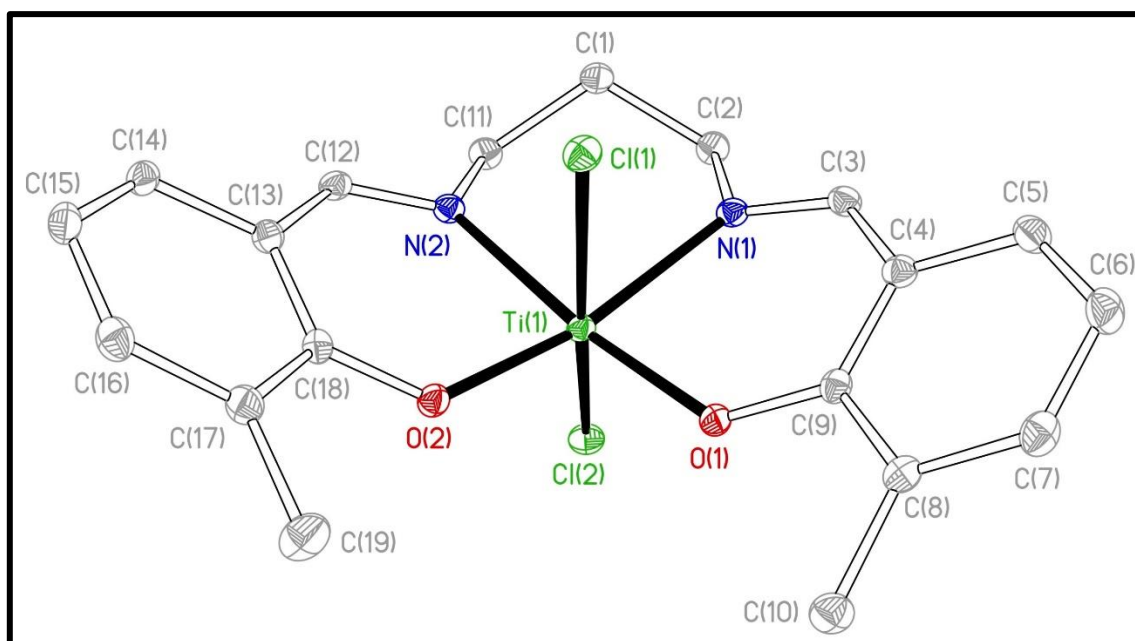
Figure 2.7: Molecular structure of [Ti(Me-Salpn)Cl$_2$] (**18**) with thermal ellipsoids drawn at 30% probability and hydrogen atoms omitted for clarity.

Table 2.3: Selected bond lengths (Å) and bond angles (°) for [Ti(Me-Salpn)Cl₂] (**18**)

Bond	Bond length(Å)	Bond	Bond length(Å)
Ti(1)-Cl(1)	2.3653(4)	Ti(1)-O(2)	1.8298(10)
Ti(1)-Cl(2)	2.3396(4)	Ti(1)-N(1)	2.1920(11)
Ti(1)-O(1)	1.8419(10)	Ti(1)-N(2)	2.1843(11)
Bond	Bond Angle(°)	Bond	Bond Angle(°)
Cl(2)-Ti(1)-Cl(1)	165.938(16)	O(2)-Ti(1)-N(1)	168.91(4)
O(1)-Ti(1)-Cl(1)	92.09(3)	O(2)-Ti(1)-N(2)	84.36(4)
O(1)-Ti(1)-Cl(2)	96.13(3)	N(1)-Ti(1)-Cl(1)	80.89(3)
O(1)-Ti(1)-N(1)	84.84(4)	N(1)-Ti(1)-Cl(2)	88.49(3)
O(1)-Ti(1)-N(2)	173.11(4)	N(2)-Ti(1)-Cl(1)	84.48(3)
O(2)-Ti(1)-Cl(1)	89.81(3)	N(2)-Ti(1)-Cl(2)	86.10(3)
O(2)-Ti(1)-Cl(2)	99.64(3)	N(2)-Ti(1)-N(1)	88.71(4)
O(2)-Ti(1)-O(1)	101.64(4)		

2.3.1.4 Crystal Structure Determination of [Ti(Salpy)Cl₂] (8):

Crystals of [Ti(Salpy)Cl₂] (**8**) suitable for X-ray diffraction studies were grown under N_2 from a solution in acetonitrile: drops of toluene were added with slow diffusion of THF as an anti-solvent. The molecular structure is illustrated in Figure 2.8. Selected bond lengths and angles are summarized in Table 2.4. The X-ray crystal structure of (**8**) revealed that it contains a six-coordinate titanium ion with distorted octahedral geometry. As expected for a Ti(IV) complex with two co-ligands, the pyridyl does not coordinate to the titanium centre, a phenomenon that was observed by Houser et al. in a copper complex with the same ligand.[3] Unusually for the Salpy ligand, the two chloride ligands occupy the axial positions, and the N_2O_2 ligand donor set occupies the equatorial plane to give a trans geometry; the corresponding isopropoxide complexes prepared by Bahlili et al. gave the corresponding β-cis geometry.[7] The equatorial angles are 99.55(7), 86.08(11), 88.55(7) and 85.81(11)° for O(1)-Ti(1)-O(2), O(1)-Ti(1)-N(2), N(2)-Ti(1)-N(3) and N(3)-Ti(1)-O(2), respectively. The Cl(1)-Ti(1)-Cl(2) angle is slightly bent toward the imine moiety leading to a less than ideal angle of 167.72(3)°. The nitrogen bonds Ti(1)-N (2.1423(3)-2.223(3) Å) are significantly longer than the Ti(1)-O bonds (1.833(3), 1.830(3)) as a result of the greater atomic size of N atom.[49] All Ti-N, Ti-O and Ti-Cl bond lengths are similar to those reported for trans [TiLCl₂] complexes (Table 2.2). However, the angle N(1)-Ti(1)-N(2) are significantly greater and the O(1)-Ti(1)-O(2) angle are significantly smaller compared to those for [TiLCl₂]. Interestingly, the pyridyl was found to be protonated, forming a hydrogen bond to a proximal chloride ion, effectively an additional molecule of HCl which is captured by the pyridyl base when HCl is liberated during the

synthesis. The presence of the HCl proved to be crucial in stabilising the complexes as will be discussed below; when the synthesis was performed in the presence of a base (to remove the liberated HCl), an intractable mixture was obtained from which no complex could be isolated.
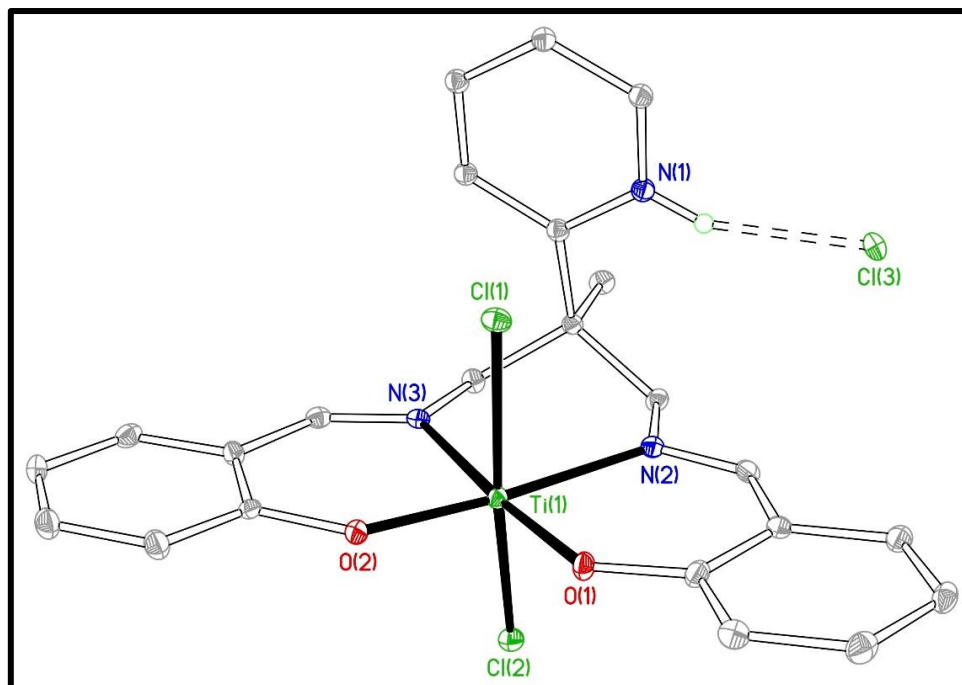
Figure 2.8: Molecular structure of [Ti(Salpy)Cl$_2$] **(8).** Displacement ellipsoids are drawn 30% probability and H atoms other than NH have been omitted for clarity.

Table 2.4: Selected bond lengths (Å) and bond angle (°) for [Ti(Salpy)Cl$_2$] (**8**)

Bond	Bond length(Å)	Bond	Bond length(Å)
Ti(1)-O(2)	1.825(2)	Ti(1)-N(2)	2.208(3)
Ti(1)-O(1)	1.827(2)	Ti(1)-Cl(2)	2.3501(6)
Ti(1)-N(3)	2.205(3)	Ti(1)-Cl(1)	2.3625(6)
Bond	**Bond Angle(°)**	**Bond**	**Bond Angle(°)**
O(2)-Ti(1)-O(1)	99.55(7)	N(3)-Ti(1)-Cl(2)	84.11(8)
O(2)-Ti(1)-N(3)	85.81(11)	N(2)-Ti(1)-Cl(2)	84.63(8)
O(1)-Ti(1)-N(3)	174.62(11)	O(2)-Ti(1)-Cl(1)	91.83(8)
O(2)-Ti(1)-N(2)	174.17(11)	O(1)-Ti(1)-Cl(1)	92.13(8)
O(1)-Ti(1)-N(2)	86.08(11)	N(3)-Ti(1)-Cl(1)	87.30(8)
N(3)-Ti(1)-N(2)	88.55(7)	N(2)-Ti(1)-Cl(1)	86.40(8)
O(2)-Ti(1)-Cl(2)	96.27(8)	Cl(2)-Ti(1)-Cl(1)	167.72(3)
O(1)-Ti(1)-Cl(2)	95.60(8)		

2.3.1.5 Crystal Structure Determination of [Ti(Me-Salpy)Cl$_2$] (12):

Single crystals suitable for X-ray crystallography were obtained for [Ti(Me-Salpy)Cl$_2$] (**12**) by slow evaporation of deuterated chloroform solution in a J. Young NMR tube at room temperature. The crystal structure of (**12**) is shown in Figure 2.9 while selected bond lengths and angles are summarized in Table 2.6. This structure makes an interesting comparison with the aforementioned complex (**18**) since (**12**) has an extra pyridyl group to coordinate. Complex (**12**) crystallizes in the monoclinic space group P2$_1$/n and contains 4 complex units and two chloroform molecules within the unit cell. The X-ray crystallography confirmed the presence of mononuclear distorted octahedral titanium (IV) species. The coordinated Salpy-Me ligand occupies the equatorial plane of the complex and displays an acute N(2)-Ti(1)-N(3) bond angle of 87.33(8)° and obtuse O(1)-Ti(1)-O(2) bond angle of 102.41(8)°. The two chloride ligands occupy the axial positions. The Ti-N bonds are Ti(1)-N(2)= 2.206(2), Ti(1)-N(3)= 2.198(2) Å. The Ti(1)-O(1)= 1.8402(18), Ti(1)-O(2)= 1.8235(18) Å . And the Ti-Cl bonds are Ti(1)-Cl(1)= 2.3168(7) Å and Ti(1)-Cl(2)= 2.3146(7) Å. The bond lengths around the titanium centre are all within the expected range based upon examples in the Cambridge structural database (1.849-12.477, mean= 2.179 Å for 740 examples (Ti-N), 1.722-2.497, mean= 1.909 Å for 1999 examples (Ti-OAr), and 1.780-3.037, mean=2.332 Å for 3010 examples (Ti-Cl)).[47] Complex (**12**) is like (**8**) in that the pyridyl does not participate in the coordination with the titanium ion.
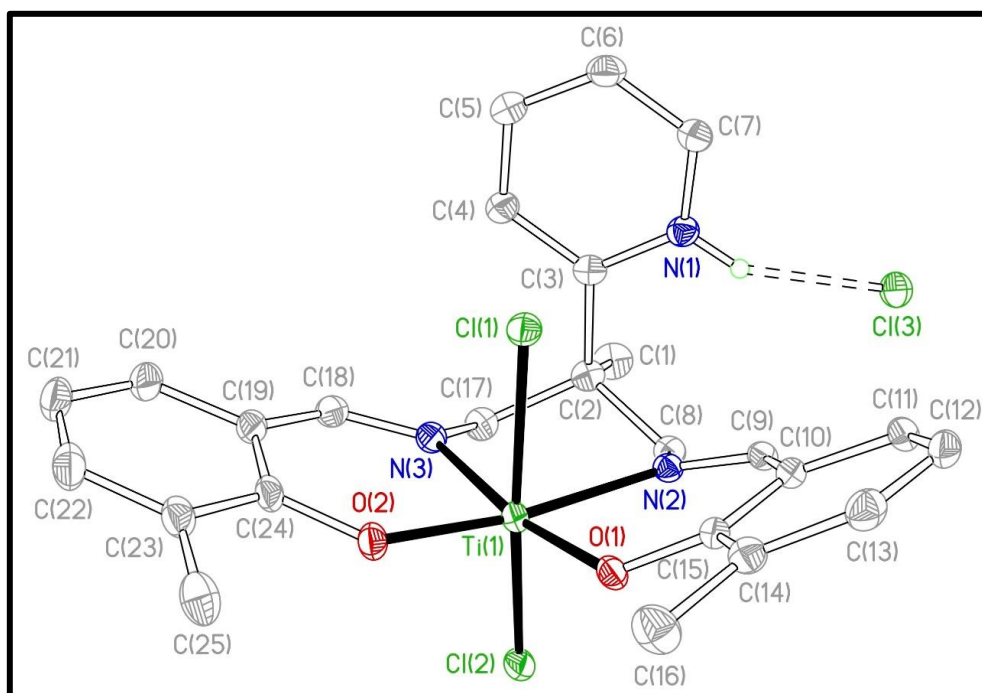
Figure 2.9: Molecular structure of [Ti(Me-Salpy)Cl$_2$] (**12**) with thermal ellipsoids drawn plot at 30%, solvent of crystallization and H atoms (other than NH) omitted for clarity.

Table 2.2: Selected bond lengths (Å) and bond angle (°) for [Ti(Me-Salpy)Cl$_2$] (**12**)

Bond	Bond length(Å)	Bond	Bond length(Å)
Ti(1)-Cl(1)	2.3618(7)	Ti(1)-O(2)	1.8235(18)
Ti(1)-Cl(2)	2.3146(7)	Ti(1)-N(2)	2.206(2)
Ti(1)-O(1)	1.8402(18)	Ti(1)-N(3)	2.198(2)
Bond	Bond Angle(°)	Bond	Bond Angle(°)
Cl(2)-Ti(1)-Cl(1)	164.52(3)	O(2)-Ti(1)-N(2)	171.51(8)
O(1)-Ti(1)-Cl(1)	90.28(6)	O(2)-Ti(1)-N(3)	85.34(8)
O(1)-Ti(1)-Cl(2)	99.44(6)	N(2)-Ti(1)-Cl(1)	83.17(5)
O(1)-Ti(1)-N(2)	84.51(8)	N(2)-Ti(1)-Cl(2)	85.79(5)
O(1)-Ti(1)-N(3)	170.49(8)	N(3)-Ti(1)-Cl(1)	83.90(6)
O(2)-Ti(1)-Cl(1)	91.79(6)	N(3)-Ti(1)-Cl(2)	84.79(6)
O(2)-Ti(1)-Cl(2)	97.78(6)	N(3)-Ti(1)-N(2)	87.33(8)
O(2)-Ti(1)-O(1)	102.41(8)		

This complex also has a protonated pyridyl and features two types of weak bonds; hydrogen bond between protonated pyridyl and the chloride atom of hydrochloric acid that is liberated during the complexation reaction (N-H·····Cl), and there is a weak van der Waals-type force between the axial chloride atom Cl(1) and the ipso-carbon in the pyridyl ring. The van der Waals radii are 1.7 Å and 1.8 Å for carbon and chloride, respectively, and the sum of these radii = 3.5 Å,[50] however, the DFT calculation (section **2.3.1.6**) indicates the distance between the two atoms (Cl and pyridyl ipso-carbon) to be 3.139 Å. The first interaction is illustrated in Figure 2.9 while the latter is more clearly exhibited in Figure 2.10.
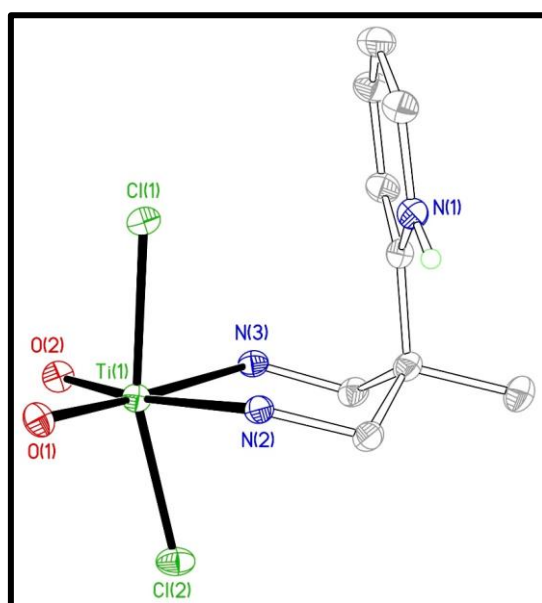
Figure 2.10: Van der waal's interaction in [Ti(Me-Salpy)Cl$_2$] (**12**)

Table 2.6 illustrates a comparison in bond lengths and angles between [Ti(Me-Salpy)Cl$_2$] (**12**) which have the pendent pyridyl moiety and [Ti(Me-Salpn)Cl$_2$] (**18**) with the same structure other than the pyridyl. It can be seen that there is almost no difference, with bond lengths and angles being similar for both, showing that the extra pyridyl and methyl groups make no significant difference to the coordination geometry.

Table 2.6: A comparison of selected bonds (Å) and angles (°) in [Ti(Me-Salpy)Cl$_2$] (**12**) and [Ti(Me-Salpn)Cl$_2$] (**18**)

	[Ti(Me-Salpy)Cl$_2$] (12)	[Ti(Me-Salpn)Cl$_2$] (18)
Ti-N	2.1982(2)	2.1920(11)
	2.206(2)	2.1843(11)
Ti-O	1.8402(18)	1.8419(10)
	1.8235(18)	1.8298(10)
Ti-Cl	2.3618(7)	2.3653(4)
	2.3146(7)	2.3396(4)
N-Ti-N	87.33(8)	88.71(4)
O-Ti-O	102.41(8)	101.64(4)
Cl-Ti-Cl	164.52(3)	165.938(16)

2.3.1.6 DFT calculation for [Ti(Salpy)Cl$_2$]:

The structure of [Ti(Salpy-H)Cl$_2$]$^+$ appeared to exhibit a non-intuitive structure, in that the TiN$_2$C$_3$ titanacycle adopts a chair-like conformation (akin to a cyclohexane ring) but with the pyridyl occupying an axial, rather than an equatorial site, as expected based upon a comparison of the sterics of pyridyl *vs.* methyl. Further analysis indicates that one of the chloride ligands has a close-contact with the pyridyl *ipso*-carbon (3.139 Å) ($\sum r_{vdw}$ = 3.5 Å for crystallographic van der Waals radii). The structure of [Ti(Salpy)Cl$_2$] was calculated using density functional theory calculations, employing the M06 functional[51] and def2-TZVP triple-ζ basis set. Calculations were executed by Dr Benjamin Ward.[52,53] The calculation slightly overestimates the Cl…C distance at 3.302 Å but analysis of the calculated structure using Bader's Quantum Theory of Atoms in Molecules[54] indicates a bond critical point (BCP) between the Cl and *ipso*-C (Figure 2.11). The BCP has electron density of 0.059 e Å^{-3} and Laplacian of +0.633 e Å^{-5}. The positive value of the Laplacian indicates a primarily ionic interaction rather than covalent, as expected for this type of interaction.
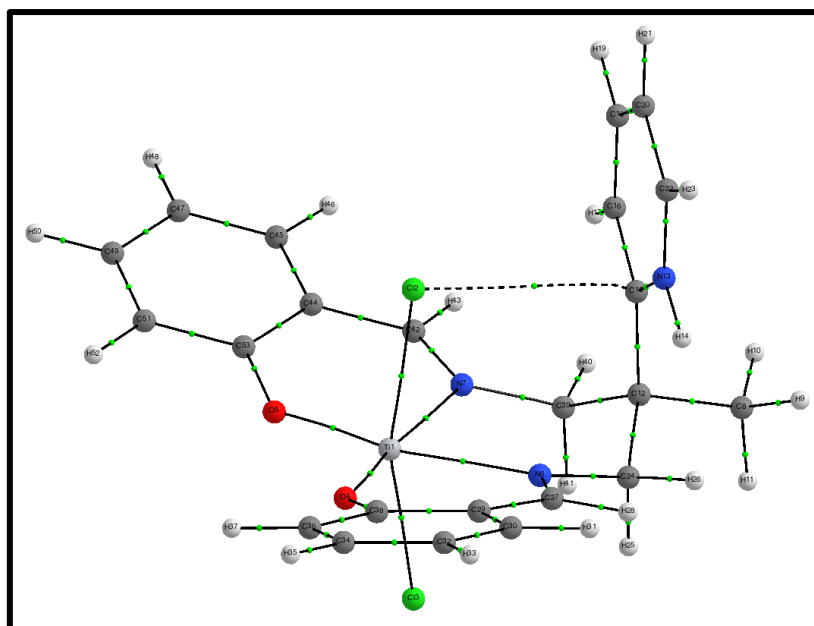
Figure 2.11: Calculated structure of [Ti(Salpy)Cl$_2$] showing the bond-critical points derived from Quantum Theory of Atoms in Molecules (QTAIM) analysis [M06 | def2-TZVP]

A Natural Bonding Orbital analysis is a useful method for providing an intuitive and easy to understand bonding scheme for molecular systems.[55–57] In addition, second-order perturbation analysis allows weak or long-range interactions to be probed, where the bonding cannot be considered truly covalent, but where interactions do exist. In this case, a donor-acceptor interaction was identified to exist between a chlorine-based lone pair and an unoccupied antibonding orbital on the pyridyl ring; this interaction is best described as p to π* and is depicted in Figure 2.12.
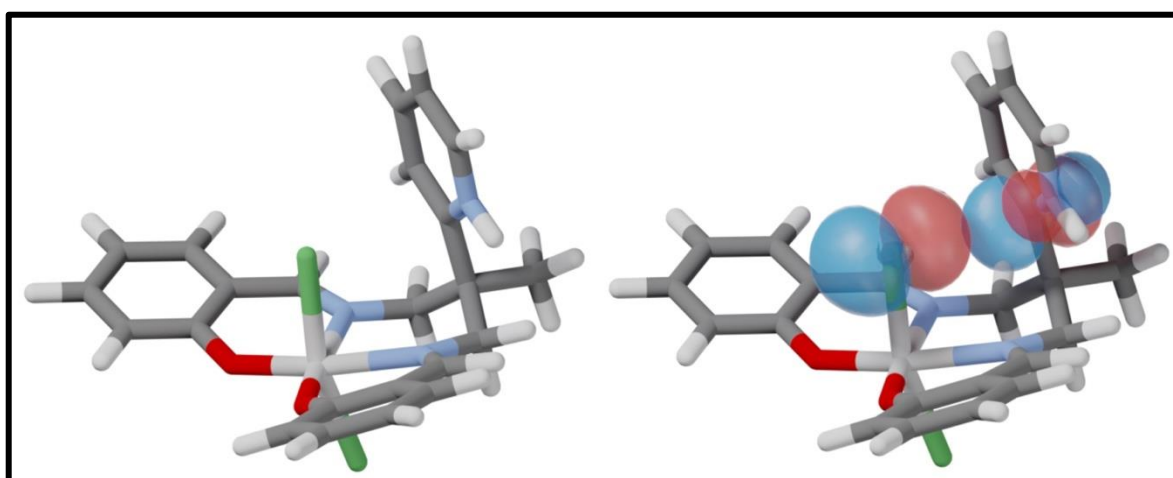
Figure 2.12: Calculated structure of [Ti(Salpy)Cl$_2$], showing the donor-acceptor interactions derived from natural bonding orbital analyses [M06 | def2-TZVP].

2.3.1.7 Crystal Structure Determination of [Ti$_2$(^{t}Bu,^{t}Bu-Salpy)Cl$_7$][Ti(^{t}Bu,^{t}Bu-Salpy)Cl] (1A):

Crystals suitable for X-ray structural determination were grown from a diethyl ether of [Ti(^{t}Bu,^{t}Bu-Salpy)Cl$_2$] (**10**) at room temperature to give the unexpected structure [Ti$_2$(^{t}Bu,^{t}Bu-Salpy)Cl$_7$][Ti(^{t}Bu,^{t}Bu-Salpy)Cl] (**1A**) in Figure 2.13. Selected bond lengths and angles are provided in Table 2.7.
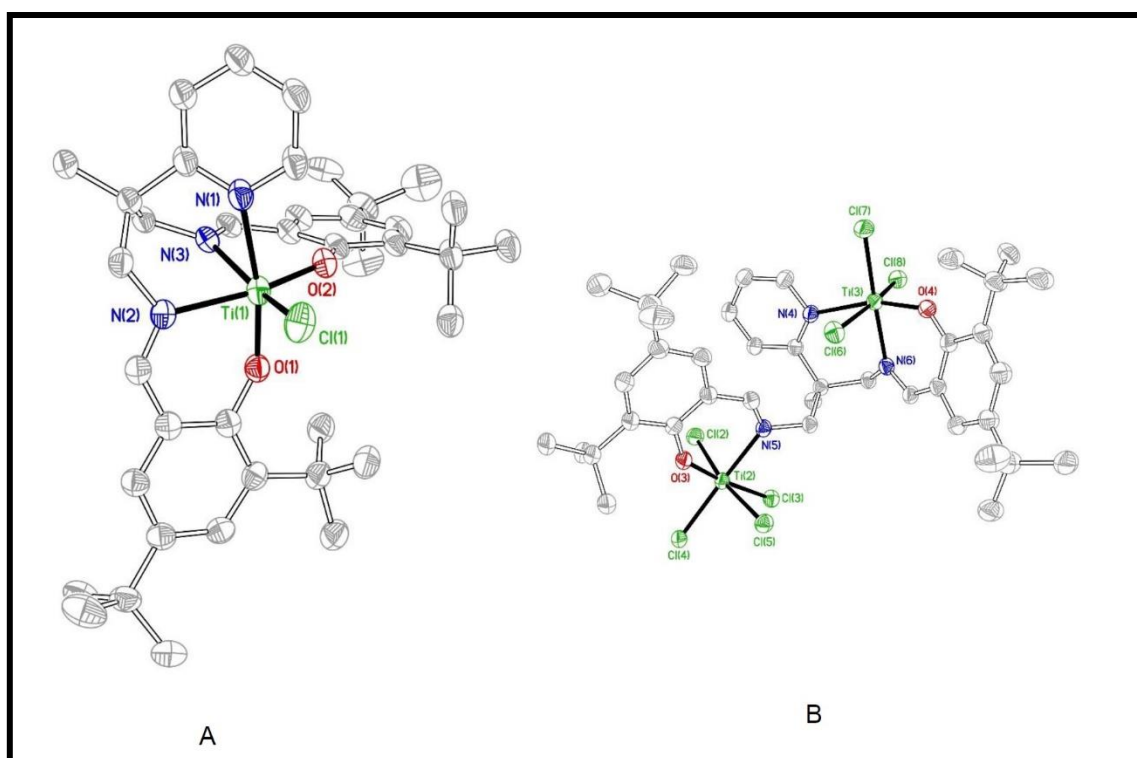
Figure 2.13: Molecular structure of [Ti$_2$(^{t}Bu,^{t}Bu-Salpy)Cl$_7$][Ti(^{t}Bu,^{t}Bu-Salpy)Cl] (**1A**) with thermal ellipsoids drawn at 30% and hydrogen atoms omitted for clarity.

Table 2.7: Selected bond lengths (Å) and bond angle (°) for (**1A**)

Bond	Bond length(Å)	Bond	Bond length(Å)
Ti(1)-O(1)	1.830(3)	Ti(1)-N(3)	2.158(3)
Ti(1)-O(2)	1.833(3)	Ti(1)-N(1)	2.223(3)
Ti(1)-N(2)	2.142(3)	Ti(1)-Cl(1)	2.2805(13)
Bond	Bond Angle(°)	Bond	Bond Angle(°)
O(1)-Ti(1)-O(2)	95.90(12)	N(2)-Ti(1)-N(1)	86.02(12)
O(1)-Ti(1)-N(2)	83.49(12)	N(3)-Ti(1)-N(1)	74.84(12)
O(2)-Ti(1)-N(2)	162.58(12)	O(1)-Ti(1)-Cl(1)	96.08(9)
O(1)-Ti(1)-N(3)	101.31(12)	O(2)-Ti(1)-Cl(1)	105.90(9)
O(2)-Ti(1)-N(3)	83.16(11)	N(2)-Ti(1)-Cl(1)	91.45(9)
N(2)-Ti(1)-N(3)	79.91(12)	N(3)-Ti(1)-Cl(1)	159.50(9)
O(1)-Ti(1)-N(1)	169.33(12)	N(1)-Ti(1)-Cl(1)	86.11(10)
O(2)-Ti(1)-N(1)	93.53(12)		

Although the spectroscopic data for complex **10** suggest a comparable structure to complexes **8** and **12**, the structure obtained from the X-ray data clearly indicate a very different structure, which contains two ionic moieties, a cationic fragment containing a κ^5-salpy and one chloride in [Ti(^{t}Bu,^{t}Bu-salpy)Cl]$^+$ (**A**), and a second species which contains one salpy ligand and two titanium ions, one of which is bound to the salpy ligand in a κ^3 fashion (i.e. with the pyridyl coordinated) and the other in a κ^2 manner via just an imine and a phenoxide (**B**). In ion **A**, the geometry around the titanium ion is best described as distorted octahedral, with the N_3O_2 donor set from the deprotonated pentadentate ligand [^{t}Bu,^{t}Bu-Salpy]$^{2-}$ in addition to the chloride ion. The four equatorial positions are occupied with one phenoxy group, one chloride ion, and two imine donors; the pyridyl and the remaining phenoxy oxygen occupy the axial positions, thus giving a β-cis arrangement of the donors. The overall +1 charge of the complex is balanced by the negatively charged ion **B**. The pyridyl Ti(1)-N(1) in the trans position is significantly longer (2.223(3) Å) than the distances of the cis imine N(2)-Ti(1), N(3)-Ti(1) bonds (2.1422(3) and 2.158(3) Å, respectively) which is consistent with the weaker interaction between the pyridyl and titanium, and consequently the pyridyl being subjected to hemi-labile donation. The Ti(1)-O(1) and Ti(1)-O(2) bond lengths are the same within experimental error (1.830(3), 1.833(3) Å). The Ti-Cl bond in ion **A** is shorter than the Ti-Cl bonds lengths in [Ti(salpy)Cl$_2$] (**8**) and [Ti(salpy)Cl$_2$] (**12**). The N(1)-Ti(1)-O(1) angle is 169.33(12)° with the two

bonds Ti(1)-N(1) and Ti(1)-O(1) not quite orthogonal to the equatorial plane and a little bent toward the imine nitrogens.

In ion **B**, both titanium ions adopt distorted octahedral geometries. The titanium with a κ^3-salpy is bound by the pyridyl nitrogen, an imine nitrogen and a phenoxy oxygen; the remaining coordination sphere is made up with three chloride ligands. The second titanium is coordinated to the nitrogen and oxygen of the ligand "arm" with the coordination sphere made up with four chloride ligands.

The high number of chloride ligands, which are known to readily hydrolyse on contact with water, precludes a rearrangement arising from hydrolysis, and the formation of complex **1A** is therefore curious and unexpected. The successful structural determinations of complexes **8** and **12** suggests that this species may arise from a rearrangement in the crystallization process, and therefore not representative of the bulk sample. One clear difference was that the crystals of **1A** were uniquely grown from diethyl ether, and so it is possible that the ether facilitates the rearrangement. One possibilty is that ether can, over time, allow dissociation of the coordinated HCl, thus leaving behind a free pyridyl donor. Since removal of HCl by adding a base (Et₃N) during the synthesis leads to a complex mixture of products, it is entirely feasible that liberating the pyridyl donor leads to a complex rearrangement, suggested in equation 2.2. Since the dissociation of HCl could be considered to be an equilibrium, the formation of a small quantity of **1A** would lead to a shift in the equilibrium by Le Chatelier's principle if the ionic species were less soluble, as is clearly the case in diethyl ether, and so this encourages the formation of the right hand side as it crystalises.

$$3[\text{Ti}(^t\text{Bu},^t\text{Bu-Salpy})\text{Cl}_2\cdot\text{HCl}] \rightleftharpoons [\text{Ti}_2\text{Cl}_7(^t\text{Bu},^t\text{Bu-Salpy})]^-[\text{Ti}(^t\text{Bu},^t\text{Bu-Salpy})\text{Cl}]^+ + {}^t\text{Bu},^t\text{Bu-H}_2\text{Salpy}\cdot\text{HCl}$$

Equation 2.5: Rearrangement of complex **10** in diethyl ether

2.3.1.8 Crystal Structure Determination of [Ti(Salpy)(η^2-O$_2$)] (1B):

Several attempts were made to grow crystals of Ti(III) complexes for X-ray analysis but their extreme solubility properties (i.e. complexes are either very soluble or completely insoluble in suitable solvents) hampered efforts. After much trying, on one occasion crystallization of [Ti(Salpy)Cl] (**1**) did give crystals upon standing for several weeks. The structure is shown in Figure 2.14. The X-ray data were twinned and gave poor quality diffraction data, and so the data are not of the required standard for publication. Nevertheless, the connectivity is almost certainly correct and confirms that the ligand successfully binds to the Ti(III) in the expected manner, as depicted in Scheme 2.18. The most interesting feature is the co-ligand. In the structure, the chloride has been replaced by a π-coordinated O$_2$, presumably arising from fortuitous air ingress during the crystallization procedure. Similar complexes of titanium bearing a π-coordinated O$_2$ have been reported in the literature and have been crystallographically characterized.[58–67] In these cases, the O$_2$ moiety adopts the same binding mode as seen in **1B** in most cases; bridging motifs are also observed in the literature.[68–70] Since the complex in this thesis is a fortuitous crystal and could not be reproduced, no further data could be obtained. Insight into the bonding was obtained with DFT calculations (undertaken by Dr. Ben Ward), which shows that titanium (III) ion donates its unpaired electron to oxygen, formally giving a Ti(IV) ion and an O$_2^{2-}$ ligand (Figure 2.15). Whilst this was not the desired structure, it gives confidence that a) a titanium(III) complex was formed (otherwise the structure from the X-ray data would not have been obtained), b) the Salpy ligand is not affected/degraded by coordinating it to Ti(III) since it is intact in the observed structure, and c) the electron from the Ti(III) can be donated to an appropriate substrate, which is critical for catalytic purposes as described later in this thesis. Given the low quality data, it is inappropriate to comment on the metric parameters for this structure, other than to note that the Salpy ligand binds in a κ^5-motif, with the pyridyl coordinating to the metal centre and adopting a *β*-cis coordination geometry, with the two imine nitrogens, one phenoxide, and the O$_2$ occupying the equatorial plane, and the pyridyl and second phenoxide in the axial positions. It is noteworthy that several crystal structures of the Salpy ligand have been obtained for the aluminium as well as titanium isopropoxide complexes; in all cases only *β*-cis coordination geometries have been observed.[7,71]
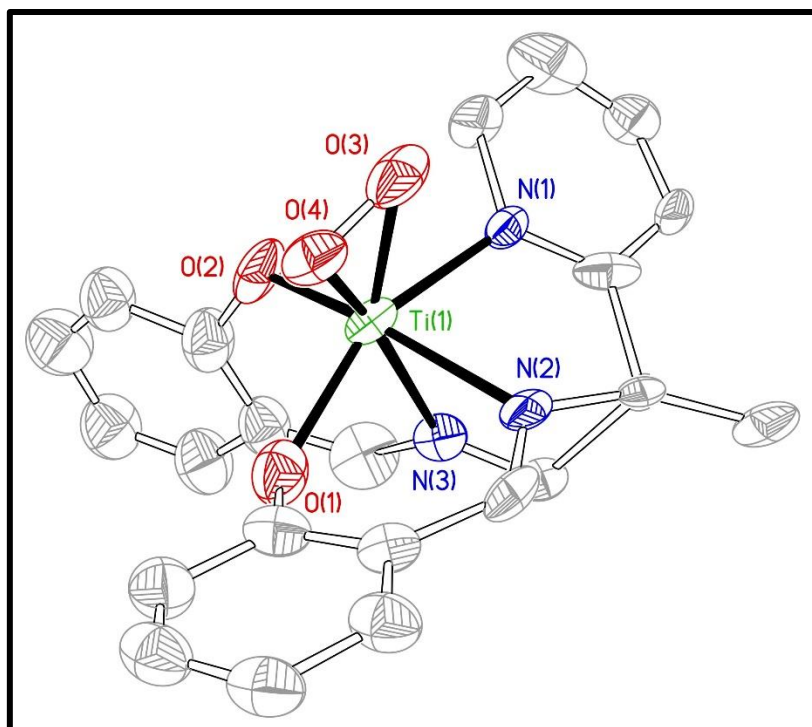
Figure 2.14: Molecular structure of [Ti(Salpy)(η^2-O$_2$)] **(1B)** Ellipsoids are shown at 30% probability level; hydrogens are omitted for clarity.
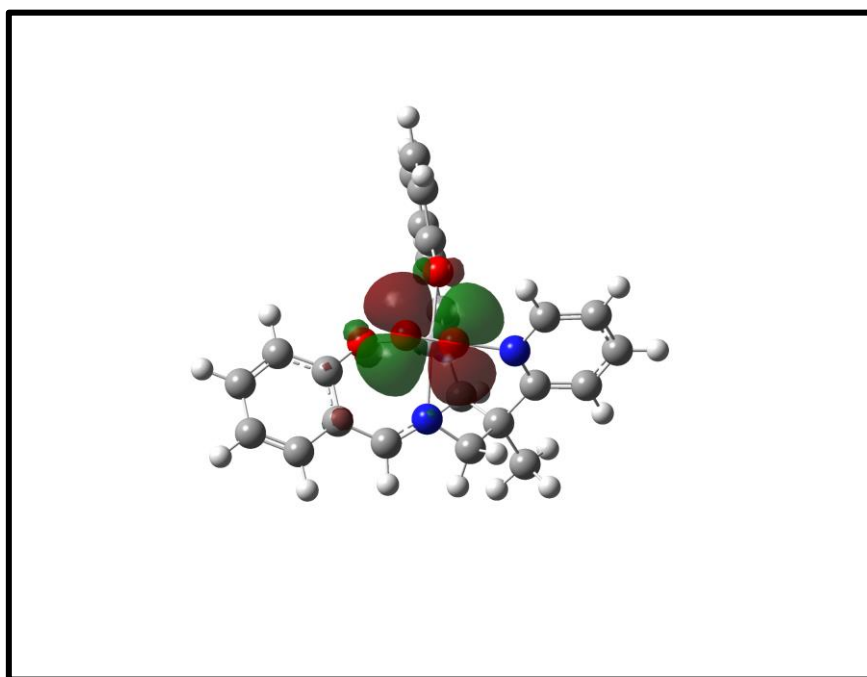
Figure 2.15: [Ti(Salpy)(η^2-O$_2$)] **(1B)**, DFT structure showing the SOMO drawn to an isosurface of 0.02 a.u. [M06 | def2-TZVP]

2.3.2 FT-IR studies :

2.3.2.1 Introduction:

Fourier transform infrared (FTIR) is considered an important analytical tool for researchers. This technique is very quick, excellent in accuracy, and comparatively sensitive.[72] In this method, samples are exposed to infrared radiation which affect the molecular vibrations in the sample and the intensities of either the transmitted or absorbed radiation are measured.[73] The IR spectrum can be divided into three regions:

a) Near-IR spectrum (13000-4000 cm^{-1})
b) Mid-IR spectrum (4000- 400 cm-1)
c) Far-IR spectrum (<400 cm^{-1})

In this study focus was placed on the mid-IR region (4000-400 cm^{-1}) which is most commonly used for routine characterization of samples. All pro-ligands, Ti(IV) and Ti(III) complexes were studied using FTIR spectroscopy. Interest has focused on selected bands which present considerable information about the structure to indicate the most probable manner in which the ligand is coordinated to the titanium ion. The coordination mode of the Schiff base ligand with the titanium atom in complexes could be determined by comparing the FTIR spectrum of the free Schiff base ligands with the spectrum of the corresponding titanium complex.

2.3.2.2 FT-IR for ligands:

There are three important functional groups in the Salen-type ligands under investigation that are important in the infrared spectra, Ar-O, C=N and O-H. Table 2.8 provides assignments of selected characteristic IR bands. In this region 4000-3000 cm^{-1} we expect to see O-H stretching vibration at about 3500 cm^{-1} in the free ligand spectrum. Yet, there are no absorption bands observed in this region but, alternatively, a weak intensity broad band can be seen at about ~2683-2543 cm ^{1} or about ~2960-2840 cm^{-1}.[74–77] This band is attributed to ν(O-H) stretching vibration; the internal hydrogen bonding with the imine nitrogen leads to a significant shift to this vibration to a lower frequency, and increasing the hydrogen bonding strength increases the frequency range such that this absorption sometimes is not observed.[76,78–86] This is especially true if the H bonding is combined with the ring resonance. Figure 2.16 illustrates the hydrogen bonding and the resonance of polar structures which leads to strong hydrogen bonding.[83]

70

These types of ligands contain intramolecular hydrogen bonding N---H-O between the nitrogen of imine group and the enolic hydrogen in the same molecule which are usually very strong.[81,82,84] To allow the hydrogen bonding to contribute with the phenyl resonance, it is required that the six-membered ring including the hydrogen bond to be planar or coplanar to the phenyl ring.[83] ligands are nearly planar with sufficient intramolecular distances that allowed the formation of intramolecular hydrogen bonds.[87] The presence of electron donating groups on the aromatic rings increases the electron density on the oxygen atom of the hydroxyl groups which makes the bond O-H stronger and the absorption bands appears more broad.[78]
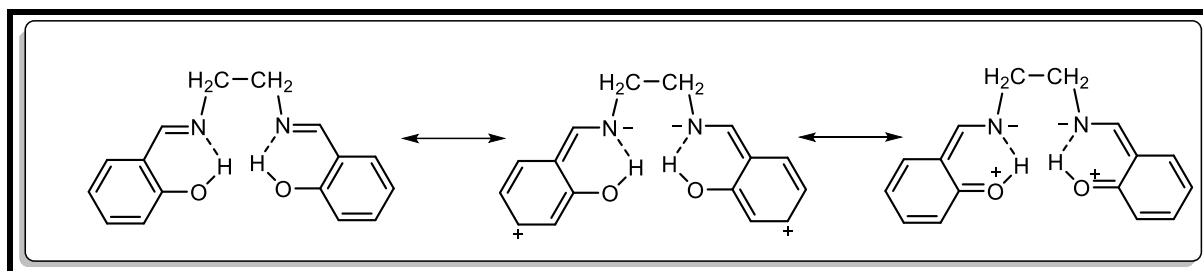
Figure 2.118: Intramolecular hydrogen bond[83]

Bands observed at ~3092-3001 cm^{-1} were assigned to aromatic C-H stretching vibration whereas the bands at ~2998-2903 cm^{-1} and ~2898-2835 cm^{-1} were assigned to the presence of symmetric and asymmetric of aliphatic C-H stretching vibration of CH_2 and CH_3.

The area from 2000-1000 cm^{-1} contains important bands. The C=N stretching frequencies lie in the range ~1640-1611 cm^{-1} and are in agreement with other similar Schiff bases.[39,88,89] The present ligands exhibited the imine v(C=N) stretching vibration with strong and sharp intensity in the range of ~1636-1618 cm^{-1}. v(C=N) stretching vibration in H_2Naphpy was the lowest for which this band observed at 1618 cm^{-1}. The shift in Naphpy ligand is due to the increased resonance because of the extra phenyl ring, which causes increased resonance about of C=N bond. The ligand H_2Salpy-Me does not exhibit this band as the bond C=N been reduced to C-N. The C-N stretching vibration appears within the 1385-1303 cm^{-1} range as reported for similar Schiff bases.[78,84]

In addition to C=N stretching vibration, these ligands show characteristic aromatic stretches v(C=C) in the range 1608-1433 cm^{-1}. However, these overlap with C-H asymmetric bending of CH_3 and alkene CH_2 and are therefore not diagnostic in this case.

The C-O phenolic stretching vibrations were observed at about 1325-1215 cm⁻¹, consistent with values for similar ligands which are found in the region ~1340-1210 cm⁻¹ [76,78,84,90].

The aromatic rings are known to give absorptions in the region 900-670 cm⁻¹ which correspond to C-H out-of-plane bending deformation vibrations.[73] Two to three strong bands in the region 884-713 cm⁻¹ of the prepared ligands are attributed to this vibration mode.

In all ligands, there were no bands assigned to $v(N-H_2)$ or $v(C=O)$ stretching vibrations that are exist in the diamine or salicylaldehyde derivatives which confirm the complete condensation, and the ligands are successfully synthesized.

Table 2.8: Assignments in FT-IR of prepared Salen-type Schiff base ligands (in cm⁻¹)

Ligand	v(C=N)	v (C=C)	v (C-N)	v (Ar-O)
H₂Salpy	1628	1578, 1497, 1472, 1456	1333	1275
H₂Salpy-Me	-	1587, 1489 1471, 1458	1385	1251
ᵗBu,ᵗBu-H₂Salpy	1624	1589,1470, 1457,1438	1361	1248
ᵗBu,OMe-H₂Salpy	1636	1602, 1590, 1465, 1456	1356	1325
Me-H₂Salpy	1631	1590, 1457, 1447, 1434	1305	1270
Cl,Cl-H₂Salpy	1636	1589,1558, 1507, 1456	1338	1215
Ad,Me-H₂Salpy	1631	1593, 1475, 1448, 1435	1315	1251
H₂Naphpy	1618	1543, 1528, 1491, 1444	1303	1258
H₂Salpn	1630	1608, 1579, 1496, 1458	1316	1273
ᵗBu,ᵗBu-H₂Salpn	1629	1589, 1465, 1439	1361	1241
Me-H₂Salpn	1628	1608, 1491, 1455, 1433	1318	1263

2.3.2.3 FT-IR for the complexes:

The reactions of Schiff base ligands with $TiCl_4(THF)_2$ (**2.26**) or $TiCl_3(THF)_3$ (**2.28**) yield mononuclear complexes where ligands are coordinated to the central titanium atom as dianionic tetradentate ligand. A vibrational spectrum offers useful information about the nature of functional groups bonded to the metal ion in a complex. Infrared spectra of the complexes were recorded in KBr pellets with a Shimadzu IRAffinity-1 FTIR spectrometer from 4000 to 400 cm^{-1}. The characteristic IR frequencies of the complexes along with their assignment are presented in tables 2.9 and 2.10.

The infrared spectra of the Schiff bases and their respective titanium complexes were very similar. In the infrared spectra of the titanium complexes, there are no broad bands in the region 3200 to 2500 cm^{-1}, assigned to the O-H stretch. The absence of this band indicates the deprotonation of the phenolic OH group upon complexation.[74,91,92] Representative IR spectra of a free ligand and the corresponding titanium complexes are presented in Figure 2.17.
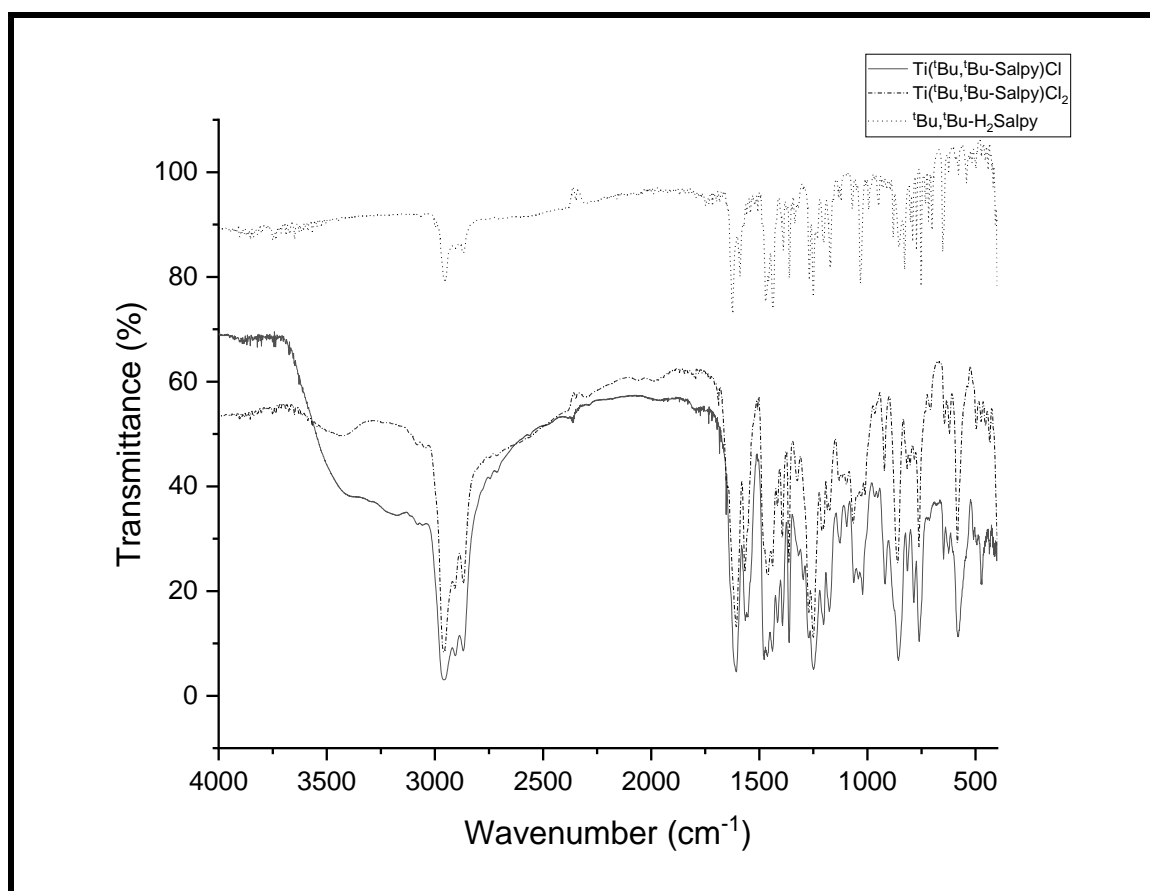
Figure 2.17: FT-IR spectrum of $^tBu,^tBu-H_2Salpy$ and the corresponding Ti(III) and Ti(IV) complexes

C-H stretching bands for aromatic CH and aliphatic CH, CH_2 and CH_3 remained at almost unchanged frequencies, with almost the same intensities compared to the free ligands. In contrast, upon complexation the imine bands $v(C=N)$ were shifted to a lower wavenumber compared to the free ligands, by 17-38 cm^{-1} for the titanium complexes bearing $^tBu,^tBu$-H_2Salpy, $^tBu,OMe$-H_2Salpy, Me-H_2Salpy, Cl,Cl-H_2Salpy and Ad, Me-H_2Salpy. This shift indicates the direct coordination of the ligand through the nitrogen of the imine group.[86,93,94] This shift can be attributed to the reduction of the electron density in the azomethine bond (C=N) when the lone pair of the imine nitrogen atom coordinate to the titanium ion.[78,79,85,95–97] This connection could be supported by the appearance of additional weak bands in the spectra of the complexes, at ~591-491 cm^{-1} corresponding to M-N stretching vibration.[94,98] This band has been assigned in the region 600-450 cm^{-1} based on previous studies.[74,85,91,93] In the Ti complexes of H_2Salpy, $H_2Naphpy$, H_2Salpn and $^tBu,^tBu$-H_2Salpn $v(C=N)$ were shifted toward higher frequency by about 8-30 cm^{-1}; the shift of this band vibration to higher wavenumber has been seen by Ueno et al. and it is also an evidence of the coordination of the imine nitrogen atoms to the titanium atom.[74,83,85,99–103]

The observed bands in the region 1600-1400 cm^{-1} were assigned to aromatic $v(C=C)$ stretching vibrations and are slightly affected by complexation(~2-16 cm^{-1}).[81,83,99]

Phenolic $v(C-O)$ stretching vibration was found in the range of ~1367-1247 cm^{-1} and are shifted to higher frequencies upon coordination, which confirms the involvement of the oxygen atoms of deprotonated phenolic groups to the metal ion. This observation is due to the replacement of the hydrogen atoms in the Schiff bases by Ti^{III} or Ti^{IV} ions, which leads to an increase in the π bond character in the Ar-O bond.[78,104] This coordination is also supported by the assignments of the weak bands in ~485-436 cm^{-1} to the new Ti-O bonds. The $v(M-O)$ stretching vibration bond have been assigned to the region ~489-370 cm^{-1}.[85,91,93,94,98] The exception for that is [Ti(Me-Salpy)Cl$_2$] (**12**) (which show a slightly downward shift of 3 cm^{-1} in $v(C-O)$ vibration, this observation is also seen by others.[75,83,93,99]

Ti-N and Ti-O bands appear as new peaks in the spectra of the complexes and are not observed in the FTIR spectra of the ligands. $v(C-N)$ bands have been reported in the region of ~1390-1350 cm^{-1} and are found in the present complexes in the 1393-1319 cm^{-1} region.[78] All the FTIR data indicates that the titanium atom was bonded to the ligand through the azomethine nitrogen and the phenolic oxygen,[78,96,99,105,106] and are therefore consistent with the proposed structures and those determined using X-ray crystallography.

Table 2.9: Assignments in FT-IR of prepared Ti(IV) complexes (in cm^{-1})

Complex	$\check{V}$(C=N)	$\check{V}$ (C=C)	$\check{V}$ (C-N)	$\check{V}$ (Ar-O)
[Ti(Salpy)Cl$_2$] (8)	1647	1602,1558, 1538, 1462	1334	1276
[Ti(Salpy-Me)Cl$_2$] (9)	-	1595,1572, 1481,1452	1387	1259
[Ti(^{t}Bu,^{t}Bu-Salpy)Cl$_2$)] (10)	1607	1567, 1478, 1462,1440	1364	1251
[Ti(^{t}Bu,OMe-Salpy)Cl$_2$] (11)	1598	1562, 1457, 1427	1393	1348
[Ti(Me-Salpy)Cl$_2$] (12)	1609	1591,1573, 1528,1453	1318	1267
[Ti(Cl,Cl-Salpy)Cl$_2$] (13)	1606	1546,1450, 1437	1364	1286
[Ti(Ad,Me-Salpy)Cl$_2$] (14)	1603	1564, 1487, 1451	1329	1260
[Ti(Naphpy)Cl$_2$] (15)	1591	1549,1511, 1460	1344	1291
[Ti(Salpn)Cl$_2$] (16)	1659	1599, 1553, 1473, 1453	1326	1277
[Ti(^{t}Bu,^{t}Bu-Salpn)Cl$_2$] (17)	1654	1612,1565, 1465,1437	1367	1247
[Ti(Me-Salpn)Cl$_2$] (18)	1609	1591, 1574, 1456, 1432	1319	1273

New absorption bands in the region ~652-599 cm^{-1} appear for the titanium complexes, which are assigned to the $\check{v}$(Ti-Cl) stretching vibrations.[94] Finally, there are no bands that is characteristic of $\check{v}$(Ti=O) in titanium complexes (strong band at ~1100-900 cm^{-1}) which suggests the existence of non-oxotitanium in the metal chelates under investigation.[41,98,107,108]

Table 2.10: Assignments in FT-IR of prepared Ti(III) complexes (in cm^{-1})

Complex	ν(C=N)	ν (C=C)	ν (C-N)	ν (Ar-O)
[Ti(Salpy)Cl] (1)	1646	1605, 1546, 1474, 1457	1341	1277
[Ti(Salpy-Me)Cl] (2)	-	1595, 1570, 1480, 1456	1385	1263
[Ti(^{t}Bu,^{t}Bu-Salpy)Cl)] (3)	1607	1563, 1478, 1464, 1440	1363	1250
[Ti(Cl,Cl-Salpy)Cl] (4)	1609	1544, 1523, 1438	1387	1288
[Ti(Naphpy)Cl] (5)	1597	1548, 1513, 1468	1343	1289
[Ti(Salpn)Cl] (6)	1659	1604,1545, 1473, 1455	1325	1290
[Ti(tBu,tBu-Salpn)Cl] (7)	1659	1612, 1565, 1461, 1440	1364	1248

2.3.3 Nuclear magnetic resonance (NMR) studies:

The ^{1}H and ^{13}C NMR spectra of the ligands and their Ti(IV) complexes were obtained in CDCl$_3$ at 400 MHz or 500 MHz at room temperature, and chemical shifts expressed in units of ppm relative to TMS. ^{1}H and ^{13}C assignments were proved when required with the use of two dimentional ^{1}H-^{1}H and ^{13}C-^{1}H NMR experiments. The ^{1}H and ^{13}C NMR data and assignments are presented in Tables 2.11-2.14.

2.3.3.1 ^{1}H and ^{13}C NMR studies for the free ligands:

The most diagnostic chemical shifts from the ^{1}H and ^{13}C NMR spectra of the ligands are presented in tables 2.11 and 2.12, respectively. Figure 2.18 depicts the numbering system used in assigning the NMR signals. ^{1}H NMR spectra of similar ligands have been reported.[76,78,109] The ^{1}H NMR spectrum of the ligands in this thesis showed a broad singlet at low field at δ= 13.19-13.82 ppm, corresponding to the phenolic protons (Ar-OH). The integration of this signal usually is less than 2.0 as a result of intramolecular hydrogen bonding that makes the signals broad (figure 2.16); traces of water in the NMR solvent can also give rise to a slightly low integration.[78,83] The high chemical shift of this signal is attributed to the

strong impact of the deshielded oxygen atom.[110] In Cl,Cl-H$_2$Salpy and H$_2$Naphpy this peak is shifted downfield (14.07, 14.55 ppm, respectively) as the H proton being less shielded due to the increased resonance and the withdrawing groups in H$_2$Naphy and Cl,Cl-H$_2$-Salpy respectively. On the other hand, as seen in Table 2.11, this peak shifted by 3.7 ppm lower in the H$_2$-Salpy-Me compared to H$_2$Salpy due to the weaking in the intramolecular hydrogen bonding between the amine nitrogen and the phenolic OH compared to the imine ligand.
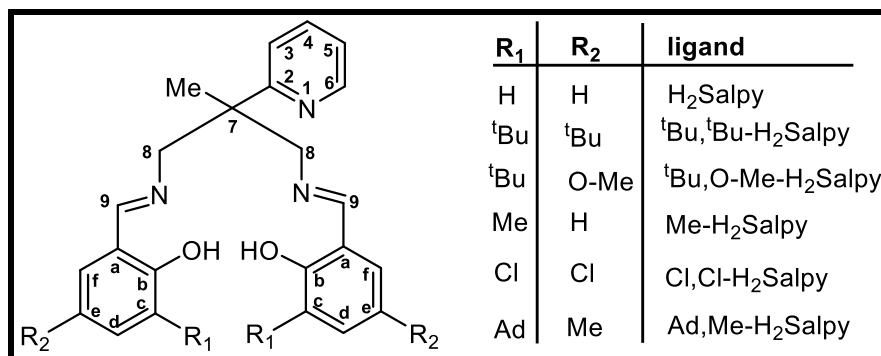
Figure 2.18: General formula of the ligand and the numbering system.

A singlet at δ=8.73-8.18 ppm appears for all ligands (except for H$_2$Salpy-Me), and is attributed to the imine proton (-N=CH, position 9), and is consistent with literature values.[17,78,86,88,93,94,110,111] The presence of this signal, and the absence of the broad peak in the region 5.0-8.0 ppm due to the free amine protons, confirm the formation of the Schiff base in the condensation reaction between diamine and salicyaldehyde. The appearance of one singlet signal for the two imine protons confirm the C$_s$ symmetry for these ligands. Also, the observation of a peak at δ= 167.34-165.02 ppm in the ^{13}C NMR spectra of the ligands (except for H$_2$Naphpy which shows this signal at 173.98 ppm) which is attributed to the corresponding imine carbon is further proof that the ligands were successfully synthesized. The (=CH) in these ligands is *sp^2* hybridized and is not terminal and known to show NMR signal at about 140 ppm.[110] Nevertheless, in these types of ligands this signal is seen at high chemical shift due to the deshielding caused by the π system and the electronegative N atom.

Each aryl group has four, three or two protons in the molecule with different environments and were observed in the range 7.77-6.62 ppm. The carbon atoms in the aryl group are observed from 161.21 ppm to 107.16 ppm. The chemical shifts for C$_b$ bonded to the phenolic oxygen were the highest value in the phenol ring and observed at ~161.27-155.07 ppm, due to the presence of the electronegative oxygen.[110] In the Salpy ligands, introducing

the electron donating group (-OMe) to the *para* position to C_b cause the greatest upfield shift to this carbon signal by 6.14 ppm compared to H_2Salpy ligand (where the substituents are hydrogen atoms). The signal for C_a bonded to the azomethine group showed at ~121.95-118.92 ppm and is the least affected carbon by the substitution on the ring.

For the pyridyl ring, present in all Salpy ligands, protons in position 6 have the highest chemical shift after the phenolic protons. The chemical shifts for H_6 were observed between 8.64-8.60 ppm; the ^{13}C chemical shifts for C_6 were observed between 149.39 and 149.07 ppm. The ^{13}C NMR signals for C_2 are following the CH=N signals with ~163.86-162.09 ppm. In general, the ^{1}H NMR and ^{13}C NMR chemical shifts in pyridyl ring are almost have the same value in all Salpy derivatives with no noticeable effect of the substituents group on the aromatic ring. The largest shift (compared to the H_2Salpy ligand) is only 0.16 and 1.71 ppm in the ^{1}H and ^{13}C NMR spectra, respectively.

The methyl protons (-Me) in the Salpy ligands appear at 1.67-1.53 ppm and the corresponding carbons appear at ~22.44-20.75 ppm, these values lie in the sp^3 hybridized carbon atom region. The sp^3 hybridized methylene carbon (-CH$_2$) when present in the middle of the molecule usually appears at about 30 ppm.[110] However, in the Salen-type ligands these groups (at position 8) shows downfield signals (^{1}H NMR~4.17-3.72, ^{13}C NMR~67.95-56.85 ppm) and this can be ascribed to the presence of electronegative nitrogen atom and the existence of π bonds adjacent to the -CH$_2$ groups which leads to deshielding of this group and as a result the signals appear more downfield.[110] In the Salpn ligands this signal appears as a triplet at δ= 3.71-3.72 due to the coupling with the adjacent CH$_2$ protons. In the Salpy ligands the adjacent carbon has no protons and ^{t}Bu,^{t}Bu-H$_2$Salpy and ^{t}Bu,OMe-H$_2$Salpy ligands ^{1}H NMR spectra shows singlet at 4.06 and 4.07 ppm, respectively, represent the four methylene protons which confirm the equivalents chemical environment of these protons. However, in H$_2$Salpy, H$_2$Salpy-Me, Me-H$_2$Salpy, Cl, Cl-H$_2$Salpy and H$_2$Naphpy the resonances appeared as two doublets, each representing one of the -CH$_2$ group protons in the ligand, with corresponding geminal proton- proton coupling constant (^{2}J$_{HH}$) is ~13.2-12.2 Hz. This happens since these protons are diasterotopic which makes them inequivalent with different chemical shifts, therefore appears as doublet signal. The reason why two doublets are appeared because the two methylene groups are chemically equivalent (a mirror plane passes between the two groups). In Ad, Me-H$_2$Salpy this signal represents second order AB quartet at δ= 4.04 ppm for the two inequivalent methylene protons (^{2}J$_{HH}$=12.2 Hz). From the above discuss it can be concluded that the chemical environment around the methylene protons strongly influences its chemical shift pattern leading to two distinct doublets, enclosed doublets, second order AB quartet or singlet as seen in Figures 2.19 and 2.20.
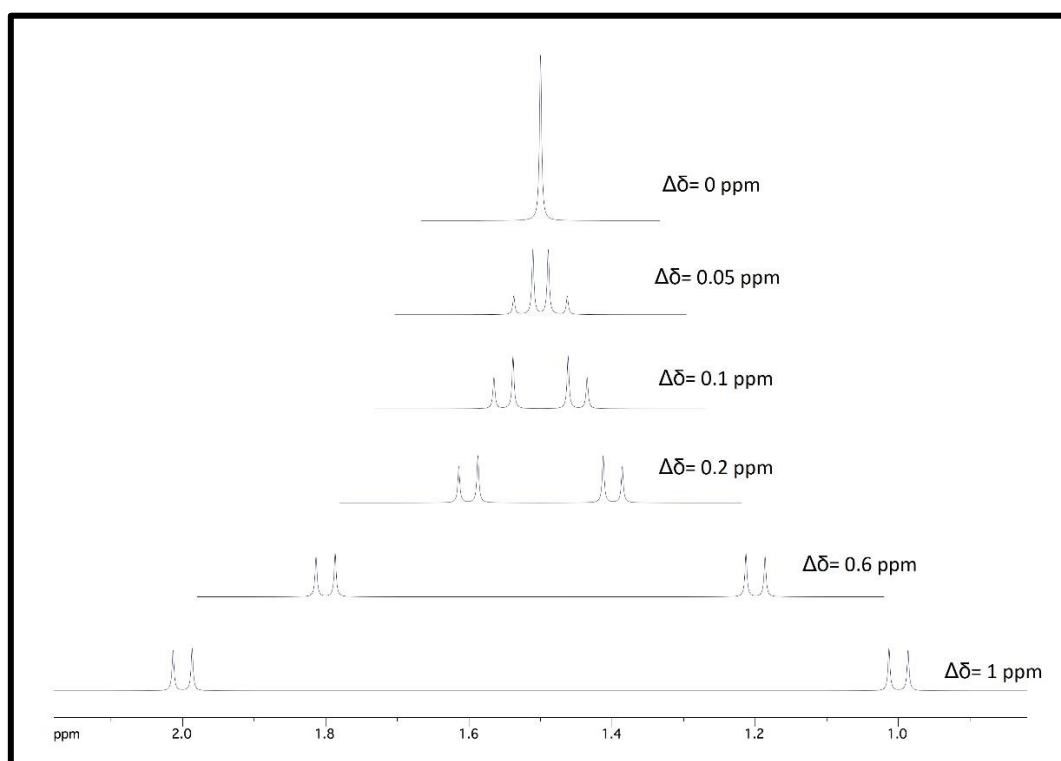
Figure 2.19: Simulated signals of methylene mutually coupled doublets; the only difference between each spectrum is the difference in chemical shift of the two signals.
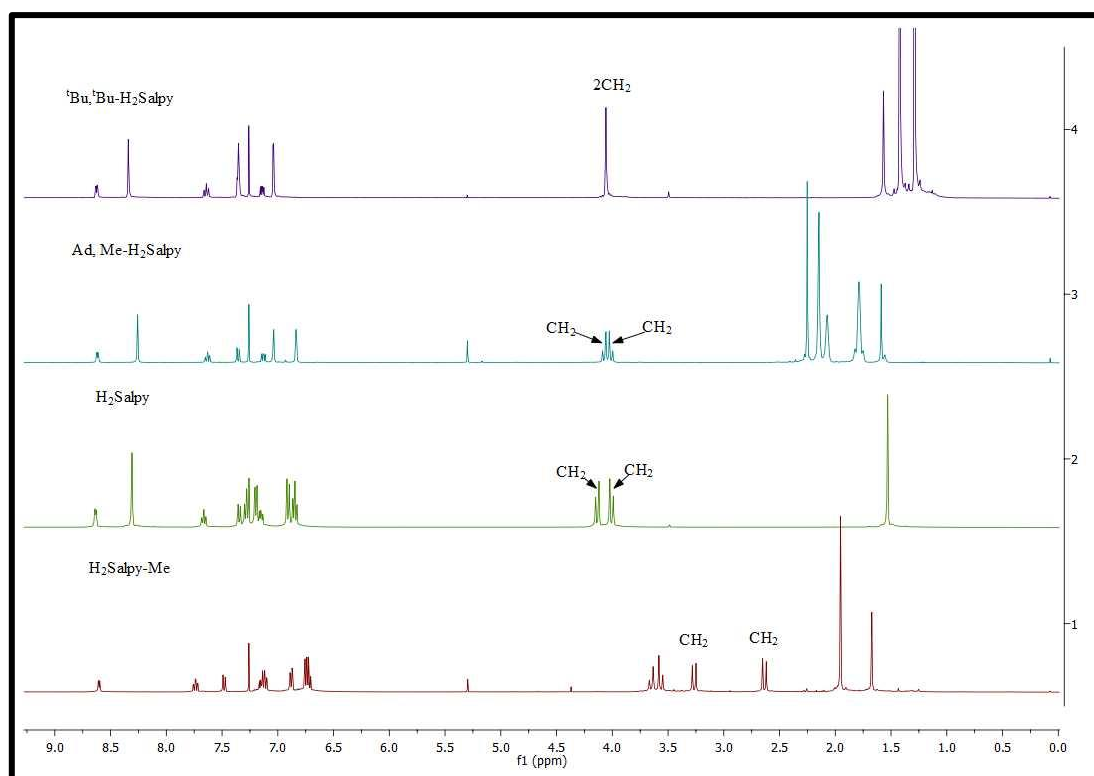
Figure 2.20: ^{1}H NMR (400 MHz, CDCl$_3$, 293 K) spectra for different ligands showing different - CH$_2$ chemical shifts.

The -OMe group NMR signal in $^tBu,OMe-H_2Salpy$ was observed as singlet at 3.75 ppm in the ^1H NMR spectrum, and at 55.94 ppm in the ^{13}C NMR spectrum and are at the same chemical shift found in OMe-H_2salen.[78]

Table 2.11: Assignment of Ligands' diagnostic ^1H NMR signals in CDCl$_3$ (δ, ppm)

Ligand	OH	H$_6$	N=CH	Ar-H	Py-H	H$_8$	-Me
H$_2$Salpy	13.19	8.64	8.31	7.28, 7,20, 6.91, 6.85	7.67, 7.33, 7.15	4.14, 4.01	1.53
H$_2$Salpy-Me	10.20	8.60	-	7.21, 7.06, 6.88, 6.81-6.62	7.74, 7,48, 7.21-7.06	3.27, 2.64	1.67
$^tBu,^tBu-H_2Salpy$	13.53	8.62	8.34	7.38-7.32, 7.04	7.64, 7.38-7.32, 7.14	4.06	1.57
$^tBu,OMe-H_2Salpy$	13.28	8.62	8.28	6.94, 6.55	7.64, 7.36, 7.14	4.07	1.58
Me-H$_2$Salpy	13.39	8.63	8.29	7.19-7.11, 7.05, 6.76	7.66, 7.36, 7.19-7.11	4.12, 4.04	1.57
Cl,Cl-H$_2$Salpy	14.07	8.61	8.18	7.38, 7.08	7.66, 7.30, 7.16	4.15, 4.05	1.56
Ad,Me-H$_2$Salpy	13.53	8.62	8.26	7.04, 6.84	7.63, 7.36, 7.13	4.07, 4.01	1.59
H$_2$Naphpy	14.55	8.76	8.73	7.77-7.64, 7.59, 7.31 6.95	7.77-7.64, 7.37, 7.25-7.17	4.17, 4.04	1.65
H$_2$Salpn	13.43	-	8.38	7.32, 7.25, 6.97, 6.88	-	3.72	-
$^tBu,^tBu-H_2Salpn$	13.82	-	8.39	7.39, 7.09	-	3.71	-
Me-H$_2$Salpn	13.74	-	8.36	7.21, 7.11, 6.82	-	3.72	-

Table 2.12: Assignment of Ligands diagnostic ^{13}C NMR signals in CDCl$_3$ (δ, ppm)

Ligand	N=CH	C$_2$	C$_6$	C$_b$	C$_a$	C$_8$	C$_7$	-Me
H$_2$Salpy	166.27	163.33	149.15	161.21	118.71	67.21	46.26	21.84
H$_2$Salpy-Me		163.37	149.07	157.54	121.95	67.95	46.67	20.75
^{t}Bu,^{t}Bu-H$_2$Salpy	167.34	163.80	149.12	158.25	118.01	67.03	46.29	22.37
^{t}Bu,OMe-H$_2$Salpy	166.84	163.65	149.12	155.07	118.06	67.16	46.31	22.36
Me-H$_2$Salpy	166.54	163.40	149.10	159.48	118.08	67.22	46.26	21.99
Cl,Cl-H$_2$Salpy	165.02	162.09	194.39	157.06	119.41	66.45	46.26	21.69
Ad,Me-H$_2$Salpy	167.24	163.74	149.09	158.57	118.50	67.41	46.39	22.44
H$_2$Naphpy	173.98	161.69	149.48	159.73	118.23	62.00	46.43	21.47
H$_2$Salpn	165.60	-	-	161.27	118.79	56.97	-	-
^{t}Bu,^{t}Bu-H$_2$Salpn	166.62	-	-	158.26	117.99	56.90	-	-
Me-H$_2$Salpn	165.76	-	-	159.57	118.09	56.85	-	-

2.3.3.2 ^{1}H and ^{13}C NMR studies of Ti(IV) complexes:

The ^{1}H NMR spectrum of the Ti(III) complexes were not informative due to the paramagnetic nature of Ti(III) compounds (no observable signals between +100 and -100 ppm at 293 K, 400 MHz). However the NMR spectra of the Ti(IV) complexes supported the proposed structures; information could be obtained by comparing the NMR data of the complexes with those of the free ligands (Table 2.13 and Table 2.14). The NMR spectra showed complete conversion to titanium complexes. The very low solubility of some complexes in deuterated solvents hindered their NMR characterization.

Upon coordination, the ^{1}H NMR spectra of the complexes shows the disappearance of the phenolic proton signals, which indicates the deprotonation and coordination of the negatively charged oxygen to the titanium cation (Ar-O-Ti).[45,93,97,99]

The imine proton signals are shifted downfield in the Salpy complexes by 1.09-0.34 ppm. This deshielding is probably as a result of the donation of the nitrogen imine lone pair to the titanium ion.[74,76,86,88,98,103,107] However, the titanium complexes with salpn ligands were shifted slightly upfield by about 0.13-0.11 ppm. The upfield shift in the imine proton signals also observed by Fonseca and others and they ascribed that to the vicinity to the metal centre.[39,93,111,112] The presence of one sharp singlet signal assigned to the two imine protons in the complexes suggests that the magnetic environment is the same for all these protons, consistent with the solid-state structures. The ^{13}C NMR spectral data of the complexes showed the displacement to downfield of the imine carbon resonance from δ 167.34, 166.84 and

166.54 ppm in ^{t}Bu,^{t}Bu-H$_2$Salpy, ^{t}Bu,O-Me-H$_2$Salpy and Me-H$_2$Salpy ligands to δ 169.88, 169.38 and 168.92 ppm, respectively, in the respective complexes.[97] Conversely, in [Ti(^{t}Bu,^{t}Bu-Salpn)Cl$_2$] (**17**) and [Ti(Me-Salpn)Cl$_2$] (**18**) this signal was shifted upfield by 0.18 and 0.66 ppm.[93,102]

The ^{13}C NMR signals of the phenolic group carbons were shifted by 2.42-2.05 ppm downfield in the complexes [Ti(^{t}Bu,^{t}Bu-Salpy)Cl$_2$] (**10**), [Ti(^{t}Bu,O-Me-Salpy)Cl$_2$] (**11**), [Ti(^{t}Bu,^{t}Bu-Salpn)Cl$_2$] (**17**) and [Ti(Me-Salpn)Cl$_2$] (**18**) and by 2.03 ppm upfield in [Ti(Me-Salpy)Cl$_2$] (**12**) compared to the proligands. In general, the aromatic ^{1}H NMR and ^{13}C NMR signals (aryl and pyridyl) showed a downfiled shift in complexes compared to the free ligands.

In the Salpy complexes, C$_2$ exhibited an upfield shift by 3.8, 6.08 and 1.2 ppm in [Ti(^{t}Bu,^{t}Bu-Salpy)Cl$_2$] (**10**), [Ti(^{t}Bu,O-Me-Salpy)Cl$_2$] (**11**) and [Ti(Me-Salpy)Cl$_2$] (**12**), respectively. Likewise, the C$_6$ carbon signals are shifted upfield in the complexes [Ti(^{t}Bu,^{t}Bu-Salpy)Cl$_2$] (**10**), [Ti(^{t}Bu,O-Me-Salpy)Cl$_2$] (**11**) and [Ti(Me-Salpy)Cl$_2$] (**12**) by about 3.55, 6.64 and 4.1 ppm, respectively.

The chemical shift of the H$_6$ resonance in pyridyl group can be an indicative of the coordinative state of pyridyl nitrogen.[3,4,113] Therefore, no or only little shift in this resonance relative to the free ligand can indicate that the pyridyl nitrogen is not coordinated to the metal. The H$_6$ proton in Ti(IV) Salpy complexes exhibited slightly downfield shift (0.23-0.12 ppm) and this can be used as an evidence that the pyridyl nitrogen does not participate in the coordination. The absence of a downfield H$_6$ signal in the spectrum of complex **10** is evidence that the solid state structure differs than the solution state structure and corresponds to a rearrangement product.

A downfield shift also observed in the ^{1}H and ^{13}C NMR shifts of the alkyl groups (-CH$_3$ and -N-CH$_2$-) in all complexes compared to the free ligands. Meanwhile, the peaks representing the four protons of the two -CH$_2$ groups in ^{t}Bu,^{t}Bu-H$_2$Salpy, ^{t}Bu,O-Me-H$_2$Salpy ligands transformed from the singlet found in the ligand to two doublets, Figure 2.21 represent the ^{1}H NMR spectra for ^{t}Bu,^{t}Bu-H$_2$Salpy and the corresponding complex and indicates the sensitivity of the CH$_2$ signals to the coordination environment. Nevertheless, that the -CH$_2$ proton chemical shifts in Salpn ligands and its titanium(IV) complexes are observed as one set of triplets confirm that the two half of these compounds are equivalent by symmetry (Figure 2.22).[79] The rest of signals show slight shifts as a result of metal complexation.

The shifting of the signal in the complexes compared to the ligands is a good indication about the successful formation of the complexes and that the Ti(IV) metal centre is coordinated to the ligand via O,N,N,O sites.[39,94] Therefore, the ^{1}H and ^{13}C NMR confirmed the dibasic

tetradentate nature of the Schiff bases under investigation which already indicated by the FT-IR and crystallographic studies.
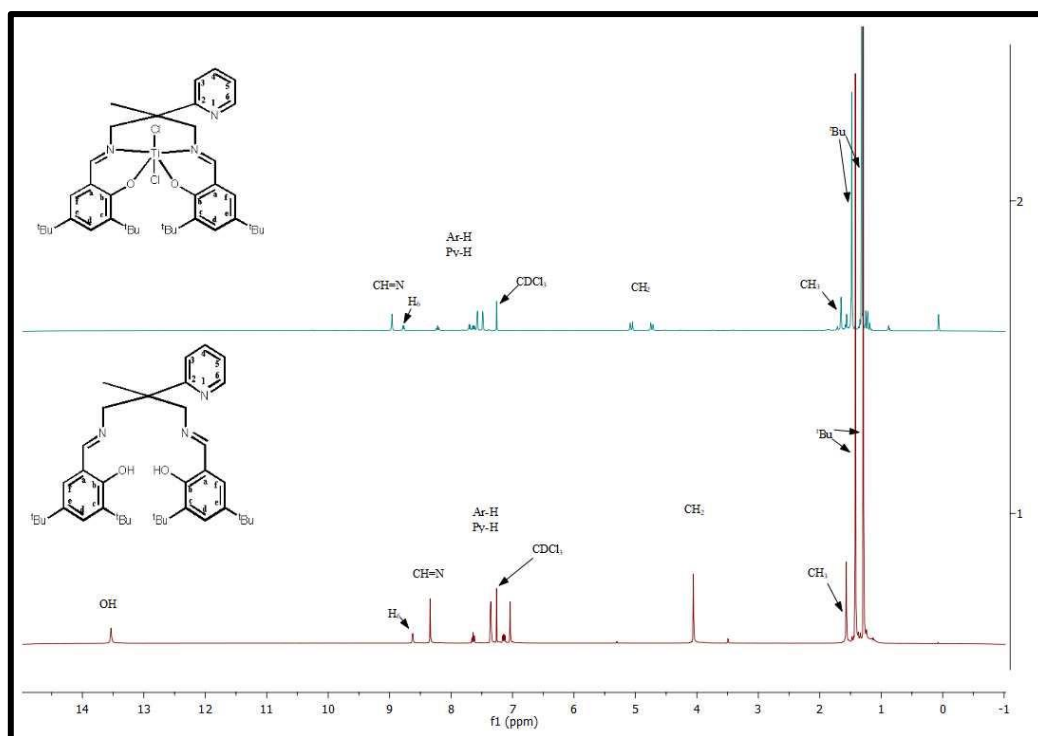
Figure 2.21: ^{1}H NMR (400 MHz, CDCl$_3$, 293 K) spectra of ^{t}B,^{t}Bu-H$_2$Salpy and its complex (**10**) with Ti(IV) in CDCl$_3$
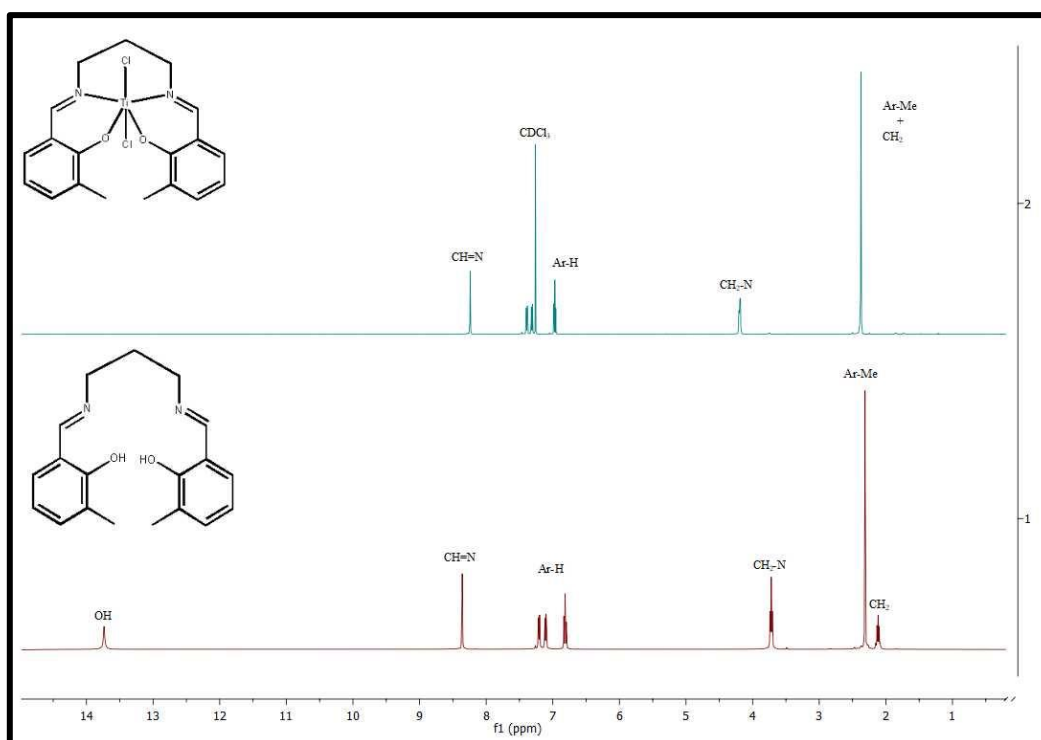
Figure 2.22: ^{1}H NMR (400 MHz, CDCl$_3$, 293 K) spectra of Me-H$_2$Salpn and [Ti(Me-Salpn)Cl$_2$] **(18)** in CDCl$_3$.

Table 2.13: Assignment of Ti(IV) complexes diagnostic ^{1}H NMR signals in CDCl$_3$ (δ, ppm)

Complex	H$_6$	N=CH	Ar-H	Py-H	H$_8$	-Me
[Ti(Salpy)Cl$_2$] (8)	8.83	9.03	7.70-7.65, 7.10, 6.83	8.23,7.70-7.65,7.6	5.09 4.85	1.69
[Ti(^{t}Bu,^{t}Bu-Salpy)Cl$_2$] (10)	8.78	8.96	7.57, 7.48	8.22,7.70, 7.63	5.07 4.73	1.65
[Ti(^{t}Bu,OMe-Salpy)Cl$_2$] (11)	8.77	8.96	7.11, 7.00	8.22, 7.71, 7.64		
[Ti(Me-Salpy)Cl$_2$] (12)	8.75	9.03	7.51, 7.37, 6.96	8.19, 7.65, 7.60	5.07 4.84	1.66
[Ti(Cl,Cl-Salpy)Cl$_2$] (13)	8.84	9.07	7.59 (4H)	8.27, 7.72, 7.55	5.15 4.90	1.70
[Ti(Naphpy)Cl$_2$] (15)	8.82	9.82	8.65-8.53, 7.99 7.85-7.79, 7.76-7,68, 7.48, 7.03	8.65-8.53, 7.76-7.68, 7.48	5.30 5.01	1.78
[Ti(Salpn)Cl$_2$] (16)	-	8.27	7.54, 7.48, 7.08, 6.91	-	4.21	-
[Ti(^{t}Bu,^{t}Bu-Salpn)Cl$_2$] (17)	-	8.26	7.57, 7.29	-	4.14	-
[Ti(Me-Salpn)Cl$_2$] (18)	-	8.24	7.39, 7.31, 6.97	-	4.19	-

Table 2.14: Assignment of some Ti(IV) complexes diagnostic ^{13}C NMR signals in CDCl$_3$ (δ, ppm)

Complex	N=CH	C$_2$	C$_6$	C$_b$	C$_a$	C$_8$	C$_7$	-Me
[Ti(^{t}Bu,^{t}Bu-Salpy)Cl$_2$] (10)	169.88	160.53	145.57	157.59	127.05	70.09	45.03	28.51
[Ti(^{t}Bu,OMe-Salpy)Cl$_2$] (11)	169.38	157.57	142.48	157.47	126.48	69.93	44.98	28.54
[Ti(Me-Salpy)Cl$_2$] (12)	168.92	162.20	145.60	157.45	125.63	69.62	45.43	28.47
[Ti(^{t}Bu,^{t}Bu-Salpn)Cl$_2$] (17)	166.44	-	-	160.31	127.07	62.90	31.46	-
[Ti(Me-Salpn)Cl$_2$] (18)	165.10	-	-	161.99	125.82	63.51	28.46	-

2.3.4 UV spectroscopic studies:

The absorption spectra of the ligands and their complexes were measured in THF in the range 200-800 nm at room temperature (Table 2.15). Titanium (IV) complexes were obtained as dark orange to red solids and Ti(III) complexes were obtained as dark green solids. All the ligands were yellow solids. Indeed, the change in colour during the complexation reactions is a good indication that the ligand has coordinated to the titanium ions. These new colours could be attributed to the ligand to metal charge transfer (LMCT) or metal to ligand charge transfer (MLCT). Since Ti(IV) ions contains an empty valence shell d^0, and do not exhibit d-d transitions. Ti(III) complexes can show d-d transitions but will we comparatively weak.

Schiff bases usually show three absorption bands due to π→π* transitions (at higher energy) in the ligands aromatic rings, n→π* transition of the nonbonding electrons located on the nitrogen of the imine groups and the third band attributed to n→π* transitions involving C=N and phenolic groups.[86,114–116]

The UV-Vis spectra of the complexes exhibited similar absorption spectra as the ligand but with some shifts in absorption maxima. A new absorption band should be found in the 300-400 nm region, however, in most cases they are difficult to distinguish as they overlapped with the strong absorptions a rise from the aromatic species of the ligands. This band can be assigned to LMCT which might be occur from the π orbitals of the ligand to the d orbitals of titanium.[78,94,109]

All titanium complexes show three sets of bands, falling in the range 261-465 for Ti(IV) complexes and in the range 246-433 nm for Ti(III) complexes. An additional band should be observed for Ti(III) complexes due to d-d transition as Ti(III) has an electronic configuration of d^1, nevertheless, this peak was not observed which might be attributed to the low concentration of the solutions (10^{-4},10^{-5} M).

A representative UV spectrum of the free ligand and the corresponding titanium complexes is presented in Figure 2.23. It can be concluded that a shift to longer wavelength in the spectral bands of the complexes with respect to the free ligands infers that the titanium-ligand interaction is strong in this type of complexes.[84,93]
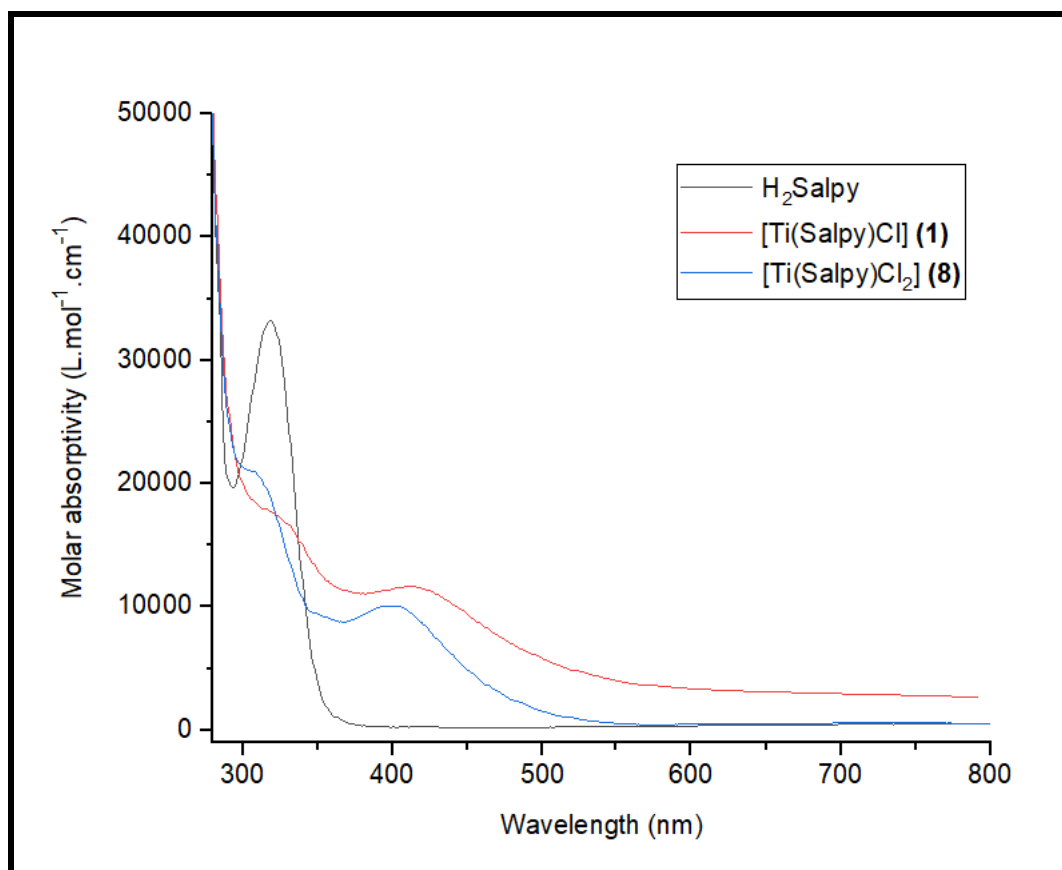
Figure 2.23: UV-Vis spectra of H$_2$Salpy ligand and its Ti(III) and Ti(IV) complexes (1×10^{-5} M in THF at 25 °C).

Table 2.15: UV-Vis spectral data of some ligands and their corresponding Ti(III) and Ti(IV) complexes.

Ligand	Electronic spectra λ_{max} (nm)	Complex	Electronic spectra λ_{max} (nm)
H$_2$Salpy	247,285,319	[Ti(Salpy)Cl] **(1)**	246, 324, 415
		[Ti(Salpy)Cl$_2$] **(8)**	262,309,398
^{t}Bu,^{t}Bu-H$_2$Salpy	235, 265, 332	[Ti(^{t}Bu,^{t}Bu-Salpy)Cl] **(3)**	261, 325, 418
		[Ti(^{t}Bu,^{t}Bu-Salpy)Cl$_2$] **(10)**	272, 325, 425
Cl,Cl-H$_2$Salpy	252, 337, 436	[Ti(Cl,Cl-Salpy)Cl] **(4)**	286, 329, 400
		[Ti(Cl,Cl-Salpy)Cl$_2$] **(13)**	270, 287, 396
H$_2$Salpn	232, 257, 319	[Ti(Salpn)Cl] **(6)**	265, 294,322
		[Ti(Salpn)Cl$_2$] **(16)**	266, 303, 387
^{t}Bu,^{t}Bu-H$_2$Salpn	250, 330	[Ti(^{t}Bu,^{t}Bu-H$_2$Salpn)Cl] **(7)**	262, 325, 410
		[Ti(^{t}Bu,^{t}Bu-H$_2$Salpn)Cl$_2$] **(17)**	261, 319, 405

2.3.5 Mass spectra:

The mass spectra of the Schiff base ligands were measured in high resolution mode using atmospheric solid analysis probe (ASAP) mass spectrometry for the most ligands. It displayed ion peaks at m/z =$[M+1]^+$ which is consistent with the molecular weight of the ligands M with an added proton. Ad,Me-H_2Salpy and H_2Salpn ligands were measured using high resolution electron ionization (EI) spectrometry which show a molecular ion peaks at m/z= 669.42 and 282.13, corresponding to $[M]^+$.

All the complexes have been analysed using high resolution mass spectra EI or ASAP. The mass spectra of the prepared complexes supported the suggested formula by showing a series of peak at different m/z ratios. The molecular ions were observed at $[M-Cl]^+$ in all Ti(IV) complexes except for **(16)** and **(17)** as it appeared at $[M]^+$ which correspond to the molecular weight of the respective compounds. However, the molecular ion in Ti(III) complexes showed at $[M]^+$, the exception is **(5)** which appeared as $[M-Cl]^+$.

2.3.6 EPR spectroscopy:

Samples for EPR measurements were prepared under an N_2 atmosphere in a glovebox. A solution of each complex was prepared by dissolving ca. 4 mg in 200 µL of dry THF (in all cases, a small quantity of dry toluene was also added to improve the quality of the glass formed in frozen solution). The solutions were transferred to a Young's EPR tube, and then cooled to 77 K before rapid transfer to the pre-cooled EPR cavity. The X-band CW EPR measurements were performed on a Bruker EMX spectrometer utilizing an ER4119HS resonator, 100 kHz field modulation at 140 K. EPR simulations were performed using the Easyspin toolbox.[117]

Computational details:

All density functional theory (DFT) calculations were carried out with ORCA (version 4.0.0.2).[118] The fully relaxed geometry optimisations were taken from crystallographic refinements using the BP86 density functional, making use of the zeroth order relativistic correction ZORA retaining one centre terms. The CoreProp basis set was used on the Ti atom, EPRII basis set was used for all C/H/N atoms and the ZORA-def2-TZVP basis sets were used for all Cl atoms.

The CW X-band EPR spectra for a representative series of the Ti(III) complexes are presented in Figure 2.24. As can be seen, all spectra display a predominantly rhombic profile

characterized by $g_1 > g_2 > g_3$. Notably, all of the g-values are lower than free spin ($g_e \approx 2.0023$), which is to be expected for a d^1 ion in which the spin-orbit coupling to empty molecular orbitals produces a negative contribution to each component of the **g**-tensor.[119,120] No hyperfine from the Ti centre can be resolved due to the low natural abundance of spin-active nucleus ($I(^{47}Ti)$ = 5/2, 7.4%; $I(^{49}Ti)$ = 7/2, 5.4%). Furthermore, no superhyperfine coupling to the spin-active ^{14}N ligand nuclei is observed, resulting from only a small amount of electron delocalisation onto the ligand, giving rise to couplings that are smaller than the intrinsic linewidth and therefore remaining unresolved. These EPR spectra are conclusive evidence of successful reduction of the Ti(IV) to Ti(III) to form a paramagnetic d^1 system, and are similar to other rare example of Ti^{3+} centred organometallic complexes presented in the literature.[121,122]

Unfortunately, due to challenges with poor solubility in a wide range of solvents and resulting difficulties in obtaining a suitable frozen glass, the spectra are affected by artefacts arising from an inhomogeneous system. The appearance of micro-crystallites in the frozen sample creates regions of defined orientation with respect to the external magnetic field, resulting in off-axis resonances.

In Figure 2.25a, the experimental spectrum for [Ti(Salpy)Cl] (**1**) is presented alongside a simulation (Fig 2.25b) to extract the spin Hamiltonian values, which are listed in Table 2.16. Also included are computational simulations based upon the DFT calculations of both the trans- (Fig 2.25c) and cis- (Fig 2.25d) isomers of this complex. Whilst neither of the calculated parameters are an exact match for the experimental spectra, we determined that the values for the cis-isomer are marginally better, and hence hereafter DFT calculations were only performed on the cis-isomer of the remaining complexes.

Pleasingly, the experimental observations are in good agreement with the spin Hamiltonian values calculated via DFT using the ORCA programme, as listed in Table 2.16. The calculations correctly identify a rhombic **g**-tensor and small unresolvable nitrogen superhyperfine couplings. Whilst there is some discrepancy between the absolute values of the experimental and calculated **g**-tensor (notably, the calculations do not correctly predict $g_{iso} > g_e$), this is within the acceptable errors arising from assumptions within the DFT methods.
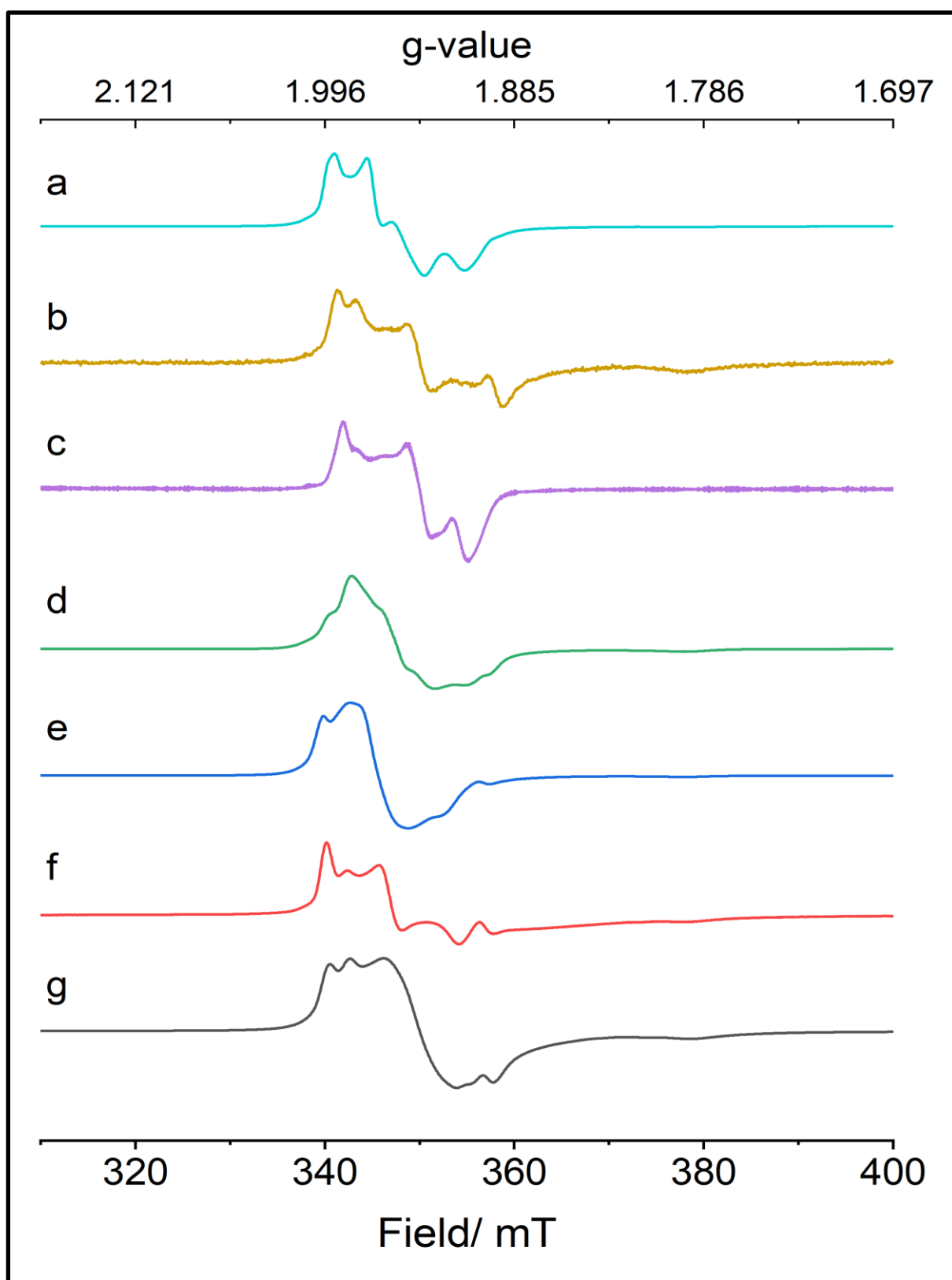
Figure 2.24: CW X-band EPR spectra (T = 140 K) of complexes (a) **4**, (b) **5**, (c) **6**, (d) **7**, (e) **1**, (f) **2** and (g) **3**. Complexes **2**, and **3** were prepared via reduction in-situ over Zn from the Ti(IV) precursor, followed by filtration (20 mM in THF + 20 μL toluene).
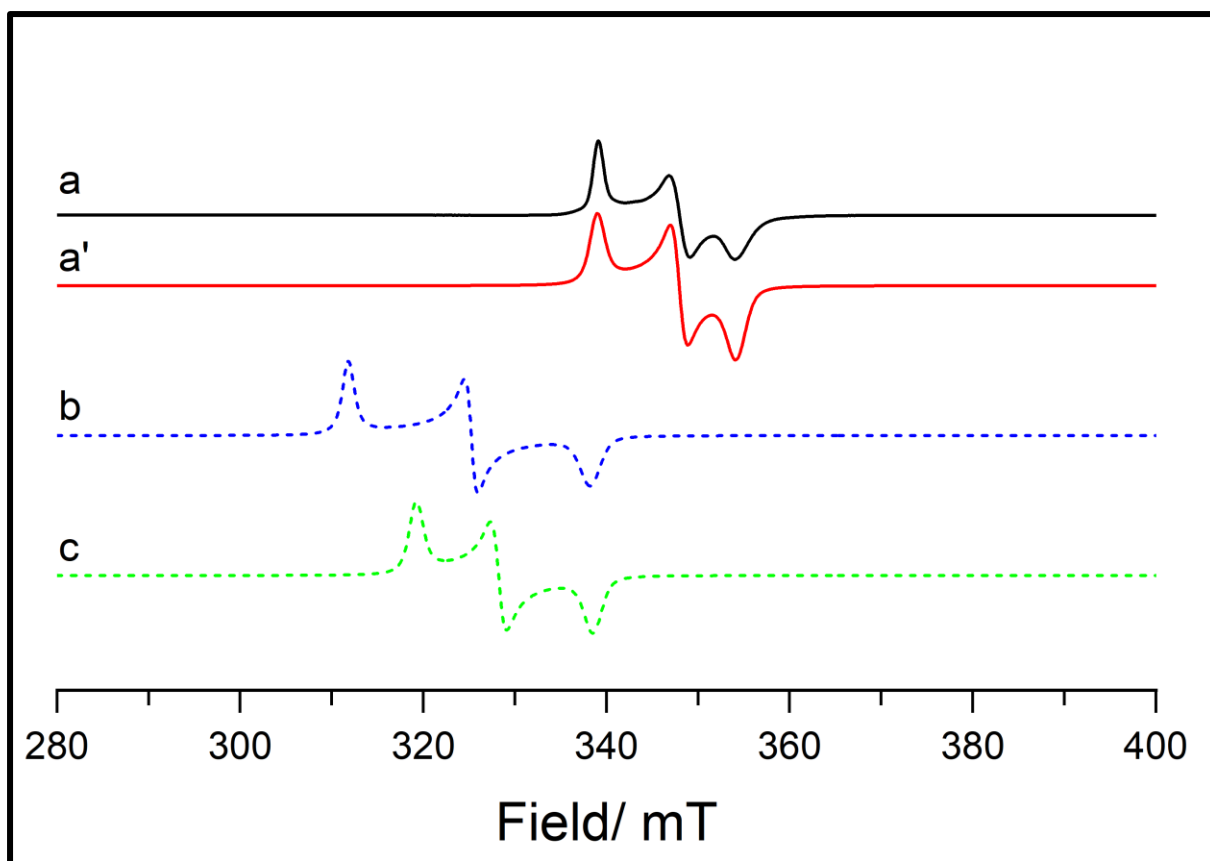
Figure 2.25: (a) Experimental (T = 140 K) and (a`) simulated CW X-band EPR spectrum of complex **1**. Simulations based on computational calculations of geometry optimised structures of (b) trans and (c) cis isomers.

Table 2.16: Experimental (via simulation) and calculated (ORCA DFT) spin Hamiltonian parameters for a series of Ti(III) complexes.

	g-tensor				Euler angle/ rad			Nucs	Superhyperfine coupling/ MHz				Euler angle/ rad		
Complex	g1	g2	g3	giso	α	β	γ		a|A1|	|A2|	|A3|	aiso	α	β	γ
Expt															
1	1.904	1.938	1.989	1.944	3.711	2.324	1.751								
DFT															
T534b Cis-1	1.992	2.054	2.112	2.053	3.711	2.324	1.751	N1	6.86	7.34	7.54	7.25	0.598	2.061	2.252
								N2	6.74	7.07	8.77	7.52	1.999	0.804	3.419
								N3	6.55	7.43	8.60	7.52	6.214	1.942	1.768
T989	1.993	2.073	2.163	2.076	3.785	0.022	1.024	N1	7.21	7.24	8.48	7.64	1.546	1.622	3.945
Trans-1								N2	7.06	7.12	8.33	7.50	1.408	1.496	3.975
								N3	2.30	2.62	2.97	2.63	2.935	0.064	3.586
T1010	1.990	2.059	2.110	2.053	6.126	0.512	1.702	N1(py)	7.28	7.86	7.99	7.71	6.002	2.230	4.144
5								N2	7.51	7.91	9.95	8.46	4.468	0.807	2.577
								N3	6.31	7.38	8.25	7.31	0.097	1.796	4.136
T1012	1.923	1.989	2.116	2.009	6.043	1.532	2.228	N1	7.91	8.10	10.04	8.68	4.496	1.242	2.603
6								N2	8.63	9.20	10.80	9.54	4.331	0.510	1.361
T1009	1.992	2.053	2.086	2.044	6.092	0.720	1.759	N1(py)	6.99	7.48	7.87	7.45	0.488	1.069	0.717
4								N2	6.38	6.74	8.33	7.15	4.286	0.835	2.583
								N3	5.96	7.19	8.14	7.10	0.069	1.793	4.199

[a] all components of the superhyperfine tensor are of the same sign (calculated as negative in the ORCA output)

2.4 Conclusion:

In this chapter, three types of ligands have been prepared by the Schiff base condensation. These are: the Salpn ligands, which were synthesised from the reaction of 1,3-diaminopropane with two equivalents of salicylaldehyde or its derivatives; Salpy ligands which were prepared from the treatment of 2-methyl-2-(pyridine-2-yl)propane-1,3-diamine (ppda) with salicylaldehyde or its derivatives in 1:2 ratio; lastly, Naphpy ligand which were obtained by the condensation of one equivalent of the ppda with two equivalents 2-hydroxynaphthaldehyde. Salpn ligands contain N_2O_2 potential donor sets with imine nitrogens and phenols oxygens donors. Salpy and Naphpy contain an additional pyridyl group which makes them N_3O_2 donor sets. All these ligands were fully characterized by mass spectrometry, FT-IR, UV-Vis, ^1H and $^{13}C\{^1H\}$ NMR spectroscopy.

A series of Ti(IV) complexes were successfully synthesized in high yields by the direct reaction of the precursor $TiCl_4(THF)_2$ and the prepared ligands in THF in 1:1 ratio. The single crystal structures of five complexes have been solved by X-ray crystallography which indicated distorted octahedral geometry around the metal centres. Due to the present the rigid tetradentate ligand, the two labile chloride ligands are forced to be in trans position while the ligand occupied the equatorial position via ONNO sites, which is unusual for the Salpy ligands. The Ti(IV) Salpy complexes were found to undergo a redistribution process in ether solution to give a separated ion pair; the formation of these products is attributed to the dissociation of coordinated HCl from the pendant pyridyl. All Ti(IV) complexes have been studied using high resolution mass spectrometry, IR and UV-Vis spectroscopies, and nuclear magnetic resonance (^1H and $^{13}C\{^1H\}$ NMR).

Seven Ti(III) complexes have been prepared by reducing the analogous Ti(IV) complexes using zinc dust as reducing agent. All these complexes have been characterized using high resolution mass spectrometry, FT-IR and UV-Vis spectroscopy, and by electron paramagnetic resonance spectroscopy (EPR). However, the ^1H NMR spectrum of the Ti(III) complexes were not informative due to their paramagnetic nature; in every case the spectra showed no evidence for any diamagnetic species which evidences the complete conversion of Ti(IV) to Ti(III).

2.5 References:

1   P. G. Cozzi, *Chem. Soc. Rev.*, 2004, **33**, 410–421.

2   Y. Gürsoy Tuncer, K. Gürpınar, N. Acar, H. Nazır, I. Svoboda, O. Atakol and E. K. İnal, *J. Mol. Struct.*, 2020, **1221**, 128789.

3   R. Shakya, A. Jozwiuk, D. R. Powell and R. P. Houser, *Inorg. Chem.*, 2009, **48**, 4083–4088.

4   S. Friedrich, M. Schubart, L. H. Gade, I. J. Scowen, A. J. Edwards and M. McPartlin, *Chem. Ber.*, 1997, **130**, 1751–1759.

5   A. Sattler, J. A. Labinger and J. E. Bercaw, *Organometallics*, 2013, **32**, 6899–6902.

6   H. Shi and Y. Yin, *Inorganica Chimica Acta*, 2014, **421**, 446–450.

7   M. A. Bahili and B. D. Ward, *unpublished results*.

8   X. Zhang, T. J. Emge and K. C. Hultzsch, *Angewandte Chemie International Edition*, 2012, **51**, 394–398.

9   S. Shaw and J. D. White, *Chem. Rev.*, 2019, **119**, 9381–9426.

10   S. J. Coles, M. B. Hursthouse, D. G. Kelly, A. J. Toner and N. M. Walker, *J. Chem. Soc., Dalton Trans.*, 1998, 3489–3494.

11   F. L. Bowden and D. Ferguson, *J. Chem. Soc., Dalton Trans.*, 1974, 460–462.

12   R. H. Holm, G. W. Everett and A. Chakravorty, in *Progress in Inorganic Chemistry*, John Wiley & Sons, Ltd, 1966, pp. 83–214.

13   P. C. H. Mitchell and D. A. Parker, *J. Chem. Soc., Dalton Trans.*, 1972, 1828–1831.

14   G. Dell'Amico, F. Marchetti and C. Floriani, *J. Chem. Soc., Dalton Trans.*, 1982, 2197–2202.

15   E. Solari, C. Floriani, A. Chiesi-Villa and C. Rizzoli, *J. Chem. Soc., Dalton Trans.*, 1992, 367–373.

16   L. E. Manxzer, J. Deaton, P. Sharp and R. R. Schrock, in *Inorganic Syntheses*, John Wiley & Sons, Ltd, 1982, pp. 135–140.

17   H. Chen, P. S. White and M. R. Gagné, *Organomet.*, 1998, **17**, 5358–5366.

18   J.-H. Kim and G.-J. Kim, *Catal. Lett.*, 2004, **92**, 123–130.

19   M. Pasquali, F. Marchetti, A. Landi and C. Floriani, *J. Chem. Soc., Dalton Trans.*, 1978, 545–549.

20   A. Chatterjee, T. H. Bennur and N. N. Joshi, *J. Org. Chem.*, 2003, **68**, 5668–5671.

21   A. Bensari, J.-L. Renaud and O. Riant, *Org. Lett.*, 2001, **3**, 3863–3865.

22   J. Streuff, M. Feurer, P. Bichovski, G. Frey and U. Gellrich, *Angew. Chem. Int. Ed.*, 2012, **51**, 8661–8664.

23   J. Streuff, *Synthesis*, 2013, **45**, 281–307.

24 W. Hao, J. H. Harenberg, X. Wu, S. N. MacMillan and S. Lin, *J. Am. Chem. Soc.*, 2018, **140**, 3514–3517.

25 G. Fachinetti, C. Floriani, M. Mellini and S. Merlino, *J. Chem. Soc., Chem. Commun.*, 1976, **0**, 300–301.

26 Y. Wang, Y. Qin, X. Wang and F. Wang, *ACS Catal.*, 2015, **5**, 393–396.

27 N. A. Jones, S. T. Liddle, C. Wilson and P. L. Arnold, *Organomet.*, 2007, **26**, 755–757.

28 W. C. Schumb and R. F. Sundström, *J. Am. Chem. Soc.*, 1933, **55**, 596–604.

29 F. Calderazzo, G. E. D. Benedetto, U. Engler, I. Ferri, G. Pampaloni and T. Wagner, *Z. Naturforsch B*, 1996, **51**, 506–516.

30 C. Eden, H. Feilchenfeld and D. Zehavi, *J. Inorg. Nucl. Chem.*, 1961, **22**, 153–155.

31 J. Balsells, P. J. Carroll and P. J. Walsh, *Inorg. Chem.*, 2001, **40**, 5568–5574.

32 A. J. Chmura, M. G. Davidson, M. D. Jones, M. D. Lunn, M. F. Mahon, A. F. Johnson, P. Khunkamchoo, S. L. Roberts and S. S. F. Wong, *Macromolecules*, 2006, **39**, 7250–7257.

33 S. Gendler, S. Segal, I. Goldberg, Z. Goldschmidt and M. Kol, *Inorg. Chem.*, 2006, **45**, 4783–4790.

34 A. Yeori, S. Groysman, I. Goldberg and M. Kol, *Inorg. Chem.*, 2005, **44**, 4466–4468.

35 S. Groysman, E. Sergeeva, I. Goldberg and M. Kol, *Eur. J. Inorg. Chem.*, 2005, **2005**, 2480–2485.

36 E. Y. Tshuva and D. Peri, *Coord. Chem. Rev.*, 2009, **253**, 2098–2115.

37 D. Peri, S. Meker, M. Shavit and E. Y. Tshuva, *Chem. Eur. J.*, 2009, **15**, 2403–2415.

38 A. Tzubery and E. Y. Tshuva, *Inorg. Chem.*, 2011, **50**, 7946–7948.

39 R. K. Gurung, C. D. McMillen, W. L. Jarrett and A. A. Holder, *Inorg. Chim. Acta*, 2020, **505**, 119496.

40 I. Kim, Y. S. Ha, D. F. Zhang, C.-S. Ha and U. Lee, *Macromol. Rapid Commun.*, 2004, **25**, 1319–1323.

41 N. F. Choudhary, P. B. Hitchcock and G. J. Leigh, *Inorg. Chim. Acta*, 2000, **306**, 24–29.

42 T. Repo, M. Klinga, M. Leskelä, P. Pietikäinen and G. Brunow, *Acta Cryst C*, 1996, **52**, 2742–2745.

43 C. Floriani, *Polyhedron*, 1989, **8**, 1717–1722.

44 J. P. Corden, W. Errington, P. Moore and M. G. H. Wallbridge, *Chem. Commun.*, 1999, 323–324.

45 B. Gao, X. Li, R. Duan and X. Pang, *New J. Chem.*, 2015, **39**, 2404–2408.

46 L. Yangang and J. Guoxin, *Chin.Sci.Bull.*, 2004, **49**, 1236–1240.

47 C. R. Groom, I. J. Bruno, M. P. Lightfoot and S. C. Ward, *Acta Cryst. B Struct. Sci. Cryst. Eng. Mater.*, 2016, **72**, 171–179.

48 A. Davis, C. A. Kilner and T. P. Kee, *Inorg. Chim. Acta*, 2004, **357**, 3493–3502.

49 B. Cordero, V. Gómez, A. E. Platero-Prats, M. Revés, J. Echeverría, E. Cremades, F. Barragán and S. Alvarez, *Dalton Trans.*, 2008, 2832–2838.

50 S. S. Batsanov, *Inorganic Materials*, 2001, **37**, 871–885.

51 Y. Zhao and D. G. Truhlar, *Theor Chem Account*, 2008, **120**, 215–241.

52 F. Weigend and R. Ahlrichs, *Phys. Chem. Chem. Phys.*, 2005, **7**, 3297–3305.

53 F. Weigend, *Phys. Chem. Chem. Phys.*, 2006, **8**, 1057–1065.

54 P. S. V. KUMAR, V. RAGHAVENDRA and V. SUBRAMANIAN, *J Chem Sci*, 2016, **128**, 1527–1536.

55 E. D. Glendening, C. R. Landis and F. Weinhold, *WIREs Computational Molecular Science*, 2012, **2**, 1–42.

56 F. Weinhold, *Journal of Computational Chemistry*, 2012, **33**, 2363–2379.

57 A. E. Reed, L. A. Curtiss and F. Weinhold, *Chem. Rev.*, 1988, **88**, 899–926.

58 Y.-C. Yang, Q.-X. Liu, Z.-H. Zhou and H.-L. Wan, *Dalton Trans.*, 2019, **48**, 16943–16951.

59 M. Rohe and K. Merz, *Chem. Commun.*, 2008, **0**, 862–864.

60 J. M. Stauber and C. C. Cummins, *Inorg. Chem.*, 2017, **56**, 3022–3029.

61 Y.-F. Deng and Z.-H. Zhou, *Inorg. Chem. Commun.*, 2008, **11**, 1064–1066.

62 J. R. Hagadorn and J. Arnold, *Inorg. Chem.*, 1997, **36**, 2928–2929.

63 M. Dakanali, E. T. Kefalas, C. P. Raptopoulou, A. Terzis, G. Voyiatzis, I. Kyrikou, T. Mavromoustakos and A. Salifoglou, *Inorg. Chem.*, 2003, **42**, 4632–4639.

64 P. Jeske, G. Haselhorst, T. Weyhermueller, K. Wieghardt and B. Nuber, *Inorg. Chem.*, 1994, **33**, 2462–2471.

65 A. Sofetis, F. Fotopoulou, C. P. Raptopoulou, T. F. Zafiropoulos, S. P. Perlepes and N. Klouras, *Polyhedron*, 2009, **28**, 3356–3360.

66 Z.-H. Zhou, Y.-F. Deng, Q.-X. Liu, H.-L. Zhang, T. C. W. Mak and Y. L. Chow, *Inorg. Chem.*, 2007, **46**, 6846–6848.

67 J. A. Kožíšková, M. Breza, M. Valko, P. Herich, L. Bučinský and J. Kožíšek, *IUCrJ*, 2021, **8**, 295–304.

68 A. Berkessel, T. Günther, Q. Wang and J.-M. Neudörfl, *Angew. Chem. Int. Ed.*, 2013, **52**, 8467–8471.

69 M. Lansing, H. Engler, T. M. Leuther, J.-M. Neudörfl and A. Berkessel, *ChemCatChem*, 2016, **8**, 3706–3709.

70 S. Kondo, K. Saruhashi, K. Seki, K. Matsubara, K. Miyaji, T. Kubo, K. Matsumoto and T. Katsuki, *Angew. Chem. Int. Ed.*, 2008, **47**, 10195–10198.

71 M. A. Bahili, E. C. Stokes, R. C. Amesbury, D. M. C. Ould, B. Christo, R. J. Horne, B. M. Kariuki, J. A. Stewart, R. L. Taylor, P. Andrew Williams, M. D. Jones, K. D. M. Harris and B. D. Ward, *Chem. Commun.*, 2019, **55**, 7679–7682.

72 N. Jaggi and D. R. Vij, in *Handbook of Applied Solid State Spectroscopy*, ed. D. R. Vij, Springer US, Boston, MA, 2006, pp. 411–450.

73 N. Asep Bayu Dani, R. Oktiani and R. Ragadhita, *Indon. J. Scie. Techn.*, 2019, **4**, 97–118.

74 A. Prakash, M. P. Gangwar and K. K. Singh, *J. Dev. Biol.*, 2011, **3**, 13–19.

75 B. S. Garg and D. Nandan Kumar, *Spectrochim. Acta A Mol. Biomol. Spectrosc.*, 2003, **59**, 229–234.

76 O. SignoriniE, R. Dockal, G. Castellano and G. Oliva, *Polyhedron*, 1996, **15**, 245–255.

77 D. N. Kumar and B. S. Garg, *Spectrochim. Acta A Mol. Biomol. Spectrosc.*, 2006, **64**, 141–147.

78 P. E. Aranha, M. P. dos Santos, S. Romera and E. R. Dockal, *Polyhedron*, 2007, **26**, 1373–1382.

79 R. Vafazadeh and M. Kashfi, *Bull. Korean. Chem. Soc.*, 2007, **28**, 1227–1230.

80 G. C. Pimentel, *The hydrogen bond*, Freeman, 1960.

81 J. A. Faniran, K. S. Patel and J. C. Bailar, *J. Inorg. Nucl. Chem.*, 1974, **36**, 1547–1551.

82 A. T. Mubarak, *Spectrochim. Acta A Mol. Biomol. Spectrosc.*, 2006, **65**, 1197–1207.

83 K. Ueno and A. E. Martell, *J. Phys. Chem.*, 1956, **60**, 1270–1275.

84 M. N. Uddin, D. A. Chowdhury and Md. A. H. Sarker, *Chiang Mai J. Sci.*, 2008, **35**, 483–494.

85 N. S. Biradar and V. H. Kulkarni, *J. Inorg. Nucl. Chem.*, 1971, **33**, 3847–3854.

86 H. Naeimi and M. Moradian, *J. Coord. Chem.*, 2010, **63**, 156–162.

87 H. H. Freedman, *J. Am. Chem. Soc.*, 1961, **83**, 2900–2905.

88 Z. Asadi and M. R. Shorkaei, *Spectrochim. Acta A Mol. Biomol. Spectrosc.*, 2013, **105**, 344–351.

89 C. R. Bhattacharjee, G. Das, P. Mondal and N. V. S. Rao, *Polyhedron*, 2010, **29**, 3089–3096.

90 Z.-L. You, Y. Lu, N. Zhang, B.-W. Ding, H. Sun, P. Hou and C. Wang, *Polyhedron*, 2011, **30**, 2186–2194.

91 M. N. Uddin, S. Khandaker, Moniruzzaman, Md. S. Amin, W. Shumi, Md. A. Rahman and S. M. Rahman, *Journal of Molecular Structure*, 2018, **1166**, 79–90.

92 N. S. Biradar, V. B. Mahale and V. H. Kulkarni, *Inorg. Nucl. Chem. Lett.*, 1972, **8**, 997–1002.

93 F. K. Ommenya, E. A. Nyawade, D. M. Andala and J. Kinyua, *J. Chem.*, 2020, **2020**, e1745236.

94 M. N. Uddin, M. S. Amin, M. S. Rahman, S. Khandaker, W. Shumi, M. A. Rahman and S. M. Rahman, *Appl. Organomet. Chem.*, 2021, **35**, e6067.

95 J. Uttamchandani and R. N. Kapoor, *Transit. Met. Chem.*, 1978, **3**, 79–81.

96 M. N. Uddin, D. A. Chowdhury and K. Hossain, *J. Chin. Chem. Soc.*, 2012, **59**, 1520–1527.

97 S. K. Che Soh and M. Shamsuddin, *J. Chem.*, 2013, **2013**, 1–8.

98 M. N. Uddin, Z. A. Siddique, N. Mase, M. Uzzaman and W. Shumi, *Appl. Organomet. Chem.*, 2019, **33**, e4876.

99 J. Liu, B.-W. Wu, B. Zhang and Y. Liu, *Turk. J. Chem.*, 2006, **30**, 41–48.

100 X. Li, B. Yang, H. Zheng, P. Wu and G. Zeng, *PLOS ONE*, 2018, **13**, e0201054.

101 G.-H. Sheng, F.-Y. Xu, F.-Y. Tian, L.-Y. Liu, Z.-L. You and H.-L. Zhu, *Synth. React. Inorg. Met. Org. Chem.*, 2014, **44**, 1247–1250.

102 A. Yardan, A. Karahan, N. B. Arslan, C. Hopa, M. Gokmen, C. Kazak and R. Kurtaran, *Synth. React. Inorg. Met. Org. Chem.*, 2015, **45**, 1224–1233.

103 A. Varshney, J. P. Tandon and A. J. Crowe, *Polyhedron*, 1986, **5**, 739–742.

104 Y.-X. Sun and X.-H. Gao, *Synth. React. Inorg. Met. Org. Chem.*, 2011, **41**, 973–978.

105 O. V. Kotova, S. V. Eliseeva, A. S. Averjushkin, L. S. Lepnev, A. A. Vaschenko, A. Yu. Rogachev, A. G. Vitukhnovskii and N. P. Kuzmina, *Russ. Chem. Bull.*, 2008, **57**, 1880–1889.

106 K. C. Gupta and A. K. Sutar, *React. Funct. Polym.*, 2008, **68**, 12–26.

107 M. N. Uddin, S. Khandaker, Moniruzzaman, Md. S. Amin, W. Shumi, Md. A. Rahman and S. M. Rahman, *J. Mol. Struct.*, 2018, **1166**, 79–90.

108 M. Gullotti and A. Pasini, *Inorg. Chim. Acta*, 1975, **15**, 129–136.

109 R. C. Felicio, E. T. G. Cavalheiro and E. R. Dockal, *Polyhedron*, 2001, **20**, 261–268.

110 A. F. Zahoor, M. Yousaf, M. Pervaiz, A. Anjum, K. G. Ali, F. M. Zahid, S. Ahmad, S. A. Bukhari and B. Parveen, *Asian J. Chem.*, 2014, **26**, 841–845.

111 J. Fonseca, J. Martinez, L. Cunha-Silva, A. L. Magalhães, M. T. Duarte and C. Freire, *Inorg. Chim. Acta*, 2010, **363**, 4096–4107.

112 B. V. Agarwala, S. Hingorani, V. Puri, C. L. Khetrapal and G. A. Naganagowda, *Transit. Met. Chem.*, 1994, **19**, 25–27.

113 B. D. Ward, S. R. Dubberley, L. H. Gade and P. Mountford, *Inorg. Chem.*, 2003, **42**, 4961–4969.

114 R. Shakya, D. R. Powell and R. P. Houser, *Eur. J. Inorg. Chem.*, 2009, **2009**, 5319–5327.

115 D. S. Wankhede, S. Hussain, N. Jadhav, P. B. Wagh, M. D. Chaudhari, A. G. Murke and O. Shankarrao, *Der Chemica Sinica*, 2013, **4**, 79–85.

116 S. K. Tadavi, J. D. Rajput, S. D. Bagul, A. A. Hosamani, J. N. Sangshetti and R. S. Bendre, *Res. Chem. Intermed.*, 2017, **43**, 4863–4879.

117 S. Stoll and A. Schweiger, *J. Magn. Reson*, 2006, **178**, 42–55.

118 F. Neese, *Wiley Interdiscip. Rev.: Comput. Mol. Sci.*, 2012, **2**, 73–78.

119 M. Brustolon and G. Giamello, Eds., *Electron paramagnetic resonance: a practitioner's toolkit*, Wiley, Hoboken, N.J, 2009.

120 V. Chechik, E. Carter and D. Murphy, *Electron paramagnetic resonance*, Oxford Univ Press, Oxford, 2016.

121 N. Rahimi, B. de Bruin and P. H. M. Budzelaar, *Organomet.*, 2017, **36**, 3189–3198.

122 S. Barroso, P. Adão, A. M. Coelho, J. C. Pessoa and A. M. Martins, *J. Mol. Cat. A*, 2016, **412**, 107–116

Chapter 3

Ring opening copolymerization of epoxides with cyclic anhydrides

3.1 Introduction:

With growing concern about the effect of plastic materials on the environment and resources, the need to develop alternatives that are biodegradable, biocompatible and renewable is increasing. Polyesters formed from the ring opening copolymerization (ROCOP) of anhydrides and epoxides has been found to be a promising alternative to petroleum-based plastics such as polyolefins (Equation 3.1).
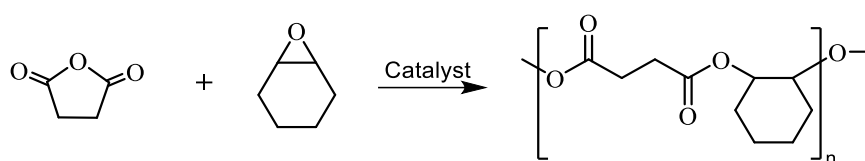
Equation 3.6: Synthesis of polyesters from epoxide and anhydride

Any Lewis acidic metal, when supported by an appropriate ligand can, in principle, be used as catalyst in the ROCOP of epoxides and cyclic anhydrides. The most successful ligands used in these types have mainly included hard Lewis base oxygen or/and nitrogen donors in manifolds such as salen,[1–3] salan,[4,5] salalen,[6] other Schiff bases,[7] corrole,[8] porphyrinato,[9–11] and β-diiminate (Figure 3.1).[12] Nevertheless, ligands with soft Lewis bases have also been employed, such as [OSSO]-type bis (phenolate).[13] Salen type complexes have been found to be more active in ROCOP compared with β-diketiminato-type and porphyrin complexes under the same conditions.[14]

There are many applications of transition metal salen complexes, as mentioned in the introduction. The most important application of these complexes is in homogeneous catalysis. Metal Salen complexes have been considered one of the most useful class of catalysts.[15] Due to the successful applications of salen-type complexes (especially aluminium, chromium, and cobalt) in the ring opening copolymerization of epoxides with cyclic anhydrides, titanium(III)- and titanium(IV)- salen type complexes have been employed as catalysts in ROCOP of various epoxides with anhydrides, which is the subject of this chapter. It is noteworthy that titanium, despite being an inexpensive and non-toxic element and commonly used in alkene polymerisation, is far less used in epoxide-anhydride ROCOP than other metals. It is this area that this thesis adds to.
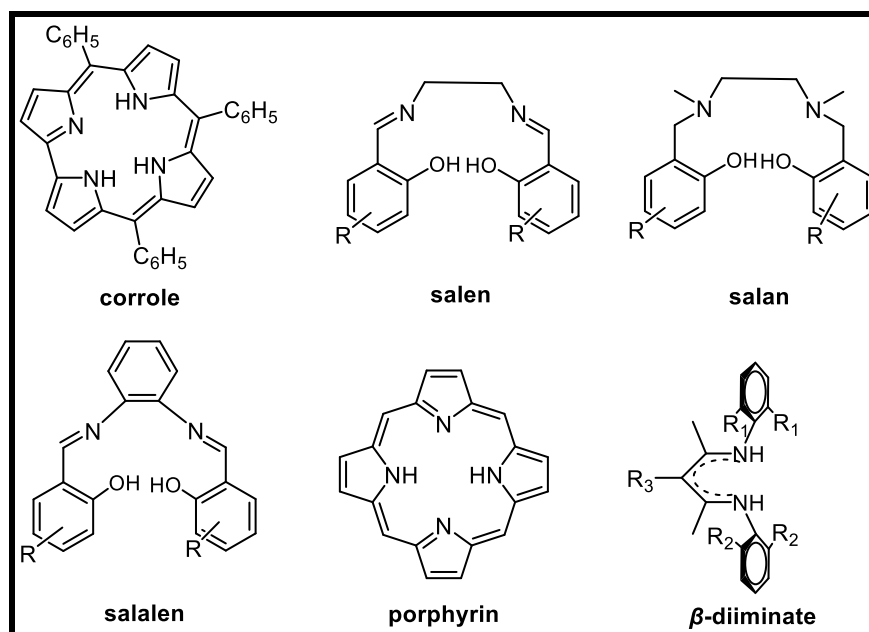
Figure 3.19: Different ligands used in ROCOP complex design.

In this thesis, the ring opening copolymerization of various epoxides with different anhydrides using Ti(III) and Ti(IV) salen-type complexes as catalyst is described in both solution and solvent-free conditions. The epoxides and anhydrides used in this thesis are listed in Figure 3.2. The epoxides and anhydrides were carefully selected to provide a variety of structural motifs including saturated, unsaturated, aliphatic, aromatic, unsubstituted and substituted rings. All epoxides and anhydrides were commercially available. To avoid any impurities that may act as chain transfer agents (CTAs) and shorten the polymer chain length,[1,16–18] all the monomers were purified prior to polymerization. Epoxides were stirred over freshly ground calcium hydride for three days then distilled under reduced pressure and degassed using three successive freeze-pump-thaw cycles, and stored under argon. All the anhydrides were purified by recrystallization followed by sublimation before use and stored in the glovebox.
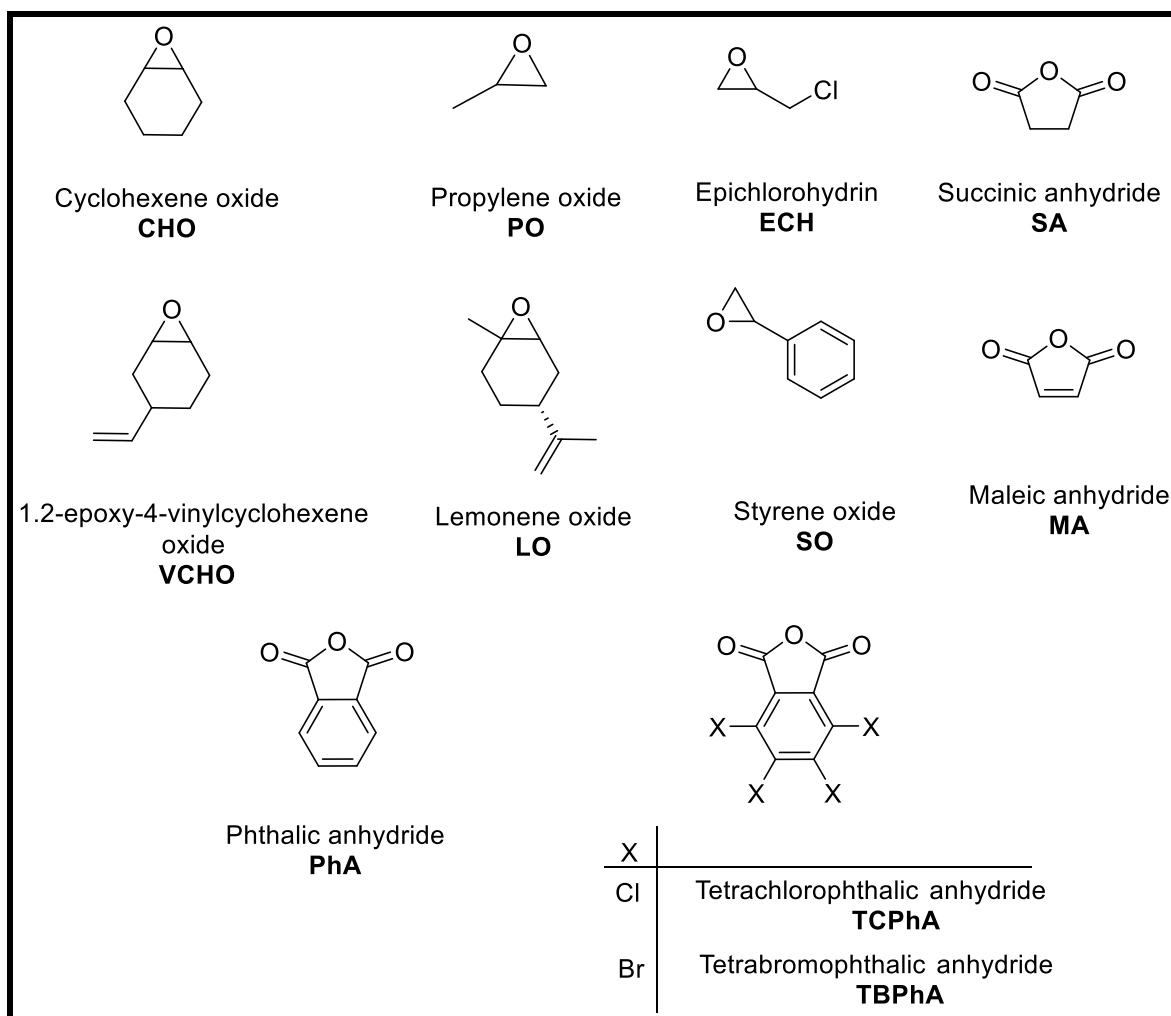
Figure 3.20: Epoxides and anhydrides used in this study

The copolymerization experiments were performed as described in the literature; in a glove box the catalyst, cocatalyst and anhydride were weighed out into an oven-dried screw cap vial equipped with a magnetic stir bar. Epoxide was then added via pipette, and after sealing the vial, it was removed from the glove box and placed in preheated aluminum heating block to the desired temperature for the certain time. The conversion was determined by taking an aliquot for ^{1}H NMR spectroscopic analysis after the appropriate amount of time. The resulting mixture was dissolved in a minimum amount of dichloromethane and precipitated using excess of methanol or hexane with vigorous stirring, before decanting the solvent. To ensure that the catalyst and the excess of monomer were removed, the precipitation was repeated three times. The polymer was collected and dried under reduced pressure. The produced polymers were characterized by ^{1}H NMR spectroscopy. Polymer molecular weights (M_n) and molecular weight distributions (PDI) were determined by Gel Permeation Chromatography (GPC).

The identity of the prepared polyesters was also verified by FTIR spectroscopy; the FTIR spectra of the polyesters confirm the existence of the ester linkage. Figure 3.3 shows an FTIR spectrum of the Poly(CHO-co-PhA) prepared using catalyst **1** in presence of PPNCl. The band at 1718 cm^{-1} is assigned to the symmetric stretching vibration of the ester carbonyl. The bands at 1256 and 1066 cm^{-1} are attributed to C-O-C asymmetric and symmetric stretching vibrations, respectively.[19]
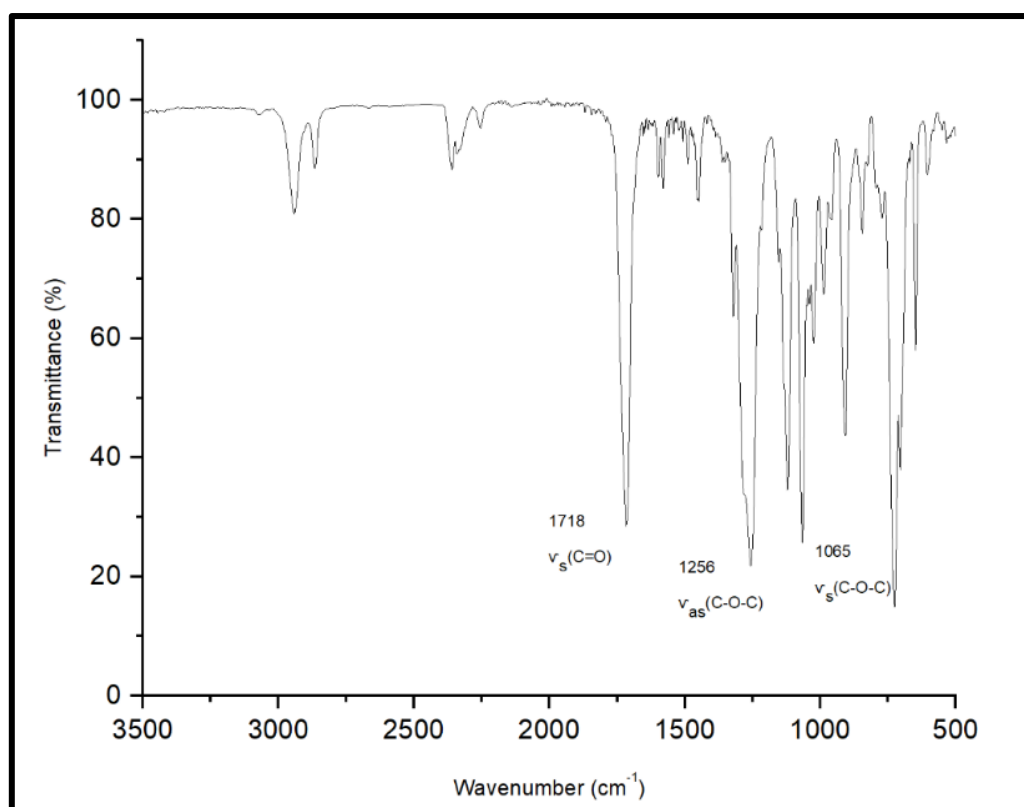
Figure 3.3: FT-IR spectrum of Poly(CHO-co- PhA) copolymer

Matrix assisted laser desorption/ionization time of flight mass spectrometry (MALDI-TOF MS) is used to investigate the microstructure of polyesters and to clarify the nature of chain end groups that formed during the initiation step. The MALDI-TOF MS spectrum of the poly(PhA-co-CHO) formed in bulk by catalyst **1** in the presence of PPNCl as a cocatalyst (entry 49) showed an m/z interval of 246 between the consecutive peaks, which corresponds to [PhA+CHO] repeating unit (Figure 3.4). This confirms the perfectly alternating polyester structure as determined previously by ^{1}H NMR spectroscopy.

It should be noted that MALDI-TOF was not able to analyse the polymer with high molecular weight which could be attributed to the lower tendency of the large molecule to volatize with this technique.[4]
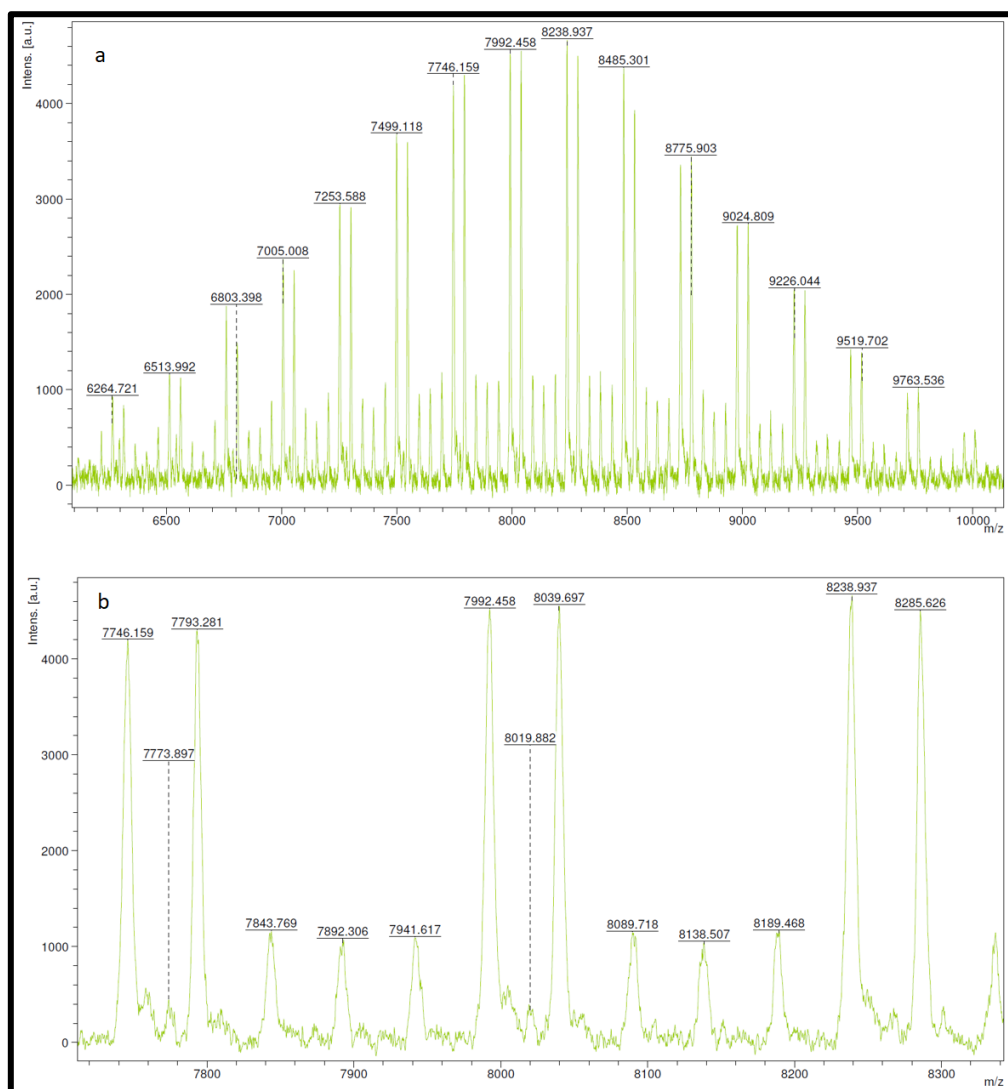
Figure 3.4: MALDI-TOF mass spectrum of poly(CHO-co-PhA) (entry 49)

The prepared polymers can be either perfectly alternating polyesters resulting from succession of epoxides with anhydrides (the ideal case), or it might contain polyether regions resulting from homopolymerization of epoxide (Scheme 3.1).

Scheme 3.36: ROCOP of cyclohexene oxide and phthalic anhydride
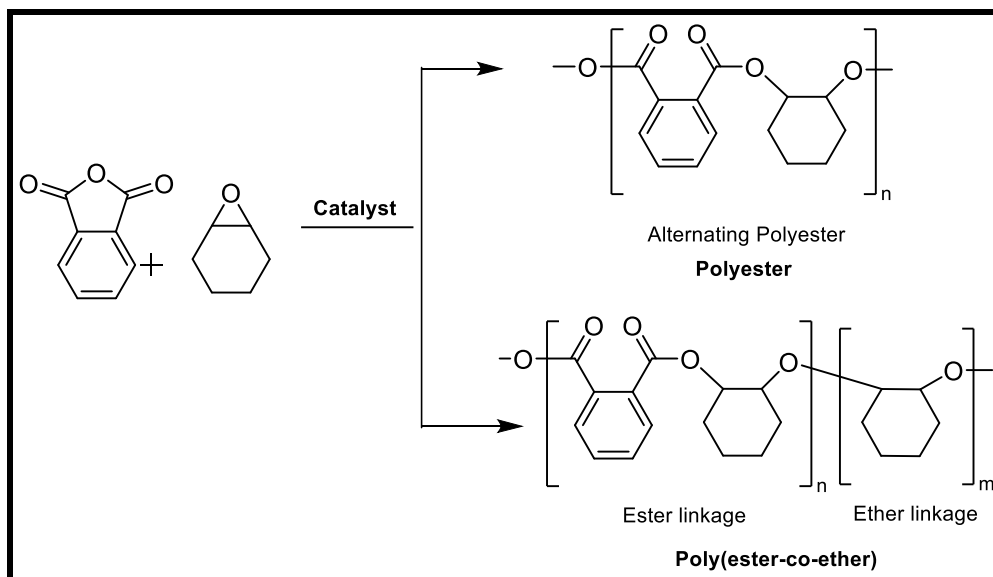
The selectivity of polyesters can be measured by comparing the integration of ester linkage (4.8-5.27 ppm) and ether linkage (3.22-3.65 ppm) in their ^1H NMR spectra.[4] An increase in the ester linkage means an increase in the selectivity (Figure 3.5).
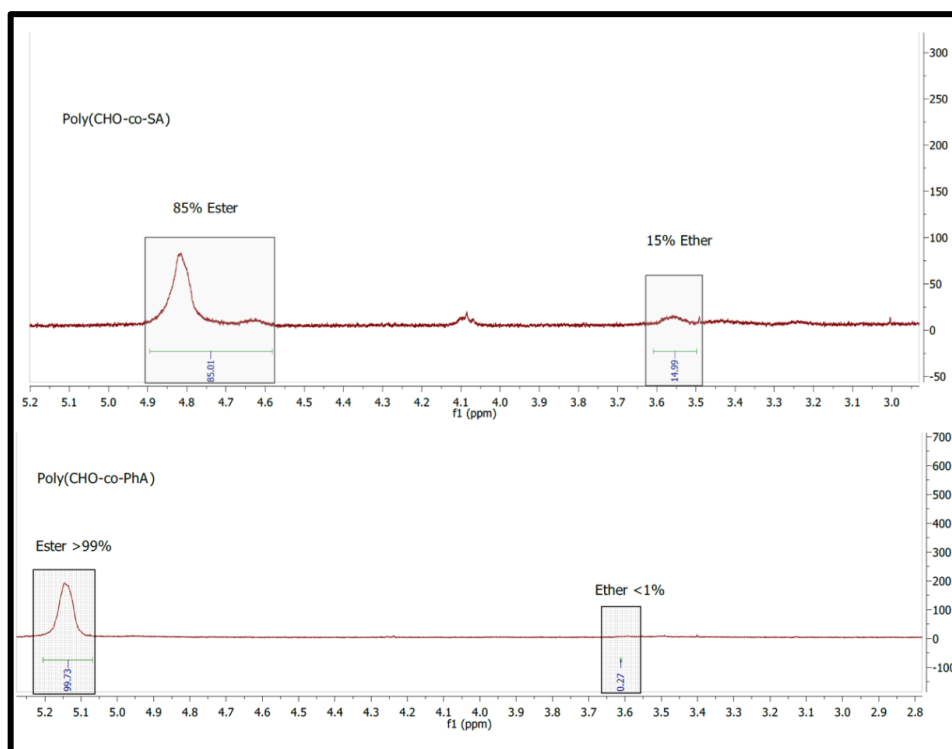
Figure 3.5: Two polymers (Poly(CHO-co-SA) and Poly(CHO-co-PhA)) with different selectivities.

ROCOP of epoxides with anhydrides requires a catalyst (LMX), where L is an ancillary ligand, X is the initiating group from which the propagation proceeds (commonly halide or an alkoxide group), and M is a metal centre. Scheme 1.3 illustrates a proposed ROCOP mechanism.[20] The initiation process involves the coordination of an epoxide; the metal alkoxide is then formed by nucleophilic ring opening of the epoxide by a halide ligand or co-catalyst to generate a metal alkoxide intermediate (which is the rate determining step). Consequently, the metal alkoxide reacts with an anhydride to provide a metal carboxylate species. The propagation reactions involve subsequent addition of monomers to metal carboxylate and alkoxide intermediates (metal alkoxide attacks the anhydride to regenerate metal carboxylate and the metal carboxylate ring opens the epoxide to reform the metal alkoxide). The termination is usually achieved by the addition of water or alcohol, but back-biting/transesterification of the polymer chain can also result in a termination step with a premature shortening of the growing polymer chain (*vide infra*).

Unfortunately, at high monomer conversions most catalysts undergo undesirable side reactions especially when using excess epoxide. These side reactions include transesterification,[2,10] epimerization,[2] and epoxide homopolymerization (Figure 3.6).[8,11,21,22] Epoxide homopolymerization leads to ether linkages and thus lowering the alternating selectivity of the obtained polymers and producing polymers that are less recyclable. Other side reactions include chain transfer reactions, in which water or alcohol trace impurities displace the growing polymer chain and form metal alkoxide or hydroxyl. This new initiating group can form a new polymer chain and thus decrease the molecular mass of the polymers.
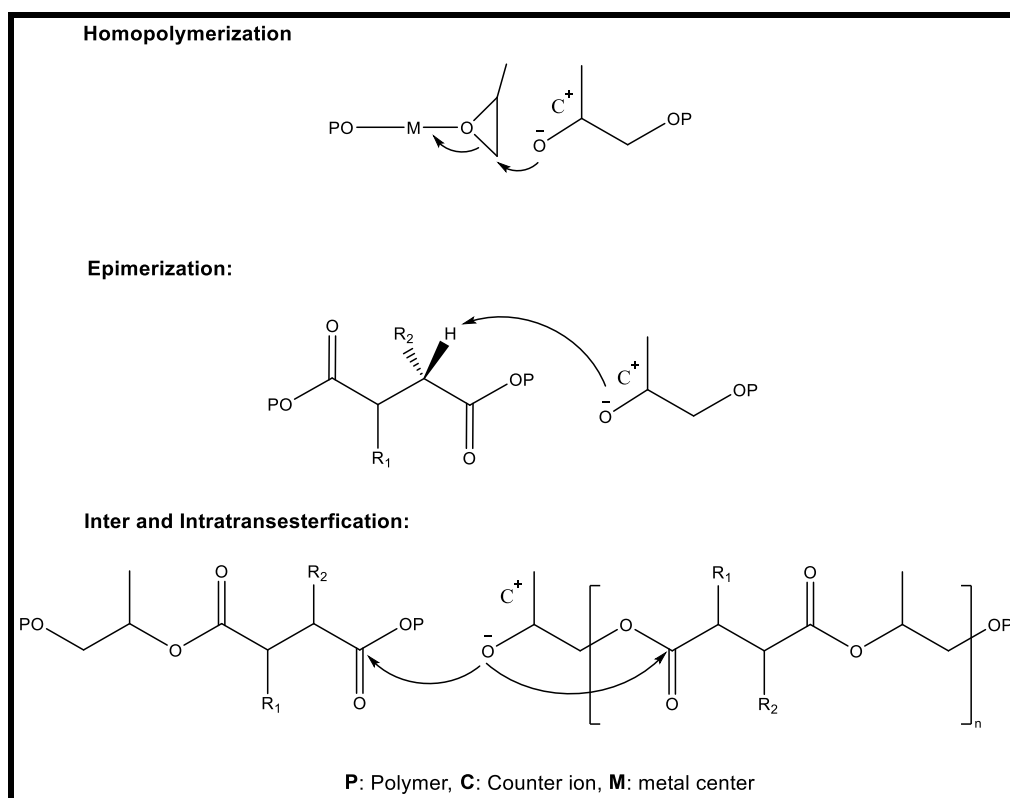
Figure 3.6: Common side reactions observed at the end of the copolymerization[23]

3.2 ROCOP optimization:

Initially, the polymerization of CHO, PO, and SO with SA and MA were performed without cocatalyst using [Ti(Salpy)Cl] (**1**) as catalyst. The experiments were conducted at 60 °C for 24 hours using [catalyst]:[epoxide]:[anhydride]= [1]:[200]:[200] in THF (0.5 ml). The polymerization results are illustrated in Table 3.1.

Table 3.1: Copolymerization of epoxides and anhydrides catalysed by **1** without cocatalyst[a]

Entry	Epoxide	Anhydride	Ester[b] (%)	Y_w[c] (%)	M_n[d] (g/mol)	DP	PDI[d]
1	CHO	SA	48	40	1804	9	6.78
2	PO	SA	86	45	5399	34	1.09
3	SO	SA	86	32	2464	11	1.00
4	SO	MA	78	32	2591	12	1.04

[a][epoxide]:[Anhydride]:[Catalyst]=200:200:1, solvent:THF, reaction temperature= 60 °C. [b] Determined from ¹H NMR spectra of dried polymer samples in CDCl₃. [c] based on isolated polymer yield. [d] determined by GPC (triple detection).

It is notable that salen-type complexes are known to form polymers with significant polyether (i.e. low ester) content with low activities when performed without a cocatalyst.[1,4,10] However, it can be seen from Table 3.1 that **1** can polymerize epoxides with anhydrides with competitive ester selectivities in the absence of a cocatalyst, exemplified by poly(PO-co-SA) (entry 2, Table 3.1 and Figure 3.7) with 86% ester linkage and M_n=5399 g/mol. In the case of CHO and SA (entry 1) the catalyst is only poorly active and the low molecular weight copolymer (M_n=1804 g/mol) obtained contains a high contribution of ether linkage (52%) and broad PDI (6.78) which indicates poor control over the polymerization process. Catalyst **1** was selective in the copolymerization of SO with SA and MA (entries 3 and 4, 86 and 78% ester respectively) but the molecular weights were lower than that with Poly(PO-co-SA). In all cases the isolated yields of polymers were between 32% and 45%.
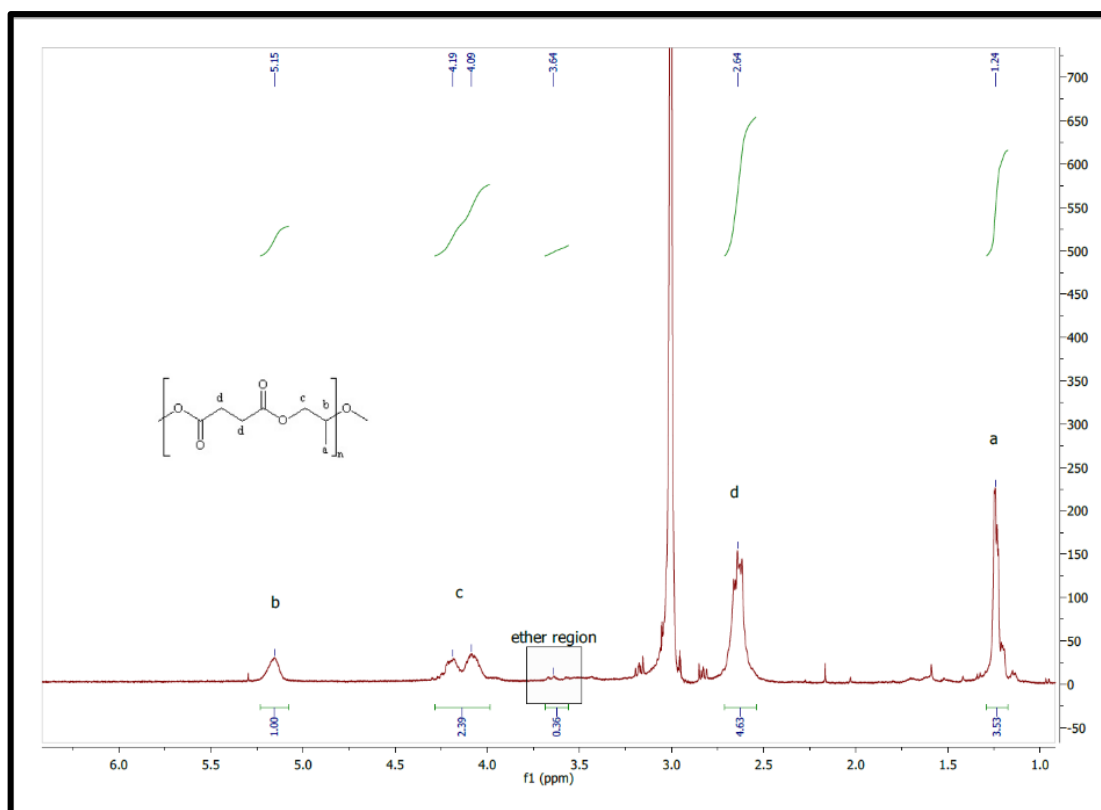
Figure 3.7: ^{1}H NMR spectrum (400 MHz, CDCl$_3$, 293 K) of the PO/SA copolymer obtained using catalyst **1** without cocatalyst (entry 2)

The exact role for the cocatalyst is not completely clear, but latest data from Coates suggest that the nucleophilic anion facilitates the initiation step by opening the first epoxide and forming an alkoxide complex (see discussion above in section 3.1), whereas the non-coordinating cation facilitates decoordination of a carboxylate-terminated polymer chain which leaves a vacant site for an epoxide to coordinate, which is then opened in an intermolecular nucleophilic attack by the non-coordinated carboxylate-terminated polymer chain.[24] The selectivity is primarily controlled by the propagation step, i.e. the cation of the cocatalyst is important for this. This explains why the selectivities are modest in Table 1, and the molecular weights are low, but the selectivities are significantly higher than one would expect without a cocatalyst which is surprising (Table 3.1, entries 2,3 and 4).

Repeating the experiments with cocatalyst (Table 3.2) clearly showed that the presence of PPNCl (nucleophile and cation source) significantly improved the catalytic activity and selectivity of the obtained polymers, emphasizing the importance of a cocatalyst in the ROCOP reaction.

Table 3.2: ROCOP of anhydrides with epoxides using **1**/PPNCl[a]

Entry	Epoxide	Anhydride	Ester[b] (%)	Y_w[c] (%)	Mn[d] (g/mol)	DP	PDI[d]
5	CHO	SA	92	51	8486	43	1.46
6	PO	SA	97	64	9071	57	1.26
7	SO	SA	91	57	20571	93	1.30
8	SO	MA	93	86	4754[e]	23	1.03[e]

[a][epoxide]:[Anhydride]:[Catalyst]:[Cocatalyst]=200:200:1:1, solvent:THF, reaction temperature= 60 °C. [b] Determined from ^{1}H NMR spectra of dried polymer samples in CDCl_3. [c] based on isolated polymer yield. [d] determined by GPC (triple detection). [e]determined by MALDI-TOF

Most of the previously reported copolymerization studies of epoxides with anhydrides showed remarkably higher reactivity and selectivity when performed in present of nucleophilic cocatalyst.[1,6,7,10,16,25,26] There are many types of cocatalysts known in ROCOP, among them bis(triphenylphosphine)iminium chloride (PPNCl) and 4-(Dimethylamino)pyridine (DMAP) (Figure 3.8) were reported as the most effective in enhancing the catalytic performance.[16,27]

Bis(triphenylphosphine)iminium chloride, **PPNCl**

4-Dimethylaminopyridine **DMAP**
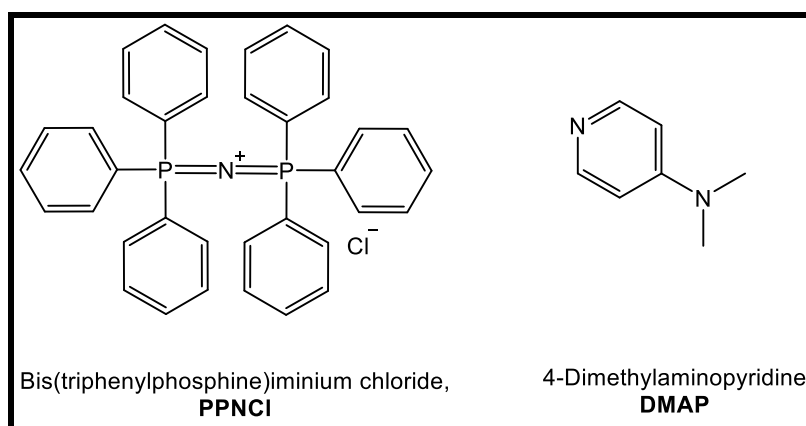
Figure 21.8: The structure of PPNCl and DMAP cocatalysts

The effect of the cocatalysts PPNCl and DMAP on the catalytic behaviour of complex **1** were tested and the results shown in Table 3.3. The results revealed that PPNCl is more efficient than with DMAP when combined with the catalyst, for example, when comparing entries 5 and 9, a higher MW was obtained with DMAP but the PDI was very large and

consistent with the uncontrolled polymerization reaction. This could be attributed to the steric bulkiness of DMAP compared to the metal salen complex which hinders its access to the metal centre, whereas the small Cl ion of PPNCl can easily reach the metal centre and initiate epoxide ring opening quicker.[17,24] Also, it could be due to the separated ion pair of PPNCl; the cation helps with the propagation so maybe there is no difference in initiation between the two but PPNCl is better at the propagation than DMAP. These observations are in agreement with Duchateau and coworkers, who studied a number of cocatalysts in epoxide/anhydride ROCOP; PPNCl showed the highest activity.[1,16,25] Also, PPNCl in combination with (salen)MCl produced one of the most active catalyst in ROCOP of epoxides with CO_2 and with the similarities between epoxide/ anhydride and epoxide/CO_2 copolymerization the same results are expected here.[28–30]

Table 3.3: Comparisons between PPNCl and DMAP as cocatalysts in the ROCOP of epoxides with anhydrides by complex **1**[a]

Entry	Epoxide	Anhydride	Cocat.	Ester[b] (%)	Y_w[c] (%)	Mn[d] (g/mol)	DP	PDI[d]
5	CHO	SA	PPNCl	92	51	8486	43	1.46
9	CHO	SA	DMAP	87	51	16489	83	6.50
6	PO	SA	PPNCl	97	64	9071	57	1.26
10	PO	SA	DMAP	-	-	-	-	-
7	SO	SA	PPNCl	91	57	20571	93	1.30
11	SO	SA	DMAP	85	43	3762	17	1.41

[a][epoxide]:[Anhydride]:[Catalyst]:[Cocatalyst]=200:200:1:1, solvent:THF, reaction temperature= 60 °C. [b] Determined from ^{1}H NMR spectra of dried polymer samples in CDCl₃. [c] based on isolated polymer yield. [d] determined by GPC (triple detection).

Since the ROCOP mechanism involves ion pairs and decoordination of a polymer chain from the metal centre it seems likely that solvent polarity and donor ability could play a significant role in dictating catalytic activity. Therefore the effect of solvent in the ROCOP by complex **1** was probed using the same monomers as discussed above. Most prior copolymerization studies used toluene as solvent;[6,13,17,25,29,31] copolymerization in THF was reported to be less active with little (or no) epoxide conversion. This has been attributed to the possible competition between the epoxide and THF for coordination with the metal centre.[8,17]

The effect is so significant because the epoxide ring opening is rate determining and therefore reducing the propensity of the epoxide to coordinate to the metal is expected to affect this step more than the other steps in the reaction. In the case of complex **1**, THF and toluene were tested as media for the copolymerization of CHO and SO with SA and PhA (Table 3.4). In contrast to the above-mentioned studies, ROCOP in THF was found to be more active and produced polymers with higher selectivities and polymer molecular weights compared to toluene. For example, the selectivity increases from 62% to 92% and the M_n increases from 1327 to 8486 g/mol when using THF instead of toluene, in addition to the very broad PDI which indicates poor polymerization control (entries 5 and 12, respectively). Also, in poly(SO-co-PhA) the selectivity was higher in THF (98%) than in toluene (93) and the molecular weight increases from 2005 to 5322 g/mol (entries 16 and 17, respectively).

Table 3.4: Comparisons between THF and toluene in the ROCOP in presence of **1**/PPNCl[a]

Entry	Epoxide	Anhydride	Solv.	Ester[b] (%)	Mn[c] (g/mol)	DP	PDI[c]
5	CHO	SA	THF	92	8486	43	1.46
12	CHO	SA	Toluene	62	1327	7	7.44
13	CHO	PhA	THF	93	6323	26	1.28
14	CHO	PhA	Toluene	73	2386	10	1.39
7	SO	SA	THF	91	20571	93	1.30
15	SO	SA	Toluene	84	103	0.5	1.67
16	SO	PhA	THF	98	5322	20	1.14
17	SO	PhA	Toluene	93	2005	7	1.20

[a][epoxide]:[Anhydride]:[Catalyst]:[Cocatalyst]=200:200:1:1, reaction temperature= 60 °C. [b] Determined from ^{1}H NMR spectra of dried polymer samples in CDCl$_3$. [c] determined by GPC (triple detection).

The purification of the anhydride prior to use is crucial, as they undergo hydrolysis which form diacids. This can be particularly problematic in older bottles of the anhydride feedstock. The presence of these diacids will affect the polyester molecular weight because they act as chain transfer agents (CTAs).[1,32] Figure 3.9 contains the infrared spectra of purified and unpurified phthalic anhydride, and illustrates the difference between the two. The

spectrum of the unpurified PhA clearly shows a very broad band at 3000 cm^{-1} which corresponds to the OH in the carboxylic acid. It also showed that the recrystallization followed by sublimation of the phthalic anhydride led to a significant decrease of phthalic acid. It was found that about 40% increase in molecular weight was achieved as a consequence to using recrystallized and sublimed PhA.[32]
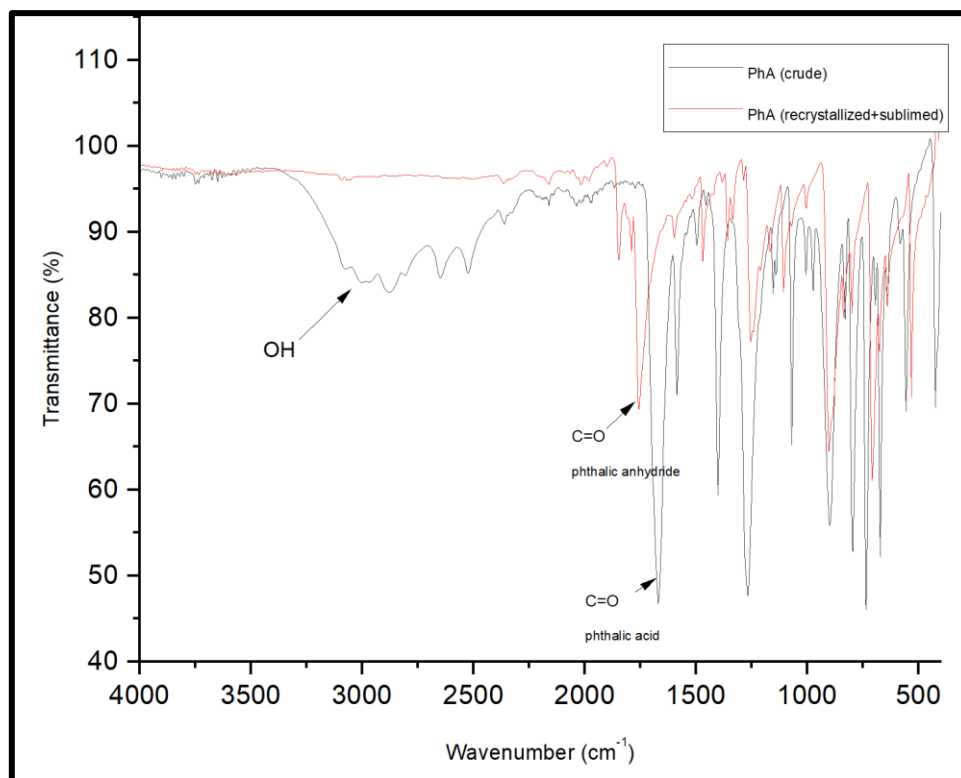
Figure 3.9: FT-IR spectra of crude and purified PhA

The relationship between PhA conversion (%) and reaction time is illustrated in Figure 3.10. The data shows that the PhA conversion increased linearly with time, and this is a strong indication that the rate of ROCOP is a zero order dependence on PhA concentration.[4]

$$y = 0.5467x - 1.2$$
$$R^2 = 0.9947$$
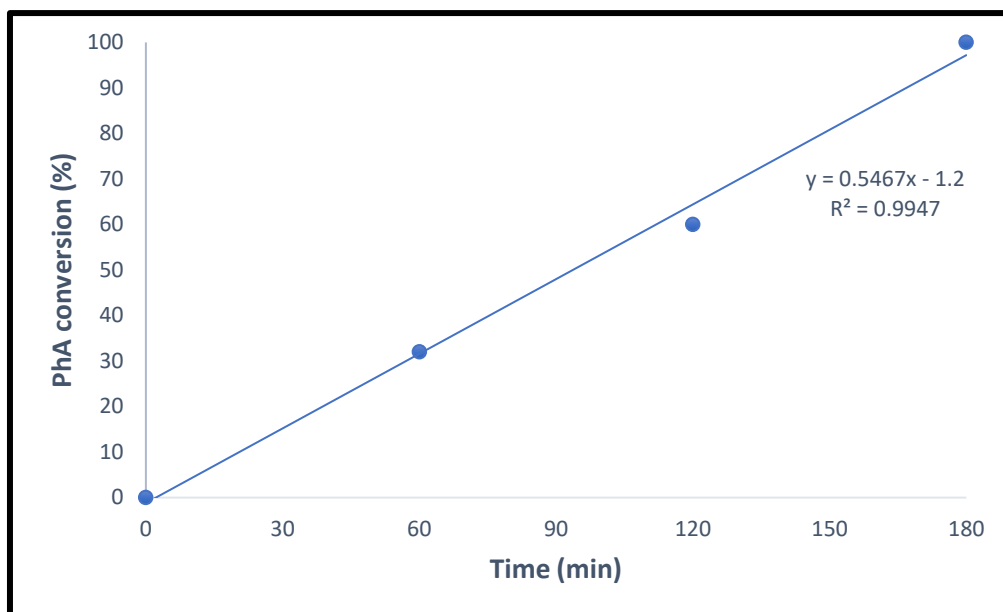
Figure 3.10: PhA conversion (determined from ^{1}H NMR spectra) vs time

As a result of the above observations, focus in this thesis was placed on utilizing PPNCl as cocatalyst and THF as solvent (if needed). The copolymerizations were performed in both solution and in bulk (no solvent other than excess epoxide).

3.3 Solution ROCOP:

The copolymerization reactions were performed as described in the literature[2] using 6.4 μ mole of the catalyst in 0.5 ml THF with [complex]:[cocatalyst]:[epoxide]:[anhydride] ratio of 1:1:200:200. The reactions were run for 24 h, which is a common timeframe for solution experiments where it is less critical to terminate the reaction precisely at the end of the anhydride conversion. To study the effect of the structure of the complexes on the copolymerization of epoxides with anhydrides, titanium complexes with different ligands were employed.

Firstly, the ring opening copolymerization of CHO, PO, and SO with SA, PhA, TCPhA and TBPhA were copolymerized at 60 °C using catalysts [Ti(Salpy)Cl] (**1**) and [Ti(Salpy)Cl₂] (**8**) in combination with PPNCl (Table 3.5). The two complexes have exactly the same ligand backbones and differ only in the central atom (Ti(III) and Ti(IV)). It can be seen that the two complexes are able to polymerize CHO with anhydrides in good selectivity (88-99%) and with relatively narrow polydispersity in most cases.

Table 3.5: ROCOP of CHO, PO, and SO with anhydrides using **1** and **8** and PPNCl[a]

Entry	Cat.	Epoxide	Anhydride	Ester[b] (%)	Y_w[c] (%)	M_n[d] (g/mol)	DP	PDI[d]
5	1	CHO	SA	92	51	8486	43	1.46
13	1	CHO	PhA	93	90	6323	26	1.28
18	1	CHO	TCPhA	89	81	9298	24	1.18
19	1	CHO	TBPhA	89	90	15714	28	1.80
20	8	CHO	SA	91	75	8467	43	1.43
21	8	CHO	PhA	97	98	16354	66	1.28
22	8	CHO	TCPhA	99	85	10076	26	1.37
23	8	CHO	TBPhA	88	75	15071	27	1.80
6	1	PO	SA	97	64	9071	57	1.26
24	1	PO	PhA	98	87	5660	27	1.06
25	1	PO	TCPhA	85	98	8124	24	1.20
26	1	PO	TBPhA	90	68	5755	11	1.39
27	8	PO	SA	94	54	11025	70	1.08
28	8	PO	PhA	98	91	10371	50	1.09
29	8	PO	TCPhA	87	86	9392	27	1.53
30	8	PO	TBPhA	87	76	4741	9	1.29
7	1	SO	SA	91	57	20571	93	1.30
16	1	SO	PhA	98	98	5322	20	1.14
31	1	SO	TCPhA	60	86	3366	8	1.14
32	8	SO	SA	91	96	20153	92	1.34
33	8	SO	PhA	96	99	6501	24	1.20
34	8	SO	TCPhA	67	90	5381	13	1.21

[a][epoxide]:[Anhydride]:[Catalyst]:[Cocatalyst]=200:200:1:1, solvent:THF, reaction temperature= 60 °C. [b] Determined from ^{1}H NMR spectra of dried polymer samples in CDCl$_3$. [c] based on isolated polymer yield. [d] determined by GPC (triple detection).

The two complexes show similar performance in the copolymerization of CHO with SA and TCPhA, whereas **8** is more reactive in case of the polymerization of PhA and TCPhA producing polyesters with higher selectivity and molecular weight (e.g. M_n= 16354 compared with 6323 g/mol in Poly(CHO-co-PhA) when using **8** and **1**, respectively, entries 21 and 13). This could point to a deactivation process with these monomers arising from the redox activity of Ti(III) compared to Ti(IV).

The copolymerization of propylene oxide (PO) with SA, TCPhA, and TBPhA using **1** produced polyesters comparable to those catalysed by **8**. Though, the copolymerization of PO and PhA using catalyst **8** has higher M_n (10371 vs 5660, entries 24 and 28).

Styrene oxide (SO) is an attractive epoxide monomer that is different from other epoxides, such as CHO and PO, due to its electron withdrawing nature. Moreover, due to its rigid structure it produces polymers with relatively high glass transition temperature (T_g).[25] However, SO was found to be more difficult to convert to the corresponding polymer when reacted with CO_2 compared to other epoxides, an observation made in the Ward research group with several other catalytic systems for epoxide/anhydride ROCOP. This is attributed to its tendency to form the cyclic styrene carbonate and its less reactive β-carbon atom.[33–35] The ROCOP of SO with anhydrides led to the corresponding semi aromatic polyesters. And as can be seen from Table 3.5 that **1** and **8** afforded alternating polyester (91% polyester linkage) with SA with high molecular mass (20571 and 20153 g/mol, entries 7 and 32). The two complexes were also able to polymerize SO and PhA with low ether linkage (2% and 4%, entries 16 and 33) with appreciable molecular weight and narrow polydispersity (PDI=1.14 and 1.20, respectively). Dachateau and coworkers found similar results when using (salophen)MX catalyst but only at elevated temperature (110 °C).[25]

The solution ROCOP of epichlorohydrin (ECH) and limonene oxide (LO) with PhA, TCPhA and TBPhA were also tested using catalyst **1** with PPNCl as cocatalyst (Table 3.6). Catalyst **1** was able to copolymerize ECH with the mentioned anhydrides producing polyesters with low ether contribution (8-6%) and with good molecular weight (6637 and 9779 g/mol) and relatively low polydispersity (1.32 and 1.17) with PhA and TCPhA (entries 35 and 36, respectively). The copolymerization of ECH and TBPhA produced lower molecular mass polymer (4558 g/mol) and high polydispersity (2.42) but the low solubility of TBPhA can hinder the reaction and cause broader PDI values to be produced.

Table 3.6: ECH and LO / anhydrides copolymerization using **1**/PPNCl[a]

Entry	Epoxide	Anhydride	Ester[b] (%)	Y_w[c] (%)	Mn[d] (g/mol)	DP	PDI[d]
35	ECH	PhA	94	97	6637	27	1.32
36	ECH	TCPhA	92	70	9779	26	1.17
37	ECH	TBPhA	92	60	4558	8	2.42
38	LO	SA	62	28	6406	25	1.45
39	LO	PhA	85	78	3775	13	1.28
40	LO	TCPhA	71	85	3848	9	1.47

[a][epoxide]:[Anhydride]:[Catalyst]:[Cocatalyst]=200:200:1:1, solvent:THF, reaction temperature= 60 °C. [b] Determined from ^{1}H NMR spectra of dried polymer samples in CDCl$_3$. [c] based on isolated polymer yield. [d] determined by GPC (triple detection).

Limonene oxide LO is a biorenewable material derived from naturally occurring limonene (cyclic monoterpene) present in citrus fruit oil and it represents a great opportunity for bio-derived polymers.[36,37] Due to its bulky and rigid structure, it is expected to result in high T_g polymers.[16] The copolymerization of LO produced polyesters with lower selectivity compared to other epoxides (62-85% ester linkage) and lower molecular mass which could be attributed to its relatively bulky structure which might require higher temperatures.[17,31] Lee and coworkers found that the ROCOP of LO with PhA with a chromium complex as catalyst did not occur at 100 °C and thus, they increased the reaction temperature to 130 °C for 24 h and at these conditions they got highly alternating polyester with 2789 g/mol and PDI=1.17.[17] However, in our study catalyst **1** produced poly(LO-co-PhA) in 85% polyester linkage and molar mass of 3775 g/mol and relatively low polydispersity (1.28) at reaction temperature of 60 °C (entry 39). It should be noted that polyesters containing LO subunits are able to undergo modification through postpolymerization modification of the vinyl group, which makes them especially attractive targets.[12]

To study the effect of the steric and electronic environment in Ti(III) Salpy complexes on catalytic performance, the copolymerization reactions were studied for [Ti(Salpy-Me)Cl] (**2**), [Ti(tBu,tBu-Salpy)Cl] (**3**), and [Ti(Cl,Cl-Salpy)Cl] (**4**) (Figure 3.11).
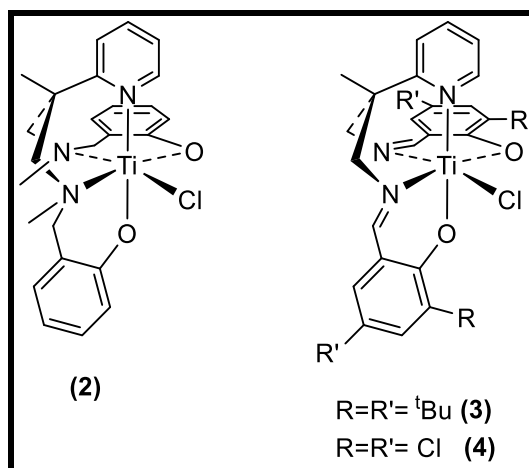
Figure 3.11: Molecular structures of complexes **2**,**3** and **4**

Table 3.7 shows the results of the copolymerization using the catalysts in Figure 3.11. The ROCOP of CHO with PhA and TCPhA in 0.5 ml THF were tested with PPNCl as cocatalyst under the same molar ratio (1:1:200:200 of catalyst:cocatalyst:epoxide:anhydride) at 80 °C for 24 h. All the complexes produced highly alternating polyesters with PhA (92-96% ester linkage) and good alternating polyesters with TCPhA (86-87% ester linkage). The highest molecular weight was obtained with **2** (14060 and 13395 g/mol with PhA and TCPhA, entries 43 and 44, respectively) however, the yields were relatively the same, which means that this complex reduces the back-biting. Complex **2** (with the reduced Salpy ligand) compared to other Salpy complexes contains sp^3 hybridized amino donors. This reduces the electrophilicity of the titanium centre and consequently facilitates the reversible epoxide/ PPNCl binding and thus can increase the activity. The same observation was found in the ROCOP of PO with CO_2, a salan chromium complex was found to be 30 times more active compared to the corresponding salen counterparts.[38,39] It was also found in the copolymerization of CHO with CO_2, that the flexibility of salalen ligands (half reduced salen ligand) facilitates the bidentate binding of the growing polymer chain and thus reduces the energy barrier to CO_2 insertion.[40]

Introducing electron withdrawing chloro substituents ortho and para to the phenoxide group in catalyst **4** results in a higher molecular weight (11731 g/mol, entry 47) compared to **1** (8011 g/mol with PhA, entry 41) That could be related to reduce the electrophilicity of the metal centre which leads to faster propagation relative to back biting and so higher molecular weight. Conversely, the complex with sterically more hindered ^{t}Bu,^{t}Bu-Salpy ligand **3** produced the lowest molar mass polyesters which could be attributed to the steric effect of the large tertiary butyl groups which makes the metal centre less accessible and therefore more back biting occurs, thus lower M_n.

Table 3.7: CHO ROCOP using different Catalyst[a]

Entry	Catal.	Anhydride	Ester[b] (%)	Y_w[c] (%)	Mn[d] (g/mol)	DP	PDI[d]
41	**1**	PhA	92	98	8011	33	1.10
42	**1**	TCPhA	86	95	10386	27	1.42
43	**2**	PhA	95	99	14060	57	1.27
44	**2**	TCPhA	87	98	13395	35	1.35
45	**3**	PhA	96	89	3414	14	1.10
46	**3**	TCPhA	87	91	7868	20	1.34
47	**4**	PhA	94	99	11731	48	1.29
48	**4**	TCPhA	87	99	10082	26	1.38

[a][epoxide]:[Anhydride]:[Catalyst]:[Cocatalyst]=200:200:1:1, solvent:THF, reaction temperature= 80 °C. [b] Determined from ^{1}H NMR spectra of dried polymer samples in CDCl$_3$. [c] based on isolated polymer yield. [d] determined by GPC (triple detection).

3.4 Bulk ROCOP:

Different studies on the ROCOP of epoxides with anhydrides show first order dependence on epoxide concentration and zero order on anhydride concentration; the rate determining step is the epoxide ring opening.[3,4,17,24,26,41,42] Running the polymerization to full conversion as a neat reaction (using excess epoxide as a reagent and solvent at the same

time) has many advantages since side reactions, such as, transesterification, epimerization, and homopolymerization can be reduced. Firstly, as the copolymerization rate depends on the epoxide concentration,[3,43,44] the copolymerization proceeds in pseudo-zero-order kinetics, which result in no noticeable decrease in the rate of copolymerization as a function of conversion, and the reaction tends to proceed much faster.[23] Moreover, the excess epoxide can be easily recovered and reused by distillation of the resulting crude polymer mixture.[2,45] The disadvantage of this approach is that the reaction must be terminated as soon as conversion reaches 100% (based upon anhydride consumption), otherwise the excess epoxide can react to afford polyether.

To study the role of the pyridyl in the ROCOP, four Salpy complexes [Ti(Salpy)Cl] (**1**), [Ti(^{t}Bu,^{t}Bu-Salpy)Cl] (**3**), [Ti(Salpy)Cl$_2$] (**8**) and [Ti(^{t}Bu,^{t}Bu-Salpy)Cl$_2$] (**10**) and four Salpn (i.e. same linker length between the imino groups but without the pyridyl) complexes [Ti(Salpn)Cl] (**6**), [Ti(^{t}Bu,^{t}Bu-Salpn)Cl] (**7**), [Ti(Salpn)Cl$_2$] (**16**) and [Ti(^{t}Bu,^{t}Bu-Salpn)Cl$_2$] (**17**) were employed in the ROCOP of CHO, PO, and ECH with PhA, TCPhA and TBPhA. Complexes **3**, **10**, **7** and **17** have been chosen based on previous studies on salen complexes with tertiary butyl groups in the 3 and 5 positions; these complexes exhibited high reactivity.[1–3,6,9,10,16,19,24]

The general stoichiometry ratio of the reactant feed is [catalyst]:[cocatalyst]:[epoxide]:[anhydride] = [1]:[1]:[2000]:[400]. Since the reaction time is largely independent of the identity of the anhydride, the reaction time can be determined by the conversion of phthalic anhydride; the reaction time will vary as a function of the identity of the epoxides and catalyst (in this case the reaction temperature was fixed at 90 °C). Once the reaction time has been determined, the same time can be used with other anhydrides, so long as the catalyst and epoxide are the same. The conversion of phthalic anhydride was measured by comparing the integrals of the aromatic protons in the unreacted phthalic anhydride (7.97 ppm) and in polyester (7.30-7.83 ppm) in the ^{1}H NMR spectra of the crude reaction mixture (Figure 3.12).[46] All the results presented below correspond to reactions quenched at full conversion of PhA.
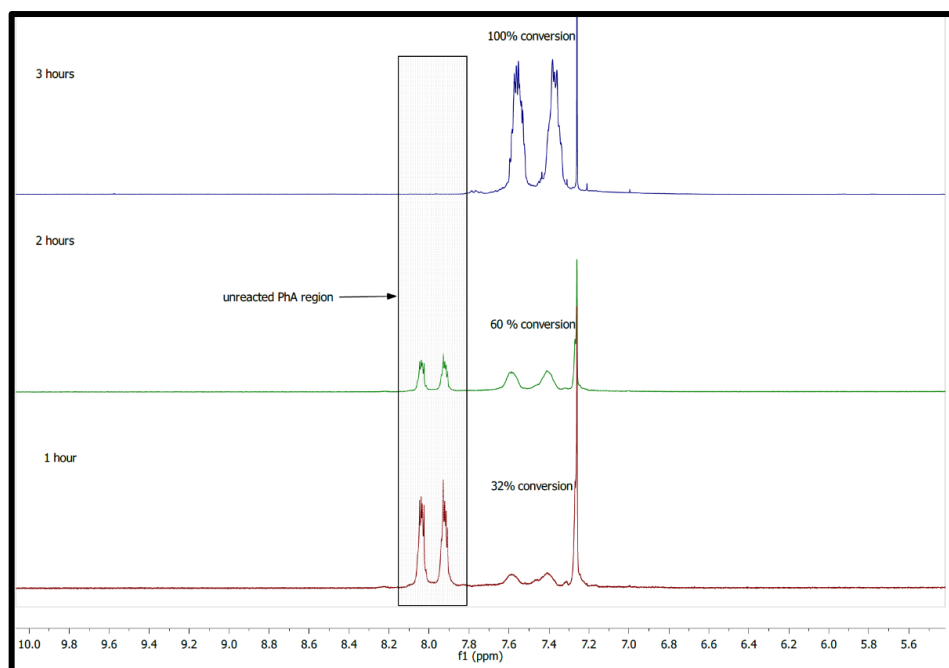
Figure 3.12: ^{1}H NMR (400 MHz, CDCl$_3$, 293 K) spectrum illustrates the conversion of PhA over time in the copolymerization with CHO using **1**/ PPNCl at 80 °C

3.4.1 Ring opening copolymerization of CHO with anhydrides:

Cyclohexene oxide (CHO) is one of the most widely used epoxides in epoxide/anhydride ROCOP. Firstly, the copolymerization of CHO with PhA, TCPhA, and TBPhA using the above mentioned 8 complexes at 90 °C (Tables 3.8 and 3.9) was investigated. Figure 3.13 gives an example of the ^{1}H NMR spectrum of the polyester produced by ROCOP of CHO with PhA. Both Ti(III) and Ti(IV) complexes are effective catalysts for the ring opening copolymerization of cyclohexene oxide with anhydrides. However, Ti(IV) catalysts are sometimes more selective (<1-6% ether linkages) and often produce polymers with higher molecular weight (molecular weights ranging from 11320- 25508 g/mol and relatively low polydispersity indices) than the Ti(III) congeners. For example, catalyst **6** produced poly(CHO-co-PhA) with selectivity >99% and molecular mass= 7715 g/mol (entry 55), whereas the analogue Ti(IV) catalyst (**16**) produced the same polymer with 98% selectivity and Mn= 11320 g/mol (entry 67).The ROCOP of CHO with TCPhA and TBPhA using Ti(III) and Ti(IV) complexes produced copolymers with higher molecular weight compared to PhA (in most cases) but broader polydispersities which could be attributed to the solubility of these anhydrides in CHO which gives the reactions a partially heterogeneous nature and can limit catalyst mixing. Complexes

with 3,5-ditertiary butyl substituents required slightly more time to reach full PhA conversion which could be related to the increased steric demands of the ligand.
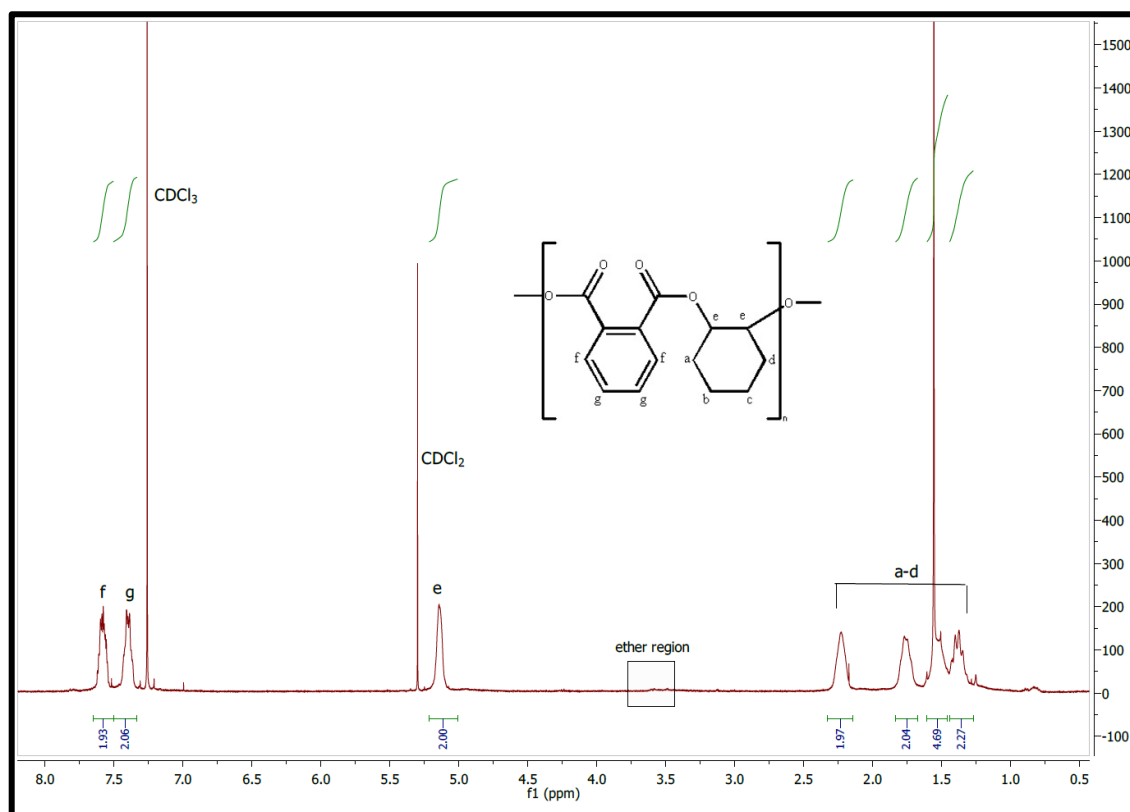
Figure 3.13: ^{1}H NMR Spectrum (400 MHz, CDCl$_3$, 293 K) of Poly(CHO-co-PhA) polyester using **17**/PPNCl (entry 70)

Generally, the Salpy complexes (Ti(III) and (IV)) gave higher selectivities and molecular weights compared with the Salpn complexes, for example catalyst **3** produced poly(CHO-co-PhA) with 88% selectivity and 14514 g/mol molecular mass (entry 53) and catalyst **7** produced this polymer in 70% and Mn= 8741 g/mol (entry 59). Ti(IV) Salpy complexes (**8** and **10**) produced polyesters with higher selectivity and molar mass compared to the analogous Ti(III) **1** and **3**. For example, the ROCOP between CHO and PhA produced polyester with M_n= 13316 g/mol and PDI=1.11 with **1** (entry 49) whereas with **8** the polymer has M_n= 25508 and PDI=1.14 (entry 61). The tBu substituted Salpy complexes with Ti(III) and Ti(IV) are less active compared to the non-substituted Salpy complexes (required more time to reach full monomer conversion). For example, the copolymerization between CHO and PhA required 90 minutes to complete with [Ti(Salpn)Cl$_2$] (**16**) (entry 67), while with [Ti(tBu,tBu-Salpn)Cl$_2$] (**17**) required 120 minutes (entry 70).

Table 3.8: ROCOP of CHO using Ti(III) complexes[a]

Entry	Cat.	Anhydride	Time (min)	Ester[b] (%)	Y_w[c] (%)	M_n[d] (g/mol)	DP	PDI[d]
49	**1**	PhA	90	>99	95	13316	54	1.11
50	**1**	TCPhA	210	83	82	11763	31	1.09
51	**1**	TBPhA	210	87	92	12704	23	1.55
52	**3**	PhA	100	>99	98	11953	49	1.10
53	**3**	TCPhA	100	88	99	14514	38	1.49
54	**3**	TBPhA	120	97	98	6720	12	1.23
55	**6**	PhA	90	>99	99	7715	31	1.22
56	**6**	TCPhA	120	77	90	8024	21	1.69
57	**6**	TBPhA	120	69	91	10933	19	1.70
58	**7**	PhA	100	97	98	11594	47	1.29
59	**7**	TCPhA	120	70	89	8741	23	1.64
60	**7**	TBPhA	120	74	97	13814	25	1.40

[a][epoxide]:[Anhydride]:[Catalyst]:[Cocatalyst]=2000:400:1:1, reaction temperature= 90 °C. [b] Determined from ^{1}H NMR spectra of dried polymer samples in CDCl$_3$. [c] based on isolated polymer yield. [d] determined by GPC (triple detection).

Compared to the solution copolymerization, the bulk copolymerization shows much higher activity as expected: the bulk copolymerization of PhA and CHO was much faster than solution copolymerization resulting in full conversion in 90-120 minutes at 90 °C. Less predictable was that the copolymers were produced with higher molar masses and lower dispersities (1.09-1.29), which may be indicative of fewer back-biting events in the shorter reaction time. However, lower selectivities were observed in the ROCOP of CHO with TCPhA and TBPhA (more ether sequences were formed) which might be related to the non-homogeneity and increased viscosity of the reaction mixture.[32]

Table 3.9: ROCOP of CHO using Ti(IV) complexes[a]

Entry	Cat.	Anhydride	Time (min)	Ester[b] (%)	Y_w[c] (%)	Mn[d] (g/mol)	DP	PDI[d]
61	**8**	PhA	90	>99	92	25508	104	1.14
62	**8**	TCPhA	180	94	99	15547	40	1.33
63	**8**	TBPhA	180	94	93	20620	37	1.67
64	**10**	PhA	100	98	94	11657	47	1.18
65	**10**	TCPhA	100	95	94	15419	40	1.39
66	**10**	TBPhA	120	98	99	11489	20	1.39
67	**16**	PhA	90	98	98	11320	46	1.12
68	**16**	TCPhA	120	99	82	14066	37	1.72
69	**16**	TBPhA	180	98	96	15496	28	1.76
70	**17**	PhA	120	97	89	14767	60	1.27
71	**17**	TCPhA	120	96	91	15272	40	1.89
72	**17**	TBPhA	210	99	99	12706	23	1.39

[a][epoxide]:[Anhydride]:[Catalyst]:[Cocatalyst]=2000:400:1:1, reaction temperature= 90 °C. [b] Determined from ^{1}H NMR spectra of dried polymer samples in CDCl$_3$. [c] based on isolated polymer yield. [d] determined by GPC (triple detection).

To study the effect of the ligand substituents on the catalytic activity, the ROCOP of CHO with PhA, TCPhA and TBPhA using **2** (with the reduced Salpy ligand) and **4** (with 3,5-dichloro ligand) were studied (Table 3.10). As seen in solution ROCOP, catalysts **2** and **4** show higher activity and produced polyester with higher masses compared to **1**. However, the selectivity is lower. For example, catalyst **2** produced poly(CHO-co-PhA) with 92% selectivity and 17923 g/mol in 60 min (entry 73, Table 3.10), whereas, the same polyester produced with >99% selectivity and 13316 g/mol in 90 min with catalyst **1** (entry 49, table 3.8).

Table 3.10: ROCOP of CHO using **2** and **4** complexes[a]

Entry	Cat.	Anhydride	Time (min)	Ester[b] (%)	Y_w[c] (%)	Mn[d] (g/mol)	DP	PDI[d]
73	**2**	PhA	60	92	99	17923	73	1.41
74	**2**	TCPhA	60	87	98	15157	39	1.55
75	**2**	TBPhA	180	70	91	12768	23	1.23
76	**4**	PhA	60	89	69	18181	74	1.13
77	**4**	TCPhA	60	84	99	17480	46	1.13
78	**4**	TBPhA	180	76	84	11523	21	1.23

[a][epoxide]:[Anhydride]:[Catalyst]:[Cocatalyst]=2000:400:1:1, reaction temperature= 90 °C. [b] Determined from ^{1}H NMR spectra of dried polymer samples in CDCl$_3$. [c] based on isolated polymer yield. [d] determined by GPC (triple detection).

3.4.2 Ring opening copolymerization of PO with anhydrides:

Propylene oxide (PO), one of the widely studied epoxides, is an attractive comonomer due to its ease of handling, low cost, and high reactivity.[2] The ROCOP of PO with PhA, TCPhA and TBPhA was studied, and the results are listed in Tables 3.11 and 3.12. Figure 3.14 contains a representative ^{1}H NMR spectrum example of the copolymer of PO with PhA.

The molecular weights obtained with PO are considerably higher than those obtained with CHO, possibly indicating that the chain propagation is faster than transesterification processes due to the lower steric demand of PO compared to CHO; the polymers contained a highly alternating microstructure across all substrate combinations (1-4% ether linkage). The polyesters produced by Ti(IV) catalysts exhibit higher masses than those produced by the Ti(III) catalysts, which may indicate a degree of catalyst instability for the reactive Ti(III) complexes. In contrast to CHO copolymerization, the Ti(III) and Ti(IV) Salpn complexes produced higher polymer molecular masses compared to Salpy. The presence of [t]Bu substituents led in most cases to higher polymer molecular mass.

In general the PO copolymerizations (electron rich epoxide) required longer reaction time to reach full PhA conversion, which is interesting since the above observations regarding molecular weight might suggest a faster reaction on the basis of sterics.[47]

Table 3.11: PO ROCOP using Ti(III) catalysts[a]

Entry	Cat.	Anhydride	Time (min)	Ester[b] (%)	Y_w[c] (%)	Mn[d] (g/mol)	DP	PDI[d]
79	**1**	PhA	120	>99	90	11687	57	1.15
80	**1**	TCPhA	120	>99	91	21628	63	1.71
81	**1**	TBPhA	120	97	87	32418	62	1.56
82	**3**	PhA	150	>99	96	11123	54	1.19
83	**3**	TCPhA	150	98	96	26586	77	1.46
84	**3**	TBPhA	150	98	97	56215	108	1.58
85	**6**	PhA	120	>99	91	17471	85	1.19
86	**6**	TCPhA	120	99	92	22767	66	1.64
87	**6**	TBPhA	120	97	99	38184	73	1.34
88	**7**	PhA	120	>99	68	15759	76	1.11
89	**7**	TCPhA	120	>99	91	28927	84	1.38
90	**7**	TBPhA	120	97	96	43447	83	1.55

[a][epoxide]:[Anhydride]:[Catalyst]:[Cocatalyst]=2000:400:1:1, reaction temperature= 90 °C. [b] Determined from ^{1}H NMR spectra of dried polymer samples in CDCl$_3$. [c] based on isolated polymer yield. [d] determined by GPC (triple detection).

Table 3.12: PO ROCOP using Ti(IV) complexes[a]

Entry	Cat.	Anhydride	Time (min)	Ester[b] (%)	Y_w[c] (%)	Mn[d] (g/mol)	DP	PDI[d]
91	**8**	PhA	120	99	85	16010	78	1.06
92	**8**	TCPhA	120	98	92	23334	68	1.42
93	**8**	TBPhA	150	96	70	42687	82	1.30
94	**10**	PhA	180	99	85	16939	82	1.11
95	**10**	TCPhA	180	98	90	31051	90	1.22
96	**10**	TBPhA	180	97	85	55955	107	1.27
97	**16**	PhA	120	99	91	17401	84	1.05
98	**16**	TCPhA	120	97	98	23419	68	1.52
99	**16**	TBPhA	180	97	64	72789	140	1.33
100	**17**	PhA	150	98	89	19622	95	1.16
101	**17**	TCPhA	180	98	93	25943	75	1.70
102	**17**	TBPhA	180	98	71	63576	122	1.27

[a][epoxide]:[Anhydride]:[Catalyst]:[Cocatalyst]=2000:400:1:1, reaction temperature= 90 °C. [b] Determined from ^{1}H NMR spectra of dried polymer samples in CDCl$_3$. [c] based on isolated polymer yield. [d] determined by GPC (triple detection).
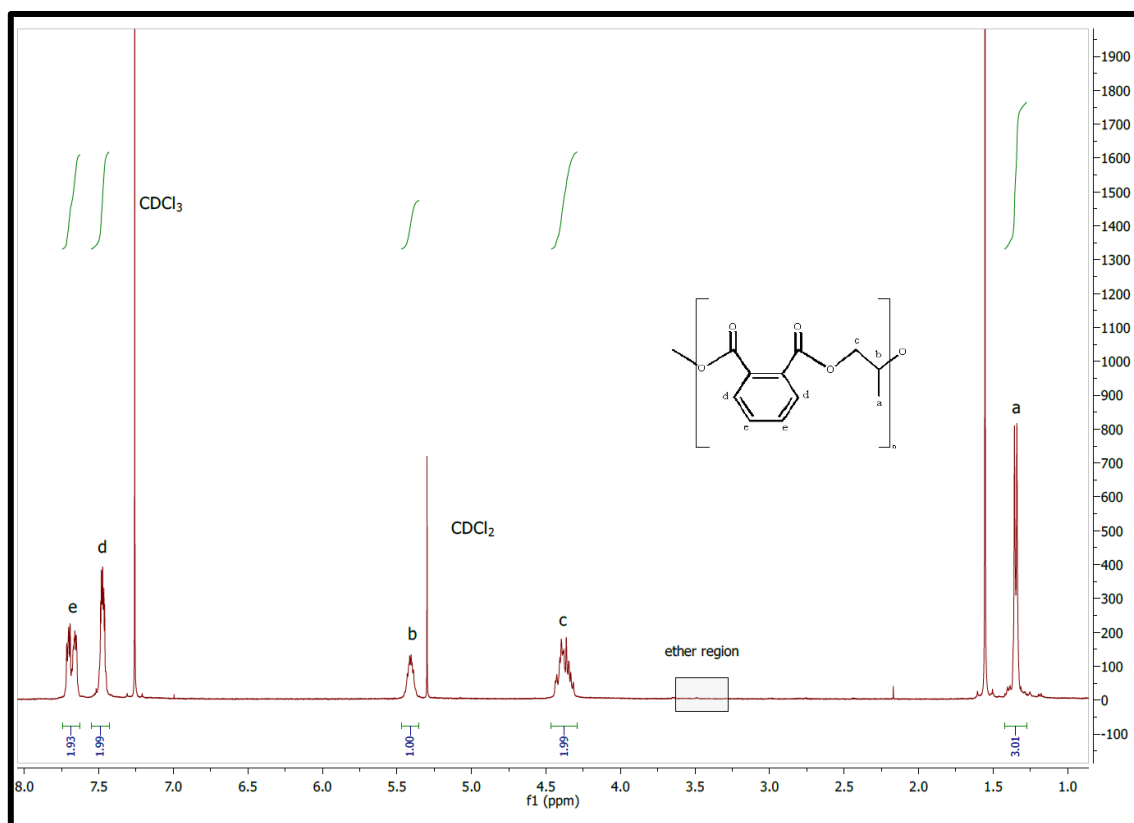
Figure 3.14: ^{1}H NMR spectrum (400 MHz, CDCl$_3$, 293 K) of Poly(PO-co-PhA) copolymer

(entry 79)

3.4.3 Ring opening copolymerization of ECH with anhydrides:

Epichlorohydrin (ECH) is considered an ideal building block for the production of chlorinated polymers. These polymers could be unique in e.g. flame retardant, resilient and dielectric properties.[48] In addition, ECH-containing polymers are suitable for post polymerization modification to introduce other functional groups via nucleophilic substitution of the pendent chloromethyl group.[49] The copolymerization of this epoxide requires a highly selective catalyst and reaction conditions that inhibit side reactions on the chloromethyl group.[50,51]

The ring opening copolymerization studies of ECH and cyclic anhydrides are relatively limited compared to other epoxides,[5,13,46,47] since the reactions are prone to side reactions on the chloromethyl group via nucleophilic substitution. This reaction supresses the propagation of some polymer chains and produces chloride anions that can reinitiate new polymer chains.[48]

As a result, lower molecular polymer mass with broader polydispersity indices are often obtained in the ROCOP of ECH with anhydrides compared to other epoxides, which emphasise its unique position in the series of epoxides that can be studied.[13,14,46]

The results of the ROCOP of ECH with anhydrides are given in Tables 3.13 and 3.14. Epichlorohydrin showed an enhanced polymerization rate to afford the polyesters with full phthalic anhydride conversion within 60 minutes (except for [t]Bu,[t]Bu-Salpy complexes **3**, **10** which required an extra 15 minutes). The polymers were produced with highly alternating structure (94-99% ester linkage). Its high reactivity could be ascribed to the presence of the electron withdrawing chloride group.[47] Although the activity was higher than other epoxide monomers, the poly(PhA-co-ECH) was produced with lower molecular weight, compared to CHO and PO, with broader PDI (1.34-1.65), which could be attributed to the stronger polarity of ECH which might lead to faster chain transfer reactions compared to successive addition.[42]

Table 3.13: ECH ROCOP of Ti(III) complexes[a]

Entry	Cat.	Anhydride	Time (min)	Ester[b] (%)	Y_w[c] (%)	Mn[d] (g/mol)	DP	PDI[d]
103	**1**	PhA	60	98	84	2331	10	1.49
104	**1**	TCPhA	120	86	50	10197	27	1.55
105	**1**	TBPhA	120	91	82	9692	17	1.79
106	**3**	PhA	75	97	85	3936	16	1.35
107	**3**	TCPhA	80	99	95	9528	25	1.74
108	**3**	TBPhA	135	98	93	7043	13	1.75
109	**6**	PhA	60	94	76	2311	10	1.45
110	**6**	TCPhA	120	99	63	9121	24	1.58
111	**6**	TBPhA	140	92	98	9797	18	1.75
112	**7**	PhA	60	98	78	2984	12	1.62
113	**7**	TCPhA	120	99	59	9105	24	1.59
114	**7**	TBPhA	140	98	87	8598	15	1.86

[a][epoxide]:[Anhydride]:[Catalyst]:[Cocatalyst]=2000:400:1:1, reaction temperature= 90 °C. [b] Determined from ^{1}H NMR spectra of dried polymer samples in CDCl$_3$. [c] based on isolated polymer yield. [d] determined by GPC (triple detection).

As with CHO and PO, Ti(IV) complexes are more active catalysts and produced polyesters with higher M_n and narrower PDI. It should be noted that Salpy complexes are more active compared to Salpn complexes, as found in the CHO copolymerization reactions. The addition of tert-butyl substituents to the ligand backbone slightly increased the polyesters' molecular mass for both Ti(III) and Ti(IV), with both Salpy and Salpn ligands. A representative ^{1}H NMR spectrum for the poly(ECH-co-TCPhA) is shown in Figure 3.15.

Table 3.14: ECH ROCOP using Ti(IV) complexes[a]

Entry	Cat.	Anhydride	Time (min)	Ester[b] (%)	Y_w[c] (%)	Mn[d] (g/mol)	DP	PDI[d]
115	**8**	PhA	60	95	78	5912	25	1.44
116	**8**	TCPhA	90	96	97	14484	38	1.78
117	**8**	TBPhA	120	97	98	10269	18	1.49
118	**10**	PhA	75	95	86	7494	31	1.48
119	**10**	TCPhA	75	99	95	15344	41	1.34
120	**10**	TBPhA	150	98	98	10632	19	1.68
121	**16**	PhA	60	95	75	3438	14	1.34
122	**16**	TCPhA	120	98	55	11153	29	1.78
123	**16**	TBPhA	140	98	88	8816	16	1.66
124	**17**	PhA	120	97	78	4215	18	1.56
125	**17**	TCPhA	120	99	76	10401	27	1.54
126	**17**	TBPhA	140	98	91	9122	16	1.58

[a][epoxide]:[Anhydride]:[Catalyst]:[Cocatalyst]=2000:400:1:1, reaction temperature= 90 °C. [b] Determined from ^{1}H NMR spectra of dried polymer samples in CDCl₃. [c] based on isolated polymer yield. [d] determined by GPC (triple detection).
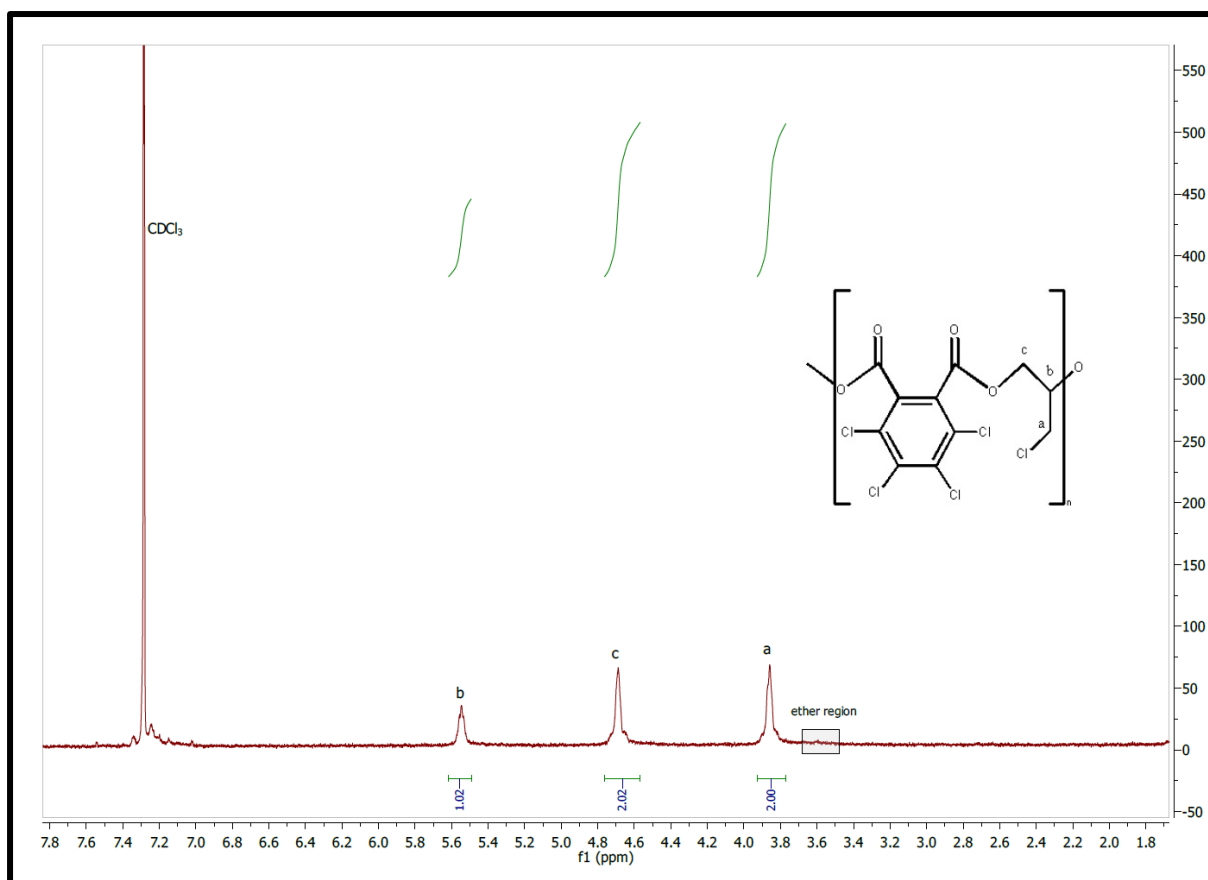
Figure 3.15: ^{1}H NMR spectrum (400 MHz, CDCl$_3$, 293 K) of poly(ECH-co-TCPhA) polyester (entry 107)

3.4.4 Ring opening copolymerization of SO and VCHO with anhydrides:

Catalyst **1** was further tested in the bulk ROCOP polymerization of styrene oxide (SO) and 4-vinyl-1-hexene-1,2-epoxide (VCHO) with PhA, TCPhA and TBPhA (Table 3.15). SO, as mentioned in the solution ROCOP section (3.3), was found to be more difficult to copolymerize due to its rigid and bulky structure. The copolymerization of TCPhA with SO resulted in an undefined product with low molecular weight (1815 g/mol, entry 128), indicating an oligomeric product, whereas no product was observed in the copolymerization with TBPhA. The ROCOP of PhA with SO required more time (150 min) and resulted in high selective polyester with M_n= 9163 and narrow PDI (1.18, entry 127).

The copolymerization of VCHO with anhydrides shows similar reactivity as found for CHO, which is expected owing to the comparable epoxide structure. However, VCHO polyesters were produced with slightly higher molar mass (the copolymerization with PhA

131

produced polyster with Mn= 15250 and 13316 g/mol with VCHO and CHO, respectively), but the difference is not significant given that VCHO has a larger molecular weight than CHO. The presence of the pendent vinyl group in VCHO makes its polyesters suitable for post polymerization modification.[12]

Table 3.15: ROCOP of SO and VCHO using **1**/PPNCl[a]

Entry	Cat.	Epoxi.	Anhydride	Time (min)	Ester[b] (%)	Y_w[c] (%)	M_n[d] (g/mol)	DP	PDI[d]
127	**1**	SO	PhA	150	98	98	9163	34	1.18
128	**1**	SO	TCPhA	180	-	-	1815	4	1.71
129	**1**	SO	TBPhA	180	-	-	-	-	-
130	**1**	VCHO	PhA	90	>99	88	15250	56	1.15
131	**1**	VCHO	TCPhA	90	97	99	15998	39	1.72
132	**1**	VCHO	TBPhA	180	96	98	13620	24	1.87

[a][epoxide]:[Anhydride]:[Catalyst]:[Cocatalyst]=2000:400:1:1, reaction temperature= 90 °C. [b]Determined from ^{1}H NMR spectra of dried polymer samples in CDCl$_3$. [c] based on isolated polymer yield. [d] determined by GPC (triple detection).

Table 3.16 gives a summary of the ROCOP of phthalic anhydride (PhA) with the different epoxides used in this study, using **1** as a catalyst and PPNCl as a cocatalyst. Catalyst **1** is selective as it produced highly alternating polyesters with all the epoxides. The biggest Mn value was found for the poly(PhA-co-VCHO) copolymer and the lowest for the poly(PhA-co-ECH) one (entries 130 and 103, respectively). The same observation was found by Bester and coworkers with chromium salophen complexes.[46]

Table 3.16: Copolymerization of PhA with different epoxides using **1**/PPNCl[a]

Entry	epoxide	Time (min)	Ester[b] (%)	Mn[c] (g/mol)	DP	PDI[c]
49	CHO	90	>99	13316	54	1.11
79	PO	120	>99	11687	57	1.15
103	ECH	60	98	2331	10	1.49
127	SO	150	98	9163	34	1.18
130	VCHO	90	>99	15250	56	1.15

[a][epoxide]:[Anhydride]:[Catalyst]:[Cocatalyst]=2000:400:1:1,reaction temperature= 90 °C. [b] Determined from ^{1}H NMR spectra of dried polymer samples in CDCl$_3$. [d] determined by GPC (triple detection).

Generally, compared to solution conditions, the copolymerizations are much faster in neat epoxide, producing polyesters with higher molecular masses in significantly less time. The copolymerization of TCPhA and TBPhA with epoxides resulted in polyesters with higher molecular weight but broader dispersities which indicate the presence of transesterification reactions.[32]

3.5 The effect of temperature on the ROCOP:

The effect of the reaction temperature on the ROCOP reactions has been studied using CHO and PhA as a representative example. CHO was chosen because of its high boiling point, giving more scope for increased reaction temperatures. The copolymerization reactions were performed at 70, 80, 90, 100, 110 and 120 °C using [Ti(salpy)Cl] **1**/ PPNCl in bulk (Table 3.17). All of the reactions were performed to full PhA conversion as determined by ^{1}H NMR spectroscopy. The data suggest that higher temperatures are more desirable for the copolymerization of CHO with PhA. Increasing the temperature led to significant decrease in copolymerization time (from 3.5 hours at 70°C to 20 minutes when using 120°C). Importantly, the selectivities are high in all experiments. Bester and co-workers found that increasing the temperature led to a decrease in the reaction time but did not affect the molecular weight M_n.[46] In contrast to Bester and co-workers study, the results herein indicate that an increase in the temperature did increase the molecular weight (e.g., from M_n=7242 at 70 °C (entry 133) to

15730 at 120 °C (entry 137), which is more than double) and with narrow polydispersity indices in all cases.

These results revealed, as expected by a consideration of the Arrhenius equation, that higher reaction temperatures shows a positive impact on the reaction rate under otherwise identical conditions.[7,13] However, higher temperatures can be detrimental to the selectivity, since copolymerization operates in kinetic control in competition with epoxide homopolymerization, and so higher temperatures can lead to lower selectivity. The data in Table 3.17 suggests that this is not the case here, which is excellent for providing rapid catalysts with no loss in control over the reaction outcome.

Table 3.17: Temperature effect on the ROCOP of CHO and PhA using **1**/PPNCl[a]

Entry	Temp.	Time (min)	Ester[b] (%)	Y_w[c] (%)	Mn[d] (g/mol)	DP	PDI[d]
133	70	210	99	94	7242	29	1.11
134	80	180	99	97	8474	34	1.28
49	90	90	99	95	13316	54	1.11
135	100	40	99	85	11982	49	1.27
136	110	30	99	83	15314	62	1.09
137	120	20	99	86	15730	64	1.09

[a][CHO]:[PhA]:[**1**]:[PPNCl]=2000:400:1:1. [b] Determined from ^{1}H NMR spectra of dried polymer samples in CDCl$_3$, [c] based on isolated polymer yield, [d] determined by GPC (triple detection).

As mentioned above, it is important to terminate bulk polymerisation reactions as soon as full anhydride conversion is reached, to avoid epoxide homopolymerization and a resulting reduction in overall selectivity. Whether or not this is important for the Ti complexes in this thesis was probed by allowing the reaction to continue beyond PhA consumption. Increasing the reaction time after the PhA full conversion did not affect the selectivity (the hompolymerization of the excess CHO did not occur), however, a noticeable reduction in molecular mass was observed with a broadening of the polydispersity (Table 3.18). This suggests that side reactions (e.g. transesterification) have taken place after the complete anhydride conversion, and is consistent with the observations above in which the solution reactions gave lower molecular weight polymers.[2,42]

Table 3.18: The effect of increased reaction time[a]

Entry	Temp.	Time (min)	Ester[b] (%)	Y_w[c] (%)	Mn[d] (g/mol)	DP	PDI[d]
135	100	40	99	85	11982	49	1.27
138	100	90	99	92	8764	36	1.5
136	110	30	99	83	15314	62	1.09
139	110	60	99	98	12054	49	1.31
137	120	20	99	86	15730	64	1.09
140	120	60	99	99	13605	55	1.32

[a][CHO]:[PhA]:[**1**]:[PPNCl]=2000:400:1:1. [b] Determined from ^{1}H NMR spectra of dried polymer samples in CDCl_3, [c] based on isolated polymer yield, [d] determined by GPC (triple detection).

3.6 Molecular weight and GPC:

The molecular weights and molecular weight distributions for all of the prepared polyesters were measured using Gel Permeation Chromatography (GPC). The GPC traces of most of the polymers showed bimodal patterns as is routine with epoxide/anhydride ROCOP.[52] However, in some polymers the GPC revealed 3,4 or 5 modal patterns. The multimodal GPC traces of the polyesters arise when the polymerization reaction contains multiple initiators. The presence of initiators in the polymerization reaction other than the catalyst will cause the propagation of multi polymer chains. Traces of protic impurities, such as water, diacids or diols resulting from hydrolysed anhydrides or epoxides, respectively, will act as chain transfer agents.[4,17,19] In addition to the possibility of the catalyst to initiate two polymers per catalyst. These impurities were found to be difficult to exclude even with using dried epoxides and sublimed anhydrides.[32]

Coates and coworkers proposed that the ROCOP catalytic cycle required an anionic six coordinate complex to initiate.[24] To detect this anion, 1 equivalent of the catalyst [Ti(Salpy)Cl] **1**, cocatalyst (PPNCl), and CHO were dissolved in 1.5 ml THF in a small ampoule charged with stirring bar. After stirring for 2 minutes, the solvent was removed *in vacuo* and the residue submitted for mass spectra analysis. The ASAP in negative mode shows a peak at m/z =

552.10 which is related to the anion [Ti(Salpy)(OR)Cl]$^-$. Repeating the experiment with 2 equivalents of CHO a new peak was observed at m/z=615.13 which attributed to [Ti(Salpy)(OR)$_2$] $^-$. This observation is consistent with reports that the copolymerization proceeds via a bis alkoxide initiator. Also, it proved that the catalyst Ti(III) does not change its oxidation state and thus the ROCOP is not a redox reaction.

3.7 Density functional calculations:

3.7.1 Experimental

Calculations were undertaken using the Gaussian 09 program.[53] The M06 functional[54] was used along with the def2-TZVP basis set[55] on all centres. Structures were optimised without symmetry constraints and the nature of each stationary point verified by a frequency calculation; minima contained no imaginary frequencies and transition states contained a single imaginary frequency that corresponded to the expected reaction coordinate. Low frequency vibrations can give rise to a substantially overestimated entropy contribution to the Gibbs free energy, and therefore all frequencies of < 100 cm^{-1} were raised to 100 cm^{-1} for the thermochemical analyses. Thermochemical analyses were also corrected for the relative concentration differences of the monomers vs. catalyst using the Sackur-Tetrode equation for translational entropy. Thermochemical corrections were applied using the Goodvibes program.[56] NBO analyses were calculated using NBO 6.0,[57] and QTAIM calculations were executed on the AIMAll program.[58] Calculations were executed by Dr Benjamin Ward.

3.7.2 Results and discussion

The mechanism for the ring-opening copolymerisation of succinic anhydride and ethylene oxide was modelled using density functional theory calculations. The mechanism was inspired by that reported by Coates *et al.*,[24] and the substrates were chosen to provide the least amount of computational complexity.

The proposed and currently accepted mechanism for Salen aluminium complexes involves an initiation process to ring-open two epoxides, giving a bis(alkoxide) complex which is anionic, i.e. [Al(Salen)(OR)$_2$]$^-$ where OR corresponds to the epoxide that has been ring-opened by a chloride anion. Previous experiments in the Ward research group have demonstrated that a similar observation is seen with the [Al(Salpy)Cl] pre-catalyst, in which the pyridyl becomes pendant to allow for a second polymer chain to be initiated. Under catalytic conditions, reaction of the alkoxide ligands with anhydride is expected to be relatively

fast, and therefore a bis(carboxylate) ligand will be formed i.e. [Al(Salen)(O$_2$CR)$_2$]$^-$ for the Salen catalyst system, which corresponds to the resting state of the catalyst until the concentration of anhydride becomes low; at this point the anhydride insertion becomes slow and the alkoxide congeners [Al(Salen)(OR)$_2$]$^-$ and [Al(Salen)(OR)(O$_2$CR)]$^-$ become the dominant forms of the catalyst. For the purpose of this computational study, an early stage in the catalytic reaction is assumed, with both epoxide and anhydride in excess relative to the catalyst; the catalytic cycle therefore starts with the bis(carboxylate) complex [Ti(Salpy)(O$_2$CMe)$_2$], and proceeds via one of the carboxylates extending the polymer chain by successive reaction with epoxide followed by anhydride. Acetate was used as a suitable starting point for the polymer chain. In reality, both carboxylates could extend the polymer chain and intermediate decoordination of carboxylate-terminated polymer chains would involve both of these ligands, but for the purposes of this study a simplified system is assumed.

The preparation of Ti(IV) complexes with a protonated pyridyl group provides the possibility that the pyridylium could act as an internal cocatalyst, removing the need for PPNCl altogether, consistent with the cyclopropenium catalyst reported by Coates.[59] Unfortunately, time constraints owing to the Covid19 pandemic meant that these studies could not be undertaken, but the possibility was probed using DFT calculations and compared to the equivalent process without the pyridylium. To this end, the mechanism was calculated twice, with the pyridyl protonated as seen in the solid state structures, and again with a non-protonated pyridyl. An energy profile is provided in Figure 3.16.
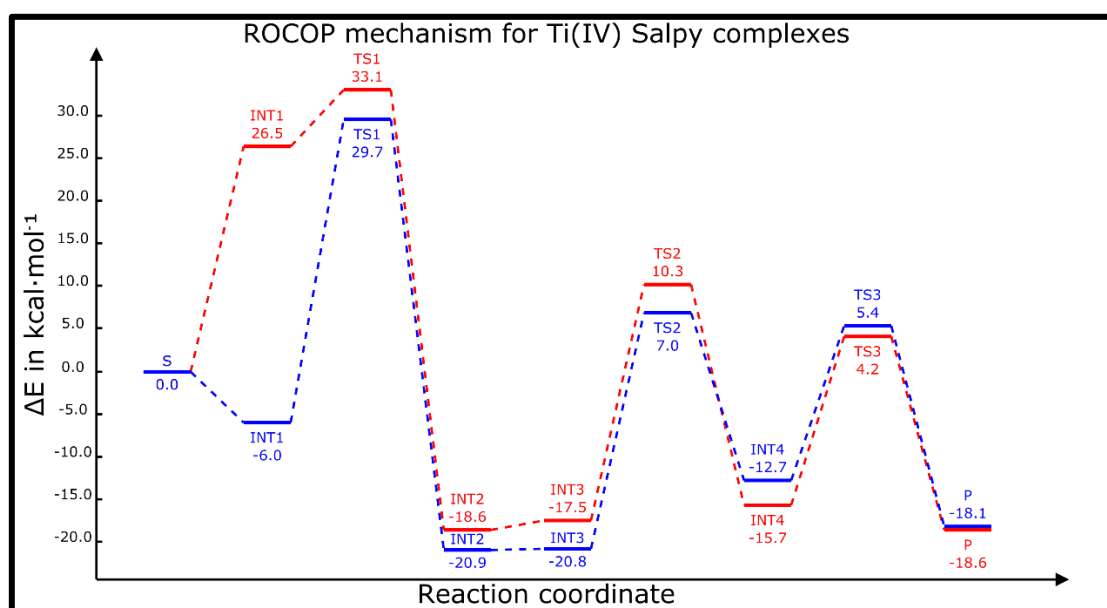
Figure 3.16: Free energy profile (363 K) for the calculated ring-opening copolymerisation mechanism by [Ti(Salpy)(O$_2$CMe)$_2$]. Blue = protonated pyridyl; red = non-protonated pyridyl [M06 | def2-TZVP].

The Coates mechanism relies on the observation that an intramolecular attack of a carboxylate ligand to open a coordinated epoxide is subject to an unacceptably high activation energy, and therefore a carboxylate-terminated polymer chain decoordinates from the metal, allowing coordination of an epoxide; the non-coordinated carboxylate subsequently undergoes intermolecular attack at one of the epoxide ring-carbons to afford a ring-opened alkoxide. It is the decoordination of a carboxylate that normally requires the presence of a co-catalyst; when PPN-Cl is added, the carboxylate decoordinates as a PPN ion-pair, which is energetically much more favourable than the simple dissociation of a charged carboxylate ligand. In Fig. 3.16, INT1 corresponds to the epoxide being coordinated and the decoordinated acetate being proximal to the coordination sphere, and therefore pre-organised for the nucleophilic attack. Without the pyridyl being protonated, INT1 lies at +26.5 kcal mol^{-1} (only slightly lower in energy than the epoxide opening transition state); The energy of this step is expected to be substantially reduced upon decoordination of the acetate as a PPN ion pair; the nature of this ion pair is not fully understood and therefore were not included in the calculations. This step is the key difference between the protonated/non-protonated pathways; when the pyridyl is protonated the decoordinated acetate is able to form a hydrogen bond to the N-H group, reducing the energy of INT1 to -6.0 kcal mol^{-1}; in the non-protonated pathway this is not possible, and the acetate is held in an energy minimum by weaker van der Waals interactions which were detected by Bader's quantum theory of atoms in molecules (QTAIM) analysis, Fig. 3.17; in this analysis a number of bond critical points (BCPs) were detected between the acetate and the Salpy ligand periphery. QTAIM analysis monitors the electron density topology and defines a BCP as a saddle point in the electron density between two atoms; a minimum in the electron density is found along the vector joining the two atoms either side of a BCP and a maximum in the perpendicular direction. A BCP does not mean that a formal bond exists, in the sense of the Lewis definition, but it does indicate a bonding-type interaction between two atoms.
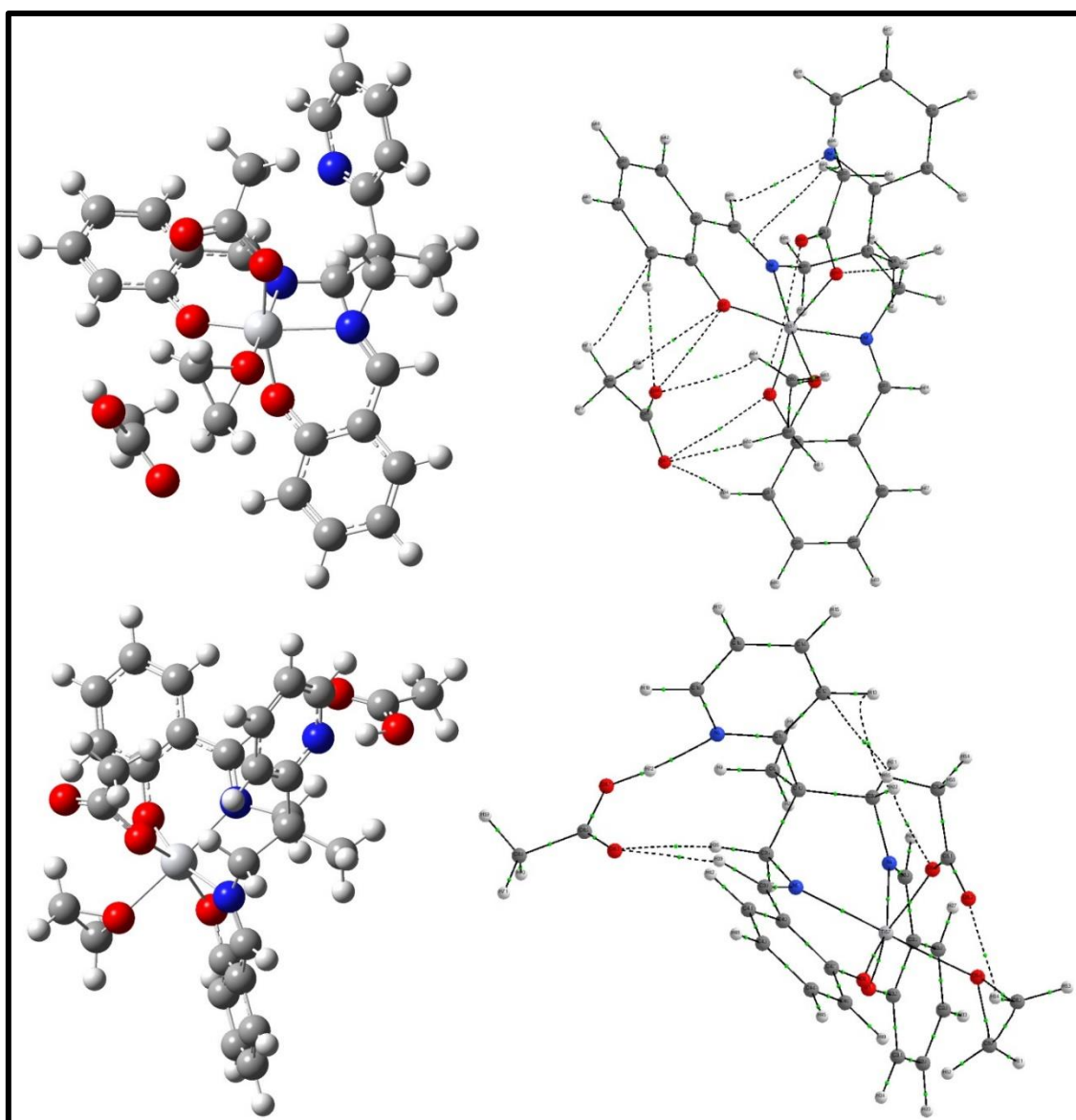
Figure 3.17: Calculated structure of INT1 (top: non-protonated pyridyl, bottom: protonated pyridyl) alongside QTAIM analyses showing the bond critical points between the non-coordinated acetate and Salpy ligand architecture [M06 | def2-TZVP].

For the protonated pathway, the decoordinated carboxylate forms a hydrogen bond with the protonated pyridylium, which explains the significant stabilisation of INT1 compared to the non-protonated pathway. This feature supports the idea that this species may not need a co-catalyst since the cationic pyridyl provides the counterion for dissociating the polymer chain, a necessary pre-requisite for chain propagation and consistent with the report by Coates that delivers a comparable effect with an aminocyclopropenium-functionalised ligand.[59] However the calculated structure explains a limitation in this regard: the energy minimum has the pyridylium proton transferred to the acetate. QTAIM analysis of the O-H…N moiety indicates

139

a O…H BCP with ρ = 2.05 e Å^{-3} and $\nabla^2(\rho)$ = –48.2 e Å^{-5}; the corresponding BCP for the H…N has ρ = 0.36 e Å^{-3} and $\nabla^2(\rho)$ = +2.15 e Å^{-5}. The value ρ corresponds to the electron density at the BCP, where a higher value indicates a stronger interaction; the value of the Laplacian $\nabla^2(\rho)$ gives an indication of the nature of the BCP interaction, where a positive value corresponds to a general depletion in electron density at the BCP (ionic interaction) and a negative value corresponds to a build-up of electron density at the BCP (covalent interaction). In the case being discussed, the QTAIM analysis indicates that the proton is formally transferred to the acetate (covalent O-H) with a significant H-bonding type interaction to the pyridyl (ionic N…H). This suggests that the concept of an internal cocatalyst is likely to have only limited effectiveness since the pyridylium is not likely to be inert enough to withstand the reaction conditions. Whilst there is an advantage of this system in that it is much easier to prepare than the cyclopropenium catalyst, these calculations point to a promising system if this deactivation process could be circumvented; possibly by replacing the N-H by N-Me. The key message from these calculations is that the pyridylium is expected to act as an alternative to PPN, but is not expected to have the same stability and point to exciting possibilities in further research.
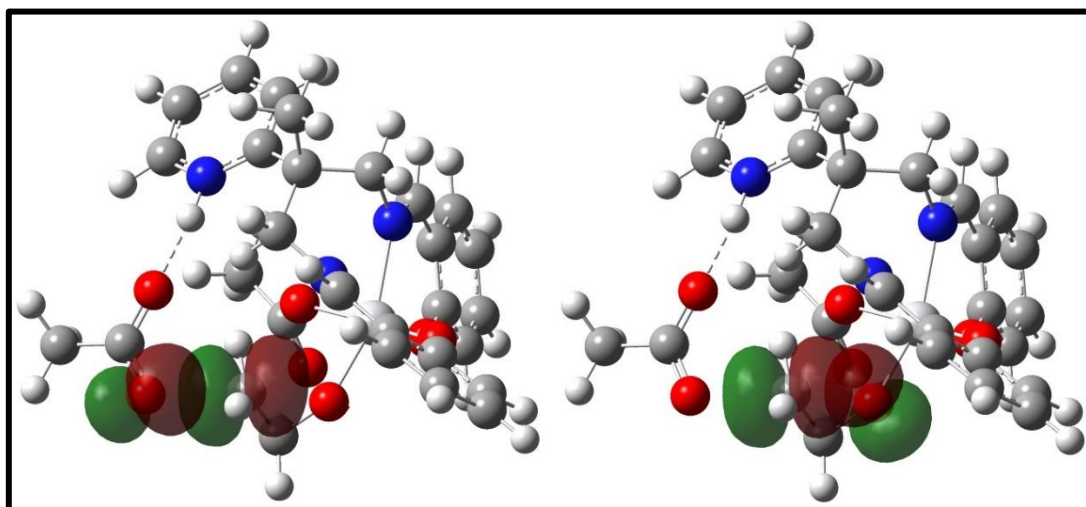
Figure 3.18: Donor-acceptor natural bonding orbital interactions for TS1 (protonated pathway) showing the forming bond (L) and breaking bond (R). Orbitals are drawn to an isovalue of 0.05 a.u. [M06 | def2-TZVP].

The transition state TS1, which corresponds to the opening of a coordinated epoxide by the non-coordinated acetate, is similar for both pathways inasmuch as the acetate undergoes an external attack upon one of the epoxide carbons; NBO analyses indicate that the attack is best described as an attack of the acetate via an sp^8 lone pair (i.e. a p orbital with some s

character) donating into a vacant p orbital on one of the epoxide carbons. The vacant p orbital on this carbon is formed by the heterolytic cleavage of the epoxide C-O bond, which splits into a C-based p orbital and an O-based p orbital (Fig. 3.18). The principal difference between the two pathways is that the attacking acetate is held in formation by a H-bond to the pyridylium group, which is not possible in the non-protonated route; this accounts for the stabilisation of the TS1 in the protonated path by 3.4 kcal mol^{-1}, but the two transition states are otherwise identical in nature. The energy of TS1 is consistent with that reported by Coates for aluminium salen complexes.[24]

As expected, the opening of an epoxide is highly exergonic, with TS1 representing the rate-determining transition state. This is consistent with experimental observations that ROCOP reactions are significantly faster when run in excess (neat) epoxide than when in a solvent such as toluene.

After adding an epoxide to the growing polymer chain, the subsequent addition of an anhydride was calculated to follow a route which is essentially identical to the generally accepted mechanism for the coordination insertion ring-opening polymerisation of cyclic esters. The anhydride initially undergoes a migratory insertion of the alkoxide-terminated polymer chain into the anhydride carbonyl group. The resulting alkoxide complex INT4 then undergoes ring-opening as the titanium migrates onto the ring-oxygen. This forms P, which is a carboxylate-terminated polymer chain and is effectively identical to the starting structure with the acetate now extended by one of each monomer. The relative energies for the two pathways are slightly different but the only one of note is that of TS2, where the coordinated (non-reacting) acetate is pushed towards the pyridyl and away from the reaction centre and is stabilised by a H-bond to the pyridylium (Fig. 3.19).
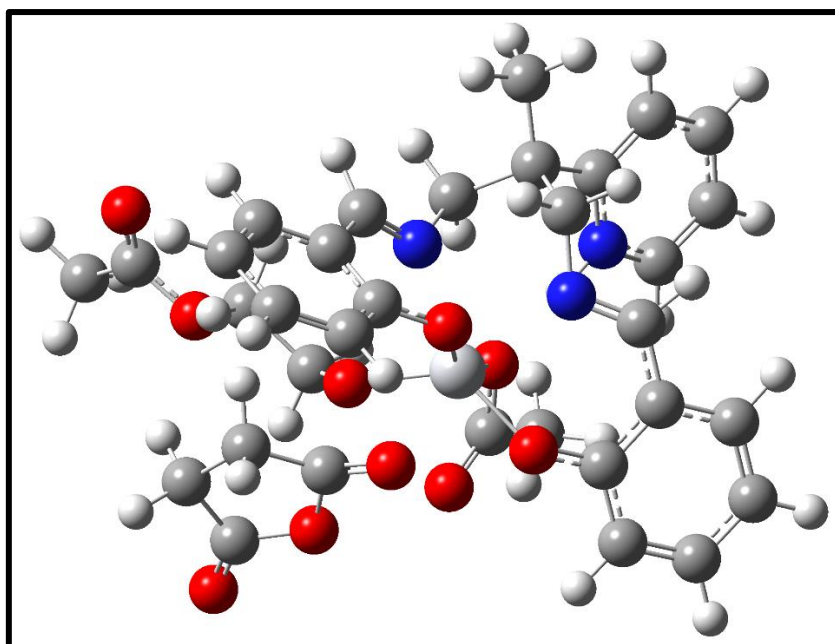
Figure 3.19: Structure of TS2 (protonated pathway) [M06 | def2-TZVP].
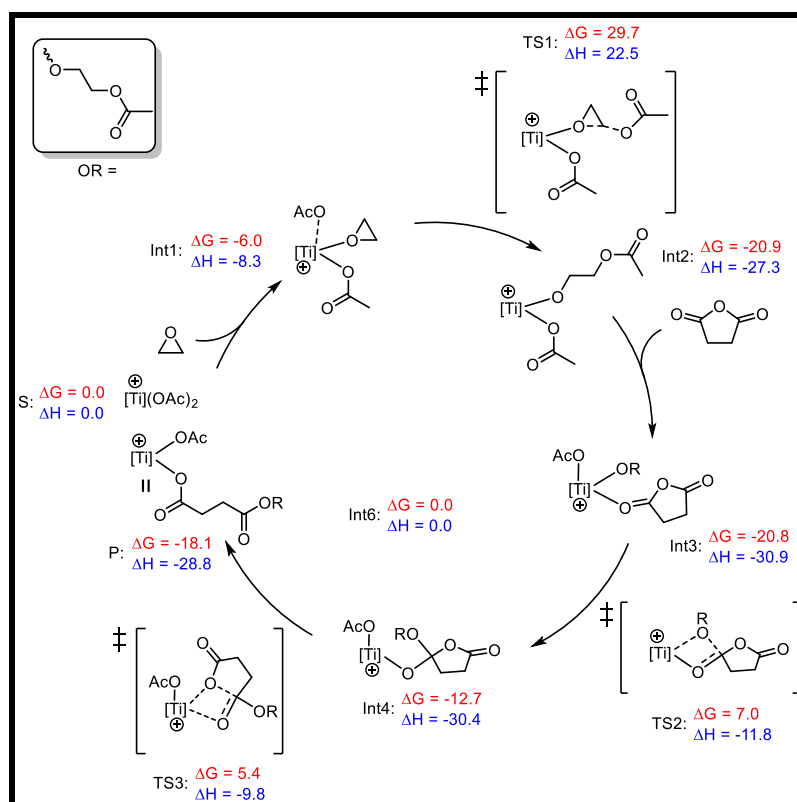
Figure 3.20: Calculated mechanism for the ROCOP of ethylene oxide with succinc anhydride by [Ti(Salpy)(OAc)₂] with a protonated pyridyl
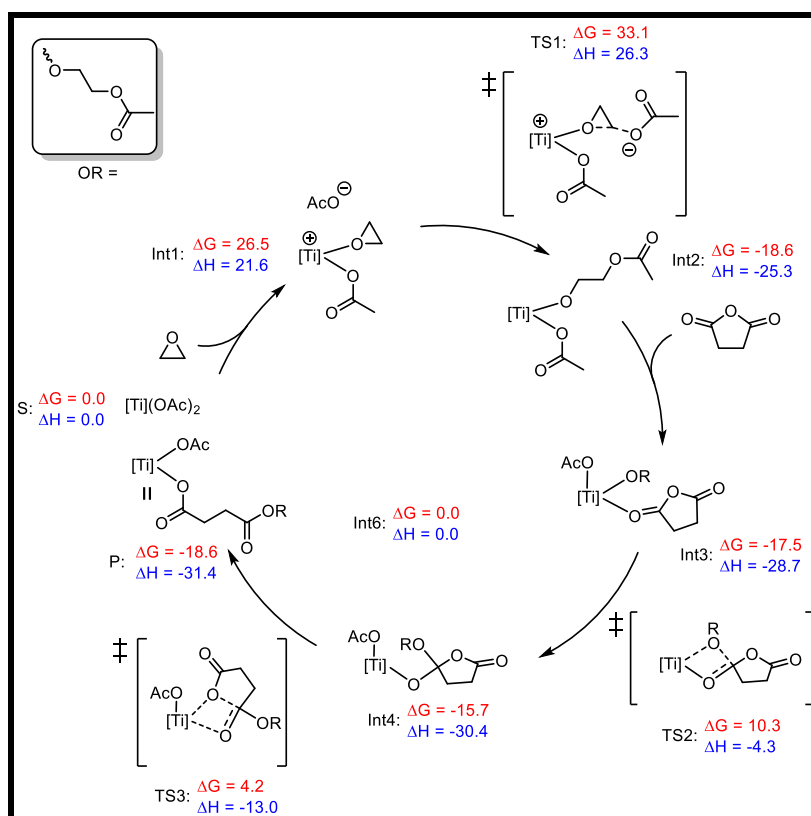
Figure 3.21: Calculated mechanism for the ROCOP of ethylene oxide with succinc anhydride by [Ti(Salpy)(OAc)$_2$] with a non-protonated pyridyl

3.8 Conclusion:

The synthesis of polyesters is attracting considerable attention as an alternative to commodity plastics. These polyesters are biodegradable, renewable, and biocompatible. In this thesis highly active catalysts for the alternating copolymerization of a range of epoxides and variety of anhydrides based upon titanium have been prepared, which is not a commonly used metal in this reaction. This work resulted in the effective synthesis of aliphatic and semi aliphatic polyesters with good M_n values and narrow PDIs.

The copolymerization was tested using [Ti(Salpy)Cl] **1** as catalyst alone (without cocatalyst) which results in good selectivity (86% ester linkage) in the case of poly(PO-co-SA) with good molecular mass. The incorporation of cocatalyst significantly improved the catalytic activity producing highly selective polymer (8% ether linkage) and higher molecular mass. PPNCl was more efficient in the copolymerization compared with DMAP.

Ring opening copolymerization of epoxides with cyclic anhydrides were performed in both solution and bulk reaction media using titanium (III) and (IV) based salen-type complexes

as catalyst and PPNCl as cocatalyst. The solution ROCOP result in polyester with highly selective polyester and good molecular masses, however due to the dilution effect the polymerization required long reaction time. A significant increase of the catalytic activity (the full anhydride conversion reached within 60-210 minutes and produced higher polyester molecular weight) was observed when the copolymerizations were performed in neat (excess of epoxides) which is in agreement with the copolymerization being first order dependence with respect to epoxides. The epoxide type significantly affected the copolymerization rates. Generally, better catalytic performance in copolymerization was achieved with Ti(IV) complexes compared to Ti(III), which is likely to reflect the greater stability of Ti(IV) complexes compared to Ti(III). This chapter demonstrates the utility of titanium in epoxide/anhydride ROCOP and it will be interesting to probe other ligand environments for this polymerisation class.

3.9 References:

1   E. Hosseini Nejad, C. G. W. van Melis, T. J. Vermeer, C. E. Koning and R. Duchateau, *Macromolecules*, 2012, **45**, 1770–1776.

2   N. J. Van Zee and G. W. Coates, *Angew. Chem. Int. Ed.*, 2015, **54**, 2665–2668.

3   D. J. Darensbourg, R. R. Poland and C. Escobedo, *Macromolecules*, 2012, **45**, 2242–2248.

4   P. K. Saini, C. Romain, Y. Zhu and C. K. Williams, *Polym. Chem.*, 2014, **5**, 6068–6075.

5   J. Liu, Y.-Y. Bao, Y. Liu, W.-M. Ren and X.-B. Lu, *Polym. Chem.*, 2013, **4**, 1439–1444.

6   X. Zhang, Y. Liu, Y. Chen, Z. Zhang, D. Fan and L. Xingqiang, *Inorg. Chem. Commun.*, 2014, **48**, 69–72.

7   D.-F. Liu, L.-Q. Zhu, J. Wu, L.-Y. Wu and X.-Q. Lü, *RSC Adv.*, 2015, **5**, 3854–3859.

8   C. Robert, T. Ohkawara and K. Nozaki, *Chem. Eur. J.*, 2014, **20**, 4789–4795.

9   A. M. DiCiccio and G. W. Coates, *J. Am. Chem. Soc.*, 2011, **133**, 10724–10727.

10 S. Huijser, E. HosseiniNejad, R. Sablong, C. de Jong, C. E. Koning and R. Duchateau, *Macromolecules*, 2011, **44**, 1132–1139.

11 N. D. Harrold, Y. Li and M. H. Chisholm, *Macromolecules*, 2013, **46**, 692–698.

12 R. C. Jeske, A. M. DiCiccio and G. W. Coates, *J. Am. Chem. Soc.*, 2007, **129**, 11330–11331.

13 G. Si, L. Zhang, B. Han, Z. Duan, B. Li, J. Dong, X. Li and B. Liu, *Polym. Chem.*, 2015, **6**, 6372–6377.

14 A. M. DiCiccio and G. W. Coates, *J. Am. Chem. Soc.*, 2011, **133**, 10724–10727.

15 C. Lv, M. Wu, S. Wang, C. Xia and W. Sun, *Tetrahedron Asymmetry*, 2010, **21**, 1869–1873.

16 E. H. Nejad, A. Paoniasari, C. G. W. van Melis, C. E. Koning and R. Duchateau, *Macromolecules*, 2013, **46**, 631–637.

17 H. K. Ryu, D. Y. Bae, H. Lim, E. Lee and K. Son, *Polym. Chem.*, 2020, **11**, 3756–3761.

18 O. Hauenstein, S. Agarwal and A. Greiner, *Nat. Commun.*, 2016, **7**, 11862.

19 R. Mundil, Z. Hošťálek, I. Šeděnková and J. Merna, *Macromol. Res.*, 2015, **23**, 161–166.

20 S. Paul, Y. Zhu, C. Romain, R. Brooks, P. K. Saini and C. K. Williams, *Chem. Commun.*, 2015, **51**, 6459–6479.

21 T. Aida and S. Inoue, *J. Am. Chem. Soc.*, 1985, **107**, 1358–1364.

22 A. Bernard, C. Chatterjee and M. H. Chisholm, *Polymer*, 2013, **54**, 2639–2646.

23 N. J. Van Zee, M. J. Sanford and G. W. Coates, *J. Am. Chem. Soc.*, 2016, **138**, 2755–2761.

24 M. E. Fieser, M. J. Sanford, L. A. Mitchell, C. R. Dunbar, M. Mandal, N. J. Van Zee, D. M. Urness, C. J. Cramer, G. W. Coates and W. B. Tolman, *J. Am. Chem. Soc.*, 2017, **139**, 15222–15231.

25 E. H. Nejad, A. Paoniasari, C. E. Koning and R. Duchateau, *Polym. Chem.*, 2012, **3**, 1308–1313.

26 D. Wannipurage, T. S. Hollingsworth, F. Santulli, M. Cozzolino, M. Lamberti, S. Groysman and M. Mazzeo, *Dalton Trans.*, 2020, **49**, 2715–2723.

27 J. M. Longo, M. J. Sanford and G. W. Coates, *Chem. Rev.*, 2016, **116**, 15167–15197.

28 D. J. Darensbourg, R. M. Mackiewicz, J. L. Rodgers and A. L. Phelps, *Inorg. Chem.*, 2004, **43**, 1831–1833.

29 D. J. Darensbourg and R. M. Mackiewicz, *J. Am. Chem. Soc.*, 2005, **127**, 14026–14038.

30 C. T. Cohen, T. Chu and G. W. Coates, *J. Am. Chem. Soc.*, 2005, **127**, 10869–10878.

31 M. Martínez de Sarasa Buchaca, F. de la Cruz-Martínez, J. Martínez, C. Alonso-Moreno, J. Fernández-Baeza, J. Tejeda, E. Niza, J. A. Castro-Osma, A. Otero and A. Lara-Sánchez, *ACS Omega*, 2018, **3**, 17581–17589.

32 Z. Hošťálek, O. Trhlíková, Z. Walterová, T. Martinez, F. Peruch, H. Cramail and J. Merna, *Eur. Polym. J.*, 2017, **88**, 433–447.

33 D. J. Darensbourg and M. W. Holtcamp, *Coord. Chem. Rev.*, 1996, **153**, 155–174.

34 R. L. Paddock, Y. Hiyama, J. M. McKay and S. T. Nguyen, *Tetrahedron Lett.*, 2004, **45**, 2023–2026.

35 F. Jutz, J.-D. Grunwaldt and A. Baiker, *J. Mol. Catal. Chem.*, 2008, **279**, 94–103.

36 R. Ciriminna, M. Lomeli-Rodriguez, P. D. Carà, J. A. Lopez-Sanchez and M. Pagliaro, *Chem. Commun.*, 2014, **50**, 15288–15296.

37   F. Isnard, M. Lamberti, C. Pellecchia and M. Mazzeo, *ChemCatChem*, 2017, **9**, 2972–2979.

38   M. R. Kember, A. Buchard and C. K. Williams, *Chem. Commun.*, 2011, **47**, 141–163.

39   D.-Y. Rao, B. Li, R. Zhang, H. Wang and X.-B. Lu, *Inorg. Chem.*, 2009, **48**, 2830–2836.

40   K. Nakano, M. Nakamura and K. Nozaki, *Macromolecules*, 2009, **42**, 6972–6980.

41   T. T. D. Chen, Y. Zhu and C. K. Williams, *Macromolecules*, 2018, **51**, 5346–5351.

42   H.-Y. Ji, B. Wang, L. Pan and Y.-S. Li, *Green Chem.*, 2018, **20**, 641–648.

43   A. Virachotikul, N. Laiwattanapaisarn, P. Wongmahasirikun, P. Piromjitpong, K. Chainok and K. Phomphrai, *Inorg. Chem.*, 2020, **59**, 8983–8994.

44   R. C. Jeske, J. M. Rowley and G. W. Coates, *Angew. Chem. Int. Ed.*, 2008, **47**, 6041–6044.

45   G. Jas and A. Kirschning, *Chem. – Eur. J.*, 2003, **9**, 5708–5723.

46   K. Bester, A. Bukowska, B. Myśliwiec, K. Hus, D. Tomczyk, P. Urbaniak and W. Bukowski, *Polym. Chem.*, 2018, **9**, 2147–2156.

47   A. M. DiCiccio, J. M. Longo, G. G. Rodríguez-Calero and G. W. Coates, *J. Am. Chem. Soc.*, 2016, **138**, 7107–7113.

48   B. Zhang, H. Li, H. Luo and J. Zhao, *Eur. Polym. J.*, 2020, **134**, 109820.

49   M. Xu, Z. Ge, X. Lu, H. Mo, Y. Ji and H. Hu, *RSC Adv.*, 2017, **7**, 47271–47278.

50   S. Carlotti, A. Labbé, V. Rejsek, S. Doutaz, M. Gervais and A. Deffieux, *Macromolecules*, 2008, **41**, 7058–7062.

51   C. G. Rodriguez, R. C. Ferrier, A. Helenic and N. A. Lynd, *Macromolecules*, 2017, **50**, 3121–3130.

52   M. J. Sanford, N. J. V. Zee and G. W. Coates, *Chem. Sci.*, 2018, **9**, 134–142.

53   M J Frisch G W Trucks H B Schlegel G E Scuseria M Robb J R Cheeseman G Scalmani V Barone B Mennucci G Petersson H Nakatsuji M Caricato X Li H P Hratchian F Izmaylov J Bloino G Zheng J Sonnenberg M Hada M Ehara K Toyota R Fukuda J Hasegawa M Ishida T Nakajima Honda O Kitao H Nakai T Vreven J Montgomery Jr J E Peralta F Ogliaro M Bearpark J J Heyd E Brothers K N Kudin V N Starover. T Keith R Kobayashi J Normand K Raghavachari Rendell J C Burant Iyengar J Tomasi M Cossi N Rega J M Millam M Klene J E Knox J B Cross V Bakken C Adamo J Jaramillo R Gomperts R E Strat. O Yazyev J Austin R Cammi C Pomelli J W Ochterski R Martin K Morokuma V G Zakrzewski G Voth P Salvador J J Dannenb. Dapprich Daniels O Farkas J B Foresman J V Ortiz J Cioslowski J Fox Gaussian 09 Revis. D01 Gaussian Inc Wallingford CT 2010.

54   Y. Zhao and D. G. Truhlar, *Theor. Chem. Acc.*, 2008, **120**, 215–241.

55   F. Weigend and R. Ahlrichs, *Phys. Chem. Chem. Phys.*, 2005, **7**, 3297–3305.

56   G. Luchini, J. V. Alegre-Requena, I. Funes-Ardoiz and R. S. Paton, *F1000Research*, 2020, **9**, 291.

57 D. Glendening, J. K. Badenhoop, A. E. Reed, J. E. Carpenter, J. E. Bohmann, C. M. Morales, C. R. Landis and F. Weinhold, *NBO 6.0, Theoretical Chemistry Institute, University of Wisconsin, Madison,* 2013.

58 T. A. Keith, AIMAll, TK Gristmill Software, Overland Park KS, USA, 2017.

59 B. A. Abel, C. A. L. Lidston and G. W. Coates, *J. Am. Chem. Soc.*, 2019, **141**, 12760–12769.

Chapter 4

Umpolung reactions

4.1 Introduction:

Over the past two decades, the metal-catalyzed conjugate addition reactions to Michael acceptors and enones has been an attractive research area. The assembly of nitrile or carbonyl at the position 1,6-, 1,4 or 1,2- of an alkyl chain by the formation of a C-C bond (Scheme 4.1) is considered as one of the most challenging tasks for new synthetic methods, as it requires the coupling of two similarly polarized positions.[1,2]
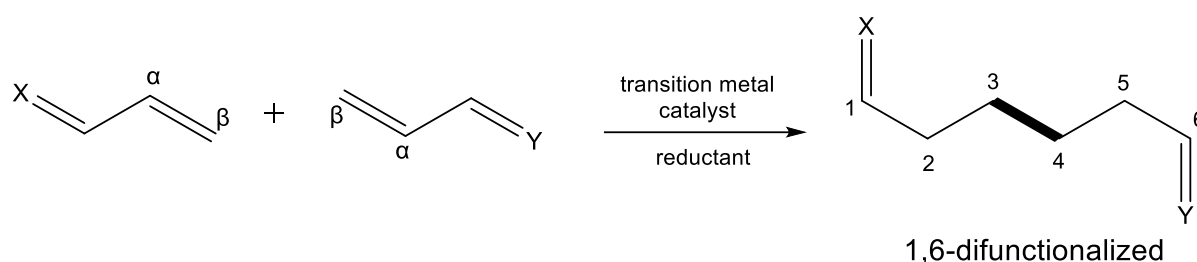
Scheme 4.37: Redox umpolung reaction

The "umpolung" concept, which is used widely in the development of synthetic methodology, can address this problem.[3,4] Electrochemical reductive or oxidative coupling procedures have been used in organic synthesis to achieve such connections.[5,6] However, the transition metal catalyzed alkyl-alkyl cross coupling reactions reported in the literature normally require laborious synthesis of metalated or halogenated coupling precursors.[2,7–9] This drawback was overcome by using easily available activated alkenes as cross- coupling partners (Scheme 4.2).[10,11] Currently, this addition can be achieved with good enantioselectivity and high yield using different catalysts;[2] in particular, the construction of asymmetric quaternary carbon centres, which is a particularly demanding challenge in synthetic organic chemistry, can be achieved with high yield.[12] Titanium(III) catalysts were found to be superior for reaching high selectivity in pinacol couplings and analogous reactions.[13–16] Notably, these Ti(III) reactions are radical reactions that are carried out with control over regio-, chemo-, and stereoselectivity, which is an advantage over the classical free radical reactions which tend to be less-easily controlled.[17,18]
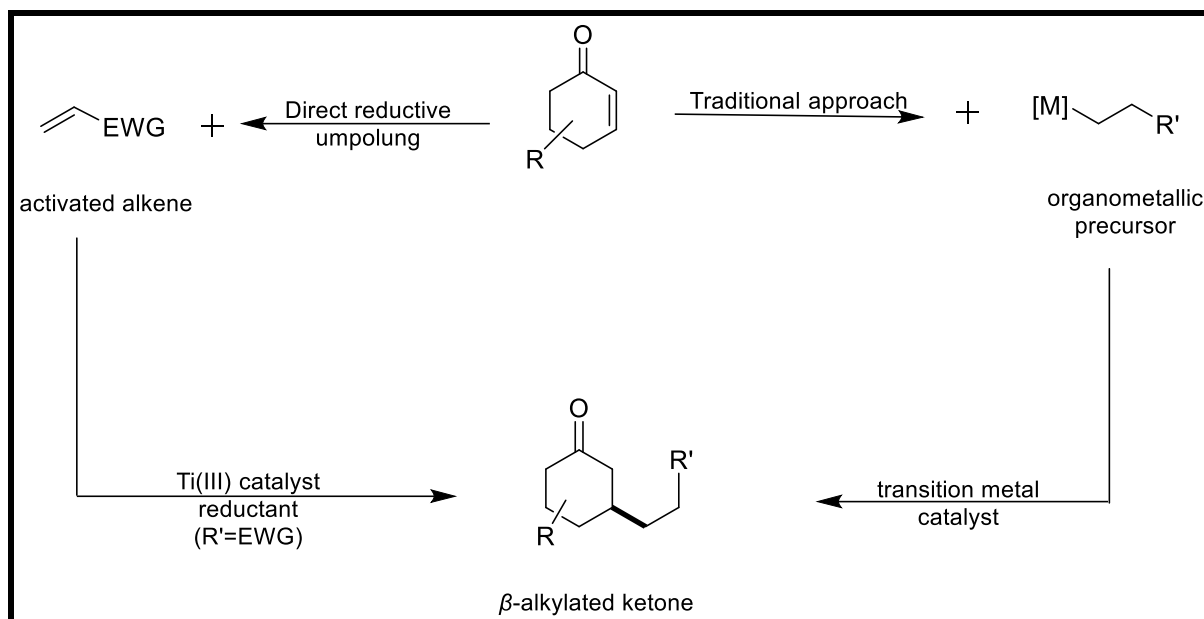
Scheme 4.38: Different methods to *β*-alkylated ketones

Titanium(III) catalysed umpolung cross coupling of Michael acceptors is a unique way to undertake conjugate β-alkylation reactions as it leads to 1,4- or 1,6-bifunctionalized compounds without the need of stoichiometric organometallic reagents.[10] The carbon-carbon bond formed by the addition of carbon nucleophile to *α,β*-unsaturated compound is activated by an electron withdrawing group.[2] The addition occurs on the *β*-carbon leading to the formation of a stabilized carbanion which protonated by the proton source. There are several parameters that can affect cross coupling reactions, such as solvent, the nature of metal ion, ligand structure, and the presence of competing catalytic species.

In this study, double reductive cross coupling reactions of enones with readily available activated alkenes were carried out to form a 1,6-difunctionalized carbon skeleton using two different a^3 synthons in one redox reaction, utilizing low valent titanium catalysts. These reactions lead to a tail-to-tail connection of two *α,β*-unsaturated compounds.

This coupling reaction was first reported in 2011 by Streuff.[1] The first attempt was to react 2-cyclohexen-1-one (**4.1**) with an excess of an inexpensive acrylonitrile (**4.2**) in the presence of titanocene dichloride (Cp$_2$TiCl$_2$) **4.3** (10%) as catalyst and Zn dust as stoichiometric reductant, which led to the formation of the cross coupling product in low yield (35%). However, repeating the reaction in presence of trimethylsilyl chloride (TMSCl) **4.4** gave complete conversion and significantly increased the yield to 87% by forming the corresponding

TMS-enol ether (**4.5**), which hydrolyzed easily to the desired product during workup (Scheme 4.3). Under these conditions several enones with varied substitution were coupled in good yield.
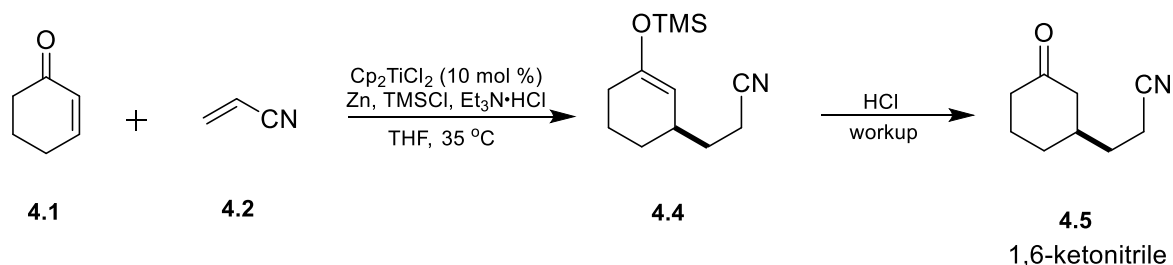
Scheme 4.39: Reductive cross coupling reaction of 2-cyclohexen-1-one with acrylonitrile

It should be noted that the TMS-enol ether intermediate (**4.4**) can be easily isolated from the reaction mixture and then employed in follow up chemistry such as Rubottom oxidation (Scheme 4.4).
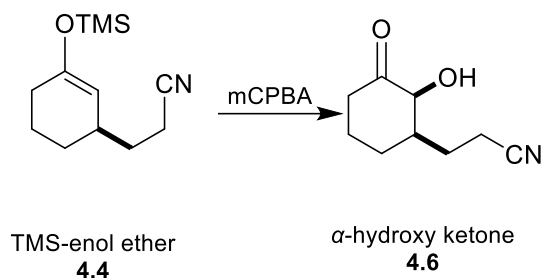
Scheme 4.40: Rubottom oxidation of TMS-enol ether (mCPBA= meta-chloroperoxybenzoic acid)

The substitution of Zn with Mn (a stronger reductant), which has often been applied in catalytic reductive coupling reactions with Cp_2TiCl_2 and other metals,[19,20] significantly reduced the yield to 55%. The addition of TMSCl found to be necessary for achieving turnover by silylation of Ti(IV)-enolate which is generated during the process.[10] The amount of $Et_3N\cdot HCl$ was carefully optimized as higher amounts led to competing reduction of the enone as reported by Ashfeld and coworkers.[21] An excess of acrylonitrile found to be essential to

suppress this reduction and other byproducts such as homocoupling of enone or its early silylation.[10]

When the reaction was undertaken without ammonium salt, only 10% conversion to the product was observed. Other ammonium salts like diisopropylethyammonium and Quinuclidinium gave slightly lower yields (64% and 78%), however, increased the acidity of the ammonium salts had a negative effect on the reaction, for example 2,4,6-collidine gave 55% conversion. The role of $Et_3N \cdot HCl$ cannot be interpreted by its acidity only but could be stem from its tendency to form a coordination complex with Ti(III) monomers **4.8**, which was found to stabilize the catalyst and thus prevent its decomposition (Scheme 4.5).[22,23]
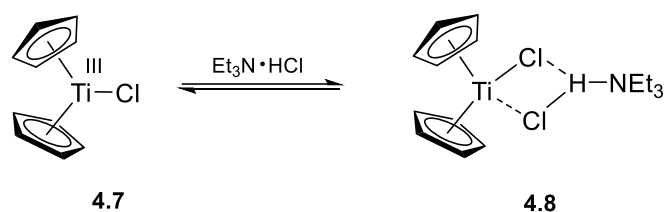
Scheme 4.41: Stabilizing impact of $Et_3N \cdot HCl$ on [Cp_2TiCl]

The most suitable solvent for these reactions was THF, which is usually employed in reactions that involved single electron transfer (SET).[10] Other solvents such as hexane, dichloromethane and diethylether gave lower yield, whereas a number of solvents such as 1,2-dimethoxyethane, toluene and chloroform gave almost no conversion to the coupling product. Lowering the catalyst amount to 3% or 5% mol gave reduction in the yield (55% and 70%, respectively) and increased the formation of products arising from competing reactions (homocoupling of **4.1** and silyl enol ether formation of the enone). Finally, performing the reaction without catalyst gave no conversion.

In this study, four Salpy complexes [Ti(Salpy)Cl] (**1**), [Ti(^{t}Bu,^{t}Bu-Salpy)Cl] (**3**), [Ti(Salpy)Cl$_2$] (**8**) and [Ti(^{t}Bu,^{t}Bu-Salpy)Cl$_2$] (**10**) and four Salpn complexes [Ti(Salpn)Cl] (**6**), [Ti(^{t}Bu,^{t}Bu-Salpn)Cl] (**7**), [Ti(Salpn)Cl$_2$] (**16**) and [Ti(^{t}Bu,^{t}Bu-Salpn)Cl$_2$] (**17**) were utilized as catalysts in the reductive umpolung cross coupling reactions of enones with nitriles. The cross coupling reactions were performed using the optimized conditions developed by Streuff;[1] in the glove box, an oven-dried screw cap vial containing a magnetic stir bar was charged with the catalyst, Zn powder, $Et_3N \cdot HCl$ and THF. The reaction mixture was stirred until the color changed from orange to green (in the case where Ti(IV) complexes were used) then, the enone cross coupling partner (fivefold excess) and TMSCl were added *via* pipette. After

sealing the vial, it was removed from the glove box and placed in preheated aluminium heating block at 35° C for 24 h. Workup was carried out and the product was purified by flash chromatography and characterized by ^{1}H and ^{13}C NMR spectroscopies and mass spectrometry.

4.2 Umpolung reductive cross coupling of 2-cyclohexen-1-one with acrylonitrile:

Direct conjugate alkylation of 2-cyclohexen-1-one (**4.1**) with an excess of the inexpensive and readily available acrylonitrile (**4.2**) was studied using Ti(III) and Ti(IV) salen type complexes as catalyst (Scheme 4.6, Table 4.1). This umpolung reaction led to the formation of C-C bonds between two equally polarized molecules under a catalyst controlled radical reaction.
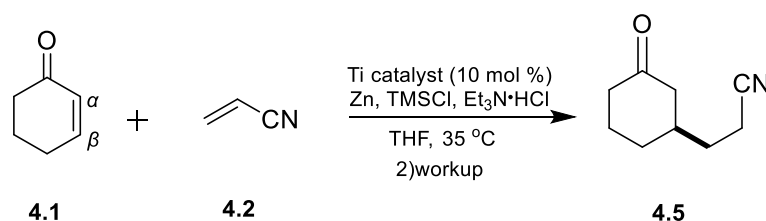
Scheme 4.42: Direct reductive umpolung reaction of 2-cyclohexen-1-one with acrylonitrile.

This reaction was first studied by Streuff in 2011 using Cp$_2$TiCl$_2$ as catalyst and zinc powder as reductant as mentioned above. The product; 3-(3-Oxocyclohexyl)propanenitrile (**4.5**) was obtained in 87% yield.[1] The same product (**4.5**) was synthesized in 1988 by Knochel et. al. from the reaction of **4.1** with a metalated nitrile **4.11** which need to be prepared in advanced (Scheme 4.7).[24]
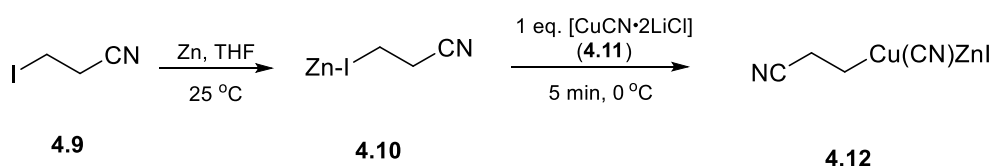
Scheme 4.43: Synthesis of the organometallic precursor for the cross coupling reaction

They first synthesized 2-cyanoethylzinc iodide (**4.10**) from the reaction of 3-iodopropionitrile (**4.9**) with zinc in THF at 25 °C, then **4.10** was transmetallated with CuCN·2LiCl (**4.11**) into the copper organometallic **4.12**, which finally coupled with **4.1** to form **4.5**. However, in this study Ti(III) will perform such connection in an easy one pot reaction of **4.1** with a readily available nitrile **4.2** without the need to the stoichiometric organometallic reagents.

Using Salen type complexes as catalysts under same conditions led to the product **4.5** but in lower (but still competitive) yields as can be seen in Table 4.1.

Table 4.1: Cross coupling yields **4.5** from **4.1**(0.5 mmol) with **4.2** (5 mmol) using Ti catalysts.[a]

Entry	Catalyst	Yield (%)[b]
1	[Ti(Salpy)Cl] (**1**)	80
2	[Ti(^{t}Bu,^{t}Bu-Salpy)Cl] (**3**)	72
3	[Ti(Salpn)Cl] (**6**)	82
4	[Ti(^{t}Bu,^{t}Bu-Salpn)Cl] (**7**)	75
5	[Ti(Salpy)Cl$_2$] (**8**)	84
6	[Ti(^{t}Bu,^{t}Bu-Salpy)Cl$_2$] (**10**)	78
7	[Ti(Salpn)Cl$_2$] (**16**)	86
8	[Ti(^{t}Bu,^{t}Bu-Salpn)Cl$_2$] (**17**)	80

[a]All reactions were carried out using 0.05 mmol of the catalyst, 2 eq. Zn, 1.3 eq. Et$_3$N·HCl, 1.5 eq. TMSCl and 1.25 ml THF at 35°C for 24h. [b] Isolated yield after flash chromatography.

In general Ti(IV) complexes gave higher yields compared to Ti(III) with the same backbone (compare entries 5-8 with entries 1-4), which could be indicative of greater stability of the Ti(IV) catalysts in storage, i.e. the Ti(III) species are better prepared in situ. The best performance was with catalyst **16** with 86% yield (entry 7) and the lowest yield was 72% with complex **3** (entry 2); these differences in isolated yield are expected to be within standard variation through the workup procedure, and so there appears little difference in reactivity based upon variation in the supporting ligand. It should be noted that the substitution in

positions 3 and 5 with ^tBu groups lower the yields by 6% (entries 2, 4, 6 and 8) which could be attributed to the steric bulk of this group and because the coupling depends on the coordination of the substrates to the metal centres (as will discussed in the mechanism section) the presence of this bulky group near to Ti centre might hamper the substrate from reaching the metal centres for the radical transformation.

The Salpy complexes were found to be lower activity compared to Salpn ones, but only slightly and with differences in yield that are not particularly significant. A lower reaction rate by Salpy complexes could be attributed to the additional bulkiness of the pyridyl (because the formation of the new C-C bond required the two intermediate molecules, the coordination complex with the enone and the coordination complex with the nitrile, to react close to each other), as well as the presence of an additional donor for the Ti centre. The small effect of the pyridyl is therefore unexpected and interesting.

4.3 Umpolung reductive cross coupling of 2-cyclopenten-1-one with acrylonitrile:

An enones with smaller ring size, cyclopentenone, was also tested as a cross coupling partner with acrylonitrile. The umpolung reaction of 2-cyclopenten-1-one (**4.13**) with acrylonitrile (**4.2**) was studied in the presence of the same titanium complexes as described above (Scheme 4.8). The conjugate reduction of cyclopenten-1-one and acrylonitrile was carried out in the dark because the cyclopenten-1-one is known to add to acrylonitrile in [2+2] addition.[25,26]
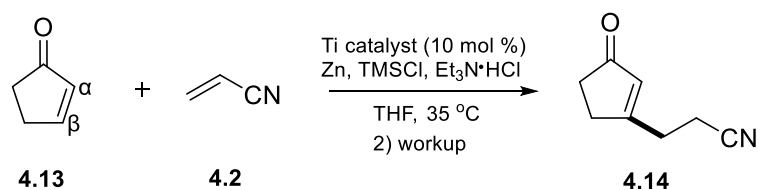
Scheme 4.44: Direct reductive umpolung reaction of 2-cyclopenten-1-one with acrylonitrile.

The product **4.14** has also been obtained previously by coupling **4.13** with the organometallic precursor **4.12** (which needs to be prepared in advance) instead of using the readily available acrylonitrile. Table 4.2 showed the yield results of reductive coupling of **4.13** with **4.2** in presence of titanium(III) and (IV) catalysts. The first observation is the low yields in all cases, and when analysing the products (both the crude and after workup solutions) by mass spectroscopy before purifying the samples by flash chromatography, there was a peak at m/z= 135.07 and this could be related to the [2+2] addition product **4.15** (Equation 4.1). This observation illustrates the strong ability of **4.13** to add to **4.2** in [2+2] addition even with light excluded and thus explains the universally low yield.

4.13   **4.2**   **4.15**
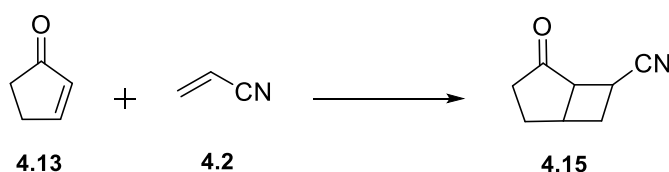
Equation 4.7: [2+2] addition of 2-cyclopenen-1-one to acrylonitrile

In the same way as found in the previous section, Ti(IV) complexes performed slightly better compared to the analogous Ti(III) complexes, for example, catalyst **1** produced **4.14** in 41% whereas **8** gave 45%(entries 9 and 13). The cross coupling reaction catalysed by complex **3** gave the lowest yield 39% (entry 10), presumably due to the steric hinderance, however, [Ti(Salpn)Cl$_2$] (**16**) produced the highest yield (with the lowest hinderance and one less competing donor), however the range of isolated yields showed only small variation overall.

156

Table 4.2: Cross coupling yields **4.14** from **4.13** (0.5 mmol) with **4.2** (5 mmol) using Ti catalysts.[a]

Entry	Catalyst	Yield (%)[b]
9	[Ti(Salpy)Cl] (**1**)	41
10	[Ti(^{t}Bu,^{t}Bu-Salpy)Cl] (**3**)	39
11	[Ti(Salpn)Cl] (**6**)	47
12	[Ti(^{t}Bu,^{t}Bu-Salpn)Cl] (**7**)	44
13	[Ti(Salpy)Cl$_2$] (**8**)	45
14	[Ti(^{t}Bu,^{t}Bu-Salpy)Cl$_2$] (**10**)	42
15	[Ti(Salpn)Cl$_2$] (**16**)	49
16	[Ti(^{t}Bu,^{t}Bu-Salpn)Cl$_2$] (**17**)	46

[a]All reactions were carried out using 0.05 mmol of the catalyst, 2 eq. Zn, 1.3 eq. Et$_3$N·HCl, 1.5 eq. TMSCl and 1.25 ml THF at 35°C for 24h. [b] Isolated yield after flash chromatography.

4.4 Umpolung reductive cross coupling of 3-methyl-2-cyclohexen-1-one with acrylonitrile:

The ability to construct quaternary carbon centres is considered as one of the most challenging targets in asymmetric catalysis.[27] To demonstrate the scope of this cross coupling reaction, 3-methyl-2-cyclohexen-1-one (**4.16**) were studied using the same optimized conditions using Ti-salen type catalysts (Scheme 4.9), although these catalysts are not chiral and so no asymmetric induction was expected, nor was it looked for.
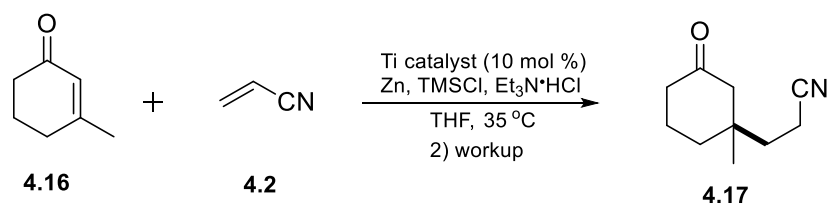
Scheme 4.45: Direct reductive umpolung reaction of 3-methyl-2-cyclohexen-1-one with acrylonitrile.

The reductive cross coupling between **4.16** and **4.2** was tested using the same titanium complexes as detailed above. Table 4.3 shows the yield of **4.17** produced from these reactions. In general, the isolated yields span only a 14% range (65%-79%) and are lower than those obtained with cyclohexeneone. This could be explained by the greater steric demand of the methyl group on the coupling carbon. The catalyst [Ti(^{t}Bu,^{t}Bu-Salpy)Cl] (**3**) was again inferior to the others and produced 65% of the cross coupling product, on the other hand, catalyst **16** gave 79% yield (entries 18 and 23, respectively). Also here, Ti(IV) complexes were more reactive compared to the Ti(III) congeners, e.g. catalyst **6** gave 75% product compared to the analogous Ti(IV) complex (**16**) which gave 79% yield.

Table 4.3: Cross coupling yields **4.17** from **4.16** (0.5 mmol) with **4.2** (5 mmol) using Ti catalysts.[a]

Entry	Catalyst	Yield (%)[b]
17	[Ti(Salpy)Cl] (**1**)	70
18	[Ti(^{t}Bu,^{t}Bu-Salpy)Cl] (**3**)	65
19	[Ti(Salpn)Cl] (**6**)	75
20	[Ti(^{t}Bu,^{t}Bu-Salpn)Cl] (**7**)	71
21	[Ti(Salpy)Cl$_2$] (**8**)	74
22	[Ti(^{t}Bu,^{t}Bu-Salpy)Cl$_2$] (**10**)	69
23	[Ti(Salpn)Cl$_2$] (**16**)	79
24	[Ti(^{t}Bu,^{t}Bu-Salpn)Cl$_2$] (**17**)	73

[a]All reactions were carried out using 0.05 mmol of the catalyst, 2 eq. Zn, 1.3 eq. Et$_3$N·HCl, 1.5 eq. TMSCl and 1.25 ml THF at 35°C for 24h. [b] Isolated yield after flash chromatography.

In general, these experiments demonstrate that the titanium complexes studied in this chapter were able to construct quaternary carbon centres smoothly from the reductive coupling of acrylonitrile with *β*-substituted enones.

4.5 Umpolung reductive cross coupling of acetophenone with phenylacetonitrile:

With the successful results for Salpy and Salpn titanium complexes as catalysts in the reductive coupling of enones with acrylonitrile, these complexes were studied as catalysts in the cross coupling reaction between nitriles and ketones to form α-hydroxyketones (Scheme 4.10). This type of coupling was studied previously using titanocene and its derivatives which were found to be effective catalysts for the construction of new C-C bonds with good yield and high stereoselectivities.[17,28,29] The cross coupling reaction of the readily available precursors acetophenone (**4.18**) with phenylacetonitrile (**4.19**) was first studied using [Ti(Salpy)Cl] (**1**), however no product was obtained. The reaction was then repeated with [Ti(Salpn)Cl] (**6**) and again no product was observed. Changing reaction temperature did not improve the result. The cross coupling in this reaction did not work with our catalysts which could be attributed to the increased steric hindrance compared to the previously studied complexes. All the precursors are big molecules compared to acrylonitrile and the catalyst itself is comparatively bigger (relative to titanocene) which could prevent the intermediate complexes from forming the new C-C bond.
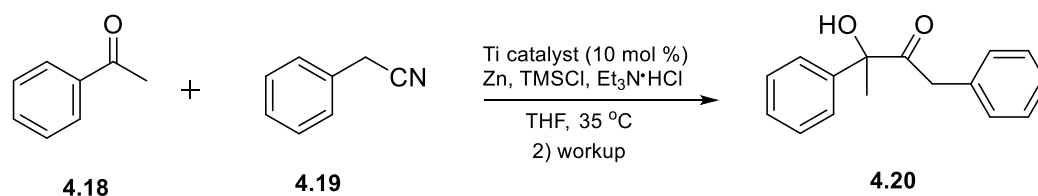
Scheme 4.46: Cross coupling of acetophenone with phenylacetonitrile

Most of the studies on titanium complexes as redox catalysts are concentrated on titanocene and its derivatives. However, there are few studies that employ salen-type complexes to mediate this reaction. The first use of titanium-salen type in redox reaction was in 1999 by Cozzi et al. in pinacol coupling of aldehydes.[30] They studied [(^{t}Bu,^{t}Bu-salen)TiCl$_2$] (**4.21**) to catalyse the coupling of benzaldehyde and they obtained 43% yield. In 2003 Chatterjee and coworkers studied the unsubstituted titanium salen complex [(salen)TiCl$_2$] (**4.22**) as a catalyst for the same reaction and they obtained 88% yield.[31] These two studies

are consistent with the conclusion determined herein that the bulk substitution on the phenyl moiety decreases the yield.

In future, the number of additives could be reduced, for example, Streuff and coworkers used a metal free reductant in their study of umpolung reductive of enone-nitrile, carbonyl-nitrile and pinacol coupling reactions.[32] They used bis(N-trimethylsilyl)-1,4-diazines (**4.26**) as a reducing agent and as a substitution for the TMSCl (Scheme 4.11); they obtained good yields with high stereoselectivities of the coupling products.
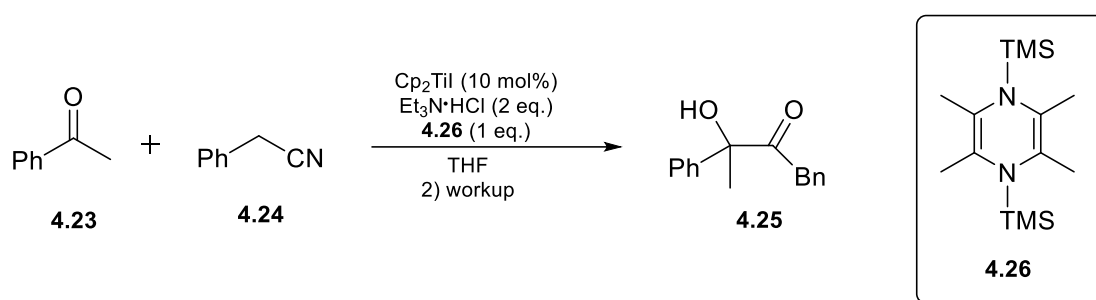
Scheme 4.47: Cross coupling reaction using metal free reductant

4.6 Mechanism:

A proposed mechanism was suggested by Streuff and coworkers, based on the observations they found during their study of cross coupling reductive umpolung reaction of several enones with a number of nitriles (70 examples), as well as using DFT calculations.[10] This mechanism is thought to be the same for the complexes in this chapter, and therefore a proposed mechanism is provided below, inspired by the work of Streuff et al (Scheme 4.12).
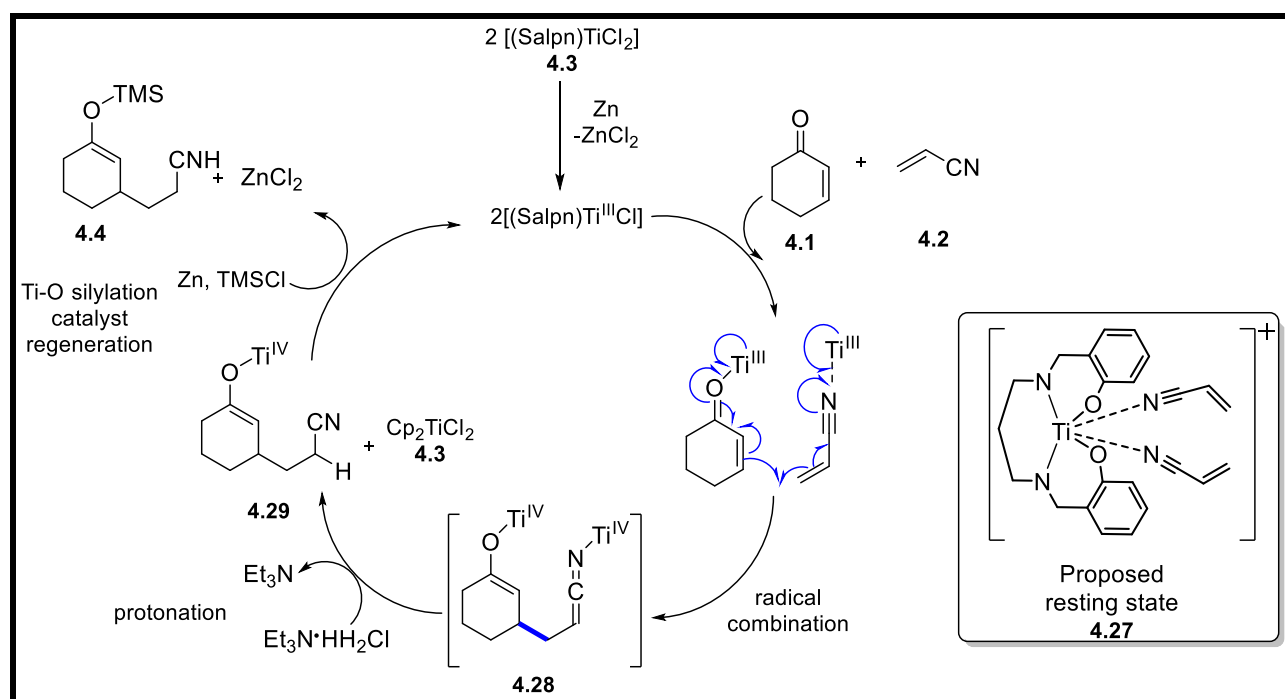
Scheme 4.48: Proposed mechanism for reductive umpolung reaction of Michael acceptors.

The reaction begins with the reduction of 2 equivalents of Ti(IV) species (**4.3**) with zinc powder to form 2 equivalents of Ti(III). Ti(III) species then coordinate to the enone **4.1** and nitrile **4.2** to form coordination complexes. The unpaired electron in fact is part located at the β-position, at the carbonyl carbon and at the titanium centre as illustrated in Scheme 4.13. The presence of these three structures was supported by the calculation of spin density distribution at the Cp_2TiCl-cyclohexenone complex, as it was mainly located at the Ti centre and partially located at the β-carbon and the carbonyl carbon. A similar case was found for the acrylonitrile-Ti(III) complex. This was also seen in DFT calculations of the [Ti(Salpy)Cl(enone)] and [Ti(Salpy)Cl(nitrile)] structures, shown in Figure 4.1. This study

explained the experimental observations: the conjugate addition (1,4-addition) at *β*-carbon was usually the preferred products. However, 1,2-addition products were formed with substrates that are sterically hindered at the *β*-position.
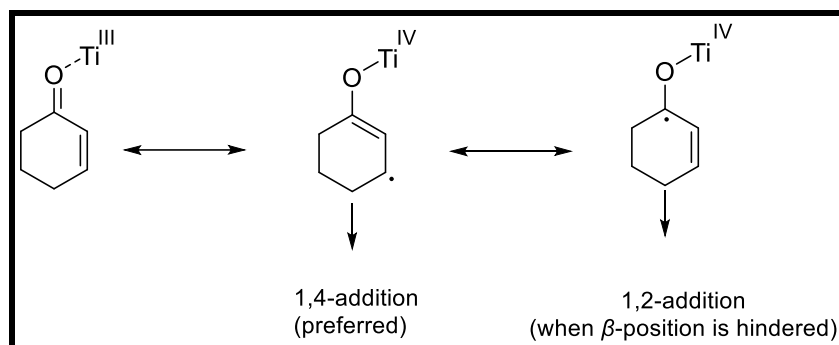
Scheme 4.49: Different forms of a Ti[III]–cyclohexenone complex.
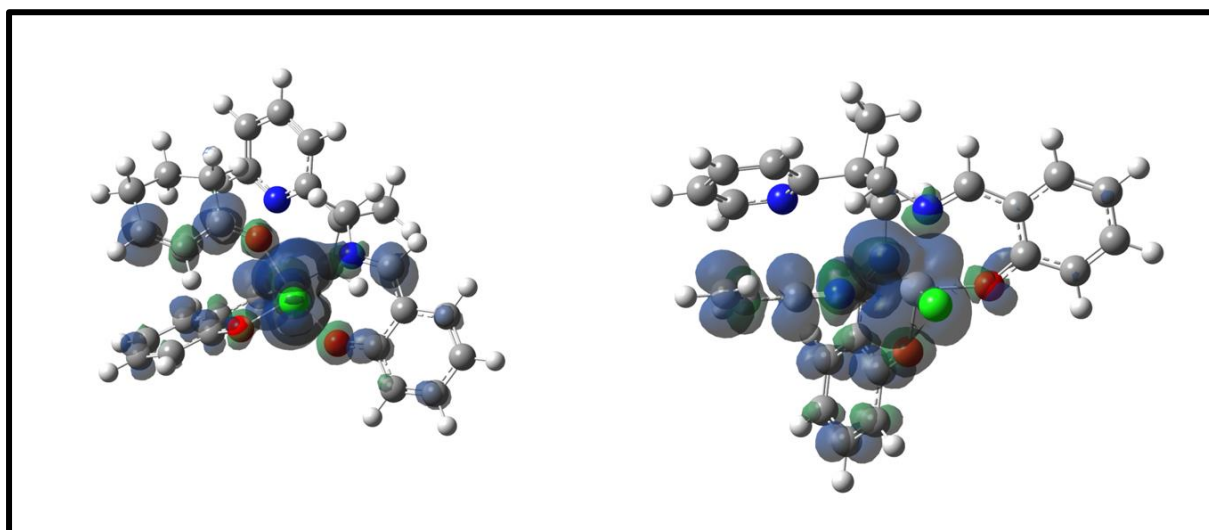
Figure 4.1: DFT-calculated structures of [Ti(Salpy)Cl(enone)] and [Ti(Salpy)Cl(nitrile)] showing the spin-density, which lies on the Ti centre and on the substrate

The Ti-nitrile and Ti-enone complexes are in equilibrium *via* ligand exchange processes. It supposed that the cationic resting state **4.27** is produced by solvation of the chloride and coordination with a second nitrile molecule (the nitrile was utilized in a 50 times excess with respect to the catalyst). Similar cationic resting state was observed previously in related enone-nitrile coupling by X-ray analysis.[17] Radical combination then takes place leading to C-

C bond formation at both *β*-carbons forming bistitanated ketamine enolate **4.28** which is quickly protonated by Et₃N·HCl to the enolate **4.29**. Titanium enolate is then displaced by TMSCl forming the crude product (silyl enol ether **4.4**) and the catalyst regenerated by reduction with Zn. The generated product then transferred to the desired 1,6-ketonitrile product after workup with dilute hydrochloric acid.

4.7 Conclusion:

Many important molecules, such as pharmaceutical agents, dyes, and polymers are produced by the formation of carbon-carbon bonds. For that, the development of new methods to perform this important connection have been the focus of numerous studies. In this work, the reductive cross coupling reaction, of which only few examples are known in the literature and with a confined number of catalytic systems, has been studied. Substituted olefins have been reacted with electron poor olefins to produce molecules that are difficult to access using conventional methods. Titanium complexes have been found to be efficient in these coupling reactions due to its tendency to undergo redox processes (between +4 and +3 oxidation states).

Titanium salen-type complexes catalyzed the double reductive alkylation of enones and readily available alkenes. It allows the selective preparation of 1,6-bifunctionalized ketonitriles *via* redox umpolung procedure under mild conditions and without the requirement of stoichiometric organometallic reagents. These complexes are able to catalyze enones with different ring sizes (2-cyclohexen-1-one and 2-cyclopenten-1-one) and also with the more hindered *β*-position (3-methyl-2-cyclohexen-1-one) leading to the formation of the quaternary carbon centres.

In conclusion, the reductive cross coupling reactions of enones with readily available nitriles catalyzed by titanium salen-type complexes have been reported for the first time. These complexes offer a cheap and environmentally friendly promising research area for the construction of inaccessible carbon-carbon bonds with an increasing number of ligand manifolds from the plethora available within the chemical literature.

4.8 References:

1   J. Streuff, *Chem. Eur. J.*, 2011, **17**, 5507–5510.

2   T. Jerphagnon, M. G. Pizzuti, A. J. Minnaard and B. L. Feringa, *Chem. Soc. Rev.*, 2009, **38**, 1039–1075.

3   J. C. Lo, J. Gui, Y. Yabe, C.-M. Pan and P. S. Baran, *Nature*, 2014, **516**, 343–348.

4   J. Streuff, *Synthesis*, 2013, **45**, 281–307.

5   M. M. Baizer, *Tetrahedron*, 1984, **40**, 935–969.

6   C.-C. Wang, P.-S. Lin and C.-H. Cheng, *Tetrahedron Lett.*, 2004, **45**, 6203–6206.

7   S. R. Harutyunyan, T. den Hartog, K. Geurts, A. J. Minnaard and B. L. Feringa, *Chem. Rev.*, 2008, **108**, 2824–2852.

8   A. Gutnov, *European Journal of Organic Chemistry*, 2008, **2008**, 4547–4554.

9   J. Christoffers, G. Koripelly, A. Rosiak and M. Rössle, *Synthesis*, 2007, **2007**, 1279–1300.

10   P. Bichovski, T. M. Haas, M. Keller and J. Streuff, *Org. Biomol. Chem.*, 2016, **14**, 5673–5682.

11   A. Rudolph and M. Lautens, *Angew. Chem. Int. Ed.*, 2009, **48**, 2656–2670.

12   K. Kikushima, J. C. Holder, M. Gatti and B. M. Stoltz, *J. Am. Chem. Soc.*, 2011, **133**, 6902–6905.

13   J. Streuff, *Chem. Rec.*, 2014, **14**, 1100–1113.

14   S. P. Morcillo, D. Miguel, A. G. Campaña, L. Á. de Cienfuegos, J. Justicia and J. M. Cuerva, *Organic Chemistry Frontiers*, 2014, **1**, 15–33.

15   S. P. Morcillo, Á. Martínez-Peragón, V. Jakoby, A. J. Mota, C. Kube, J. Justicia, J. M. Cuerva and A. Gansäuer, *Chemical Communications*, 2014, **50**, 2211–2213.

16   A. Gansäuer, D. von Laufenberg, C. Kube, T. Dahmen, A. Michelmann, M. Behlendorf, R. Sure, M. Seddiqzai, S. Grimme, D. V. Sadasivam, G. D. Fianu and R. A. Flowers II, *Chem. Eur. J.*, 2015, **21**, 280–289.

17   J. Streuff, M. Feurer, G. Frey, A. Steffani, S. Kacprzak, J. Weweler, L. H. Leijendekker, D. Kratzert and D. A. Plattner, *J. Am. Chem. Soc.*, 2015, **137**, 14396–14405.

18   J. Streuff and A. Gansäuer, *Angew. Chem. Int. Ed.*, 2015, **54**, 14232–14242.

19   S. P. Morcillo, D. Miguel, S. Resa, A. Martín-Lasanta, A. Millán, D. Choquesillo-Lazarte, J. M. García-Ruiz, A. J. Mota, J. Justicia and J. M. Cuerva, *J. Am. Chem. Soc.*, 2014, **136**, 6943–6951.

20   A. Rosales, J. Muñoz-Bascón, E. Roldan-Molina, M. A. Castañeda, N. M. Padial, A. Gansäuer, I. Rodríguez-García and J. E. Oltra, *J. Org. Chem.*, 2014, **79**, 7672–7676.

21   A. D. Kosal and B. L. Ashfeld, *Org. Lett.*, 2010, **12**, 44–47.

22   A. Gansäuer, C. Kube, K. Daasbjerg, R. Sure, S. Grimme, G. D. Fianu, D. V. Sadasivam and R. A. Flowers, *J. Am. Chem. Soc.*, 2014, **136**, 1663–1671.

23   A. Gansäuer, M. Behlendorf, D. von Laufenberg, A. Fleckhaus, C. Kube, D. V. Sadasivam and R. A. Flowers, *Angew. Chem. Int. Ed.*, 2012, **51**, 4739–4742.

24   M. C. P. Yeh and P. Knochel, *Tetrahedron Lett.*, 1988, **29**, 2395–2396.

25   D. I. Schuster, George. Lem and N. A. Kaprinidis, *Chem. Rev.*, 1993, **93**, 3–22.

26   P. Krug, A. Rudolph and A. C. Weedon, *Tetrahedron Letters*, 1993, **34**, 7221–7224.

27   M. Sidera, P. M. C. Roth, R. M. Maksymowicz and S. P. Fletcher, *Angew. Chem. Int. Ed.*, 2013, **52**, 7995–7999.

28   S. Wiesler, S. L. Younas, D. Kratzert and J. Streuff, *J. Organomet. Chem.*, 2020, **919**, 121327.

29   M. Feurer, G. Frey, H.-T. Luu, D. Kratzert and J. Streuff, *Chem. Commun.*, 2014, **50**, 5370–5372.

30   M. Bandini, P. G. Cozzi, S. Morganti and A. Umani-Ronchi, *Tetrahedron Lett.*, 1999, **40**, 1997–2000.

31   A. Chatterjee, T. H. Bennur and N. N. Joshi, *J. Org. Chem.*, 2003, **68**, 5668–5671.

32   G. Frey, J. N. Hausmann and J. Streuff, *Chem. Eur. J.*, 2015, **21**, 5693–5696.

Chapter 5

Experimental and

characterization data

5.1 General experimental details:

Unless otherwise specified, all reagents were used as received from commercial sources without further purification. All glassware was dried overnight in the oven at 150 °C before use. All manipulations involving air and water sensitive compounds were performed under an atmosphere of dry, oxygen-free nitrogen or argon using glovebox or standard Schlenk techniques with rigorous exclusion of air and moisture. Water and air sensitive complexes were stored in screw cap vials under nitrogen in a glovebox. All monomers and solvents were purified and dried prior to use and stored under nitrogen or argon atmosphere unless otherwise noted. Solvents used were dried using appropriate drying agents. Hexane, Pentane, dichloromethane and toluene were dried by pushing the solvents through an alumina drying column included in a MBraun SPS800 solvent purification system. Tetrahydrofuran was refluxed over melted potassium for 3 days then distilled under argon. Diethyl ether was dried over sodium wire and benzophenone for three days and then distilled under argon. The freshly distilled solvents were degassed by three successive freeze-pump-thaw cycles and stored in Teflon valve ampules. Deuterated solvents were stirred over calcium hydride ($CDCl_3$, CD_2Cl_2 and THF-d_8) or molten potassium (C_6D_6) for three days then distilled under reduced pressure. 2-methyl-2-(pyridine-2-yl)propane-1,3-diamine (ppda) was prepared according to a previously reported method.[1] Anhydrides were sublimed before used and stored in the glovebox. Epoxides were dried over calcium hydride then distilled under reduced pressure and stored under argon. ROCOP cocatalysts (bis(triphenylphosphoranylidene)ammonium chloride (PPNCl) and 4-(diamethylamino)pyridine (DMAP)) were used as received. All cross coupling precursors were purified using three successive freeze-pump-thaw cycles and stores under nitrogen.

Vials and glassware used in the catalytic reactions were dried in an oven at 150 °C overnight and exposed to vacuum-nitrogen cycles three times. All catalytic reactions have been carried out in a 7 ml screw cap vails (2 ml in case of propylene oxide copolymerizations) equipped with a small stirring magnetic bar under inert atmosphere.

5.1.1 Instruments and measurements:

1. NMR spectra were obtained at 25°C and were measured at ^1H resonance frequency of 400 MHz or 500 MHz (100 MHz and 125 MHz for ^{13}C respectively) using Bruker Avance HD III spectrometers. ^1H and ^{13}C NMR signals are reported in parts per million (ppm) relative to TMS (δ=0) and were referenced internally to the protio solvent (^1H) or solvent (^{13}C) signals. Coupling constants (J) are given in hertz. Two dimensional ^1H-^1H and ^1H-^{13}C NMR correlation experiments were used

to confirm the ^{1}H and ^{13}C assignments. NMR samples for the complexes were prepared in the glovebox in 5 mm J young valved NMR tubes.

2- Infrared spectra for the complexes were measured as KBR pellets and recorded on a Shimadzu IRAffinity-1 FTIR spectrometer from 4000 to 400 cm^{-1}. The KBr was oven-dried at 150°C for two days before use. All the ligands and catalytic products were measured by ATR on a Shimadzu IRAffinity 1S FTIR spectrometer.

3- UV-Vis spectra were recording using a Shimadzu UV-1900 UV-VIS spectrophotometer in the range 200-800/1100 nm on solutions ranging in concentration from 1×10^{-4} to 1×10^{-6} M.

4- Electron paramagnetic resonance (EPR) spectra of Ti(III) complexes were recorded using Bruker EMX X-band utilizing an ER4119HS resonator, 100 kHz field modulation at 140 K. The frequency of microwave was kept at ca. 9.5 GHz. All measurements were performed at low temperature. Samples for the measurements were obtained by dissolving ca. 4 mg in ~150 µl THF + 20 µl toluene and placed in 4 mm young tubes. EPR spectra were simulated using the EasySpin toolbox within Matlab programme to extract the spin Hamiltonian parameters.[2]

5- Low and high resolution mass spectra were performed by the analytical services within the university (EI, ASAP).

6- Gel permeation chromatography (GPC): The polydispersity (PD) and number average molecular weights (Mn) were determined by Agilent 1260 Infinity II equipped with triple detectors (refractive index, light scattering and viscometer). The GPC columns were eluted with THF at a rate of 1 ml per minute and were calibrated with polystyrene standards. Samples were prepared by dissolving 3 mg of the polymer in 1 ml THF and then filtered through 0.2 µm filter to the GPC vials.

7- MALDI mass spectra were measured using Bruker AutoFlex speed MALDI-ToF mass spectrometer operating in positive mode. The polymer samples were dissolved in THF at 10 mg per 1 ml. The matrix used was trans-2-[3-(4-tert-butylphenyl)-2-methyl-2-propenylidene]malononitrile (DCTB) and was dissolved in THF at 20 mg/ml. Sodium acetate used as cationization agent. Solutions of polymer, matrix and salt were mixed in ratio of 20:100:1, respectively. After being vortex-mixed, 0.5 µl was hand spotted on the MALDI target plate and left to dry. The plate was inserted into the machine and the spectra were recorded in both positive linear and reflectron modes.

8- X-ray data for all the structures in this thesis were measured by the EPSRC National Crystallography Service at the university of Southampton (for [Ti(Salpy)Cl] **(1)**, [Ti(Salpy)Cl$_2$] **(8)**, and [Ti(^{t}Bu,^{t}Bu-Salpy)Cl$_2$] **(10)**) or by Dr. Benson Kariuki at Cardiff University ([Ti(Me-Salpy)Cl$_2$] **(12)**, [Ti(^{t}Bu,^{t}Bu-Salpn)Cl$_2$] **(17)**, and [Ti(Me-

Salpn)Cl$_2$] **(18)**). The structures solved and refined by Dr. Benjamin Ward using the SHELX software suite.[3]

Note: In some spectra a molecule of tetrahydrofuran or diethyl ether are present which remained even after drying under vacuum at 80 °C.

5.1.2 Ring Opening Copolymerization general procedure:

The copolymerization experiments were performed as described in the literature using 6.4 μ mole of the catalyst in 0.5 ml solvent with [complex]: [cocatalyst]: [epoxide]: [anhydride] ratio of 1:1:200:200 or without solvent in the ratio of 1:1:2000:400.[4] After sealing the vial, it was removed from the glove box and placed in preheated aluminum heating block to the desired temperature for the certain time. The conversion can be determined by taking an aliquot for ^{1}H NMR analysis after the appropriate amount of time. When judged complete, the resulting mixture was dissolved in a minimum amount of dichloromethane and precipitated using excess of methanol or hexane with vigorous stirring, before decanting the solvent. To ensure that the catalyst and the excess of monomer were removed, the precipitation was repeated three times. The polymer was collected and dried under reduced pressure. The polymers were characterized by ^{1}H NMR spectroscopy. The degree of alternating microstructure was determine by integrating the ester and ether regions of the ^{1}H NMR spectra.

5.1.3 Cross coupling reactions general procedure:

The cross coupling reactions were performed as found in literature;[5,6] in the glove box, a screw cap vial containing a magnetic stir bar was charged with 0.05 mmol of [Ti(salen-type)Cl$_2$] or [Ti(salen-type)Cl], 1mmol Zn powder, 0.65 mmol Et$_3$N·HCl, 1.25 ml THF, 0.5 mmol substrate, 2.5 mmol cross coupling partner and 1.5 eq TMSCl. The reaction was stirred for 24 h at 35° C in an aluminum heating block. Workup was carried out by the addition of 4 ml of 1 N aqueous HCl and CH$_2$Cl$_2$ and stirring for 03 min. at room temperature. The mixture was then transferred into a separating funnel containing 20 ml CH$_2$Cl$_2$ and 20 ml H$_2$O. The organic layer was separated, and the aqueous layer washed with additional CH$_2$Cl$_2$ (3x10 ml). The combined organic layers were dried, concentrated, and purified by flash chromatography (hexane/EtOAc 3:2 or 2:1, R_f =0.30-0.40). Thin layer chromatography (TLC) was performed using E. Merck silica gel 60 precoated plates and visualized by heating. Silica gel 60 (particle size 0.35-0.70 nm) was used for flash chromatography.

5.2 Synthesis and characterization of Ligands:

5.2.1 Synthesis and characterization of H₂Salpy ligand:
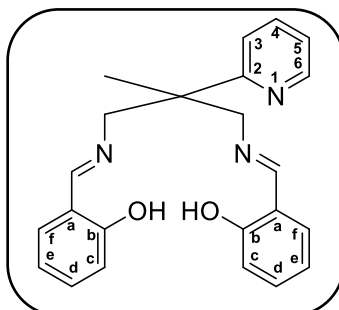
This ligand was prepared as described in previous work by the Schiff base condensation of 2-methyl-2-(pyridine-2-yl)propane-1,3-diamine (2 g, 12.1 mmol) with 2 equivalents of salicylaldehyde (2.96 g, 24.2 mmol) in methanol (50 ml).[7] The solution was stirred for 3 hours at 50 °C giving a yellow solution which then allowed to cool to room temperature. After cooling to room temperature, a yellow precipitate was formed which then filtered and washed with cold methanol. The product was dried in vacuo for 2 hours. Yield: 3.94 g (87%).

Properties of H₂Salpy:

Formula: $C_{23}H_{23}N_3O_2$.

Nature: Crystalline yellow solid.

Molecular weight: 373.46 g/mol.

Yield: 87%

^{1}H NMR (400 MHz, CDCl₃): δ 13.19 (s, 2H,OH), 8.64 (ddd, ^3J = 4.8 Hz, ^4J =1.8 Hz, ^5J = 0.9 Hz, 1H, H₆), 8.31 (s, 2H,CH=N), 7.67 (td, ^3J = 7.7 Hz,^4J =1.5 Hz, 1H, H₄), 7.35 (d, ^3J = 8 Hz, 1H,H₃), 7.28 (td, ^3J = 8.4 Hz, ^4J =1.2 Hz, 2H,H_c), 7.20 (dd, ^3J =7.6 Hz, ^4J = 1.4 Hz, 2H, H_e), 7.15 (ddd, ^3J = 7.5 Hz, ^3J =4.8 Hz, ^4J = 1.0 Hz, 1H, H₅), 6.91 (d, ^3J = 8.3 Hz, 2H, H_f), 6.85 (t, ^3J = 7.5 Hz, 2H, H_d), 4.14 (d, ^2J = 12.3 Hz, 2H, CHH), 4.01 (d, ^2J = 12.3 Hz, 2H, CH<u>H</u>), 1.53 (s, 3H, CH₃). ^{13}C{^{1}H} NMR (101 MHz, CDCl₃): δ 166.27(CH=N), 163.33(C₂), 161.21(C_b), 149.15(C₆), 136.71(C₄), 132.48 (C_c), 131.51(C_e), 121.80 (C₅), 121.34(C₃), 118.82(C_d), 118.71(C_a), 117.08(C_f), 67.21(CH₂-N), 46.26(py-<u>C</u>-CH₃), 21.84(CH₃). HRMS for [M+H]⁺ (ASAP): calcd. for ($C_{23}H_{24}N_3O_2$): 374.1869; found: 374.1868.

FT-IR (cm⁻¹): 3051 ν(C-H_aromatic), 2997 ν(C-H_aliphatic), 2965 ν(C-H_aliphatic), 2860 ν(C-H_aliphatic), 1628s ν(C=N_imine), 1578m, 1497m, 1472, 1456m ν(C=N_py, C=C_aromatic), 1431, 1419 1376, 1333

v(C-N), 1275s v(Ar-O), 1208w, 1154, 1117, 1036, 1018, 989, 949, 891, 849m, 762vs v(C-H oop bend), 654, 629, 587, 552, 474 cm^{-1}.UV-Vis (THF) λ_{max}: 247, 285, and 319 nm.

5.2.2 Synthesis and characterization of H$_2$Salpy-Me ligand:

The synthesis of this ligand was accomplished in two steps: first, reduction of H$_2$Salpy ligand to H$_2$Salpy-H. Then, methylation of H$_2$Salpy-H$_2$.

5.2.2.1 Synthesis and characterization of H$_2$Salpy-H:
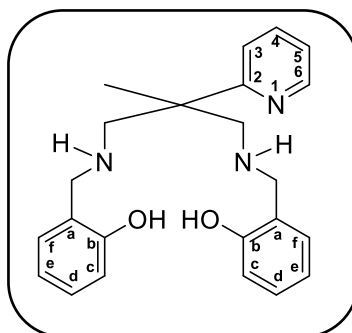
H$_2$Salpy-H was prepared according to a modified procedure found in literature.[7] 2 g of H$_2$Salpy ligand (5.36 mmol) was dissolved in methanol (50 ml) in 100 ml round bottom flask and 3 equivalents of sodium borohydride (0.608 g, 16.09 mmol) was added gradually at 0 °C. The resulting mixture was stirred at room temperature for 6 hours, then the solvent evaporated yielding white product. Aqueous saturated sodium bicarbonate (100 ml) was added and then extracted with Et$_2$O (3×100 ml). The combined organic layers washed two times with 100 ml of water then dried over anhydrous magnesium sulphate and the solvent removed under reduced pressure to yield pale pink sticky product (1.2 g, 60%).

Properties of H$_2$Salpy-H:

Formula: C$_{23}$H$_{27}$N$_3$O$_2$.

Nature: Pale pink sticky product.

Molecular weight: 377.49 g/mol.

Yield: 60%

^{1}H NMR (400 MHz, CDCl$_3$): δ 8.54 (d, ^3J = 4.2 Hz, 1H, H$_6$), 7.68 (t, ^3J = 7.6 Hz, 1H, H$_4$), 7.31 (d, ^3J = 7.6 Hz, 1H, H$_5$), 7.21 – 7.08 (m, 3H, H$_3$,Ar-H), 6.97 (d, ^3J = 7.2 Hz, 2H, Ar-H), 6.81 – 6.71 (m, 4H, Ar-H), 3.96 (d, ^2J = 13.9 Hz, 2H, CH$_2$), 3.88 (d, ^2J = 13.8 Hz, 2H, CH$_2$), 3.13 (d, ^2J = 11.4 Hz, 2H, CH$_2$), 2.86 (d, ^2J = 11.4 Hz, 2H, CH$_2$), 1.46 (s, 3H, CH$_3$).

5.2.2.2 Synthesis and characterization of H$_2$Salpy-Me:
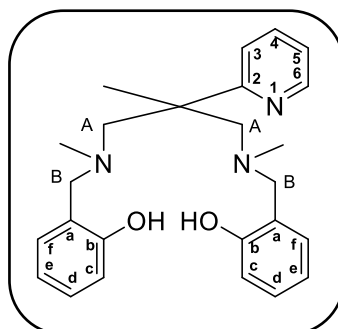
The methylation was performed following the procedure used by Hultzsch et al., 1.8 g (4.77 mmol) of H$_2$Salpy-H$_2$ was dissolved in acetonitrile (40 ml) and aqueous formaldehyde (37%, 3.58 ml, 44.36 mmol) was added.[8] The solution was stirred for 15 min. at room temperature, and then Sodium cyanoborohydride (1.11 g, 17.65 mmol) was added and stirring continued. After 15 min., 2 ml glacial acetic acid was added dropwise. After 5 hours of constant stirring at room temperature the solvent was evaporated and 100 ml of aqueous saturated sodium bicarbonate was added. The product was extracted with 100 ml Et$_2$O three times and the combined organic layers were washed with water (2×100 ml). The extract was dried over MgSO$_4$ and the solvent removed under reduced pressure to yield a white product (1.34 g, 69%).

Properties of H$_2$Salpy-Me:

Formula: C$_{25}$H$_{31}$N$_3$O$_2$.

Nature: White solid.

Molecular weight: 405.54 g/mol.

Yield: 69%

^{1}H NMR (400 MHz, CDCl$_3$): δ 10.20 (s, 2H, OH), 8.60 (ddd, ^3J = 4.7 Hz, ^4J = 1.9 Hz, ^5J = 0.9 Hz, 1H, H$_6$), 7.74 (td, ^3J = 7.8 Hz, ^4J =1.9 Hz, 1H, H$_4$), 7.48 (d, ^3J = 8.0 Hz, 1H, H$_3$), 7.21 – 7.06 (overlapping, 3H,H$_5$,H$_d$), 6.88 (dd, ^3J = 7.4 Hz, ^4J = 1.3 Hz, 2H, H$_c$), 6.81 – 6.62 (m, 4H, H$_e$,H$_f$), 3.65 (d, ^2J = 13.7 Hz, 1H,CHH^B), 3.56 (d, ^2J =13.7 Hz, 1H, CHH^B), 3.27 (d, ^2J = 13.2 Hz, 1H,CHH^A), 2.64 (d, ^2J =13.2 Hz, 1H, CHH^A), 1.95 (s, 6H, N-CH$_3$), 1.67 (s, 3H,-CH$_3$). ^{13}C{^{1}H} NMR (126 MHz, CDCl$_3$): δ 163.37(C$_2$), 157.54 (C$_b$), 149.07 (C$_6$), 137.18 (C$_4$), 128.84 (C$_d$), 128.66 (C$_c$), 122.13 (C$_3$), 121.99 (C$_5$), 121.95 (C$_a$), 119.12 (C$_e$), 116.02 (C$_f$), 67.95 (CH$_2$A), 63.91 (CH$_2$B), 46.67 (py-C-CH$_3$), 43.80 (CH$_3$N), 20.75 (CCH$_3$). HRMS for [M+H]$^+$ (ASAP): calcd. for (C$_{25}$H$_{32}$N$_3$O$_2$): 406.2495, found: 406.2493.

FT-IR (cm^{-1}): 3055 ν(C-H$_{aromatic}$), 3001 ν(C-H$_{aromatic}$), 2961 ν(C-H$_{aliphatic}$), 2912 ν(C-H$_{aliphatic}$), 2869 ν(C-H$_{aliphatic}$), 1587m , 1489m 1471m, 1458 ν(C=N$_{py}$, C=C$_{aromatic}$), 1429, 1415, 1397, 1385 ν(C-N), 1337, 1275, 1251s ν(Ar-O), 1174, 1128, 1093, 1006s, 977, 930, 874, 835, 794, 753vs ν(C-H oop bend), 721, 647, 623, 551, 497, 455, 430, 418 . UV-Vis (THF) λ$_{max}$: 274, and 286 nm.

5.2.3 Synthesis and characterization of ^{t}Bu,^{t}Bu-H$_2$Salpy ligand:
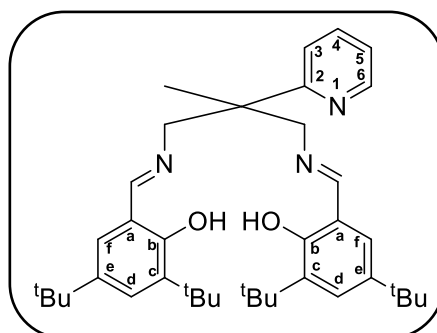
In a 100 round bottom flask, 1.01 g of ppda (6.12 mmol) was dissolved in methanol (30 ml) then a solution of 3,5-di-tert-butylsalicyaldehyde (2 eq., 2.87 g, 12.24 mmol) in methanol (20 ml) was added. After 3 hours of stirring at 50 °C, the reaction was cooled to room temperature and the pale-yellow precipitate was filtered and washed with cold MeOH. The ligand was dried under reduced pressure. Yield: 3.58 g (98%).

Properties of ^{t}Bu,^{t}Bu-H$_2$Salpy:

Formula: C$_{39}$H$_{55}$N$_3$O$_2$.

Nature: Pale yellow solid.

Molecular weight: 597.89 g/mol.

Yield: 98%

^{1}H NMR (400 MHz, CDCl$_3$): δ 13.53 (s, 2H,OH), 8.62 (ddd, ^3J = 4.8 Hz,^4J =1.8 Hz, ^5J =0.8 Hz, 1H, H$_6$), 8.34 (s, 2H, CH=N), 7.64 (td, ^3J = 7.7 Hz, ^4J =1.9 Hz, 1H, H$_4$), 7.38 – 7.32 (overlapping m, 3H, H$_3$, H$_d$), 7.14 (ddd, ^3J = 7.5 Hz, ^3J =4.8, ^4J = 1.0 Hz, 1H, H$_5$), 7.04 (d, ^4J = 2.4 Hz, 2H, H$_f$), 4.06 (s, 4H, -CH$_2$), 1.57 (s, 3H, -CH$_3$), 1.42 (s, 18H, -C(CH$_3$)$_3$), 1.29 (s, 18H, -C(CH$_3$)$_3$). ^{13}C{^{1}H} NMR (101 MHz, CDCl$_3$): δ 167.34 (CH=N), 163.80 (C$_2$), 158.25 (C$_b$), 149.12(C$_6$), 140.04 (C$_e$), 136.75 (C$_4$), 136.48 (C$_c$), 127.04 (C$_d$), 126.08 (C$_f$), 121.61 (C$_3$), 121.36 (C$_5$), 118.01 (C$_a$), 67.03 (CH$_2$-N), 46.29 (py-$\underline{C}$-Me), 35.18 ($\underline{C}$(CH$_3$)$_3$), 34.25 ($\underline{C}$(CH$_3$)$_3$), 31.63 (C($\underline{CH_3}$)$_3$), 29.55(C($\underline{CH_3}$)$_3$), 22.37(-CH$_3$). HRMS for [M+H]$^+$ (ASAP): calcd. for (C$_{39}$H$_{56}$N$_3$O$_2$): 598.4373; found: 598.4373.

FT-IR (cm^{-1}): 3066 ν(C-H$_{aromatic}$), 3000 ν(C-H$_{aromatic}$), 2953 ν(C-H$_{aliphatic}$), 2906 ν(C-H$_{aliphatic}$), 2870 ν(C-H$_{aliphatic}$), 1624s ν(C=N$_{imine}$), 1589m, 1470s, 1457, 1438s ν(C=N$_{py}$, C=C$_{aromatic}$), 1389m, 1361m ν(C-N), 1335, 1269m, 1248s ν(Ar-O), 1203, 1173, 1133, 1070, 1033, 994, 948, 881m, 854m, 828s, 791m, 773m, 752s ν(C-H oop bend), 652m, 579, 542, 498, 442, 418. UV-Vis (THF) λ$_{max}$: 235, 265, and 332 nm.

5.2.4 Synthesis and characterization of ^{t}Bu,OMe-H$_2$Salpy ligand:

The precursor for the ligand ^{t}Bu,OMe-H$_2$Salpy (3-tert-butyl-5-methoxy salicylaldehyde) was prepared according to a known method using Duff reaction.[9]

5.2.4.1 Synthesis and characterization of 3-tert-butyl-5-methoxy salicylaldehyde:
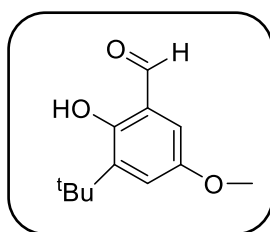
A mixture of 3-tert-butyl-4-hydroxyanisole (9.25 g, 51.32 mmol) and hexamethylenetetramine (14.40 g, 102.64 mmol) in glacial acetic acid (50 ml) was stirred at 110 °C. After 2 hours, an aqueous solution of H$_2$SO$_4$ (33%, 50 ml) was added at 75 °C. The solution was heated again at 110 °C for another 3 hours and then was extracted with diethyl ether (2×100 ml). The organic layer was washed with water (2×100 ml), then a saturated solution of sodium carbonate (2×100 ml) and finally saturated sodium chloride solution (100 ml). The organic phase was dried over anhydrous magnesium sulphate, filtered and the solvent removed under vacuum. The crude product was dissolved in dichloromethane (10 ml) and purified by column chromatography over silica using DCM as an eluent, to yield the product as yellow oil (5.42 g, 51% yield).

Properties of 3-tert-butyl-5-methoxy salicylaldehyde:

Formula: C$_{12}$H$_{16}$O$_3$.

Nature: Yellow oil.

Molecular weight: 208.26 g/mol.

Yield: 51%

^{1}H NMR (400 MHz, CDCl$_3$) δ 11.51 (s, 1H, OH), 9.84 (s, 1H, CHO), 7.18 (d, ^4J = 3.1 Hz, 1H,Ar-H), 6.81 (d, ^4J = 3.1 Hz, 1H, Ar-H), 3.81 (s, 3H,O-CH$_3$), 1.41 (s, 9H, C(CH$_3$)$_3$). ^{13}C{^{1}H} NMR

(101 MHz, CDCl$_3$) δ 196.77(CHO), 156.33 (C-OH), 152.15 (C-OCH$_3$), 140.28 (C-C(CH$_3$)$_3$), 123.99 (C-CHO), 119.93 (Ar-C), 111.84 (Ar-C), 55.88 (O-CH$_3$), 35.11 (C(CH$_3$)$_3$), 29.23 (C(CH$_3$)$_3$).

5.2.4.2 Synthesis and characterization of ^{t}Bu,OMe-H$_2$Salpy ligand:
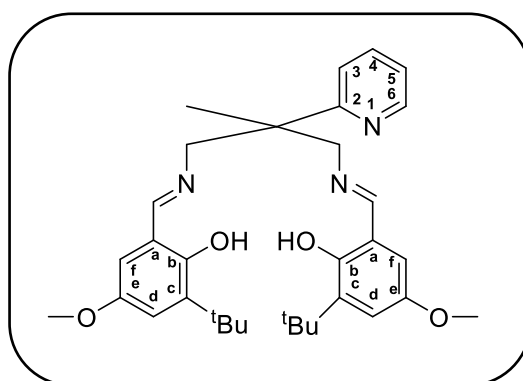
To a stirred solution of ppda (1.56 g, 9.46 mmol) in methanol (20 ml), 2 equivalents of 3-tert-butyl-5-methoxy salicylaldehyde (3.94 g, 18.92 mmol) in methanol (30 ml) was added dropwise. The solution was stirred for 3 h at 50 °C. The resulting yellow precipitate formed was filtered and washed with cold methanol then the solvent was removed under vacuum to yield the product as yellow powder (3.75 g, 73% yield).

Properties of ^{t}Bu,OMe-H$_2$Salpy :

Formula: C$_{33}$H$_{43}$N$_3$O$_4$.

Nature: Yellow solid.

Molecular weight: 545.72 g/mol.

Yield: 73%

^{1}H NMR (400 MHz, CDCl$_3$): δ 13.28 (s, 2H, OH), 8.62 (d, ^3J = 4.9 Hz, 1H, H$_6$), 8.28 (s, 2H, CH=N), 7.64 (t, ^3J = 8.0 Hz, 1H, H$_4$), 7.36 (d, ^3J = 8.0 Hz, 1H, H$_3$), 7.14 (t, ^3J = 6.2 Hz, 1H, H$_5$), 6.94 (s, 2H, H$_d$), 6.54 (s, 2H, H$_f$), 4.07 (s, 4H, -CH$_2$), 3.75 (s, 6H, O-CH$_3$), 1.58 (s, 3H, -CH$_3$), 1.40 (s, 18H, -C(CH$_3$)$_3$). ^{13}C{^{1}H} NMR (101 MHz, CDCl$_3$): δ 166.84(CH=N), 163.65 (C$_2$), 155.07 (C$_b$), 151.26 (C$_e$), 149.12 (C$_6$), 139.10 (C$_c$), 136.50 (C$_4$), 121.67 (C$_5$), 121.38 (C$_3$), 118.35 (C$_d$), 118.06 (C$_a$), 111.64 (C$_f$), 67.16 (CH$_2$-N), 55.94 (O-CH$_3$), 46.31 (py-C-Me), 35.13 (C(CH$_3$)$_3$), 29.38 (C(CH$_3$)$_3$), 22.36 (CH$_3$). HRMS for [M+H]$^+$ (ASAP): calcd. for (C$_{33}$H$_{44}$N$_3$O$_4$): 546.3332; found: 546.3330.

FT-IR (cm^{-1}): 3066 ν(C-H$_{aromatic}$), 3000 ν(C-H$_{aromatic}$), 2947 ν(C-H$_{aliphatic}$), 2887 ν(C-H$_{aliphatic}$), 2835 ν(C-H$_{aliphatic}$), 1636 ν(C=N$_{imine}$), 1602, 1590s, 1465s, 1456s ν(C=N$_{py}$, C=C$_{aromatic}$), 1430

vs, 1386, 1356 v(C-N), 1325s v(Ar-O), 1277, 1258, 1235, 1195, 1150, 1057s, 1048, 1011, 993, 956, 833s, 786vs v(C-H oop bend), 764, 756, 649, 625, 518, 471, 458, 438, 419. UV-Vis (THF) λ_{max}: 281, and 353 nm.

5.2.5 Synthesis and characterization of Me-H₂Salpy ligand:
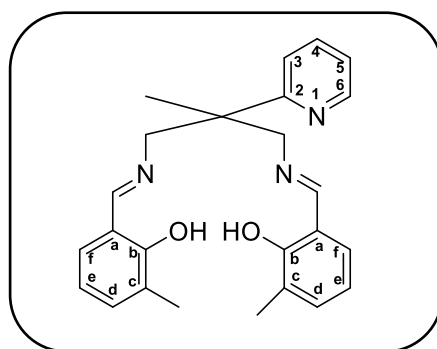
2-methyl-2-(pyridine-2-yl) propane-1,3-diamine (ppda) (1 g, 6.05 mmol) was dissolved in methanol (20 ml). A solution of 2-hydroxy-3-methyl benzaldehyde (1.65 g,1.47 ml, 12.1 mmol) in methanol (30 ml) was added dropwise to the amine solution with stirring. The stirring solution was heated at 50 °C for 3 h, yielding yellow solution. The solvent was removed under reduced pressure to give a crude product as yellow waxy solid. The product was purified by recrystallization from MeOH. (2.28 g, 94% yield).

Properties of Me-H₂Salpy:

Formula: $C_{25}H_{27}N_3O_2$.

Nature: Yellow waxy solid.

Molecular weight: 401.51 g/mol.

Yield: 94%

^{1}H NMR (400 MHz, CDCl₃) δ 13.39 (s, 2H, OH), 8.63 (d, ^3J = 4.1 Hz, 1H, H₆), 8.29 (s, 2H, CH=N), 7.66 (t, ^3J = 7.5 Hz, 1H, H₄), 7.36 (d, ^3J = 8.0 Hz, 1H, H₃), 7.19-7.11 (overlapping m, 3H, H₅, H_f), 7.05 (d, ^3J = 7.5 Hz, 2H, H_d), 6.76 (t, ^3J = 7.5 Hz, 2H, H_e), 4.12 (d, ^2J = 12.2 Hz, 2H, -C_HH), 4.04 (d, ^2J = 12.3 Hz, 2H, -CH_H), 2.24 (s, 6H, Ar-CH₃), 1.57 (s, 3H, -CH₃). ^{13}C{^{1}H} NMR (101 MHz, CDCl₃): δ 166.54(CH=N), 163.40(C₂), 159.48(C_b), 149.10(C₆), 136.69(C₄), 133.41(C_f), 129.20(C_d), 126.00(C_c), 121.72(C₅), 121.38(C₃), 118.18(C_e), 118.08(C_a), 67.22(N-CH₂), 46.26(py-C-Me), 21.99(CH₃), 15.63(Ar-CH₃). HRMS for [M+H]$^+$ (ASAP): calcd. for (C₂₅H₂₈N₃O₂): 402.2182; found: 402.2177.

FT-IR (cm^{-1}): 3092 ν(C-H$_{aromatic}$), 3055 ν(C-H$_{aromatic}$), 2979 ν(C-H$_{aliphatic}$), 2888 ν(C-H$_{aliphatic}$), 2847 ν(C-H$_{aliphatic}$), 1631s ν(C=N$_{imine}$), 1590, 1457, 1447, 1434s ν(C=N$_{py}$, C=C$_{aromatic}$), 1381m, 1318, 1305 ν(C-N), 1270 ν(Ar-O), 1249, 1160, 1084, 1050, 1039, 994w, 947m, 845s, 785m, 773s, 744vs ν(C-H oop bend), 713m, 658, 638, 625, 576m, 532, 488, 464, 447, 414. UV-Vis (THF) λ$_{max}$: 273, and 324 nm.

5.2.6 Synthesis and characterization of Cl,Cl-H$_2$Salpy ligand:
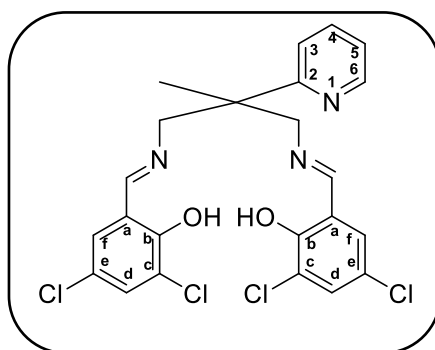
To a solution of ppda (1 g, 6.05 mmol) in methanol (20 ml), a solution of 3,5-dichlorosalicyaldehyde (2.31 g, 12.1 mmol, 2 eq.) in a mixture of DCM/MeOH (15 ml/15 ml) was added dropwise while the solution was stirred at 50 °C. A deep orange solution was formed, and the stirring was continued for 4 hours. The solvent was removed under reduced pressure and the resulting precipitate was washed with methanol, purified by recrystallization from petroleum ether/ dichloromethane, then dried under vacuum to give a dark orange powder (2.81 g, 91% yield).

Properties of Cl,Cl-H$_2$Salpy:

Formula: C$_{23}$H$_{19}$Cl$_4$N$_3$O$_2$.

Nature: Dark orange solid.

Molecular weight: 511.22 g/mol.

Yield: 91%

^{1}H NMR (400 MHz, CDCl$_3$): δ 14.07 (s, 2H, OH), 8.61 (ddd, ^3J= 4.8 Hz,^4J =1.8 Hz, ^5J= 0.9 Hz, 1H, H$_6$), 8.18 (s, 2H, CH=N), 7.66 (td, ^3J= 7.8 Hz, ^4J =1.9 Hz, 1H, H$_4$), 7.38(d, ^4J =2.5 Hz, 2H, H$_d$), 7.30 (d, ^3J= 8.0,1H, H$_3$), 7.16 (ddd, ^3J= 7.5 Hz, ^3J=4.8 Hz, ^4J =1.0 Hz, 1H, H$_5$), 7.08 (d, ^4J= 2.5 Hz, 2H, H$_f$), 4.15 (dd, ^2J= 12.5 Hz, ^4J= 0.9 Hz, 2H, -C$\underline{H}$H), 4.05 (dd, ^2J= 12.4 Hz, ^4J= 1 Hz, 2H, -CH$\underline{H}$), 1.56 (s, 3H, -CH$_3$). ^{13}C{^{1}H} NMR (101 MHz, CDCl$_3$): δ 165.02 (CH=N), 162.09 (C$_2$), 157.06 (C$_b$), 149.39 (C$_6$), 137.02 (C$_4$), 132.57 (C$_d$), 129.24 (C$_f$), 123.05 ($\underline{C}$-Cl), 122.71 ($\underline{C}$-

Cl), 122.19 (C_5), 121.28 (C_3), 119.41 (C_a), 66.45 (-CH_2), 46.26 (py-$\underline{C}$-CH_3), 21.69 (-CH_3). HRMS for $[M+H]^+$ (ASAP): calcd. for ($C_{23}H_{20}Cl_4N_3O_2$): 512.0280; found: 512.0288.

FT-IR (cm^{-1}): 3077 v(C-$H_{aromatic}$), 3031 v(C-$H_{aromatic}$), 2969 v(C-$H_{aliphatic}$), 2929 v(C-$H_{aliphatic}$), 2852 v(C-$H_{aliphatic}$), 1636vs v(C=N_{imine}), 1589, 1558, 1507, 1456vs v(C=N_{py}, C=$C_{aromatic}$), 1374, 1338 v(C-N), 1293, 1214s v(Ar-O), 1182m, 1050, 994w, 944, 910w, 855m, 788, 732s v(C-H oop bend), 703, 667, 647, 565, 518, 471, 456, 438, 428, 419. UV-Vis (THF) λ_{max}: 252, 337 and 436 nm.

5.2.7 Synthesis and characterization of Ad, Me-H_2Salpy ligand:

The precursor of this ligand has been prepared in two steps:

Firstly: synthesis of 2-(1-adamantyl)-*p*-cersol from *p*-cresol as described below:

5.2.7.1 Synthesis and characterization of 2-(1-adamantyl)-p-cersol:
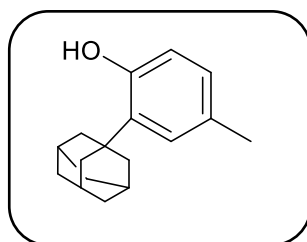
2-(1-adamantyl)-*p*-cersol was prepared according to a literature procedure.[10] In a 250 ml round bottom flask equipped with magnetic stir bar, p-cresol (4.23 g, 39.07 mmol) and 1-adamantanol (6.09 g, 40 mmol) were dissolved in dichloromethane (50 ml) at room temperature. Concentrated H_2SO_4 (2.25 ml) was added dropwise over 20 min period and stirred continued for an additional 30 minutes. After that, ice water (50 ml) was added slowly and the mixture was neutralized by adding NaOH (2M, *ca.* 40 ml). The resulting white slurry was extracted with DCM (3×50 ml) and the organic layers were combined, washed with brine (50 ml) and dried over Na_2SO_4. The solution then filtered and concentrated to yield a sticky white product which was dissolved in methanol (50 ml) and refluxed for one hour. After cooling, the solution was filtered, and the precipitate extracted with methanol (2× 50 ml). The extraction portions were combined and the solvent removed *in vacuo* giving a white powder (5.97 g, 63% yield).

Properties of 2-(1-adamantyl)-p-cersol:
Formula: $C_{17}H_{22}O$.

Nature: White solid.

Molecular weight: 242.36 g/mol.

Yield: 63%

^{1}H NMR (400 MHz, CDCl$_3$): δ 7.08 (d, ^3J = 7.0 Hz, 1H, Ar-H), 6.94 (d, ^3J = 7.1 Hz, 1H, Ar-H), 6.76 (d, ^3J = 7.3 Hz, 1H, Ar-H), 4.97 (s, 1H, OH), 2.51 (s, 3H, Ar-CH$_3$), 2.37 (s, 6H, Ad), 2.31 (s, 3H, Ad), 2.02 (s, 6H, Ad).

Secondly:

5.2.7.2 synthesis of 3-adamantyl-2-hydroxy-5-methylbenzaldehyde:
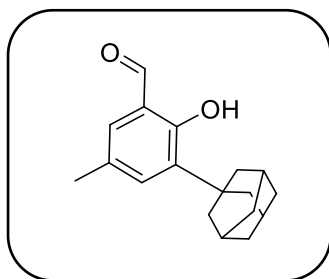
3-adamantyl-2-hydroxy-5-methylbenzaldehyde was prepared according to a procedure described elswere.[10] 2-(1-adamantyl)-*p*-cersol (4.37 g, 18.03 mmol) and two equivalents of hexamethylenetetramine (5.06 g, 36.06 mmol) were dissolved in glacial acetic acid (100 ml) in 250 ml round bottom flask equipped with magnetic stir bar and heated at 110 °C for 5 hours. The yellow solution allowed to cool to 90 °C and water (150 ml) was added dropwise over 30 minutes period. When the mixture cools to room temperature, an off-white suspension formed which was isolated by filtration, treated with methanol (50 ml) and stirred for one hour. After that, the precipitate was collected, washed with methanol, and dried under reduced pressure giving the desired product as an off-white powder (2.34 g, 48% yield).

Properties of 3-adamantyl-2-hydroxy-5-methylbenzaldehyde:

Formula: C$_{18}$H$_{22}$O$_2$.

Nature: Off-white solid.

Molecular weight: 270.37 g/mol.

Yield: 48%

^{1}H NMR (400 MHz, CDCl$_3$): δ 11.64 (s, 1H, OH), 9.82 (s, 1H, CHO), 7.27 (s, 1H, Ar-H), 7.16 (s, 1H, Ar-H), 2.32 (s, 3H, Ar-CH$_3$), 2.16 – 2.03 (m, 9H, Ad), 1.78 (s, 6H, Ad).

5.7.2.3 Synthesis and characterization of Ad, Me-H₂Salpy ligand:
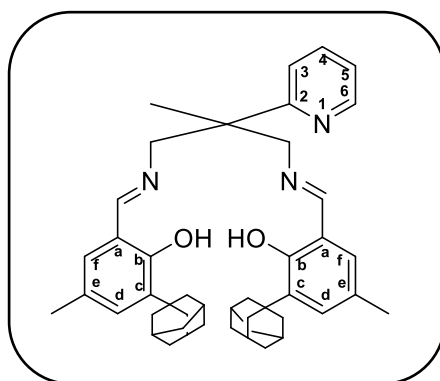
2 equivalents of 3-adamantyl-2-hydroxy-5-methybenzaldehyde (1.63 g, 6.05 mmol) were dissolved in MeOH/DCM (20ml/20 ml) and added gradually to a stirred solution of ppda (0.5 g, 3.03 mmol) in methanol (10 ml). The reaction mixture was stirred at 50 °C for four hours and allowed to cool. The pale-yellow precipitate was filtered, washed with cold methanol and dried under vacuum to yield the desired ligand (1.58 g, 78% yield).

Properties of Ad, Me-H₂Salpy:

Formula: $C_{45}H_{55}N_3O_2$.

Nature: Pale yellow solid.

Molecular weight: 669.95 g/mol.

Yield: 78%

^{1}H NMR (400 MHz, CDCl₃): δ 13.53 (s, 2H,OH), 8.62 (dd, ^3J = 4.8 Hz, ^4J =1.0 Hz, 1H, H₆), 8.26 (s, 2H, CH=N), 7.63 (td, ^3J = 7.8 Hz, ^4J =1.9 Hz, 1H,H₄), 7.36 (d, ^3J = 8.0 Hz, 1H, H₃), 7.13 (dd, ^3J = 7.5 Hz, ^4J =4.8 Hz, 1H, H₅), 7.04 (d, ^4J = 1.9 Hz, 2H, H_f), 6.84 (d, ^4J = 1.5 Hz, 2H, H_d), 4.07 (d, ^2J = 12.2 Hz, 2H,-C<u>H</u>H), 4.01 (d, ^2J = 12.2 Hz, 2H, -CH<u>H</u>), 2.25 (s, 6H, Ar-CH₃), 2.15 (s, 12H, Ad), 2.07 (s, 6H, Ad), 1.83-1.74 (m, 12H, Ad), 1.59 (s, 3H, -CH₃). ^{13}C{^{1}H} NMR (101 MHz, CDCl₃): δ 167.24 (CH=N), 163.74 (C₂), 158.57 (C_b), 149.09 (C₆), 137.50 (C_c), 136.51 (C₄), 130.54 (C_f), 129.63 (C_d), 126.67 (C_e), 121.63 (C₅), 121.43 (C₃), 118.50 (C_a), 67.14 (-CH₂), 46.39 (py-<u>C</u>-Me), 40.39 (Ad), 37.33 (Ad), 37.07 (Ad), 29.26 (Ad), 22.44 (CH₃), 20.80 (Ar-CH₃). HRMS for [M]$^+$ (EI): calcd. for ($C_{45}H_{55}N_3O_2$): 669.4288; found: 669.4315.

FT-IR (cm^{-1}): 3063 ν(C-H_aromatic), 2961 ν(C-H_aliphatic), 2903 ν(C-H_aliphatic), 2849 ν(C-H_aliphatic), 1631s ν(C=N_imine), 1593, 1475,1448s, 1435 ν(C=N_py, C=C_aromatic), 1366, 1315 ν(C-N), 1264, 1251 ν(Ar-O), 1232, 1188, 1170, 1117, 1070, 1042, 994, 980, 871, 854, 822, 785s, 768, 753s ν(C-H oop bend), 704, 657, 633, 625, 568, 557, 523, 510, 458, 443, 429, 416. UV-Vis (THF) λ_max: 297, and 335 nm.

5.2.8 Synthesis and characterization of H₂Naphpy ligand:
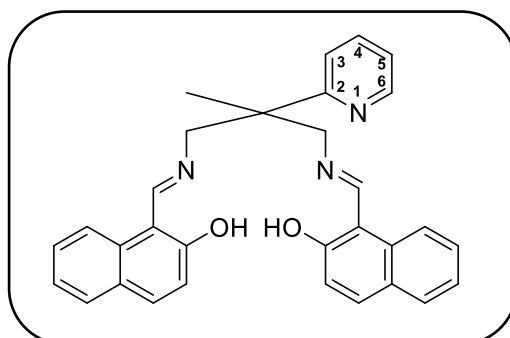
In 100 ml two-nick round bottom flask, a solution of ppda (2 g, 12.1 mmol) in dry ethanol was stirred at 40 °C under argon for 30 min. Afterward, 2 equivalents (4.17 g, 24.2 mmol) of 2-hydroxy-1-naphthaldehyde (which was recrystallized from methanol prior to use) was added gradually. After 5 hours, the solution allowed to cool to room temperature and the dark yellow precipitate was filtered and washed with cold ethanol. The product then dried *in vacuo*. Yield (4.29 g, 75%).

Properties of H₂Naphpy:

Formula: $C_{31}H_{27}N_3O_2$.

Nature: Dark yellow solid.

Molecular weight: 473.58 g/mol.

Yield: 75%

^{1}H NMR (400 MHz, CDCl₃): δ 14.55 (s, 2H, OH), 8.76 (d, ^3J = 4.9 Hz, 1H, H₆), 8.73 (overlapping, 2H, CH=N), 7.77-7.64 (m, 5H, Ar-H,H₄), 7.59 (d, ^3J = 7.7 Hz, 2H, Ar-H), 7.37 (d, ^3J = 8.0 Hz, 1H, H₅), 7.31 (t, ^3J = 7.7 Hz, 2H, Ar-H), 7.25-7.17 (overlapping, 3H, Ar-H, H₃), 6.95 (d, ^3J = 9.2 Hz, 2H, Ar-H), 4.17 (d, ^2J = 12.9 Hz, 2H, -C<u>H</u>H), 4.04 (d, ^2J = 12.9 Hz, 2H, -CH<u>H</u>), 1.65 (s, 3H, -CH₃). ^{13}C{^{1}H} NMR (101 MHz, CDCl₃): δ 173.98(CH=N), 161.69(C₂), 159.73(Ar-C), 149.48(C₆), 137.26 (Ar-C), 137.11 (C₄), 133.54(Ar-C), 129.26(Ar-C), 128.11(Ar-C), 126.58(Ar-C), 123.84(Ar-C), 123.05(C₃), 122.59(Ar-C), 121.56(C₅), 118.23(Ar-C), 107.16(Ar-C), 62.00(-CH₂), 46.43(py-<u>C</u>-Me), 21.47(-CH₃). HRMS for [M+H]$^+$ (ASAP): calcd. for (C₃₁H₂₈N₃O₂): 474.2182; found: 474.2180.

FT-IR (cm^{-1}): 3157 ν(C-H$_{aromatic}$), 3054 ν(C-H$_{aromatic}$), 3031 ν(C-H$_{aromatic}$), 2998 ν(C-H$_{aliphatic}$), 2974 ν(C-H$_{aliphatic}$), 2870 ν(C-H$_{aliphatic}$), 1618s ν(C=N$_{imine}$), 1543, 1528, 1491, 1444 ν(C=N$_{py}$, C=C$_{aromatic}$), 1400, 1350m, 1303m ν(C-N), 1258 ν(Ar-O), 1209, 1183, 1159, 1140, 1122, 1012, 992m, 973, 937, 891, 859, 830s, 794, 752s, 744vs ν(C-H oop bend), 681, 648,625, 535, 517, 503, 438, 423, 413. UV-Vis (THF) λ$_{max}$: 280, 313, 363, 403, and 426 nm.

5.2.9 Synthesis and characterization of H₂Salpn ligand:
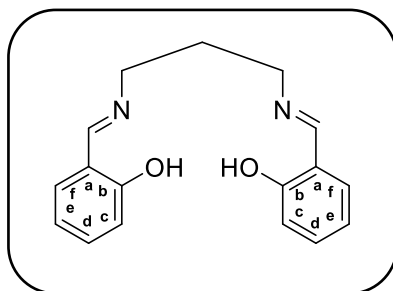
The Schiff base ligand H$_2$Salpn was prepared by standard methods: 10 mmol of 1,3-diaminoprpane (0.83 ml, 0.74 g) was added dropwise to a magnetically stirred methanolic solution of 20 mmol salicylaldehyde (1.67 ml, 2.44 g). The reaction mixture was heated at 50 °C for three hours. After cooling to ambient temperature, the precipitate was filtered off, washed with methanol, and dried *in vacuo* to give a yellow powder (2.59 g, 92% yield).

Properties of H$_2$Salpn:

Formula: C$_{17}$H$_{18}$N$_2$O$_2$.

Nature: Yellow solid.

Molecular weight: 282.34 g/mol.

Yield: 92%

^{1}H NMR (400 MHz, CDCl$_3$): δ 13.43 (s, 2H, OH), 8.38 (s, 2H, CH=N), 7.32 (ddd, ^3J = 8.3 Hz, ^3J =7.3 Hz, ^4J =1.0 Hz, 2H, H$_d$), 7.25 (dd, ^3J =7.6 Hz, ^4J =1.2 Hz, 2H, H$_f$), 6.97 (dd, ^3J = 8.3 Hz, ^4J =1.0 Hz, 2H, H$_c$), 6.88 (td, ^3J =7.6 Hz, ^4J =1.1 Hz, 2H, H$_e$), 3.72 (td, ^3J = 6.6 Hz, ^4J =1.0 Hz, 4H, N-CH$_2$), 2.13 (p, ^3J = 6.6 Hz, 2H, -CH$_2$-).^{13}C{^{1}H} NMR (101 MHz, CDCl$_3$): δ 165.60 (CH=N), 161.27 (C$_b$), 132.43 (C$_d$), 131.41 (C$_f$), 118.89 (C$_e$), 118.79 (C$_a$), 117.14 (C$_c$), 56.97 (N-CH$_2$), 31.85 (-CH$_2$-). HRMS for [M]$^+$ (EI): calcd. for (C$_{17}$H$_{18}$N$_2$O$_2$): 282.13628; found: 282.1369.

FT-IR (cm^{-1}): 3050 ν(C-H$_{aromatic}$), 2996 ν(C-H$_{aliphatic}$), 2947 ν(C-H$_{aliphatic}$), 2898 ν(C-H$_{aliphatic}$), 2870 ν(C-H$_{aliphatic}$), 1630s ν(C=N$_{imine}$), 1608s, 1579, 1496s, 1458 ν(C=C$_{aromatic}$), 1419m, 1387, 1360, 1337, 1316 ν(C-N), 1273s ν(Ar-O), 1210, 1199, 1145, 1124, 1102, 1083, 1052, 1030, 1007, 975, 883s, 854s, 778, 750vs ν(C-H oop bend), 735s, 663, 639, 571, 556, 522, 464m, 420, 411. UV-Vis (THF) λ$_{max}$: 232, 257, and 319 nm.

5.2.10 Synthesis and characterization of ᵗBu,ᵗBu-H₂Salpn ligand:
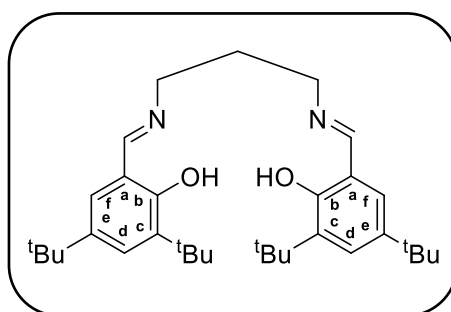
The procedure was similar to that described for the preparation of most Schiff base ligands in this thesis. A solution of 1,3-diaminopropane (0.42 ml, 0.37 g, 5 mmol) in methanol (10 ml) was added to a methanolic solution of 3,5-di-tert-butylsalicyaldehyde (2.34 g, 20 mmol) and the mixture was stirred at 50°C for two hours. The precipitate was collected by filtration, washed with MeOH and dried under reduced pressure to yield the titled ligand as yellow powder (2.16 g, 85% yield).

Properties of ᵗBu,ᵗBu-H₂Salpn:

Formula: $C_{33}H_{50}N_2O_2$.

Nature: Yellow solid.

Molecular weight: 506.78 g/mol.

Yield: 85%

^{1}H NMR (400 MHz, CDCl₃): δ 13.82 (s, 2H,OH), 8.39 (s, 2H, CH=N), 7.39 (d, ^4J =2.0 Hz, 2H, H$_d$), 7.09 (d, ^4J = 2.1 Hz, 2H, H$_f$), 3.71 (t, ^3J = 6.5 Hz, 4H, CH₂-N), 2.13 (p, ^3J = 6.5 Hz, 2H, -CH₂-), 1.46 (s, 18H, C(CH₃)₃), 1.31 (s, 18H, C(CH₃)₃). ^{13}C{^{1}H} NMR (101 MHz, CDCl₃): δ 166.62 (CH=N), 158.26 (C$_b$), 140.19 (C$_e$), 136.83 (C$_c$), 127.04 (C$_d$), 125.98 (C$_f$), 117.99 (C$_a$), 56.90 (CH₂-N), 35.19 (C(CH₃)₃), 34.28 (C(CH₃)₃), 31.87 (-CH₂-), 31.65 (C(CH₃)₃), 29.58 (C(CH₃)₃). HRMS for [M+H]⁺ (ASAP): calcd. for (C₃₃H₅₁N₂O₂): 507.3951; found: 507.3950.

FT-IR (cm⁻¹): 3083 ν(C-H$_{aromatic}$), 3002 ν(C-H$_{aromatic}$), 2955 ν(C-H$_{aliphatic}$), 2908 ν(C-H$_{aliphatic}$), 2866 ν(C-H$_{aliphatic}$), 1629s ν(C=N$_{imine}$), 1589, 1465s, 1439vs ν(C=C$_{aromatic}$), 1389, 1361s ν(C-N), 1271, 1251s, 1241 ν(Ar-O), 1200, 1171s, 1110, 1091, 1058, 1035, 1024, 984m, 880m, 830s, 801s, 772s ν(C-H oop bend), 730, 714, 700, 646m, 590, 543, 515, 500, 484, 473, 463, 446, 436, 433, 421, 412. UV-Vis (THF) λ$_{max}$: 250, and 330 nm.

5.2.11 Synthesis and characterization of Me-H₂Salpn ligand:
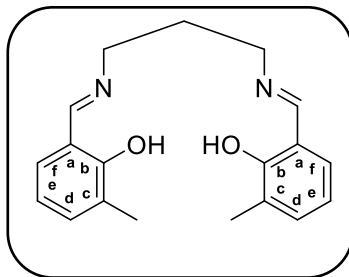
(0.56 ml, 0.5 g, 6.75 mmol) of 1,3-diaminopropane was dissolved in methanol (20 ml) and a methanolic solution of 2-hydroxy-3-methybenzaldehyde was added gradually. The resulting yellow solution was then heated at 50 °C for three hours. The solution allowed to cool to room temperature and then kept in freezer overnight whereupon a yellow precipitate formed. The precipitate was filtered off, washed with cold methanol and the solvent evaporated under reduced pressure (1.87 g, 89% yield).

Properties of Me-H₂Salpn:

Formula: $C_{19}H_{22}N_2O_2$.

Nature: Yellow solid.

Molecular weight: 310.40 g/mol.

Yield: 89%

^{1}H NMR (400 MHz, CDCl₃) δ 13.74 (s, 2H, OH), 8.36 (s, 2H, CH=N), 7.21 (d, ^3J = 7.3 Hz, 2H, H$_d$), 7.11 (dd, ^3J = 7.6 Hz, ^4J =0.9 Hz, 2H, H$_f$), 6.82 (t, ^3J = 7.5 Hz, 2H, H$_e$), 3.72 (t, ^3J = 6.6 Hz, 4H, CH₂-N), 2.31 (s, 6H, Ar-CH₃), 2.12 (p, ^3J = 6.6 Hz, 2H, -CH₂-).^{13}C{^{1}H} NMR (101 MHz, CDCl₃) δ 165.76 (CH=N), 159.57 (C$_b$), 133.39 (C$_d$), 129.07 (C$_f$), 126.08 (C$_c$), 118.26 (C$_e$), 118.09 (C$_a$), 56.85 (CH₂-N), 31.91 (-CH₂-), 15.62 (C(C̲H₃)). HRMS for [M+H]⁺ (ASAP): calcd. for ($C_{19}H_{23}N_2O_2$): 311.1760; found: 311.1761.

FT-IR (cm⁻¹): 3055 ν(C-H$_{aromatic}$), 3008 ν(C-H$_{aromatic}$), 2980 ν(C-H$_{aliphatic}$), 2915 ν(C-H$_{aliphatic}$), 2845 ν(C-H$_{aliphatic}$), 1628s ν(C=N$_{imine}$), 1608, 1491, 1455s, 1433s ν(C=C$_{aromatic}$), 1376, 1347, 1318 ν(C-N), 1263s ν(Ar-O), 1249s, 1100, 1082m, 1032, 989, 971m, 842s, 772s, 742vs ν(C-H oop bend), 708m, 633, 621, 527, 483, 458,420. UV-Vis (THF) λ$_{max}$: 272, and 323 nm.

5.3 Synthesis and characterization of Ti(IV) complexes:

Titanium (IV) complexes with Salen-type ligand in this thesis have been prepared using TiCl$_4$ or TiCl$_4$(THF)$_2$ precursor and both gave good results with no considerable difference in the yield. However, as the reaction of TiCl$_4$ with THF is exothermic and vigorous, TiCl$_4$(THF)$_2$ was used in the synthesis.

5.3.1 Synthesis and characterization of [Ti(Salpy)Cl$_2$] (8):
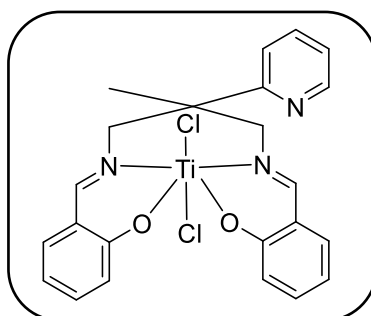
A solution of TiCl$_4$(THF)$_2$ (0.2 g, 0.59 mmol) in dry THF (~20 ml) was added dropwise to a stirred solution of H$_2$Salpy (1 eq., 0.23 g, 59 mmol) in dry THF (~20 ml) under argon. The resulting mixture was refluxed at 70 °C for one hour. After cooling to ambient temperature, the solution was filtered using filter canula and the precipitate washed with dry Et$_2$O (3×10 ml). The orange precipitate then dried under high vacuum (10^{-6} mbar) at 80 °C for 3 hours (0.26 g, 91% yield).

Properties of [Ti(Salpy)Cl$_2$]:

Formula: C$_{23}$H$_{21}$Cl$_2$N$_3$O$_2$Ti.

Nature: Orange solid.

Molecular weight: 490.21 g/mol.

Yield: 91%

The lack of solubility of this complex hampered its full characterization; ^{13}C{^{1}H} NMR data could not be measured. ^{1}H NMR data were acquired with 265 scans.

^{1}H NMR (500 MHz, CDCl$_3$): δ 9.03 (s, 2H, CH=N), 8.83 (d, ^3J = 7 Hz, 1H, H$_6$), 8.23 (td, ^3J = 8.0 Hz, ^4J =1.8 Hz, 1H, H$_4$), 7.70-7.65 (m, 3H, H$_c$, H$_5$), 7.60 (d, ^3J = 8.5 Hz, 1H, H$_3$), 7.53 (ddd, ^3J = 8.4 Hz, ^3J =7.4 Hz, ^4J =1.7 Hz, 2H, H$_d$), 7.10 (td, ^3J = 7.5 Hz, ^4J = 0.9 Hz, 2H, H$_e$), 6.83 (d, ^3J = 8.1 Hz, 2H, H$_f$), 5.09 (d, ^2J = 14.7 Hz, 2H, CHH), 4.85 (d, ^2J = 14.3 Hz, 2H, CHH), 1.69 (s, 3H, CH$_3$). HRMS for [M-Cl]$^+$ (EI): calcd. for (C$_{23}$H$_{21}$ClN$_3$O$_2$Ti): 454.0802; found: 454.0791.

FT-IR (KBr pellet, cm^{-1}): 3046 ν(C-H$_{aromatic}$), 2997 ν(C-H$_{aliphatic}$), 2965 ν(C-H$_{aliphatic}$), 2931 ν(C-H$_{aliphatic}$), 2870 ν(C-H$_{aliphatic}$),1647 ν(C=N$_{imine}$), 1602s, 1558s, 1538, 1462s, ν(C=N$_{py}$, C=C$_{aromatic}$), 1384, 1334 ν(C-N), 1276s ν(Ar-O), 1250s, 1221s, 1150m, 1121, 1087, 1030m, 998s, 912s, 901s, 830s, 767s, 660s, 651s, 623, 599 ν(Ti-Cl), 589, 554m, 533, 491 ν(Ti-N), 474m, 415s. UV-Vis (THF) λ_{max}: 262, 309, and 398 nm.

5.3.2 Synthesis and characterization of [Ti(Salpy-Me)Cl$_2$] (9):
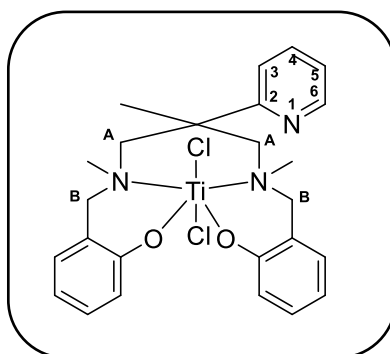
A solution of TiCl$_4$(THF)$_2$ (0.45 g, 1.35 mmol) in dry THF (~20 ml) was added dropwise to a stirred solution of H$_2$Salpy-Me (1 eq., 0.55 g) in dry THF (~15 ml) under argon. The resulting mixture was refluxed at 70 °C for one hour. After cooling to ambient temperature, the solution was filtered using filter canula and the precipitate washed with dry Et$_2$O (3×10 ml). The bright orange precipitate then dried under high vacuum (10^{-6} mbar) at 80 °C for 3 hours (0.59 g, 84% yield).

Properties of [Ti(Salpy-Me)Cl$_2$]:

Formula: C$_{25}$H$_{29}$Cl$_2$N$_3$O$_2$Ti.

Nature: Bright orange solid.

Molecular weight: 522.29 g/mol.

Yield: 84%

The lack of solubility of this complex hampered its full characterization; ^{13}C{^{1}H} NMR data could not be measured and the ^{1}H NMR not fully characterized. ^{1}H NMR data were acquired with multiple scans.

^{1}H NMR (500 MHz, CD$_2$Cl$_2$): 8.81 (dd, ^3J = 5.76 Hz,^4J = 0.94 Hz, 1H, H$_6$), 8.30 (t, ^3J = 7.2 Hz, 1H, H$_4$), 7.81 (d, ^3J = 8.3 Hz, 1H, H$_3$), 7.74 (t, ^3J = 8.3 Hz, 1H, H$_5$), 7.48-6.73 (overlapping, 8H, Ar). HRMS for [M-Cl]$^+$ (EI): calcd. for (C$_{25}$H$_{29}$ClN$_3$O$_2$Ti): 486.1427; found: 486.1035.

FT-IR (cm^{-1}): 3063 ν(C-H$_{aromatic}$), 3029 ν(C-H$_{aromatic}$), 2965 ν(C-H$_{aliphatic}$), 2875 ν(C-H$_{aliphatic}$), 1595m, 1572, 1481s, 1452s ν(C=N$_{py}$, C=C$_{aromatic}$), 1387 ν(C-N),, 1259s ν(Ar-O), 1158, 1111, 1041, 895s, 807w 760s ν(C-H oop bend), 638 ν(Ti-Cl), 547 ν(Ti-N), 474 ν(Ti-O).

5.3.3 Synthesis and characterization of [Ti(^{t}Bu,^{t}Bu-Salpy)Cl$_2$] (10):
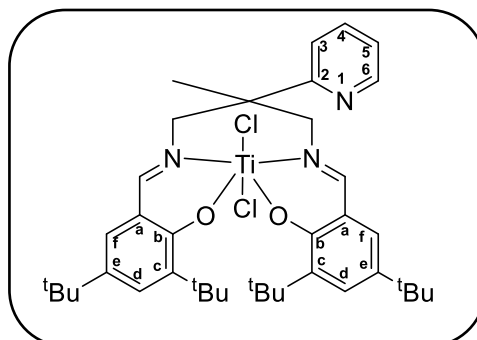
To a Schlenk tube containing ^{t}Bu,^{t}Bu-H$_2$Salpy ligand (1 g, 1.67 mmol) in THF (20 ml), 1 equivalent of TiCl$_4$(THF)$_2$ (0.56 g) in THF (15 ml) was added dropwise at room temperature. The orange red solution was refluxed at 70 °C for one hour. The solvent removed under reduced pressure and dry pentane (15 ml) was added. The mixture was stirred for 2 minutes before filtering it. The washing process was repeated 3 times and then the precipitate was dried *in vacuo* for 3 hours (1.1 g, 92% yield).

Properties of [Ti(^{t}Bu,^{t}Bu-Salpy)Cl$_2$]:

Formula: C$_{39}$H$_{53}$Cl$_2$N$_3$O$_2$Ti.

Nature: Orange red solid.

Molecular weight: 714.64 g/mol.

Yield: 92%

^{1}H NMR (400 MHz, CDCl$_3$): δ 8.96 (s, 2H, CH=N), 8.78 (dd, ^3J = 5.9 Hz, ^4J =1.2 Hz, 1H, H$_6$), 8.22 (td, ^3J = 8.1, ^4J =1.5 Hz, 1H, H$_4$), 7.70 (d, ^3J = 8.2 Hz, 1H, H$_3$), 7.63 (t, ^3J = 6.7 Hz, 1H$_5$), 7.57 (d, ^4J = 2.4 Hz, 2H, H$_d$), 7.48 (d, ^4J = 2.3 Hz, 2H, H$_f$), 5.07 (d, ^2J = 14.9 Hz, 2H, -CHH), 4.73 (d, ^2J = 14.6 Hz, 2H, -CHH), 1.65 (s, 3H, -CH$_3$), 1.48 (s, 18H, C(CH$_3$)$_3$), 1.32 (s, 18H, C(CH$_3$)$_3$). ^{13}C{^{1}H} NMR (126 MHz, CDCl$_3$): δ 169.88 (CH=N), 160.53 (C$_2$), 157.59 (C$_b$), 145.65 (C$_6$), 145.57 (C$_4$), 142.58 (C$_c$), 137.10 (C$_e$), 131.85 (C$_d$), 131.09 (C$_f$), 127.05 (C$_a$), 126.44 (C$_3$), 124.81 (C$_5$), 70.09 (CH$_2$-N), 45.03 (py-C-Me), 35.86 (C(CH$_3$)$_3$), 34.71(C(CH$_3$)$_3$), 31.43 (C(CH$_3$)$_3$), 30.46 (C(CH$_3$)$_3$), 28.51 (-CH$_3$). HRMS for [M-Cl]$^+$ (ASAP): calcd. for (C$_{39}$H$_{53}$ClN$_3$O$_2$Ti): 678.3306; found: 678.3314.

FT-IR (KBr pellet, cm^{-1}): 3084 ν(C-H$_{aromatic}$), 3048 ν(C-H$_{aromatic}$), 2959 ν(C-H$_{aliphatic}$), 2909 ν(C-H$_{aliphatic}$), 2870 ν(C-H$_{aliphatic}$), 1607s ν(C=N$_{imine}$), 1567m, 1478, 1462m, 1440m ν(C=N$_{py}$, C=C$_{aromatic}$), 1416, 1394, 1364m ν(C-N), 1325, 1272s, 1251s ν(Ar-O), 1202, 1175, 1066, 1011, 921, 860s, 761s ν(C-H oop bend), 644 ν(Ti-Cl), 620, 585s ν(Ti-N), 497, 473, 436 ν(Ti-O), 419. UV-Vis (THF) λ_{max}: 272, 325, and 425 nm.

5.3.4 Synthesis and characterization of [Ti(^{t}Bu,OMe-Salpy)Cl$_2$] (11):
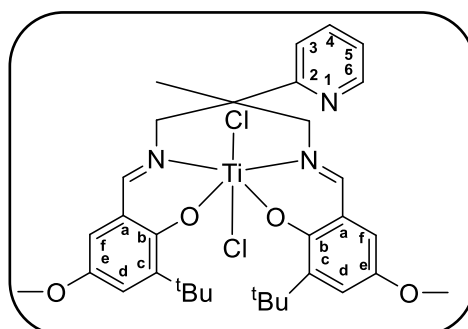
To a Schlenk tube containing ^{t}Bu,OMe-H$_2$Salpy (0.31 g, 0.92 mmol) in THF (20 ml), 1 equivalent of TiCl$_4$(THF)$_2$ (0.50 g) in THF (15 ml) was added dropwise at room temperature. The red solution was refluxed at 70 °C for one hour. The solvent removed under reduced pressure and dry pentane (15 ml) was added. The mixture was stirred for 2 minutes before filtering it. The washing process was repeated 3 times and then the precipitate was dried *in vacuo* for 3 hours (0.5 g, 82% yield).

Properties of [Ti(^{t}Bu,OMe-Salpy)Cl$_2$]:

Formula: C$_{33}$H$_{41}$Cl$_2$N$_3$O$_4$Ti.

Nature: Red solid.

Molecular weight: 662.48 g/mol.

Yield: 82%

^{1}H NMR (500 MHz, CDCl$_3$): δ 8.96 (d, ^4J= 0.9Hz, 2H,CH=N), 8.77 (dd, ^3J = 5.8 Hz, ^4J = 1.4 Hz, 1H, H$_6$), 8.22 (td, ^3J = 8.1 Hz, ^4J =1.5 Hz, 1H, H$_4$), 7.71 (d, ^3J = 8.2 Hz, 1H, H$_3$), 7.64 (t, ^3J = 6.8 Hz, 1H, H$_5$), 7.11 (d, ^4J = 3.1 Hz, 2H, H$_d$), 7.00 (d, ^4J = 3.1 Hz, 2H, H$_f$), 5.05 (d, ^2J = 14.8 Hz, 2H, -CHH), 4.74 (d, J = 14.7 Hz, 2H, -CHH), 3.83 (s, 6H, O-CH$_3$), 1.64 (s, 3H, -CH$_3$), 1.45 (s, 18H, C(CH$_3$)$_3$). ^{13}C{^{1}H} NMR (126 MHz, CDCl3): δ 169.38 (CH=N), 157.57 (C$_2$), 157.47 (C$_b$), 154.61 (C$_e$), 145.69 (C$_4$), 142.48 (C$_6$), 139.57 (C$_c$), 127.72 (C$_5$), 126.48 (C$_a$), 124.85 (C$_3$), 122.56 (C$_d$), 115.34 (C$_f$), 69.93 (CH$_2$-N), 56.04 (O-CH$_3$), 44.98 (Py-C-Me), 35.80 (C(CH$_3$)$_3$),

30.28($\underline{C}(CH_3)_3$), 28.54 (-CH_3). HRMS for [M-Cl]$^+$ (EI): calcd. for ($C_{33}H_{41}ClN_3O_4Ti$): 626.22596; found: 626.2279.

FT-IR (KBr pellet, cm^{-1}): 3079 ν(C-H$_{aromatic}$), 3000 ν(C-H$_{aromatic}$), 2954 ν(C-H$_{aliphatic}$), 2969 ν(C-H$_{aliphatic}$), 2836 ν(C-H$_{aliphatic}$), 1598s ν(C=N$_{imine}$), 1562s, 1457s, 1427s ν(C=N$_{py}$, C=C$_{aromatic}$), 1394, 1348s ν(C-N), 1322, , 1348 ν(Ar-O), 1250s, 1218s, 1200s, 1159s, 1057, 930w, 853vs,780w ν(C-H oop bend), 760m, 638 ν(Ti-Cl), 595m, 559 ν(Ti-N), 485 ν(Ti-O), 434. UV-Vis (THF) λ$_{max}$: 270, 332, and 439 nm.

5.3.5 Synthesis and characterization of [Ti(Me-Salpy)Cl₂] (12):
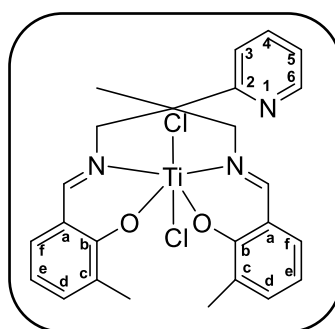
To a Schlenk tube containing Me-H$_2$Salpy (0.2 g, 0.49 mmol) in THF (20 ml), 1 equivalent of TiCl$_4$(THF)$_2$ (0.17 g) in THF (15 ml) was added dropwise at room temperature. The dark orange solution was refluxed at 70 °C for one hour. The solvent removed under reduced pressure and dry diethyl ether (15 ml) was added. The mixture was stirred for 2 minutes before filtering it. The washing process was repeated 3 times and then the precipitate was dried *in vacuo* for 3 hours (0.19 g, 73% yield).

Properties of [Ti(Me-Salpy)Cl₂]:

Formula: $C_{25}H_{25}Cl_2N_3O_2Ti$.

Nature: Dark orange solid.

Molecular weight: 518.26 g/mol.

Yield: 73%

^{1}H NMR (500 MHz, CDCl$_3$): δ 9.03 (d, ^4J= 1.5 Hz, 2H, CH=N), 8.75 (dd, ^3J = 5.8 Hz, ^4J =1.3 Hz, 1H, H$_6$), 8.19 (td, ^3J = 8.1 Hz, ^4J =1.7 Hz, 1H, H$_4$), 7.65 (d, ^3J = 8.3 Hz, 1H, H$_3$), 7.60 (ddd, ^3J = 7.5 Hz, ^3J =5.9 Hz, ^4J =1.0 Hz, 1H, H$_5$), 7.51 (dd, ^3J = 7.7 Hz, ^4J =1.0 Hz, 2H, H$_f$), 7.37 (d, ^3J = 7.4 Hz, 2H, H$_d$), 6.96 (t, ^3J = 7.6 Hz, 2H, H$_e$), 5.07 (d, ^2J = 14.6 Hz, 2H, -C$\underline{H}$H), 4.84 (d, ^2J = 14.5 Hz, 2H, -CH$\underline{H}$), 2.28 (s, 6H, Ar-CH$_3$), 1.66 (s, 3H, -CH$_3$). ^{13}C{^{1}H} NMR (126 MHz, CDCl$_3$): δ 168.92 (CH=N), 162.20 (C$_2$), 157.45 (C$_b$), 145.60 (C$_6$), 142.64 (C$_4$), 137.71 (C$_d$), 133.13 (C$_f$), 126.12 (C$_3$), 125.96 (C$_c$), 125.63 (C$_a$), 124.83 (C$_5$), 122.79 (C$_e$), 69.62 (N-CH$_2$), 45.43 (Py-$\underline{C}$-

Me), 28.47 (-CH$_3$), 16.00 (Ar-CH$_3$). HRMS for [M-Cl]$^+$ (EI): calcd. for (C$_{25}$H$_{25}$ClN$_3$O$_2$Ti): 482.1109; found: 482.1107.

FT-IR (KBr pellet, cm^{-1}): 3089 ν(C-H$_{aromatic}$),3049 ν(C-H$_{aromatic}$), 2963 ν(C-H$_{aliphatic}$), 2922 ν(C-H$_{aliphatic}$), 2866 ν(C-H$_{aliphatic}$), 1609vs ν(C=N$_{imine}$), 1591, 1573s, 1528, 1453 ν(C=N$_{py}$, C=C$_{aromatic}$), 1380, 1369, 1318 ν(C-N), 1267s ν(Ar-O), 1232, 1167, 1135, 1105, 1087, 1060, 1001, 992, 956, 880s, 777m, 759s ν(C-H oop bend), 744s, 663s, 612 ν(Ti-Cl), 622, 608s, 589, 569 ν(Ti-N), 521, 488, 472s, 445, 428s, 415. UV-Vis (THF) λ$_{max}$: 267, 311, and 410 nm.

5.3.6 Synthesis and characterization of [Ti(Cl,Cl-Salpy)Cl₂] (13):
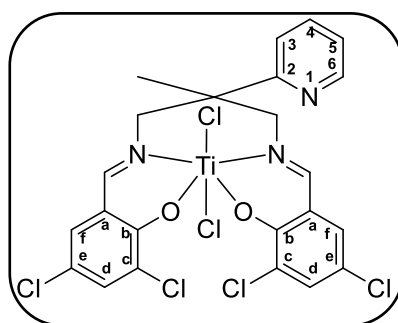
To a Schlenk tube containing Cl,Cl-H$_2$Salpy (0.92 g, 1.79 mmol) in THF (20 ml), 1 equivalent of TiCl$_4$(THF)$_2$ (0.6 g) in THF (15 ml) was added dropwise at room temperature. The red orange solution was refluxed at 70 °C for one hour. The solvent removed under reduced pressure and dry diethyl ether (15 ml) was added. The mixture was stirred for 2 minutes before filtering it. The washing process was repeated 3 times and then the precipitate was dried *in vacuo* for 3 hours (0.97 g, 86% yield).

Properties of [Ti(Cl,Cl-Salpy)Cl₂]:

Formula: C$_{23}$H$_{17}$Cl$_6$N$_3$O$_2$Ti.

Nature: Red orange solid.

Molecular weight: 627.98 g/mol.

Yield: 86%

^{1}H NMR (400 MHz, CDCl$_3$): δ 9.07 (s, 2H, CH=N), 8.84 (dd, ^3J= 5.4 Hz, ^4J=1.5 Hz, 1H, H$_6$), 8.27 (td, ^3J= 8.1 Hz, ^4J=1.2 Hz, 1H, H$_4$), 7.72 (dd, ^3J= 6.7 Hz, ^4J=1.2 Hz, 1H, H$_3$), 7.59 (s, 4H, H$_d$, H$_f$), 7.55 (d, ^3J= 8.5 Hz, 1H, H$_5$), 5.15 (d, ^3J= 14.5 Hz, 2H, CH$_2$), 4.90 (d, ^3J= 14.4 Hz, 2H, CH$_2$), 1.70 (s, 3H$_3$).LRMS for [M-Cl]$^+$ (ASAP): calcd. for (C$_{23}$H$_{17}$Cl$_6$N$_3$O$_2$Ti): 591.92136; found: 591.9221.

FT-IR (KBr pellet, cm^{-1}): 3093 ν(C-H$_{aromatic}$), 3042 ν(C-H$_{aromatic}$), 2971 ν(C-H$_{aliphatic}$), 2927 ν(C-H$_{aliphatic}$), 2857 ν(C-H$_{aliphatic}$), 1606s ν(C=N$_{imine}$), 1546s, 1450s, 1437s ν(C=N$_{py}$, C=C$_{aromatic}$), 1389, 1364 ν(C-N), 1288s ν(Ar-O), 1238, 1219m, 1202m, 1131, 1106, 1065, 99m7, 960w, 881s, 795s ν(C-H oop bend), 740m, 706w, 612s ν(Ti-Cl), 565s, 559 ν(Ti-N), 535s, 506, 439, 421m. UV-Vis (THF) λ_{max}: 270, 287, and 396 nm.

5.3.7 Synthesis and characterization of [Ti(Ad, Me-Sal)Cl$_2$] (14):
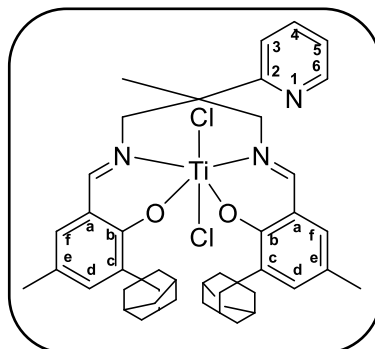
To a Schlenk tube containing Ad,Me-H$_2$Salpy (0.19 g, 0.28 mmol) in THF (20 ml), 1 equivalent of TiCl$_4$(THF)$_2$ (0.09 g) in THF (15 ml) was added dropwise at room temperature. The dark red solution was refluxed at 70 °C for one hour. The solvent removed under reduced pressure and dry hexane (15 ml) was added. The mixture was stirred for 2 minutes before filtering it. The washing process was repeated 3 times and then the precipitate was dried *in vacuo* for 3 hours (0.20 g, 91% yield).

Properties of [Ti(Ad, Me-Salpy)Cl$_2$]:

Formula: C$_{45}$H$_{53}$Cl$_2$N$_3$O$_2$Ti.

Nature: Dark red solid.

Molecular weight: 786.71 g/mol.

Yield: 91%

^{1}H NMR (500 MHz, CDCl3) δ 10.29 (dd, ^3J = 5.9 Hz, ^4J =1.2 Hz, 1H, H$_6$), 8.42 (s, 1H, CH=N), 8.35 (s, 1H, CH=N), 7.95 (td, ^3J = 7.8Hz, ^4J =1.7Hz, 1H,H$_4$), 7.74 (d, ^3J = 8.1 Hz, 1H, H$_3$), 7.53 (ddd, J =, , Hz, 1H), 7.13 (dd, ^3J = 7.3 Hz, ^4J =5.9 Hz, ^5J =1.3 Hz, 1H, H$_5$),7.37 (d, ^4J = 1.8 Hz, 1H, Ar),7.19 (d, ^4J = 1.9 Hz, 1H, Ar), 7.02 (s, 1H, Ar), 6.97 (s, 1H, Ar), 4.94 (d, ^2J = 12.8 Hz, 2H,-CHH), 4.60 (d, ^2J = 13.1 Hz, 2H, -CHH), 3.84 (d, ^2J = 12.9 Hz, 1H, -CH<u>H</u>), 3.73 – 3.70 (overlaping, 1H, -CH<u>H</u>), 2.30 (s, 3H, 3H, Ar-CH$_3$), 2.28 (s, 3H, 3H, Ar-CH$_3$), 2.27 – 2.21 (m, 12H, Ad), 2.17 – 2.12 (m, 6H, Ad), 1.86 – 1.74 (m, 12H, Ad),1.64 (s, 3H, -CH$_3$).^{13}C{^{1}H} NMR (126 MHz, CDCl$_3$): δ 168.90 (C=N), 168.20 (C=N), 163.79 (C$_2$), 160.83 (C$_{Ar}$), 158.49 (C$_{Ar}$), 151.87 (C$_{Ar}$), 139.51 (C$_{Ar}$), 138.31 (C$_{py}$), 137.81 (C$_{Ar}$), 135.59 (C$_{Ar}$), 134.75 (C$_{Ar}$), 132.38 (C$_{Ar}$),

130.09 (C$_{py}$), 128.06 (C$_{py}$), 127.21 (C$_{Ar}$), 125.53 (C$_{py}$), 124.76 (C$_{Ar}$), 123.64 (C$_{Ar}$), 118.26 (C$_{Ar}$), 68.74 (-CH$_2$), 45.44 (py-$\underline{C}$-Me), 41.38 (Ad), 40.89 (Ad), 40.57 (Ad), 37.54 (Ad), 37.25 (Ad), 37.22 (Ad), 37.17 (Ad), 36.88 (Ad), 29.19 (Ad), 29.06 (Ad), 25.90 (CH$_3$), 21.03 (Ar-CH$_3$), 20.83 (Ar-CH$_3$). HRMS for [M-Cl]$^+$ (ASAP): calcd. for (C$_{45}$H$_{53}$ClN$_3$O$_2$Ti): 750.3306; found: 750.3311.

FT-IR (KBr pellet, cm^{-1}): 3045 ν(C-H$_{aromatic}$), 2903 ν(C-H$_{aliphatic}$), 2847 ν(C-H$_{aliphatic}$), 1603s ν(C=N$_{imine}$), 1564, 1487, 1451s ν(C=N$_{py}$, C=C$_{aromatic}$), 1367, 1329 ν(C-N), 1313, 1260s ν(Ar-O), 1229s, 1186, 1170, 1103, 1066, 1012, 980w, 867s, 815m, 787m, 757m ν(C-H oop bend), 713, 657, 640, 603 ν(Ti-Cl), 588 ν(Ti-N), 535, 456, 436 ν(Ti-O). UV-Vis (THF) λ$_{max}$: 266, 320, and 417 nm.

5.3.8 Synthesis and characterization of [Ti(Naphpy)Cl$_2$] (15):
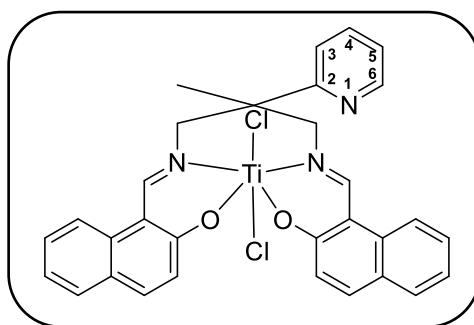
To a Schlenk tube containing H$_2$-Naphpy (0.3 g, 0.63 mmol) in THF (20 ml), 1 equivalent of TiCl$_4$(THF)$_2$ (0.21 g) in THF (15 ml) was added dropwise at room temperature. The dark red solution was refluxed at 70 °C for one hour. The solvent removed under reduced pressure and dry Et$_2$O (15 ml) was added. The mixture was stirred for 2 minutes before filtering it. The washing process was repeated 3 times and then the precipitate was dried *in vacuo* for 3 hours (0.34 g, 92% yield).

Properties of [Ti(Naphpy)Cl$_2$]:
Formula: C$_{31}$H$_{25}$Cl$_2$N$_3$O$_2$Ti.
Nature: Dark red solid.
Molecular weight: 590.33 g/mol.
Yield: 92%
^{1}H NMR (500 MHz, CDCl$_3$): δ 9.82 (s, 2H, CH=N), 8.82 (dd, ^3J = 5.8 Hz, ^4J =1.3 Hz, 1H, H$_6$), 8.65 − 8.53 (m, 3H, Ar-H,Py-H), 7.99 (d, ^3J = 9.0 Hz, 2H, Ar-H), 7.85 − 7.79 (m, 2H, Ar-H), 7.76 − 7.68 (m, 3H, Ar-H, Py-H), 7.48 (dd, ^3J = 9.7 Hz, ^4J = 5.1 Hz, 3H, Ar-H, Py-H), 7.03 (d, ^3J = 8.9 Hz, 2H, Ar-H), 5.30 (d, ^2J = 14.6 Hz, 2H, -C$\underline{H}$H), 5.01 (d, ^3J = 14.0 Hz, 2H, -CH$\underline{H}$),

1.78 (s, 3H, -CH$_3$). HRMS for [M-Cl]$^+$ (EI): calcd. for (C$_{31}$H$_{25}$ClN$_3$O$_2$Ti): 554.11093; found: 554.1122.

FT-IR (KBr pellet, cm^{-1}): 3174 ν(C-H$_{aromatic}$), 3061 ν(C-H$_{aromatic}$), 2974 ν(C-H$_{aliphatic}$), 2872 ν(C-H$_{aliphatic}$), 1632s ν(C=N$_{imine}$), 1591m, 1549s, 1511m, 1460s ν(C=N$_{py}$, C=C$_{aromatic}$), 1377, 1344 ν(C-N), 1291s ν(Ar-O), 1249s, 1197m, 1167, 1146, 1101, 1034, 1007, 969m, 834m, 750s, 652 ν(Ti-Cl), 599, 545m, 527m ν(Ti-N), 409. UV-Vis (THF) λ$_{max}$: 266, 337, and 465 nm.

5.3.9 Synthesis and characterization of [Ti(Salpn)Cl$_2$] (16):
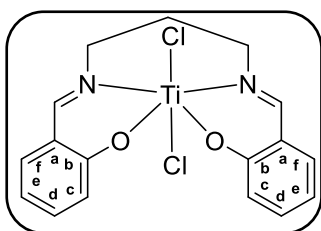
A solution of TiCl$_4$(THF)$_2$ (0.4 g, 1.19 mmol) in dry THF (~20 ml) was added dropwise to a stirred solution of H$_2$Salpn (1 eq., 0.34 g) in dry THF (~15 ml) under argon. The resulting mixture was refluxed at 70 °C for one hour. After cooling to ambient temperature, the orange solution was filtered using filter canula and the precipitate washed with dry Et$_2$O (3×10 ml). The orange precipitate then dried under high vacuum (10^{-6} mbar) at 80 °C for 3 hours (0.45 g, 94% yield).

Properties of [Ti(Salpn)Cl$_2$]:

Formula: C$_{17}$H$_{16}$Cl$_2$N$_2$O$_2$Ti.

Nature: Orange solid.

Molecular weight: 399.09 g/mol.

Yield: 94%

The lack of solubility of this complex hampered its full characterization; ^{13}C{^{1}H} NMR data could not be measured. ^{1}H NMR data were acquired with 265 scans.

^{1}H NMR (500 MHz, CDCl$_3$): δ 8.27 (s, 2H, CH=N), 7.54 (td, ^3J = 7.8 Hz, ^4J =1.6 Hz, 2H, H$_d$), 7.48 (dd, ^3J = 7.9 Hz, ^4J =1.4 Hz, 2H, H$_f$), 7.08 (t, ^3J = 7.5 Hz, 2H, H$_e$), 6.91 (d, ^3J = 8.2 Hz, 2H, H$_c$), 4.21 (t, ^3J = 5.2 Hz, 4H, N-CH$_2$), 2.40 (p, ^3J = 5.1 Hz, 2H, -CH$_2$-). HRMS for [M]$^+$ (EI): calcd. for (C$_{17}$H$_{16}$Cl$_2$N$_2$O$_2$Ti): 398.00628; found: 398.0066.

FT-IR (KBr pellet, cm^{-1}): 3152 v(C-H$_{aromatic}$), 3105 v(C-H$_{aromatic}$), 2987 v(C-H$_{aliphatic}$), 2877 v(C-H$_{aliphatic}$), 1659 v(C=N$_{imine}$), 1599s, 1553m, 1473s, 1453 v(C=C$_{aromatic}$), 1326 v(C-N), 1277s v(Ar-O), 1218, 1156, 1109, 1033m, 908s, 874, 805s, 760s v(C-H oop bend), 634 v(Ti-Cl), 608s, 535 v(Ti-N), 481, 452 v(Ti-O), 419. UV-Vis (THF) λ_{max}: 266, 303, and 387 nm.

5.3.10 Synthesis and characterization of [Ti(^{t}Bu,^{t}Bu-Salpn)Cl$_2$] (17):
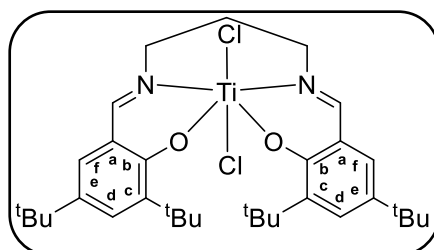
To a Schlenk tube containing ^{t}Bu,^{t}Bu-H$_2$Salpn (0.3 g, 0.59 mmol) in dry THF (20 ml), 1 equivalent of TiCl$_4$(THF)$_2$ (0.19 g) in THF (15 ml) was added dropwise at room temperature. The red orange solution was refluxed at 70 °C for one hour. The solvent removed under reduced pressure and dry hexane (15 ml) was added. The mixture was stirred for 2 minutes before filtering it. The washing process was repeated 3 times and then the precipitate was dried *in vacuo* for 3 hours (0.33 g, 90% yield).

Properties of [Ti(^{t}Bu,^{t}Bu-Salpn)Cl$_2$]:

Formula: C$_{33}$H$_{48}$Cl$_2$N$_2$O$_2$Ti.

Nature: Orange solid.

Molecular weight: 623.53 g/mol.

Yield: 90%

^{1}H NMR (400 MHz, CDCl$_3$): δ 8.26 (s, 2H, CH=N), 7.57 (d, ^4J = 2.4 Hz, 2H, H$_d$), 7.29 (d, ^4J = 2.4 Hz, 2H, H$_f$), 4.14 (t, ^3J = 5.6 Hz, 4H, CH$_2$-N), 2.39 (p, ^3J = 5.6 Hz, 2H, -CH$_2$-), 1.56 (s, 18H, C(CH$_3$)$_3$), 1.32 (s, 18H, C(CH$_3$)$_3$). ^{13}C{^{1}H} NMR (126 MHz, CDCl$_3$): δ 166.44 (CH=N), 160.31 (C$_b$), 145.10 (C$_e$), 137.04 (C$_c$), 130.65 (C$_d$), 129.82 (C$_f$), 127.07 (C$_a$), 62.90 (N-CH$_2$), 35.89 (C(CH$_3$)$_3$), 34.64 (C(CH$_3$)$_3$), 31.46 (-CH$_2$-), 30.51 (C(CH$_3$)$_3$), 27.93 (C(CH$_3$)$_3$). HRMS for [M]$^+$ (ASAP): calcd. for (C$_{33}$H$_{48}$Cl$_2$N$_2$O$_2$Ti): 620.2619; found: 620.2637.

FT-IR (KBr pellet, cm^{-1}): 3083 v(C-H$_{aromatic}$), 2960 v(C-H$_{aliphatic}$), 2907 v(C-H$_{aliphatic}$), 2868 v(C-H$_{aliphatic}$), 2744 v(C-H$_{aliphatic}$), 1659, 1612s v(C=N$_{imine}$), 1565m, 1465, 1437m v(C=C$_{aromatic}$), 1415, 1394, 1367m v(C-N), 1327, 1270s, 1247 vs v(Ar-O), 1207, 1183, 1137, 1075, 1029, 965, 920, 856s, 817, 761s v(C-H oop bend), 622m v(Ti-Cl), 582s v(Ti-N), 478 v(Ti-O), 454, 419. UV-Vis (THF) λ_{max}: 261, 319, and 405 nm.

5.3.11 Synthesis and characterization of [Ti(Me-Salpn)Cl₂] (18):
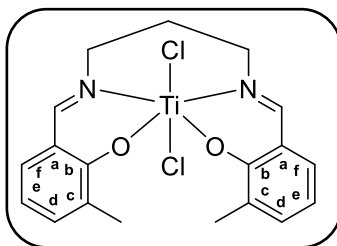
A solution of $TiCl_4(THF)_2$ (0.22 g, 0.64 mmol) in dry THF (~20 ml) was added dropwise to a stirred solution of Me-H₂Salpn (1 eq., 0.20 g) in dry THF (~15 ml) under argon. The resulting mixture was refluxed at 70 °C for one hour. After cooling to ambient temperature, the solution was filtered using filter canula and the precipitate washed with dry Et₂O (3×10 ml). The dark orange precipitate then dried under high vacuum (10^{-6} mbar) at 80 °C for 3 hours (0.23 g, 82% yield).

Properties of [Ti(Me-Salpn)Cl₂]:

Formula: $C_{19}H_{20}Cl_2N_2O_2Ti$.

Nature: Orange solid.

Molecular weight: 427.15 g/mol.

Yield: 82%

^{1}H NMR (500 MHz, CDCl₃): δ 8.24 (s, 2H, CH=N), 7.39 (dd, ^3J = 7.4 Hz, ^4J = 0.7 Hz, 2H, H_d), 7.31 (dd, ^3J = 7.5 Hz, ^4J = 0.7 Hz, 2H, H_f), 6.97 (t, ^3J = 7.6 Hz, 2H, H_e), 4.19 (t, ^3J = 5.8 Hz, 4H, CH₂-N), 2.40 – 2.35 (overlapping, 8H, -CH₂-, Ar-CH₃). ^{113}C{^{1}H} NMR (126 MHz, CDCl₃): δ 165.10 (CH=N), 161.99 (C_b), 136.78 (C_d), 132.05 (C_f), 126.12 (C_c), 125.82 (C_a), 122.55 (C_e), 63.51 (CH₂-N), 28.46 (-CH₂-), 16.08 (C($\underline{C}$H₃)). HRMS for [M-Cl]$^+$ (EI): calcd. for ($C_{19}H_{20}ClN_2O_2Ti$): 391.06873; found: 391.0688.

FT-IR (KBr pellet, cm^{-1}): 3062 ν(C-H$_{aromatic}$), 3031 ν(C-H$_{aromatic}$), 2983 ν(C-H$_{aromatic}$), 2912 ν(C-H$_{aromatic}$), 2847 ν(C-H$_{aromatic}$), 1609s ν(C=N$_{imine}$), 1591, 1574s, 1456, 1432 ν(C=C$_{aromatic}$), 1407m, 1379, 1319 ν(C-N), 1273s ν(Ar-O), 1231s, 1112, 1084m, 1052, 973, 890s, 787s, 757s ν(C-H oop bend), 651s ν(Ti-Cl), 638, 605s, 557 ν(Ti-N), 535, 519, 491, 463, 439s ν(Ti-O), 413. UV-Vis (THF) λ$_{max}$: 266, 308, and 398 nm.

5.4 Synthesis and characterization of Ti(III) complexes:

Ti(III) complexes were prepared by reduction of Ti(IV) using 1/2 equivalent of Zn in THF as described below:

5.4.1 Synthesis and characterization of [Ti(Salpy)Cl] (1):
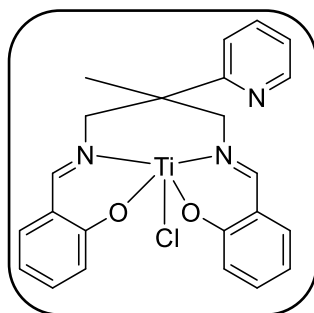
In 100 ml Schlenk tube, 0.5 g (1.02 mmol) of [Ti(Salpy)Cl$_2$], Zn powder (0.03 g, 0.51 mmol) and 40 ml THF were stirred at room temperature under argon atmosphere overnight. During which, the color of the suspension was change from orange to green. The reaction mixture was filtered, washed with dry THF (2×10 ml) and dried *in vacuo* to yield the product as green solid (0.3 g, 65% yield).

Properties of [Ti(Salpy)Cl]:

Formula: C$_{23}$H$_{21}$ClN$_3$O$_2$Ti.

Nature: Green solid.

Molecular weight: 454.76 g/mol.

Yield: 65%

^{1}H NMR (CDCl$_3$): no visible resonance above baseline, + 50 to -50 ppm. HRMS for [M]$^+$(EI): calcd. for (C$_{23}$H$_{21}$ClN$_3$O$_2$Ti): 454.0802; found 454.0813.

FT-IR (KBr pellet, cm^{-1}): 3060 ν(C-H$_{aromatic}$), 2974 ν(C-H$_{aliphatic}$), 2934 ν(C-H$_{aliphatic}$), 2874 ν(C-H$_{aliphatic}$), 1646s ν(C=N$_{imine}$), 1605, 1546, 1474s, 1457 ν(C=N$_{py}$, C=C$_{aromatic}$) ,1407, 1341 ν(C-N), 1277s ν(Ar-O), 1254, 1223, 1154m, 1126, 1031, 904m, 828, 762s ν(C-H oop bend), 651, 599 ν(Ti-Cl), 532, 491 ν(Ti-N), 456, 418 cm^{-1}. UV-Vis (THF) λ_{max}: 246, 324, and 415 nm. EPR spectrum (140 K): g_{iso} =1.944.

5.4.2 Synthesis and characterization of [Ti(Salpy-Me)Cl] (2):
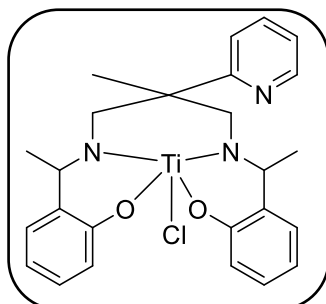
Zn (0.029 g, 0.43 mmol), [Ti(Salpy-Me)Cl$_2$] complex (0.45 g, 0.86 mmol) were dissolved in dry THF and stirred under argon for 19 hours. The mixture was filtered, washed with THF (2×10 ml) and dried under reduced pressure to leave a green solid (0.29 g, 70% yield).

Properties of [Ti(Salpy-Me)Cl]:

Formula: C$_{25}$H$_{29}$ClN$_3$O$_2$Ti.

Nature: Green solid.

Molecular weight: 486.84 g/mol.

Yield: 70%.

^{1}H NMR (CDCl$_3$): no visible resonance above baseline, + 50 to -50 ppm. HRMS for [M]$^+$(EI): calcd. for (C$_{25}$H$_{29}$ClN$_3$O$_2$Ti): 486.1428; found 486.1436.

FT-IR (KBr pellet, cm^{-1}): 3060 ν(C-H$_{aromatic}$), 2968 ν(C-H$_{aliphatic}$), 2874 ν(C-H$_{aliphatic}$), 1595s, 1570, 1480s, 1456s ν(C=N$_{py}$, C=C$_{aromatic}$), 1385 ν(C-N), 1263s ν(Ar-O), 1197, 1157, 1111, 1038, 898s, 764s ν(C-H oop bend), 633s ν(Ti-Cl), 547 ν(Ti-N), 468 ν(Ti-O).

5.4.3 Synthesis and characterization of [Ti(^{t}Bu,^{t}Bu-Salpy)Cl] (3):
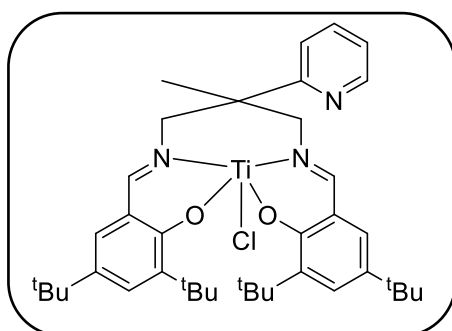
0.6 g [Ti(tBu,tBu-Salpy)Cl$_2$] (0.84 mmol) and Zn powder (0.027 g, 0.42 mmol) were stirred in THF (50 ml) overnight under inert atmosphere. After the stirring, the solvent was removed under reduced pressure to dryness and 30 ml dry dichloromethane was added. After stirring for few minutes, the reaction mixture was filtered into a new Schlenk tube and the solvent was removed from the filtrate *in vacuo* to yield the titled compound as a dark green precipitate (0.38 g, 67% yield).

Properties of [Ti(ᵗBu,ᵗBu-Salpy)Cl]:

Formula: $C_{39}H_{53}ClN_3O_2Ti$.

Nature: Dark green solid.

Molecular weight: 679.19 g/mol.

Yield: 67%

^{1}H NMR (CDCl$_3$): no visible resonance above baseline, + 50 to -50 ppm. HRMS for [M]$^+$ (ASAP): calcd for $C_{39}H_{53}ClN_3O_2Ti$: 676.3353, found: 676.3376.

FT-IR (KBr pellet, cm^{-1}): 3082 ν(C-H$_{aromatic}$), 3055 ν(C-H$_{aromatic}$), 2954 ν(C-H$_{aliphatic}$), 2908 ν(C-H$_{aliphatic}$), 2870 ν(C-H$_{aliphatic}$), 1607s ν(C=N$_{imine}$), 1563m, 1478s, 1464, 1440 ν(C=N$_{py}$, C=C$_{aromatic}$), 1415, 1394, 1363s ν(C-N), 1297, 1272, 1250s ν(Ar-O), 1203, 1176, 1126, 1061, 1022, 919m, 857s,785m, 761s ν(C-H oop bend), 648 ν(Ti-Cl), 625, 581 ν(Ti-N), 471, 437 ν(Ti-O), 412. UV-Vis (THF) λ_{max}: 261, 325, and 418 nm.

5.4.4 Synthesis and characterization of [Ti(Cl,Cl-Salpy)Cl] (4):
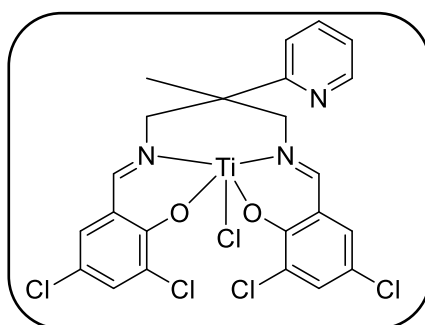
[Ti(Cl,Cl-Salpy)Cl$_2$] (0.4 g, 0.64 mmol), ½ equivalent of Zn (0.32 g, 0.32 mmol) and 40 ml THF were stirred for 20 hours at room temperature. After which, the solvent was removed under reduced pressure and the green residue was dissolved in 30 ml DCM. After stirring for 5 minutes the solvent was filtered and the solvent was removed from the filtrate *in vacuo* to yield the desired complex (0.21 g, 55% yield).

Properties of [Ti(Cl,Cl-Salpy)Cl]:

Formula: $C_{23}H_{17}Cl_5N_3O_2Ti$.

Nature: Green solid.

Molecular weight: 592.53 g/mol.

Yield: 55%

^{1}H NMR (CDCl$_3$): no visible resonance above baseline, + 50 to -50 ppm. HRMS for [M]$^+$ (ASAP): calcd for $C_{23}H_{17}Cl_5N_3O_2Ti$: 587.9290, found: 587.9308.

FT-IR (KBr pellet, cm^{-1}): 3087 ν(C-H$_{aromatic}$), 3050 ν(C-H$_{aromatic}$), 2970 ν(C-H$_{aliphatic}$), 2929 ν(C-H$_{aliphatic}$), 2871 ν(C-H$_{aliphatic}$), 1609vs ν(C=N$_{imine}$), 1544s, 1523,1438s ν(C=N$_{py}$, C=C$_{aromatic}$), 1387 ν(C-N), 1288s ν(Ar-O), 1218m, 1198, 1184, 1104, 1059, 997w, 880s, 793s ν(C-H oop bend), 740m, 705w, 651, 612m ν(Ti-Cl), 559 ν(Ti-N), 535, 503, 472, 437, 421. UV-Vis (THF) λ$_{max}$: 286, 329, and 400 nm. EPR spectrum (140 K): g_{iso} = 2.044.

5.4.5 Synthesis and characterization of [Ti(Naphpy)Cl] (5):
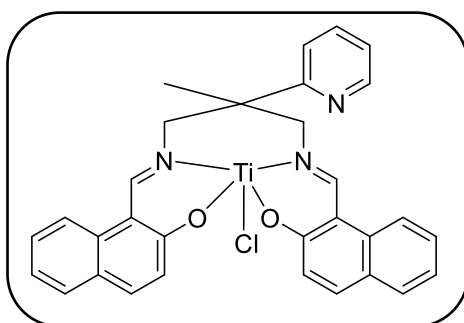
In the glove box, [Ti(Naphpy)Cl$_2$] complex (0.55 g, 0.93 mmol) and ½ equivalent zinc powder were dissolved in 50 ml dry THF. The solution was stirred under argon overnight. The solid was filtered, washed with THF (2×10 ml) and dried under reduced pressure to obtain a green solid (0.36 g, 69% yield).

Properties of [Ti(Naphpy)Cl]:

Formula: $C_{31}H_{25}ClN_3O_2Ti$.

Nature: Green solid.

Molecular weight: 554.88 g/mol.

Yield: 69%.

^{1}H NMR (CDCl$_3$): no visible resonance above baseline, + 50 to -50 ppm. HRMS for [M-Cl]$^+$ (ASAP): calcd for $C_{31}H_{25}N_3O_2Ti$: 519.1426, found: 519.1415 nm.

FT-IR (KBr pellet, cm^{-1}): 3133 ν(C-H$_{aromatic}$),3062 ν(C-H$_{aromatic}$), 2973 ν(C-H$_{aliphatic}$), 2872 ν(C-H$_{aliphatic}$), 1626s ν(C=N$_{imine}$), 1597s, 1548s, 1513m, 1468s ν(C=N$_{py}$, C=C$_{aromatic}$), 1406, 1377m, 1343 ν(C-N), 1289s ν(Ar-O), 1250s, 1196s, 1167, 1146, 1094, 1061, 1034, 968m, 839s, 780, 749vs ν(C-H oop bend), 652 ν(Ti-Cl), 620, 598, 574, 540, 523 ν(Ti-N), 519, 435, 420. UV-Vis (THF) λ_{max}: 270, 333, and 433. EPR spectrum (140 K): g_{iso} = 2.053.

5.4.6 Synthesis and characterization of [Ti(Salpn)Cl] (6):
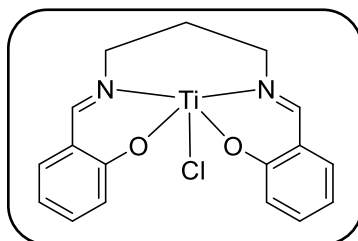
Zn (0.025 g, 0.38 mmol), [Ti(Salpn)Cl$_2$] (0.6 g, 0.75 mmol) and THF (50 ml) were stirred overnight at room temperature. The precipitate was isolated via canula filtration, washed with THF (2×10 ml) and dried under reduced pressure to yield the titled complex as a green solid (0.37 g, 67% yield).

Properties of [Ti(Salpn)Cl]:

Formula: C$_{17}$H$_{16}$ClN$_2$O$_2$Ti.

Nature: Green solid.

Molecular weight: 363.64 g/mol.

Yield: 67%

^{1}H NMR (CDCl$_3$): no visible resonance above baseline, + 50 to -50 ppm. HRMS for [M]$^+$ (ASAP): calcd for C$_{17}$H$_{16}$ClN$_2$O$_2$Ti: 363.0380, found: 363.0382.

FT-IR (KBr pellet, cm^{-1}): 3142 ν(C-H$_{aromatic}$), 3095 ν(C-H$_{aromatic}$), 2976 ν(C-H$_{aliphatic}$), 2874 ν(C-H$_{aliphatic}$), 1659s ν(C=N$_{imine}$), 1604s,1545s, 1474s, 1455 ν(C=C$_{aromatic}$), 1325 ν(C-N), 1290s ν(Ar-O), 1210, 1155s, 1110, 1030m, 906s, 874m, 803m, 761s ν(C-H oop bend), 629 ν(Ti-Cl), 540 ν(Ti-N), 597m, 483, 451 ν(Ti-O), 419. UV-Vis (THF) λ_{max}: 265, 294, 322 and 448 nm. EPR spectrum (140 K): g_{iso} = 2.009

5.4.7 Synthesis and characterization of [Ti(ᵗBu,ᵗBu-Salpn)Cl] (7):
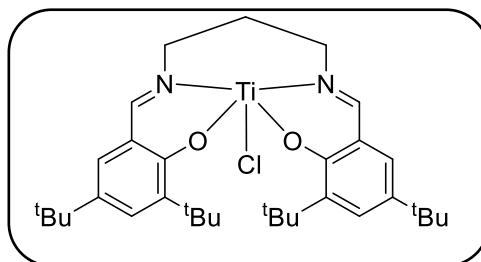
A mixture of [Ti(ᵗBu,ᵗBu-Salpn)Cl$_2$] complex (0.6 g, 0.96 mmol), Zn (0.033 g, 0.48 mmol) and 50 ml THF were stirred under argon overnight. The solvent was removed under reduced pressure and then redissolved in DCM (30 ml). The solution was filtered, and the solvent was removed from the filtrate *in vacuo* to yield a green solid (0.34 g, 60% yield).

Properties of [Ti(ᵗBu,ᵗBu-Salpn)Cl]:

Formula: C$_{33}$H$_{48}$ClN$_2$O$_2$Ti.

Nature: Green solid.

Molecular weight: 588.08 g/mol.

Yield: 60%

^{1}H NMR (CDCl$_3$): no visible resonance above baseline, + 50 to -50 ppm. HRMS for [M]$^+$ (ASAP): calcd for C$_{33}$H$_{48}$ClN$_2$O$_2$Ti: 585.2931, found: 585.2939.

FT-IR (KBr pellet, cm^{-1}): 3158 ν(C-H$_{aromatic}$), 3087 ν(C-H$_{aromatic}$), 2959 ν(C-H$_{aliphatic}$), 2908 ν(C-H$_{aliphatic}$), 2869 ν(C-H$_{aliphatic}$), 1659, 1612s ν(C=N$_{imine}$), 1565, 1560s, 1461, 1440 ν(C=C$_{aromatic}$), 1415, 1393, 1364s ν(C-N), 1272s, 1248s ν(Ar-O), 1202, 1183, 1049, 919, 856s, 760s ν(C-H oop bend), 620 ν(Ti-Cl), 582s ν(Ti-N), 479 ν(Ti-O), 418. UV-Vis (THF) λ_{max}: 262, 325, and 410 nm.

5.5 Synthesis of titanium precursors:

5.5.1 Synthesis of TiCl$_3$(THF)$_3$:
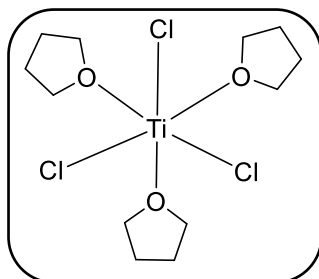
This complex was prepared according to previously reported method.[11] 10 g of $(TiCl_3)_3 \cdot AlCl_3$ was dissolved in 10 ml toluene in a Youngs tap fitted glass ampule under N$_2$ atmosphere. The ampule was then cooled to -50 °C using dry ice + acetone bath then excess of THF (100 ml) was added via canula to the stirred solution. This reaction is too exothermic and the aim of adding toluene is to work as a heat sink during the THF addition. The blue mixture was then refluxed (70 °C) overnight then allowed to cool to room temperature and the solution was filtered using filter canula. The blue precipitate was washed with THF and dried under reduced pressure for 4 hours at room temperature to yield 18 g of product (97%).

5.5.2 Synthesis of TiCl$_4$(THF)$_2$:
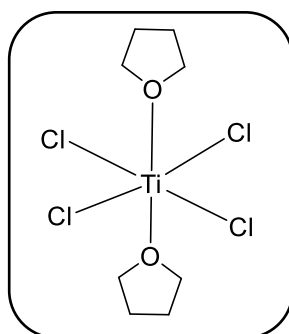
TiCl$_4$(THF)$_2$ was synthesized according to a modified known procedure.[12] Titanium tetrachloride (5 ml, 8.65 g, 45.6 mmol) was dissolved in methylene chloride (80 ml) in a Schlenk tube equipped with a magnetic stirring bar. After cooling to 0 °C, anhydrous THF (8 ml, 7.11 g, 98.6 mmol) was added dropwise and slowly to prevent a violent exothermic reaction and the reaction mixture was stirred under argon for 1 hour at room temperature. The solvent removed under reduced pressure. The resulting bright yellow solid was washed with pentane

(3×30 ml) and dried under reduced pressure giving the desired complex, $TiCl_4(THF)_2$ (13.86 g, 91% yield).

5.6 Cross coupling products:

5.6.1 3-(3-Oxocyclohexyl))Propanenitrile:
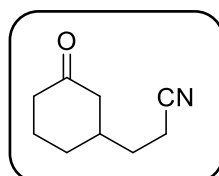
Isolated as a colorless oil after purified by flash chromatography (Hexane/EtOAc 3:2, phosphomolybdic acid stain PMA, $R_f = 0.36$).

^{1}H NMR (400 MHz, $CDCl_3$): δ 2.52 – 2.32 (m, 3H), 2.33 – 2.19 (m, 2H), 2.15 – 2.02 (m, 2H), 2.01 – 1.85 (m, 2H), 1.79 – 1.53 (m, 3H), 1.40 (ddd, $^2J = 14.3$ Hz, $^3J = 6.0$ Hz, $^4J = 2.7$ Hz, 1H). ^{13}C{^{1}H} NMR (101 MHz, $CDCl_3$): δ 210.08 (C=O), 120.64 (C≡N), 47.26, 41.33, 37.90, 31.83, 30.61, 24.87, 14.90. HRMS for [M+H]$^+$ (ASAP): calcd for $C_9H_{14}NO$: 152.1075, found: 152.1070.

FT-IR (cm^{-1}): 2937, 2360, 2243 (C≡N), 1702 v(C=O), 1446, 1422, 1345, 1315, 1227, 1167, 1103, 1065, 944, 914, 730.

5.6.2 3-(3-Oxocyclopentyl)Propanenitrile:
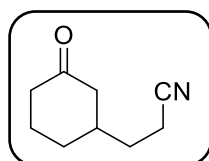
Isolated as a colorless oil after purified by flash chromatography (Hexane/EtOAc 3:2, phosphomolybdic acid stain PMA, $R_f = 0.4$).

^{1}H NMR (400 MHz, $CDCl_3$): δ 2.50 – 2.37 (m, 3H), 2.36 – 2.11 (m, 4H), 1.92 – 1.73 (m, 3H), 1.59 – 1.44 (m, 1H). ^{13}C NMR (101 MHz, $CDCl_3$) δ 217.56 (C=O), 119.25 (C≡N), 44.46, 38.46, 36.28, 31.13, 29.10, 15.95. HRMS for [M+H]$^+$ (ASAP): calcd for $C_8H_{12}NO$: 138.0919, found: 138.0913.

FT-IR (cm^{-1}): 2951, 2887, 2237 (C≡N), 1731 ν(C=O), 1455, 1405, 1340,1252, 1161, 981, 840, 732.

5.6.3 3-(1-methyl-3-oxocyclohexyl)propanitrile:
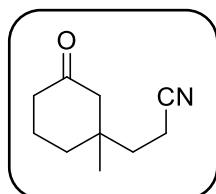
Isolated as a colorless oil after purified by flash chromatography (Hexane/EtOAc 2:1, phosphomolybdic acid stain PMA, R_f = 0.3).

^{1}H NMR (400 MHz, CDCl$_3$) δ 2.30 – 2.19 (m, 4H), 2.15 – 2.05 (m, 2H), 1.89 – 1.78 (m, 2H), 1.68 – 1.61 (m, 2H), 1.60 – 1.53 (m, 2H), 0.91 (s, 3H, CH$_3$).^{13}C{^{1}H} NMR (101 MHz, CDCl$_3$): δ 210.38 (C=O), 119.78 (C≡N), 52.83, 40.76, 38.33, 37.05, 35.43, 24.09, 21.87, 11.93. HRMS for [M]$^+$ (EI): calcd for C$_{10}$H$_{15}$NO: 165.1148, found: 165.1150.

5.7 Reference:

1   S. Friedrich, M. Schubart, L. H. Gade, I. J. Scowen, A. J. Edwards and M. McPartlin, *Chem. Ber.*, 1997, **130**, 1751–1759.

2   S. Stoll and A. Schweiger, *J. Magn. Reson.*, 2006, **178**, 42–55.

3   G. M. Sheldrick, Acta Crystallogr. Sect. C Struct. Chem., 2015, **71**, 3–8.

4   N. J. Van Zee and G. W. Coates, *Angew. Chem. Int. Ed.*, 2015, **54**, 2665–2668.

5   J. Streuff, *Chem. – Eur. J.*, 2011, **17**, 5507–5510.

6   P. Bichovski, T. M. Haas, M. Keller and J. Streuff, *Org. Biomol. Chem.*, 2016, **14**, 5673–5682.

7   R. Shakya, A. Jozwiuk, D. R. Powell and R. P. Houser, *Inorg. Chem.*, 2009, **48**, 4083–4088.

8   X. Zhang, T. J. Emge and K. C. Hultzsch, *Angew. Chem. Int. Ed.*, 2012, **51**, 394–398.

9   H. Shi and Y. Yin, *Inorganica Chim. Acta*, 2014, **421**, 446–450.

10 A. Sattler, J. A. Labinger and J. E. Bercaw, *Organometallics*, 2013, **32**, 6899–6902.

11 N. A. Jones, S. T. Liddle, C. Wilson and P. L. Arnold, *Organometallics*, 2007, **26**, 755–757.

12 L. E. Manxzer, J. Deaton, P. Sharp and R. R. Schrock, in *Inorganic Syntheses*, John Wiley & Sons, Ltd, 1982, pp. 135–140.

General conclusion:

In this thesis two types of ligands have been prepared: Salpn ligands and Salpy ligands. Salpn ligands were obtained by the condensation of 1 equivalent of 1,3-diaminopropane with 2 equivalents of salicylaldehyde or its derivatives. Three ligands of this type have been prepared: H_2Salpn, $^tBu,^tBu-H_2Salpn$ and $Me-H_2Salpn$. These ligands can coordinate to a metal via the imine nitrogens and the phenol oxygens, which are invariably deprotonated, and thus offer a (usually) planner N_2O_2 core, leaving two axial sites available for co-ligands. The Salpy ligand contains an additional central pyridyl donor, and it therefore contains five donor groups (N_3O_2). Salpy ligands were prepared by the Schiff base condensation of 1 equivalent of of 2-methyl-2-(pyridine-2-yl)propane-1,3-diamine (ppda) with two equivalents of salicylaldehyde derivatives. H_2Salpy, $^tBu,^tBu-H_2Salpy$, $Me-H_2Salpy$, and $Cl,Cl-H_2Salpy$ were all prepared from commercially available precursors whereas the precursors of $Ad,Me-H_2Salpy$ and $^tBu,OMe-H_2Salpy$ have been prepared by literature methods. $H_2Naphpy$ was prepared from the treatment of ppda with two equivalents of 2-hydroxy-1-naphthaldehyde. All of these ligands contain two ionizable phenol protons which make them bivalent anionic ligands when deprotonated.

All of the ligands were characterized using ^1H NMR, $^{13}C\{^1H\}$ NMR, IR and UV-Vis spectroscopies and by high resolution mass spectrometry. The NMR studies revealed that these ligands are symmetrical with the two arms being identical. The strong hydrogen bonds between the nitrogen of the imine group and the enolic hydrogen in the same molecule were reflected by the disappearance of the OH bands in the IR spectra. The UV-Vis spectra of these ligands usually show three absorption bands due to $\pi \rightarrow \pi^*$ transitions (at higher energy) in the ligands aromatic rings, $n \rightarrow \pi^*$ transition of the nonbonding electrons located on the nitrogen of the imine groups and the third band attributed to $n \rightarrow \pi^*$ transitions involving C=N and phenolic groups.

A series of titanium (IV) and (III) complexes bearing different ligands were successfully synthesized. Ti(IV) complexes were synthesized in high yields by the direct reaction of the precursor $TiCl_4(THF)_2$ and the pro-ligands in THF. The solid state structures of five complexes have been determined by single crystal X-ray crystallography, which indicated distorted octahedral geometry around the metal centres. Due to the present the rigid tetradentate ligand, the two labile chloride ligands are forced to be in trans position while the ligand occupied the equatorial position via ONNO sites, which is unusual for the Salpy ligands since they normally

adopt a β-cis geometry. The Ti(IV) Salpy complexes were found to undergo a redistribution process in ether solution to give a separated ion pair; the formation of these products is attributed to the dissociation of coordinated HCl from the pendant pyridyl. All Ti(IV) complexes have been studied using high resolution mass spectrometry, IR and UV-Vis spectroscopies, and nuclear magnetic resonance (^{1}H and ^{13}C{^{1}H}) spectroscopies. The ^{1}H NMR studies revealed that the pyridyl donor did not coordinate to the metal centre. The X-ray crystallographic studies found that the protonated pyridyl formed a hydrogen bond to a chloride ion in the lattice, effectively an additional molecule of HCl which is captured by the pyridyl base when HCl is liberated during the synthesis. The presence of the HCl proved to be crucial in stabilising the complexes.

Seven Ti(III) complexes were prepared by reducing the analogous Ti(IV) complexes using zinc dust. These complexes were studied using high resolution mass spectrometry, IR, UV-Vis spectroscopies, and by the Electron paramagnetic resonance (EPR) spectroscopy, as well as by high resolution mass spectrometry and FT-IR spectroscopy. However, the ^{1}H NMR spectra of the Ti(III) complexes were not informative due to the paramagnetic nature of the complexes; in every case the spectra showed no evidence for any diamagnetic species which is consistent with the complete conversion of Ti(IV) to Ti(III).

The titanium complexes were probed as catalysts in the ring opening copolymerization of various epoxides with different cyclic anhydrides. This work resulted in the effective synthesis of aliphatic and semi aliphatic polyesters with good M_n values and narrow PDIs. Examining the copolymerization of propylene oxide (PO) with succinc anhydride (SA) without cocatalyst using the Salpy complex [Ti(Salpy)Cl] (**1**) as catalyst resulted in polyester with good selectivity and yield, whereas, most of salen-type complexes known to form significant polyether content when performed without a cocatalyst. However, the incorporation of cocatalyst significantly improved the catalytic activity producing highly selective polymer and higher molecular mass. PPNCl was more efficient in the copolymerization compared with DMAP.

The ROCOP reactions were carried out in both solution and solvent free conditions. The epoxides and anhydrides were carefully selected to provide a variety of structural motifs including saturated, unsaturated, aliphatic, aromatic, unsubstituted and substituted rings. All epoxides and anhydride were commercially available.

The solution ROCOP result in polyester with highly selective polyester and good molecular weights, however due to the dilution effect the polymerization reactions required longer times (24 h). A significant increase of the catalytic activity (the full anhydride conversion reached within 60-210 minutes and produced higher polyester molecular weight) was

observed when the copolymerizations were performed in neat (excess of epoxide) which is in agreement with the copolymerization being first order dependence with respect to epoxide concentration. The epoxide type significantly affected the copolymerization rates. Generally, better catalytic performance in copolymerization was achieved with Ti(IV) complexes compared to Ti(III), which is likely to reflect the greater stability of Ti(IV) complexes compared to Ti(III).

The titanium Salen-type complexes were tested for catalytic activity in the reductive cross coupling reaction, of which only few examples are known in the literature and with a confined number of catalytic systems. Titanium salen-type complexes catalyzed the double reductive alkylation of enones and readily available alkenes. It allows the selective preparation of 1,6-bifunctionalized ketonitriles *via* redox umpolung procedure under mild conditions and without the requirement of stoichiometric organometallic reagents. These complexes offer a cheap and environmentally friendly promising research area for the construction of inaccessible carbon-carbon bonds with an increasing number of ligand manifolds from the plethora available within the chemical literature.

Appendices:

x-ray crystal structure data

Table 1. Crystal data and structure refinement for [Ti(^{t}Bu,^{t}Bu-Salpn)Cl$_2$] (17).

Identification code	sa3a
Empirical formula	$C_{33}H_{48}Cl_2N_2O_2Ti$
Formula weight	623.53
Temperature	150(2) K
Wavelength	1.54184 Å
Crystal system	Triclinic
Space group	$P\bar{1}$
Unit cell dimensions	a = 11.4842(4) Å α = 107.370(3) °
	b = 15.9617(8) Å β = 90.171(3) °
	c = 20.3647(6) Å γ = 107.608(4) °
Volume	3377.9(2) Å^3
Z	4
Density (calculated)	1.226 Mg/m^3
Absorption coefficient	3.829 mm^{-1}
F(000)	1328
Crystal size	0.251 × 0.021 × 0.019 mm^3
θ range for data collection	4.060 to 76.941 °
Index ranges	-12 ≤ h ≤ 14, -20 ≤ k ≤ 19, -17 ≤ l ≤ 25
Reflections collected	34272
Independent reflections	14057 [R(int) = 0.0638]
Completeness to θ = 67.684 °	100.0%
Absorption correction	Gaussian
Max. and min. transmission	1.000 and 0.782
Refinement method	Full-matrix least-squares on F^2
Data / restraints / parameters	14057 / 0 / 745
Goodness-of-fit on F^2	1.017
Final R indices [I>2σ(I)]	R_1 = 0.0473, wR_2 = 0.1022
R indices (all data)	R_1 = 0.0755, wR_2 = 0.1178
Extinction coefficient	n/a
Largest diff. peak and hole	0.315 and -0.387 e.Å^{-3}

Table 2. Crystal data and structure refinement for [Ti(Me-Salpn)Cl$_2$] (18).

Identification code	sa7
Empirical formula	$C_{19}H_{20}Cl_2N_2O_2Ti$
Formula weight	427.17
Temperature	160.00 K
Wavelength	1.54184 Å
Crystal system	Monoclinic
Space group	$P2_1/n$
Unit cell dimensions	a = 10.2845(2) Å α = 90 °
	b = 17.4323(3) Å β = 110.200(2) °
	c = 11.1498(2) Å γ = 90 °
Volume	1876.01(6) Å^3
Z	4
Density (calculated)	1.512 Mg/m^3
Absorption coefficient	6.622 mm^{-1}
F(000)	880
Crystal size	0.267 × 0.127 × 0.092 mm^3
θ range for data collection	4.929 to 76.748 °
Index ranges	$-12 \leq h \leq 12, -21 \leq k \leq 21, -13 \leq l \leq 13$
Reflections collected	17893
Independent reflections	3919 [R(int) = 0.0273]
Completeness to θ = 67.684 °	100.0%
Absorption correction	Gaussian
Max. and min. transmission	1.000 and 0.479
Refinement method	Full-matrix least-squares on F^2
Data / restraints / parameters	3919 / 0 / 237
Goodness-of-fit on F^2	1.045
Final R indices [I>2σ(I)]	$R_1 = 0.0258$, $wR_2 = 0.0696$
R indices (all data)	$R_1 = 0.0280$, $wR_2 = 0.0715$
Extinction coefficient	n/a
Largest diff. peak and hole	0.275 and -0.421 e.Å^{-3}

Table 3. Crystal data and structure refinement for [Ti(Salpy)Cl$_2$] (8).

Identification code	sa4
Empirical formula	C$_{23}$ H$_{22}$ Cl$_3$ N$_3$ O$_2$ Ti
Formula weight	526.68
Temperature	100(2) K
Wavelength	1.54178 Å
Crystal system	Orthorhombic
Space group	P2$_1$2$_1$2$_1$
Unit cell dimensions	a = 9.102 Å $\quad$ α = 90 °
	b = 14.93030(10) Å $\quad$ β = 90 °
	c = 16.75730(10) Å $\quad$ γ = 90 °
Volume	2277.24(2) Å^3
Z	4
Density (calculated)	1.536 Mg/m^3
Absorption coefficient	6.645 mm^{-1}
F(000)	1080
Crystal size	0.140 × 0.100 × 0.060 mm^3
θ range for data collection	3.965 to 68.214 °
Index ranges	−10 ≤ h ≤ 10, −17 ≤ k ≤ 17, −20 ≤ l ≤ 20
Reflections collected	39924
Independent reflections	4148 [R(int) = 0.0215]
Completeness to θ = 67.679 °	99.6%
Absorption correction	Semi-empirical from equivalents
Max. and min. transmission	1.00000 and 0.66956
Refinement method	Full-matrix least-squares on F^2
Data / restraints / parameters	4148 / 288 / 355
Goodness-of-fit on F^2	0.983
Final R indices [I>2σ(I)]	R_1 = 0.0246, wR_2 = 0.0702
R indices (all data)	R_1 = 0.0247, wR_2 = 0.0703
Absolute structure parameter	0.475(14)
Extinction coefficient	n/a
Largest diff. peak and hole	0.367 and −0.322 e.Å^{-3}

Table 4. Crystal data and structure refinement for [Ti(Me-Salpy)Cl$_2$] (12).

Identification code	sa6
Empirical formula	C$_{27}$H$_{28}$Cl$_9$N$_3$O$_2$Ti
Formula weight	793.47
Temperature	160.0 K
Wavelength	1.54184 Å
Crystal system	Monoclinic
Space group	$P2_1$/n

Unit cell dimensions

	a = 11.8344(2) Å	α = 90 °
	b = 19.0552(3) Å	β = 110.089(2) °
	c = 16.4679(3) Å	γ = 90 °

Volume	3487.69(11) Å^3
Z	4
Density (calculated)	1.511 Mg/m^3
Absorption coefficient	8.674 mm^{-1}
F(000)	1608
Crystal size	0.203 × 0.175 × 0.047 mm^3
θ range for data collection	3.681 to 76.765 °
Index ranges	$-14 \le h \le 14, -23 \le k \le 23, -20 \le l \le 20$
Reflections collected	35112
Independent reflections	7311 [R(int) = 0.0503]
Completeness to θ = 67.684 °	100.0%
Absorption correction	Gaussian
Max. and min. transmission	1.000 and 0.533
Refinement method	Full-matrix least-squares on F^2
Data / restraints / parameters	7311 / 0 / 382
Goodness-of-fit on F^2	1.029
Final R indices [I>2σ(I)]	R_1 = 0.0419, wR_2 = 0.1036
R indices (all data)	R_1 = 0.0543, wR_2 = 0.1126
Extinction coefficient	n/a
Largest diff. peak and hole	1.007 and -0.611 e.Å^{-3}

Table 5. Crystal data and structure refinement for [Ti$_2$(^{t}Bu,^{t}Bu-Salpy)Cl$_7$][Ti(^{t}Bu,^{t}Bu-Salpy)Cl] (1A).

Identification code	sa5
Empirical formula	$C_{86}H_{126}Cl_8N_6O_6Ti_3$
Formula weight	1767.22
Temperature	100(2) K
Wavelength	1.54178 Å
Crystal system	Monoclinic
Space group	P2$_1$/c
Unit cell dimensions	a = 18.5479(3) Å α = 90 °
	b = 26.5071(4) Å β = 111.033(2) °
	c = 20.5973(4) Å γ = 90 °
Volume	9452.0(3) Å^3
Z	4
Density (calculated)	1.242 Mg/m^3
Absorption coefficient	4.583 mm^{-1}
F(000)	3736
Crystal size	0.080 × 0.070 × 0.025 mm^3
θ range for data collection	2.552 to 68.243 °
Index ranges	–22 ≤ h ≤ 22, –30 ≤ k ≤ 31, –24 ≤ l ≤ 24
Reflections collected	133170
Independent reflections	17267 [R(int) = 0.0794]
Completeness to θ = 67.679∞	99.8%
Absorption correction	Semi-empirical from equivalents
Max. and min. transmission	1.00000 and 0.89961
Refinement method	Full-matrix least-squares on F^2
Data / restraints / parameters	17267 / 144 / 1063
Goodness-of-fit on F^2	1.081
Final R indices [I>2σ(I)]	R_1 = 0.0613, wR_2 = 0.1747
R indices (all data)	R_1 = 0.0775, wR_2 = 0.1857
Extinction coefficient	n/a
Largest diff. peak and hole	0.990 and -0.523 e. Å^{-3}

Table 6. Crystal Structure Determination of [Ti(Salpy)(η²-O²)] (1B):

Identification code	sa1
Empirical formula	C23 Cl1.97 N3 O4 Ti
Formula weight	499.90
Temperature	100(2) K
Wavelength	0.71075 Å
Crystal system	Triclinic
Space group	P-1
Unit cell dimensions	a = 12.6173(3) Å a= 91.583(4) °
	b = 13.6034(5) Å b= 97.667(3) °
	c = 17.9243(9) Å g = 108.427(3) °
Volume	2884.7(2) Å3
Z	4
Density (calculated)	1.151 Mg/m3
Absorption coefficient	0.506 mm-1
F(000)	986
Crystal size	0.170 x 0.030 x 0.020 mm3
θ range for data collection	2.024 to 27.489 Å
Index ranges	-16<=h<=16, -17<=k<=17, -23<=l<=23
Reflections collected	22614
Independent reflections	22614 [R(int) = ?]
Completeness to theta = 25.242 °	99.9%
Refinement method	Full-matrix least-squares on F2
Data / restraints / parameters	22614 / 81 / 640
Goodness-of-fit on F2	1.723
Final R indices [I>2sigma(I)]	R1 = 0.1302, wR2 = 0.3435
R indices (all data)	R1 = 0.2202, wR2 = 0.3585
Extinction coefficient	n/a
Largest diff. peak and hole	1.471 and -0.594 e.Å-3

Note on **(1B)** refinement: The data were twinned and of poor quality (low I/σ(I)), leading to a structure unsuitable for publication. In particular, there were large residual electron density peaks evident in the Fourier difference map, which could indicate a minor component

corresponding to chlorination of the phenoxide rings (ca. 25% occupancy). The bond distances for the phenoxide chlorines are erratic, ranging from 2.1-2.7Å and this is a best-guess approximation. The major component is clearly the Salpy ligand used in the synthesis of the complex. the central coordination sphere is likely to be correct but no further inference should be drawn from these data other than the formation of an O_2 complex.